University of Salerno
Department of Chemistry and Biology

PhD in
SCIENCE AND TECHNOLOGY FOR
CHEMICAL,PHARMACEUTICAL AND FOOD INDUSTRY"
XII CYCLE - Chemistry Curriculum
2013/2014

New Chemical Topologies Based on Calixarene Threading

Roberta Ciao





University of Salerno
Department of Chemistry and Biology

Ph.D in
SCIENCE AND TECHNOLOGY FOR CHEMICAL, PHARMACEUTICAL, AND FOOD INDUSTRY"
XII CYCLE - Chemistry Curriculum
2011-2014

Ph.D. Thesis

New Chemical Topologies

Based on Calixarene Threading

Roberta Ciao

Supervisors

Prof. Placido Neri

University of Salerno

Prof. Yoram Cohen

University of Tel Aviv

Counter Supervisor

Prof. Francesco De Riccardis

University of Salerno

Coordinator

Prof. Gaetano Guerra

University of Salerno

CHAPTER I

CHAPTER II

CHAPTER III

CHAPTER IV

FIGURE LISTS

Abstract

Recently, Neri et al. have introduced an efficient method to obtain *endo*-cavity complexation and *through-the-annulus* threading of large calixarenes by exploiting the inducing effect of the weakly coordinating tetrakis[3,5-bis-trifluoromethyl)phenyl]borate (TFPB-) anion. The corresponding calix[6]-arene/dialkylammonium pair can be considered a versatile recognition motif, which can be used for the construction of a large variety of calixarene-threaded architectures.

This Ph. D. thesis deals with the exploration of the stereochemical features of the threading of hosts containing multiple cavities. Therefore, the synthesis of double- and triple-calixarenes is reported, which is followed by the subsequent study of their threading abilities with dialkylammonium axles.

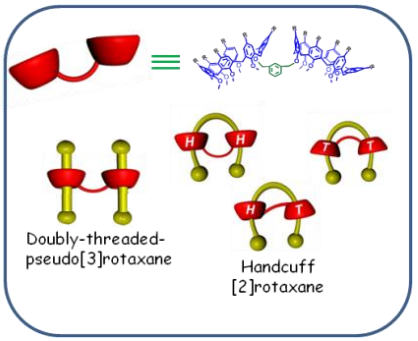

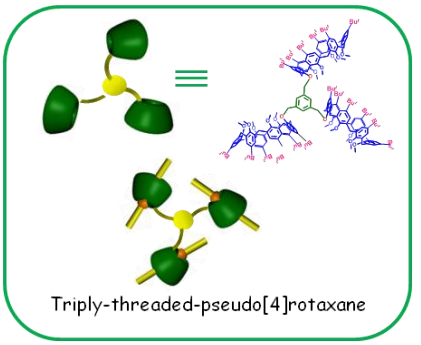

The results confirmed the now well-known *endo-alkyl* rule of calix[6]arenes that give the inclusion of alkyl chains inside the calix-cavity. On this basis, we were then able to build new attractive chemical topologies. In particular, doubly-threaded pseudo[3]rotaxane structures have been obtained by the threading of double-calixarene hosts with mono-ammonium axles. The subsequent extention to triple-calixarene hosts, in which three macrocycles are covalently linked to one another by means of an appropriate spacer, gave triply-threaded pseudo[4]rotaxane structures.

Because of the three-dimensional nonsymmetrical nature of the calix[6]arene wheels, by threading double-calixarene hosts with bis-ammonium axles three examples of beautiful stereoisomeric calixarene-based handcuff rotaxanes were obtained, which could be termed as *head-to-head* (*H,H*), *head-to-tail* (*H,T*), and *tail-to-tail* (*T,T*).

On the basis of these results, it is conceivable that the extension of this approach could lead to novel mechanically interlocked architectures with high-order topologies.

E il tempo che hai perso per la tua rosa,
a rendere importante la tua rosa

CHAPTER I

Introduction

The main interpretation of supramolecular chemistry as the chemistry that goes beyond the covalent bond is inherent to its original foundation by Lehn.[1] In particular, anyone who approaches to that branch of chemistry is introduced to the weak interactions between molecular components. These interactions can be recognized within these supramolecular structures and lead to a superior organization of the matter. Supramolecular chemistry has found quite different applications, ranging from chemistry to biological mimicry, including nanotechnology and computing at the molecular level.

Starting from the Lehn's approach[1] as the basic foundation of supramolecular chemistry, during the 90s of the last century there has been a gradual development of a new field: *supramolecular topology.* This field of research, will be introduced in the first chapter, and afterward will be used to frame the subject of the experimental work of this thesis, that is, the development of new supramolecular architectures based on calixarene[2] macrocycles. Such compounds are able to accommodate guest molecules in their cavities and therefore are well suitable to give systems of higher complexity.

---

[1] Lehn, J.-M. "*Supramolecular Chemistry - Concepts and Perspective: Molecules*" VHC, Weinheim, **1995**.

[2] C. D. Gutsche, *Calixarenes. An Introduction*, RCS, Cambridge (UK), 2008.

1. Supramolecular Topology Outline

1.1 Supramolecular Topology. An informal discussion

The *rubber geometry* metaphor, which we frequently encounter leafing through the classics on the subject, is particularly useful to introduce topology,[3] the mathematic's branch that classifies its objects by their connectivity. Through the use of transformations such as contraction or expansion of distances and angles in order to establish equivalence relationships, it marks a clear boundary with the Euclidean geometry. The rigidity of the objects is essential for the latter, whilst for the former two objects are equivalent as long as they can convert one into the other by steps that do not involve tearing or gluing, which is a *homeomorphism:* [4] a sewing needle and a pipe, a donut and a cup of coffee, Euclidean objects completely different, are topologically equivalent.

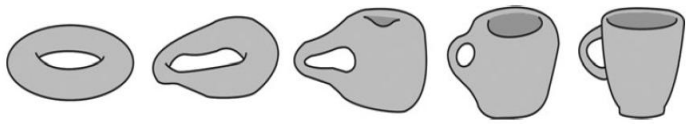

Figure. 1 – Classical topological transformation: a donut that becomes a cup. The two objects are equivalent, since both are geometrical toruses.

Euclidean geometry and topology are two complementary approaches to molecular structure which show alternative aspects of the chemical aggregates. However, in Euclidean geometry the key idea is that of *geometrically equivalent or congruent figures.* Two figures are called congruent if an intellectual transformation allows one figure to be "placed on the other" so that the two figures exactly coincide in all the geometrical

[3] P. Mezey, *Shape in Chemistry*, VCH Publishers, New York (New York), 1993, pag. 50
[4] *Ibid*., 51.

properties. In Euclidean geometry, squares A and B (Figure 2), which have the same side lengths and areas, would be said to be equivalent (or *congruent* in mathematical terminology). Square C, which differs in size, is not equivalent but is said to be *similar.* Clearly, triangle D and circle E are entirely different objects.

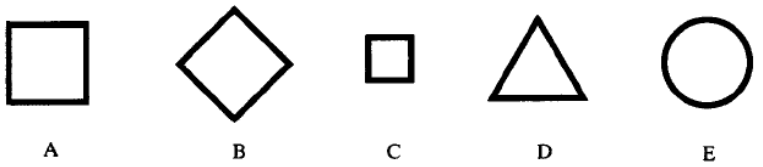

Figure 2. Some simple objects for the consideration of Euclidean geometry.

In topological geometry however, we consider different properties such as connectivity: lengths, angles and size are no longer considered. Topologically, two objects are identical if one can be deformed into the other in a continuous fashion as long as nothing is broken or no holes are punched through during the process.

If we now look again at the object in **Figure 3**, we can see that in terms of topology they are all equivalent, since given complete freedom to distort lengths and angles, any one object can be transformed into any other. Indeed, they are all simply different representations of the same topological object, a closed curve. When considering the transformation of any object into another in topological geometry, one may consider the object to be totally flexible with no restriction on length and angle changes. However, connectivity is a property that must remain unchanged and for this question the circle, square and triangle are termed *homeomorphic*.[5]

[5] Walba D.M., T*etrahedron,* **1985**, *41,* 3161**.**

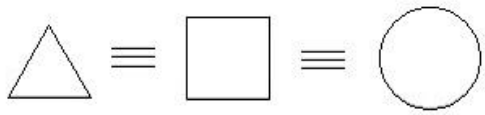

Figure 3. Topologically *equivalent* constructions .

If we consider the circle and the knot in Figure 4: both are closed curves, but they are topologically distinct. So we can see that while normal chemical isomerism such as stereoisomerism arises from the consideration of Euclidean properties (bond types, angles), to classify topological isomers, we must consider topological geometry.[6]

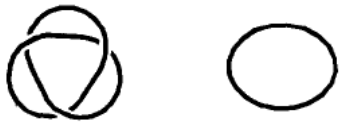

Figure 4. Two topologically distinct closed curve structures

It is clear that, topologically, a molecule is simply a collection of vertices (atoms) connected to each other by edges (bonds), with no regard to angles or lengths, considering only the connectivity.

The above dIscussion of the topology of one dimensional constructions such as closed curves and lines is directly transferable to molecular structures once the ***molecular graph*** is defined. A graph is a simply collection of vertices bound together by lines,[7] in correspondence with its atoms and bonds. We define the molecular graph as simply the graph where nuclei define the points and bonds define the edges (Figure. 5).

[6] Breault, G.A.; Hunter, C. A.; Mayers P.C., *Tetrahedron*, **1999**, *55*, 5265.
[7] N. J. Turro, *Angew. Chem. Int. Ed. Engl.*, 1987, 25, 887.

Thus, the molecular graph is exactly the common structural formula embedded in a 3D-space.

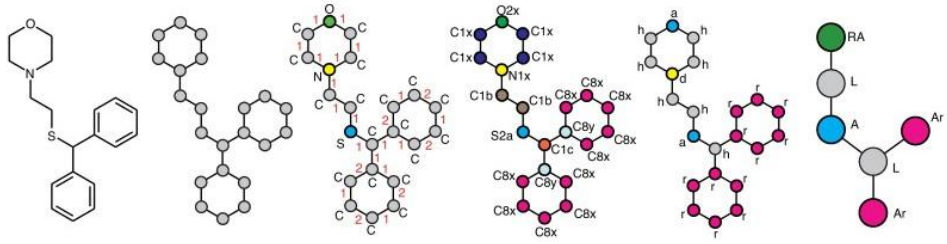

Figure. 5. Structure and graph of a fungicide. From the most structural to the most essential.

Embedding in 3D-space imparts ***extrinsic topological properties*** to a construction. Two constructions which are topologically equivalent in a 3D-space are termed ***isotopic.*** All isotopic constructions are homeomorphic. Not all homeomorphic constructions, however, are isotopic. The distinct character of the mirror image of trefoil knots, or of the linked and separated rings, are extrinsic ***topological properties.*** *These* constructions are homeomorphic, but not isotopic. Any topological chirality must necessarily be a property of embedding of an object in some space and is an extrinsic property - all mirror image objects are homeomorphic. Topological stereochemistry involves a collection of extrinsic topological properties deriving from the embedding of molecular graphs in a 3D-space.

The graphological footprint of a supramolecular architectures, whatever discernes it from a molecular entity in the topology of its graph, is the ***non-planarity***.[8] In fact, if the three-dimensional structure is projected on a plane, a graph whose lines intersect in an irreversible way is obtained (**Figure 6)**. It is impossible to remove the overlapping by a topological transformation.

[8] O. E. Polansky, "Elements of Graph Theory for Chemists", in D. Bonchev (ed.), *Chemical Graph Theory: Introduction and Fundamentals*, Taylor and Francis, London (UK), **1991**, 58.

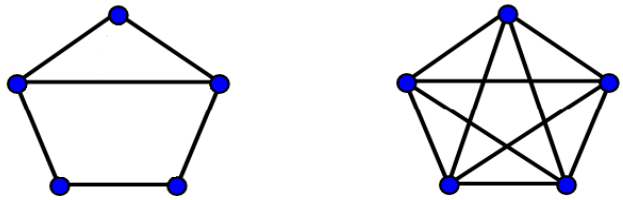

Figure 6. On the left a planar graph, where you can move the internal bond above the structure and avoid overlapping; on the right a non-planar graph.

Going to the insertion of a graph in three-dimensional space, the topoisomerism is evidently a stereochemical property and it is therefore subjected to the same wording as the stereoisomerism (i.e. there will be topological enantiomers and topological diastereoisomers). It becomes clear that, to a higher complexity of the construct corresponds to a higher number of topological stereoisomers that it is possible to find. Although, to date, the math has not yet produced a consolidated and comprehensive survey of the stereotopological tools, in chemistry it has been suggested a conjecture[9,10] which involves the occurence of topological enantiomers when at least one of the following elements in the graph is present:[11] an oriented ring, a chiral ring, a chiral knot, a chiral non-planar graph. The condition given for the topological diastereoisomerism is, instead, more elastic, since it requires that the graphs are just not planar (they do not need be topologically chiral).

The topological isomerism of molecules becomes more interesting when chirality is considered. For molecules to be topologically chiral, they must remain non-superimposable with their mirror image under all distortions. In fact, the necessary and sufficient condition for topological chirality is that

[9] *Ibid.*, 3167.
[10] P. Mezey, *Shape in Chemistry*, VCH Publishers, New York (New York), **1993**, 73.
[11] E. Flapan, *"Topological Chirality and Symmetries of Non-rigid Molecules*", in D. Buck, E. Flapan (eds.), *Applications of Knot Theory*, American Mathematical Society, Providence (Rhode Island), **2009**, 21.

any presentation of the construction must be topologically distinct from its mirror image. This implies that no presentation may be converted into its mirror by continuous deformation in the 3D-space. This property implies that the graph of the molecule is non-planar. Molecular systems with an intrinsically non-planar graph are scarce. If any rigidly achiral presentation ***is*** found for a construction, topological chirality is ruled out. Of course, such a presentation must possess an improper axis of symmetry.[12] This constraint readily allows topological chirality to be ruled out for most molecular graphs. Specifically, any ***planar*** presentation of a molecular graph is rigidly achiral in the 3D-space. It possesses at least one σ plane (the plane in which it is embedded), and is therefore a rigidly achiral presentation. Most topologically non-planar one-dimensional objects contain either a link, knot, or non-planar graph. The non-planar graphs are intrinsically non-planar, the links and knots are non-planar when embedded in a 3D-space. For example the trefoil knot is chiral, whereas a figure-of-eight knot is achiral (**Figure 7**).

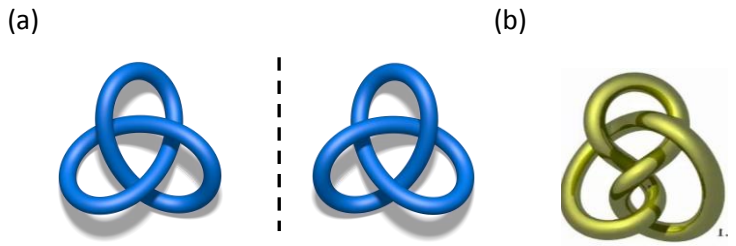

Figure 7. (a) A right and left handed trefoil knot; (b) an achiral figure-of-eight knot.

[12] O. E. Polansky, "Elements of Graph Theory for Chemists", in D. Bonchev (ed.), *Chemical Graph Theory: Introduction and Fundamentals*, Taylor and Francis, London (United Kingdom), *Nature*, **1991**, 58.

1.2. *DNA topological isomerism*

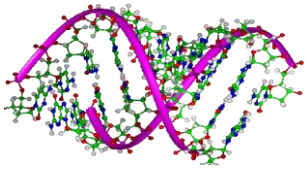

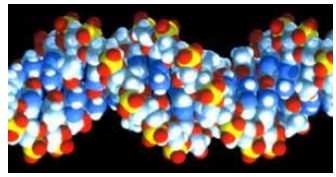

Nature gives us the most emblematic example of structural complexity through the topological isomerism of DNA. After the discovery in 1953 of the double helix by Watson and Crick,[13] the scientific community was puzzled to explain how it was possible that the strand of human DNA, even one meter long, wrapped on itself, could be in the cell's nucleus, which has a size of about five millionths of a meter. In addition, remained to explain what was the mechanism by which the structure was carried out to expose the nucleotide bases during replication and transcription. It took some time before realizing that the answer lays in topology, in particular in the theory of knots. It became soon clear that it was necessary to think DNA as a twisted band in space, a kind of node (open), whose geometry can be modified by enzymes which were responsible for relax (remove) the tensions created in the double helix DNA afterwards the transcription or other cellular processes and therefore involve a change in DNA topology (Figure 8). Knot theory will be important here, because while the effects of enzymes on DNA can not be seen directly, it is possible to realize the changes induced in its geometry.

[13] *J. D. W*atson, F. H. Crick, *Nature*, **1953**, *171*, 964.

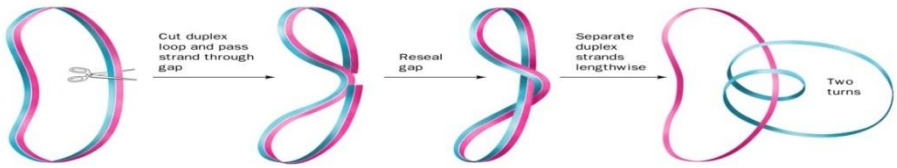

Figure 8. Topoisomerase General mechanism

In practice, these enzymes, called topoisomerases[14], resolve the helix supercoiling, producing DNA breakage at the phosphodiester bond level (Figure 8) and allowing the opening of the replication fork without excessive torsional stress.

These results encouraged the scientific research and shortly thereafter followed a successful series of articles in which even more intriguing topologies were characterized, such as knots and catenanes, of both artificial[15,16] and natural DNA (Figure 9).[17,18,19] Thus, from simple [2]catenanes up to networks of thousands of interlocked circular DNA were found in mitochondrial of trypanosomes.

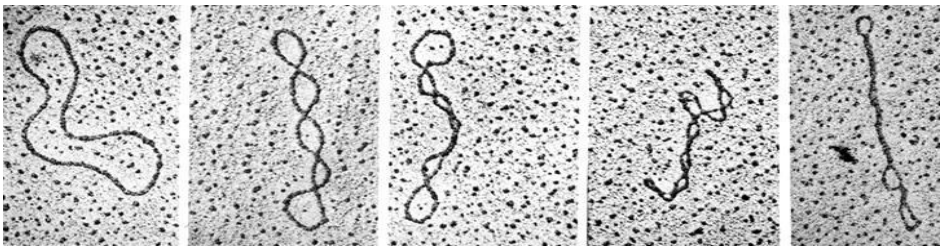

[14] A. D. Bates, A. Maxwell, *DNA Topology*, 2nd ed., Oxford University Press, Oxford (United Kingdom), 2005,. 26.
(b) Wang, J. C. , *Untangling the Double Helix: DNA Entanglement and the Action of the DNA Topoisomerases;* CSHL Press: Cold Spring Harbor, **2009**
[15] L. F. Liu, R. E. Depew, J. C. Wang, *J. Mol. Biol.*, **1976**, *106*, 439.
[16] N. C. Seeman, "Synthetic DNA Topology", in J. P. Sauvage, C. Diederich – Buchecker (eds.), *Molecular Catenanes, Rotaxanes, and Knots*, Wiley – VCH, Weinheim (Germany), **1999**, 323.
[17] B. Hudson, J. Vinograd, *Nature*, **1967**, *216*, 647 – 652.
[18] D. A. Clayton, J. Vinograd, *Nature*, **1967**, *216*, 652 – 657.
[19] P. T. Englund, S. L. Hajduk, J. C. Maraini, *Annu. Rev. Biochem.*, **1982**, *51*, 695 – 726.

Figure 9. Micrograph of DNA topological isomers by the action of DNA topoisomerase.

1.3. **Supramolecular topologies: from paper to laboratory**

Now we will discuss the most important complex architectures that have been obtained from experimental chemistry to date. Leafing through the classics of supramolecular chemistry one easily comes across in topologically complex structures and this shows the fervent interest in this attractive field of research. In particular, we intend to focus our attention to rotaxanes, catenanes, and knots.

1.3.1 Catenanes and rotaxanes[20]

Rotaxanes and catenanes are interpenetrated structures topologically more relevant in the literature. Both derive from the same precursor known as pseudorotaxane (**Figure 10**).

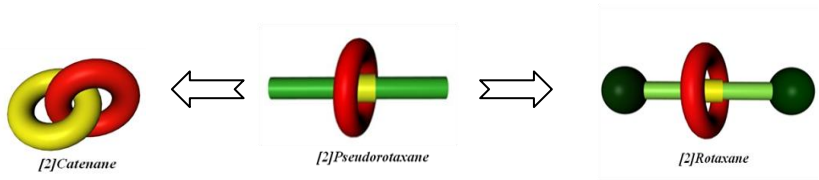

Figure 10. A pseudorotaxane: common precursor to catenane and rotaxane

Specifically, a pseudorotaxane is a supramolecular system consisting of a linear molecule, the "axle", stuck in a cyclic molecule, the "wheel", in

[20] *Molecular Catenanes, Rotaxanes and Knots: A Journey Through the World of Molecular Topology* (eds Sauvage, J.-P. & Dietrich-Buchecker, C.) Wiley-VCH, Weinheim, **1999**.

which the two units are held together only by secondary chemical forces, such as hydrogen bonds, electrostatic interactions, or π-π stacking interactions. The peculiarity of pseudorotaxane systems is that they can "disassemble" by means of the "pulling out" of the two parts.

A rotaxane can be seen as a pseudorotaxane in which the ends of the linear component are covalently linked to groups bulky enough to not allow the "parade" of the axle (stoppering) (Figure 11).

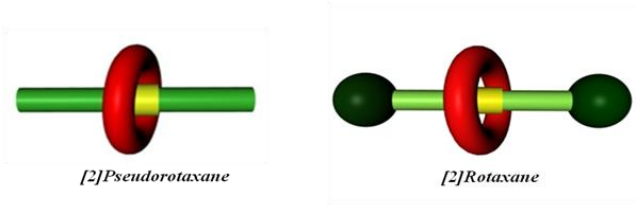

Figure 11. Pseudorotaxane & rotaxane

Starting from the pseudorotaxane we can get a different kind of interlocked structure if a suitably functionalized axis is subjected to a *macrocyclization* reaction rather than a *stoppering* reaction, as previously discussed. The interlocked structure thus obtained is called "**catenane**" (**Figure 12**) and it consists of two cyclic interpenetrated molecules that cannot be separated unless that a covalent bond is broken (Figure 12). [2]

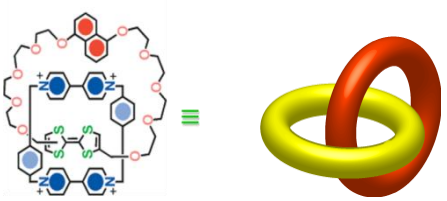

Figure 12. A catenane structure and its cartoon representation.

The nomenclature for interpenetrated systems provides to indicate, in square brackets, the number of constituents that make up the system,

followed by the name of the given system (pseudorotaxane, rotaxane and catenane) (Figure 13).

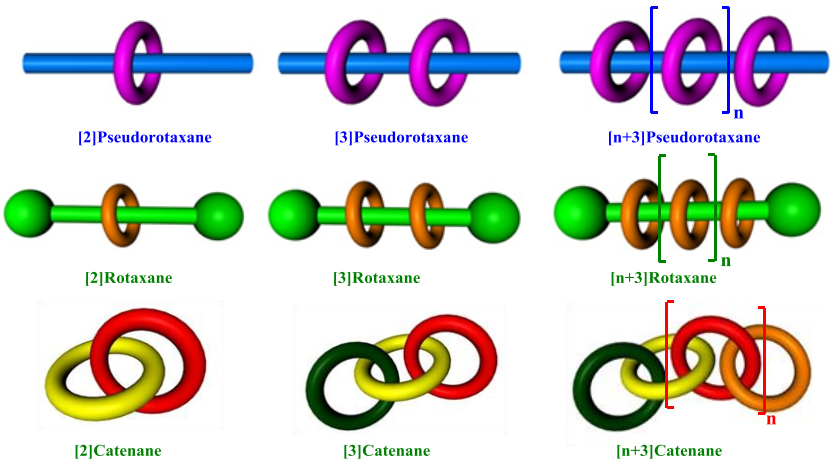

Figure 13. Nomenclature pseudorotaxanes rotaxanes and catenanes

The first examples date back as far as 1960, when Wasserman,[21] with the so-called “statistical approach”, began to cyclize an thirty-eight carbon atom ester by *acyloin condensation*, then reducing it with deuterium chloride by Clemmensen reaction. The *acyloin condensation* of the same substrate in presence of a macrocycle led to a mixture of topoisomers, including the [2]catenane. Wasserman proved the goodness of the synthesis by purifying the small amount of interlocked compound from the starting materials by column chromatography and by checking carbon-deuterium stretching with infrared spectroscopy (**Figure 14**).

[21] E. Wasserman, *J. Am. Chem. Soc*., **1960**, *82*, 4433.

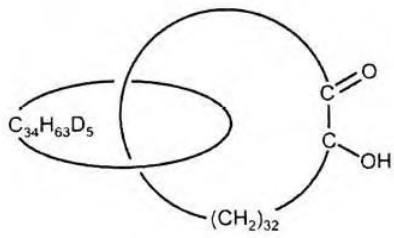

Figure 14. Wasserman [2]catenane

Notwithstanding the very low yields (ca.1%), the most interesting aspect of this work concerned the introduction of the concept of ***mechanical bond*** in chemistry and the definition of the field of ***chemical topology***. However, the insertion of a linear bifunctional molecule through a macrocycle is a strategy that is still used today, the so-called ***threading***.

The success of Wasserman prompted further scientific researches to develop new synthetic routes with improved yields. Thus, Schill and Lüttingraus published in 1964 the first ***template synthesis*** strategy of a [2]catenane.[22] The rather long synthesis (Figure 15) took advantage of the acetal formed by a substituted cyclic catechol with bis-(12-chlorododecyl) ketone. The introduction of an amino group to give a nucleophilic intramolecular substitution, followed by acetal removal and oxidation phenol, brought the desired architecture. In this methodology the role of the acetal intermediate is crucial, because the intramolecular cyclization on nitrogen is forced by the tetrahedral geometry of the protected carbonyl carbon. This synthetic approach was subsequently used for the construction of the first [3]catenane.[23]

[22] G. Schill, A. Luttingraus, *Angew. Chem. Int. Ed. Engl*., **1964**, *3*, 546 – 547.
[23] G. Schill, K. Rissler, H. Fritz, W. Vetter, *Angew. Chem. Int. Ed. Engl*., **1981**, *20*, 187.

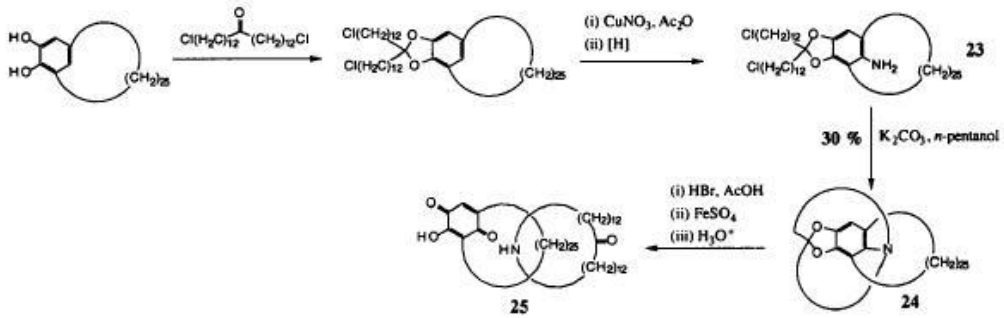

Figura 15. Schill and Lüttingraus [2]catenane by template synthesis

In the early 80's, Sauvage[24] developed a very effective ***template synthesis*** strategy, taking advantage of the use of metal coordination centers. With this methodology he assembled a polyether bridged [2]catenane.[25,26,27] A phenanthroline formed a complex with copper (I) threading a pre-formed macrocycle (Figure 16). A bis-iodide terminal polyether was used to bridge the free phenolic functions under *high dilution* conditions. Finally, the metal was removed with cyanide.

a)

[24] J.-P. Sauvage, C. O. Diederich-Buchecker, *Chem. Rev.* **1987**, *87*, 795.
[25] J.-P. Sauvage, C. O. Diederich-Buchecker, *Tetrahedron Lett.*, **1983**, *24*, 5091.
[26] C. O. Diederich-Buchecker, J.-P. Sauvage, J. P. Kintzinger, *Tetrahedron Lett.*, **1983**, *24*, 5095.
[27] C. O. Diederich-Buchecker, J.-P. Sauvage, J.-M. Kern, *J. Am. Chem. Soc*., **1984**, *106*, 3043.

b)

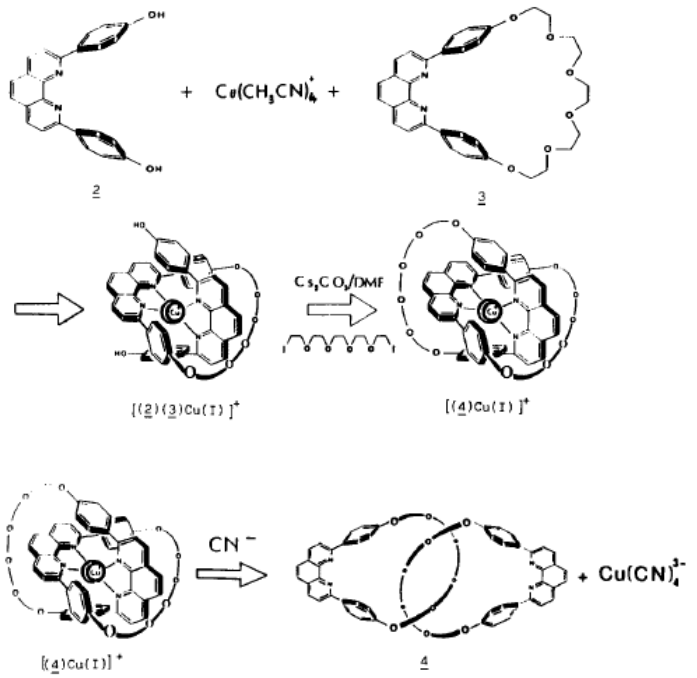

Figure 16. Schematic representation of the synthesis of a catenane by the metal template effect.

The template effect can also come into play by exploiting electrostatic interactions. This strategy was widely investigated by the group of F. Stoddart,[28,29] and is specific for aromatic compounds, as it develops on their packing interactions. In fact, π-donor/π-acceptor interactions between electron-poor paraquat (*N*,*N*-dimethyl-*4*,*4*'-bipyridinium) and electron-rich hydroquinone or napthoquinone moieties were utilized in order to preorganize a pseudorotaxane that can then be functionalized with appropriate groups to give a rotaxane or a catenane.

[28] Raymo, F.M.; Stoddart. J. F. *Organic Template-Directed Syntheses of Catenanes, Rotaxanes, and Knots* in *Molecurlar Catenanes, Rotaxanes, and Knots.* Sauvage. J.-P., Dietrich-Buchecker. C. Eds.Wiley-VCH, **1999**, 143.
[29] J. F. Stoddart, *Chem. Brit*., **1991**, *27*, 714.

Quite different is the Hunter method,[30] that uses H-bonding and π-π interaction. With this method a **34%** yield of catenane was obtained from a one-pot double macrocyclization reaction (**Figure 17**).

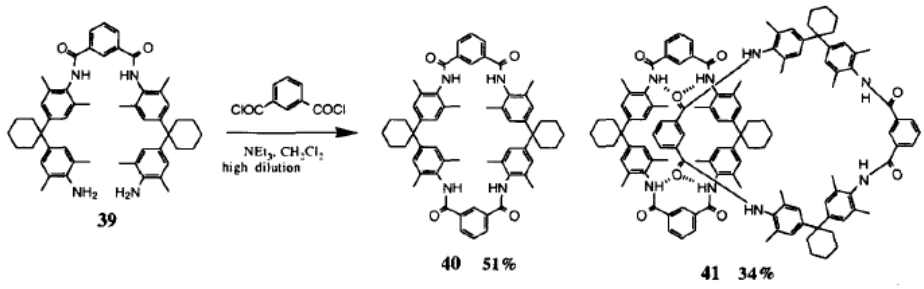

Figure 17. A supramolecular self-assembly process that results in a 34% yield of [2]-catenane in a one-pot double-macrocyclization reaction

After this short background, required to introduce the reader into the world of interlocked structures, it is important to illustrate the procedures allowing their synthesis. Hereinafter, it is shown how scientists have developed, over the years, synthetic strategies able to realize complex interlocked structures with increased efficiency. From the simplest structure, the rotaxane, we will move on to catenanes until we will come to a growing of complexity in knot structures.

As in asymmetric synthesis, where absolute stereochemistry is controlled, control of topological stereochemistry has required the development of new synthetic strategies. The key step in any synthesis is the generation of an intermediate that contains latent topological properties: the latent topology is realised by macrocyclisation of this intermediate. In fact, as mentioned above, the synthesis of the more complex catenane must proceed via the simpler pseudo-rotaxane.

[30] C. A. Hunter, *J. Am. Chem. Soc*., **1992**, *114*, 5303.

These intermediates are often not isolated and may only be present in the reaction mixture in very small amounts, but it is their properties that define the limits on the yields of catenane.

Chemists working in this field soon realised that it was possible to trap the latent topological properties of the pseudo-rotaxane by capping the ends of the linear molecule with two bulky stopper groups to prevent the unthreading (Figure 18).[31]

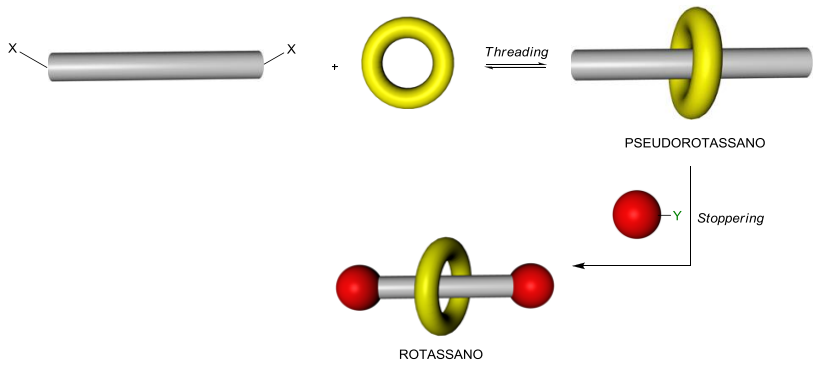

Figura 18. Rotaxane obtained by *threading* e *stoppering*.

One special feature in common to all pseudorotaxane structures is related to their ability to "disassemble" due to the unthreading of the axle with respect to the wheel portion. Therefore, the structure can be defined as "interpenetrated" but not "interlocked", whereas an "interlocked" structure requires the presence of mechanical restriction between the constitutive components as in the case of rotaxanes. Thus, strictly speaking, rotaxanes are not topological isomers of their separate components, because they accept continuous deformations of the graphs until they are split. However, in experimental practice this

[31] J. W. Steed, D. R. Turner, K. J. Wallace, *Core Concepts in Supramolecular Chemistry and Nanochemistry*, John Wiley and Sons, Chichester (United Kingdom), **2007**, 136.

fracture does not occur if it is not accompanied by the breaking of a covalent bond, making these structures quite peculiar.

In addition to *threading,* a rotaxane can also be assembled by ***clipping***, i.e. by closing the wheel around the axle. This method, shown in Figure 19, provides an initial complexation of a preformed dumbbell with a half wheel and subsequent [1 +1] cyclization reaction with an appropriate species.

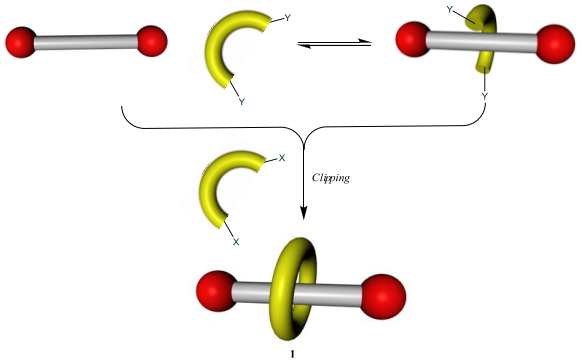

Figure 19. Cartoon representation of the clipping strategy for the synthesis of a rotaxane.

In order to achieve high yields, is an essential prerequisite that balance is strongly shifted in the direction of complex formation. In this way, it is possible to minimize the formation of unthreaded cyclic species.

A further synthetic method is known as ***slipping strategy***, when, by temperature increasing, the macrocycle possesses enough energy to overtake one of the stoppers, slipping it reversibly. This approach takes advantage from rotaxane kinetic stability. In fact, cooling the dynamic complex, it becomes kinetically trapped as rotaxane.

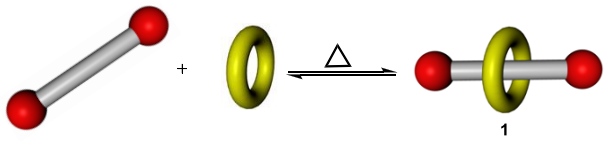

Figure 20. Cartoon representation of a *slipping* strategy for the synthesis of a rotaxane

Catenanes also follow the same synthetic strategies used for rotaxanes as summarized in Figure 21.

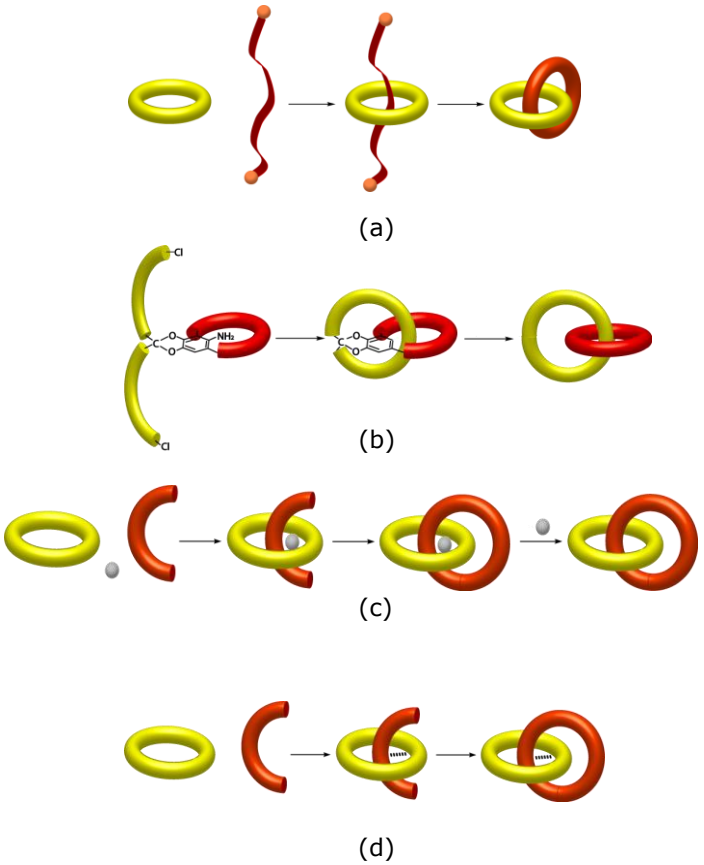

Figure 21. Cartoon representation of (a) a statistical, (b) a directed, (c) a metal templated synthesis and (d) electrostatic interaction or H-bonding templated synthesis for a catenane.

1.3.2 Molecular knots

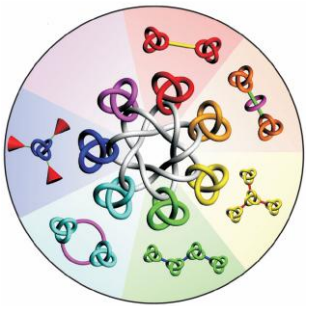

Knots and links are all around us (Figure 22). Be they functional or decorative, we encounter them constantly, when, for example, tying simple bow knots in our shoelaces or the four-in-hand knot in a necktie. These entangled and interlocked entities have also developed strong spiritual and symbolic meanings as human culture has advanced from prehistory, and now embody many tenets of both religious and secular societies. However, from a scientific point of view, the attention given to these systems is mainly due to their presence in natural systems such as DNA and proteins. In fact, aside from the DNA knottiness, of which has been exhaustively discussed in the previous pages, examples of natural macromolecules that contain knots, such as the protein lactoferrin and the enzyme ascorbic acid oxidase[32] are known (Figure 22).

(a) (b)

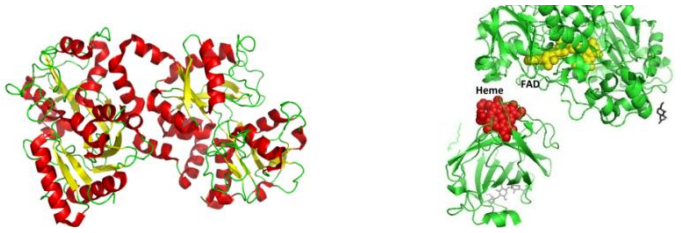

[32] C. Liang, K. Mislow, *J. Am. Chem. Soc,.* **1995**,117, 4201
C. Liang, K. Mislow, J. Am.Chem. Soc. **1994**, 116, 11189

Figura 22. (a) Lactoferrin structure, (b) acid ascorbic structure

Following the mathematical rigorism, a knot is defined as a closed curve in the three- dimensional space that does never not intersect.[33] Its representation on a plane is a "*projection"*. If knot projection intersects no more than two points, it is isomorphous to a loop, which is equivalent to a *trivial knot*: a twisted knot admits at least three intersections. A knot is "oriented" when it is possible to choose a traveling direction along it. It is clearly lawful to block together more than one knot to form a chain. From the just given definitions, it is clear the high lushness of this approach with a literally imaginable unlimited number of knot and chains, so that mathematicians have classified them in various tabs.[34] For our purposes the most suitable is the one using the Alexander-Briggs notation (Figure 23).[35] This notation takes advantage of a descriptor x^{y}_{z} that represents a knot or link, where *x* is the minimum number of nodes, or crossing points of any projection of the knot or link, *y* is the number of components (in a knot, y = 1 and is usually not displayed in the Alexander-Briggs notation), and z is the order of the knot among its peers with the same number of nodes and components, which describes, when embedding the knot or link on a sphere, the number of handles that must be added such that no crossings are observed.

[33] C. Adams, *The Knot Book. An Elementary Introduction to the Mathematical Theory of Knots*, W. H. Freeman and Company, New York (New York), 1994, pag. 2.
[34] *Ibid*., 31.
[35] R. S. Forgan, J.-P. Sauvage, J. F. Stoddart, *Chem. Rev.*, **2011**, *111*, 5434.

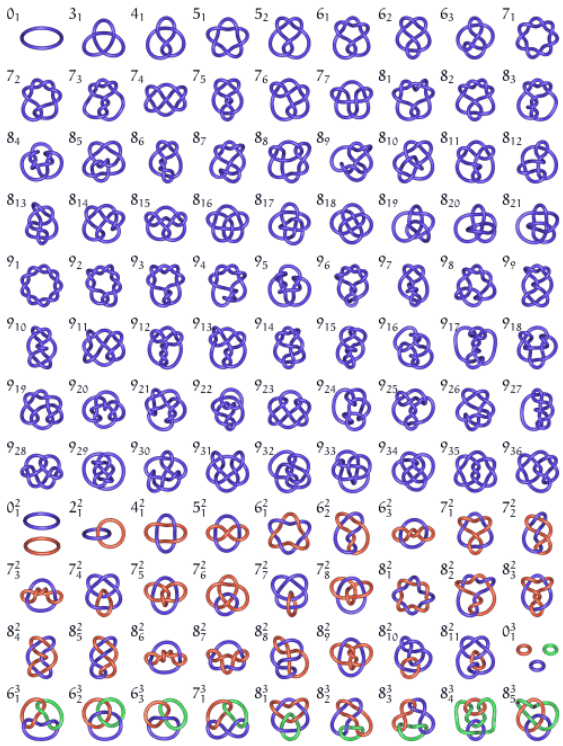

Figura 23. A schematic tabulation of simple knots and links, accompanied by their trivial names and descriptors using the Alexander-Briggs notation.

However, the above described simplicity of method has not deterred chemists to employ commonly used names. Thus, for example, it is usual to refer to knot 3_1 with the term *trefoil knot,* for his clear similary with the plant. The 2_1^2 knot is called *Hopf ring* (corresponding to catenane), whereas 4_1^2 one is called *Solomon ring*. The advantage to use similar practical terminology finds its counterpart in an apparent loss of information about architecture topology.

The search for an appropriate nomenclature that allows to draw the supramolecular assembly graph from its name is a problem still open at the present. At the dawn of the millennium, Vögtle[36] e co-workers have devised a very rigorous systematic, but unfortunately equally abstruse and poorly

[36] O. Safarowski, B. Windisch, A. Mohry, F. Vögtle, *J. Prakt. Chem*., **2000**, *342*, 437.

manageable. At the moment, it is common to name catenanes or knots that have Alexander-Briggs zenith greater than or equal to 2 and to precede, between brackets, the number of interlocked units making up the architecture. e.g. [3]catenane (*3* denoting the number of interlocked rings). The limitations of this approach are obvious; for example, *Hopf knot* and *Solomon Knot* are expressed with the same word of [2]catenane.

The search for aesthetically appealing molecules has been a goal of chemistry since its origins. In fact, nowadays chemists know how to create all types of exotic molecules. For example, Sauvage is a chemical has been primarily interested to *trefoil knot* which is the "simplest example of a *non-trivial first* knot' (Figure 24). It is known to mathematicians as 3_1, because it is formed by three crossings: is a *first knot* because, it is not separable into its components and, as such, it is the cornerstone of the mathematical knots theory.

Figure 24. *Trefoil knot rapresentation*

Knots such as *trefoil knot* inspireed the scientific community for several years. *A*part from their aesthetic beauty, an interesting aspect that surrounds these architectures is related to their properties in relation to chirality. In fact, in the particular case of the trefoil, due to the asymmetric nature of the structure, two form of *trefoil knot* are known, a left-handed and a right-handed. Therefore, the object is chiral and, as a consequence of this peculiarity, it exists as two enantiomers (**Figure 25**).

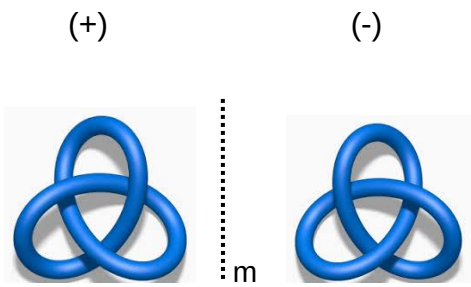

Figure 25. A visualization of the inherent topological chirality of Trefoil Knots, wherein the two nonsuperimposable mirror images which comprise the (+) and (-) isomers are displayed side-byside about a mirror plane, **m.**

Returning to Sauvage, his interest for this molecular architecture was such that immediately, in collaboration with Buchecker, he realized its synthesis (**Figure 26**). In fact, just after the development of the *template* method, he[37] was able to intertwine a phenanthroline double helix, through intramolecular cyclization.

[37] J.-P. Sauvage, C. O. Diederich-Buchecker, *Angew. Chem. Int. Ed. Eng*., **1989**, *28*, 189.

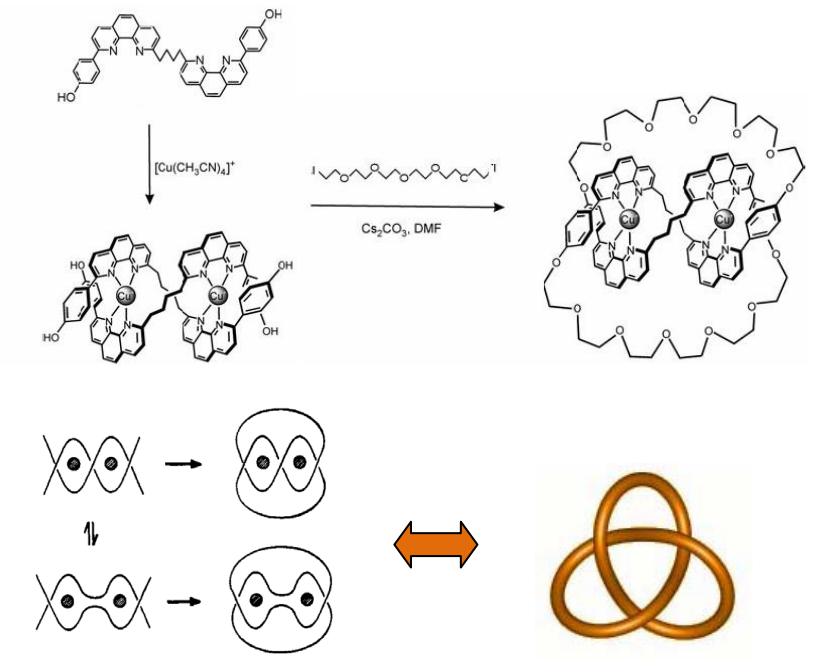

Figure 26. Knot Sauvage Synthesis.

The yields in the first instance were scarce, but they were optimized by changing the bridging groups between the aromatic units and by exploiting a metathesis reaction in order to close the macrocycle (76%) (**Figure 27**).[38]

Figure 27 Sauvage Trefoil Knot Synthesized via the metathesis.

[38] (a) Dietrich-Buchecker, C., Rapenne, G. Sauvage, J. P. *Chem. Commun*. **1997,** 2053.
(b) G. A. Breault, C. A. Hunter, P. C. Mayers, *Tetrahedron*, **1999**, *55*, 5265 .

More recently, Vögtle was successful in joining a macrocyclic trefoil by exploiting an appropriate hydrogen-bonding. This discovery led to a series of differently functionalized chiral knots 3_1.[39] By suitable changes to the modern synthetic protocols, various laboratories have enriched the literature with even more intricate geometrical knots, among which the above mentioned Solomon and Borromean ring (**Figure 28**).[40]

Figure 28. Examples of decorative Solomon Link (on the left) on an Italian mosaic tile; A schematic diagram of Solomon ring; Examples of Borromean Rings depicted in art, religion, and science. Schematic diagram showing metal template approch to Borromean Ring synthesis.

The latter, recalling to mind the heraldic family crest of a prestigious Italian Renaissance family from which it is named. It is composed of three macrocycles not concatenated but interlocked, for which the breaking of just one causes the dissociation of the others two. The building of this architecture is not trivial job. For example, the ring by ring assembly requires that they lie on orthogonal planes: a condition that is obtained through weak coordinating interactions (**Figure 29**).

[39] F. Vogtle, A. Hunten, E. Vogel, S. Buschbeck, O. Safarowsky, J. Recker, A.-H. Parham, M. Knott, W. M. Muller, U. Muller, Y.Okamoto, T. Kubota, W. Lindner, E. Francotte, S. Grimme, *Angew. Chem*. **2001**, 113, 2534; *Angew. Chem. Int. Ed.* **2001**, 40, 2468; O. Lukin,W. M. MQller, U. MQller, A. Kaufmann, C. Schmidt, J. Leszczynski, F. Vogtle, *Chem. Eur. J*., **2003**, 9, 3507.
[40] R. S. Forgan, J.-P. Sauvage, J. F. Stoddart, *Chem. Rev.*, **2011**, *111*, 5448.

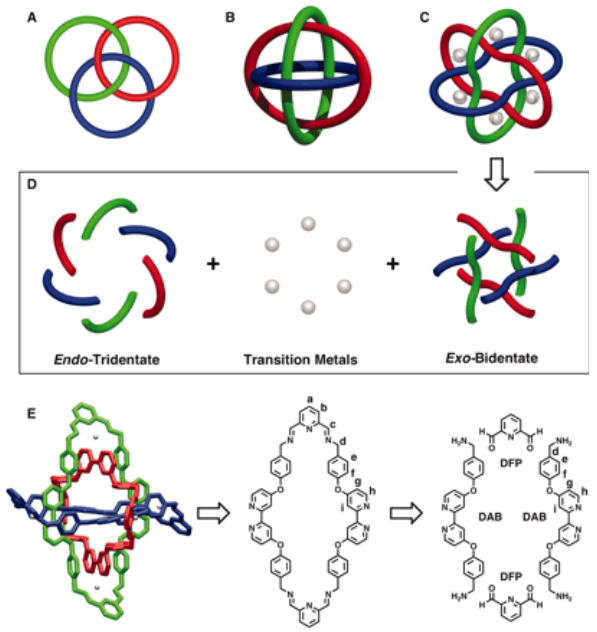

Figura 29. Schematic rapresentation of Borromean rings and molecular equivalents of its constituents.

At the peak of this *crescendo* in topological complexity, we come to discuss the most complex systems made in laboratory up to now: *olimpiadane and suitanes*. The first,[41] represent the most ambitious outcome at the present obtained in the context of catenane architectures, because they consist of five linearly interlocked macrocycles (**Figure 30**). Their synthesis, carried out by Stoddart,[42] provides that the architecture is composed of two crown ethers and three cycle-bis(paraquat-*p*-phenylene) units.

[41] D. B. Amabilino, P. R. Ashton, V. Balzani, S. E. Boyd, A. Credi, J. Y. Lee, S. Menzer, J. F. Stoddart, M. Venturi, D. J. Williams, *J. Am. Chem. Soc*., **1998**, *120*, 4295.
[42] D.B. Amabilino, P. R. Ashton, A. S. Reder, N. Spencer, J. F. Stoddart, *Angew. Chem. Int. Ed. Engl*., **1994**, *33*, 1286.

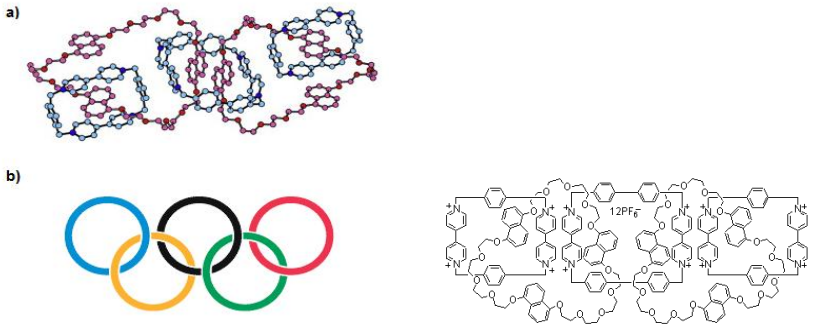

Figure 30. Stoddart olympiadane of. a) X-ray Structure b) on the left the symbol of the Internation Olympic Games from which it takes its name and on the right its structure

Suitanes, instead, consist of two units, one of which has a central body which exhibits a number of arms capable of recognizing cyclic molecules. These latter are connected with spacers to give the second unit, as if it was a suit sewn on the central body: an analogy used by its inventor, Stoddart.[43] The number of protruding limbs is inserted between "suit" and "ane" in square brackets according a supramolecular chemistry custom. Thus, the simplest member of the series would be a suit[2]ane, a linear structure in which the suit surrounds the body with limbs protruding outwards in opposite directions (**Figure 31**), such that there is no easy way by which the suit can be removed from the body. Thus, the suit[2]ane depicted in Figure 32 was synthesized upon recognition of two [24]crown-8 molecules which were linked to a planar molecule bearing two bis-benzilammonium arms.

[43] A. R. Williams, B. H. Northrop, T. Chang, J. F. Stoddart, A. J. P. White, D. J. Williams, *Angew. Chem. Int. Ed.*, **2006**, *45*, 6665.

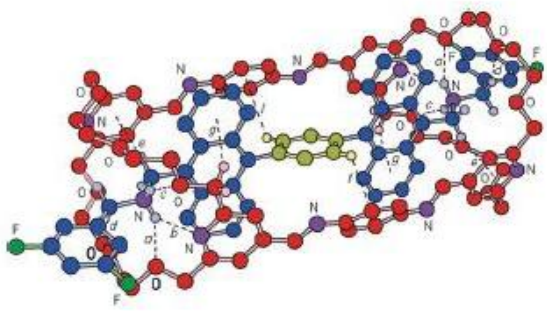

Figura 31. Ball-and-stick representation of the solid-state structure of a suit[2]ane

1.4. Topological and functional complexity [44]

1.4.1 Rotaxanes and catenanes as supramolecular devices

After the journey trough the classifications, now we will show how the topological complexity can imply a functional aspect. This will be done through a number of molecular machines representing the most natural evolution in the synthesis of such interlocked structures.

Artificial molecular machines capable of converting chemical, photochemical and electrochemical energy into mechanical motion represent a high-impact, fast-growing field of interdisciplinary research. These molecular-scale systems utilize a “bottom-up” approach centered on the design and manipulation of molecular assemblies and are potentially capable of delivering efficient actuation at length scales dramatically smaller than traditional microscale actuators. Much of the inspiration to construct such molecular devices and machines comes from the outstanding progress in molecular biology that has begun to reveal the functioning of the natural nanodevices, which are essential for life. Mechanically interlocked molecules, such as rotaxanes, are one of the most suitable candidates for molecular machines because the mechanical bond allows a large variety of

[44] V. Balzani, A. Credi, M. Venturi, *Molecular Devices and Machines. A Journey into the Nanoworld*, Wiley – VCH, Weinheim (Germany), **2003**.

mutual arrangements of the molecular components, while conferring stability to the system. The interlocked architecture limits the amplitude of the intercomponent motion in the three dimensions; the stability of a specific arrangement is determined by the strength of the intercomponent interactions; and such interactions can be modulated by external stimulation.

These systems, initially gained interest due to their peculiar topology and the associated synthetic challenge, but recent efforts have showed that they are also attractive as nanoscale switches for molecular electronics and nanoelectromechanical systems because of their electrical properties and bi- or multistable behavior.

In general, these devices consist of at least two structures, one fixed and one sliding, which are mutually interlocked. The fixed part has a pair of sites of the same or different affinity against the complementary sliding one. In the first case, the sliding unit will oscillate between two identical stations. In the second, however, it will have a preferential status, from which the system may be removed by chemical stimulus, usually hydrogen acids or oxidizing agents, electronic or light, thus through reversible transformations. Let us see some examples.

Molecular shuttles.[45]

One of the first examples found in the literature of artificial molecular machine of a single component, is known as *molecular clamp* (**Figure 32)**.[46]

[45] V. Balzani, A. Credi, F. Raymo, J. F. Stoddart, *Angew. Chem. Int. Ed*., **2000**, *39*, 3372.
[46] P. R. Ashton, R. Ballardini, V. Balzani, I. Baxter, A. Credi, M. C. T. Fyfe, M. T. Gandolfi, M. Gòmez-Lòpez. M.-V. Martìnez-Dìaz, A. Piersanti, N. Spencer, J. F. Stoddart, M. Venturi, A. J. P. White, D. J. Williams, *J. Am. Chem. Soc*. **1998**, *120*, 11932.

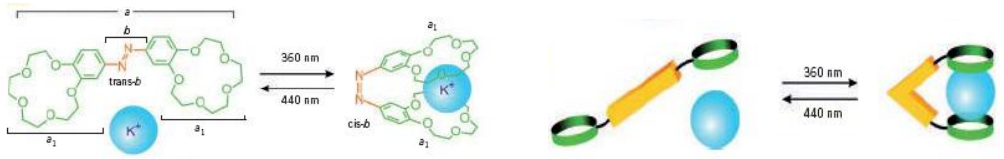

Figura 32. A molecular clamp by light activated, structure (on the left) and cartoon representation(on the right).

The system consists of two cyclic molecules (crown ethers) (a_1), connected by a central unit (*b*) that can give isomerization of the double bond after irradiation with an appropriate wavelength. In the ground state the central double bond has a *trans* stereochemistry; by beaming the system at 360 nm the *cis-isomer* is obtained leading to a closeness of the two units a_1. This structural change of the central unit enables the system to complex a potassium ion (K^+). Using light of 440 nm or leaving the system in the dark, the reverse process occurs, with consequent release of potassium ion (K^+). This mechanical action is comparable to a nanometric clamp which could be a prototype of systems able to "clean up" a body waste.

In a rotaxane, the movement of the ring along the axle corresponds, on a molecular level, to a "shuttle" motion along a track. An example of this type is represented by bistable rotaxane shown in Figure **33**. It is comprised of a ring component that encircles a dumbbell-shaped component. The interaction between the two components is such that the ring can choose between one of the two recognition sites along the rod section of the dumbbell component. If two recognition sites with very different binding affinities can be grafted into the rod section of the dumbbell component, a bistable [2]rotaxane with switchable properties can be obtained (**Figure 33**) without damage to its molecular structure.

In particular, the dumbbell component *f* bears two separate units, f_1 e f_2; the first unit is a ammonium site, the second unit is a di-pyridine cationic one which has donors-acceptors properties. These units represent two potential "stations" for the ring because it can interact with both *f*1, through the formation of hydrogen bonding, and *f*2, through a donor-acceptor interaction.[47] Initially the ring lies on the station f_1 because the first type of interaction is stronger than the second; however, upon deprotonation of ammonium unit f_1 with a base, the interaction becames weaker, which would lead to a switching to station f2.

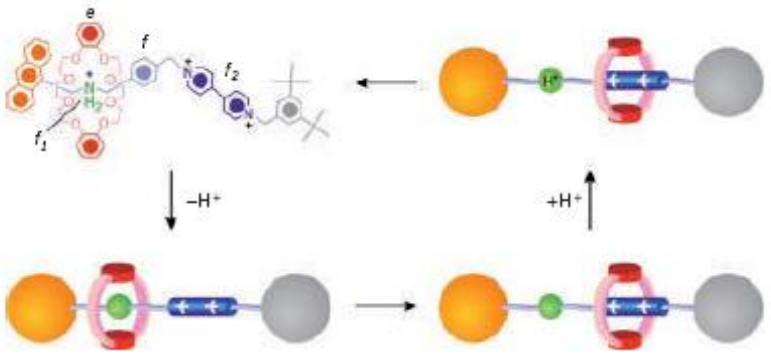

Figura 33. Molecular Shuttle driven by chemical impulses

An acid addition will be able to restore the ammonium unit f_1 which would become free to interact again with ring *e.* The alternate movement of *e* between f1 and f2 can be repeated several times due to the reversibility of the acid/base reaction. However, keep in mind that, the subsequent additions of acid and base lead to the formation of waste products, which cannot be eliminated, but accumulate, until they can impair the functioning of the system.

[47] a) M.V. Martìnez-Dìaz, N. Spencer, J. F. Stoddart, *Angew. Chem.* **1997**, *109*, 1991; *Angew. Chem. Int. Ed. Engl.* **1997**, *36*, 1904;

A higher level of complexity both in design and in construction of molecular machines is largely demonstrated by the system shown in **Figure 34**. It is a rotaxane constituted by a ring component *g*, with electron-donor characteristics, and a linear component consisted of several subcomponents: 1) a ruthenium complex *h* which is able to absorb light and to act as a stopper; 2) two units, j_1 and j_2, with electron-acceptor properties, which are the two "stations" on which it may stop the ring *g*; 3) a rigid spacer *i* and a second stopper *k*.

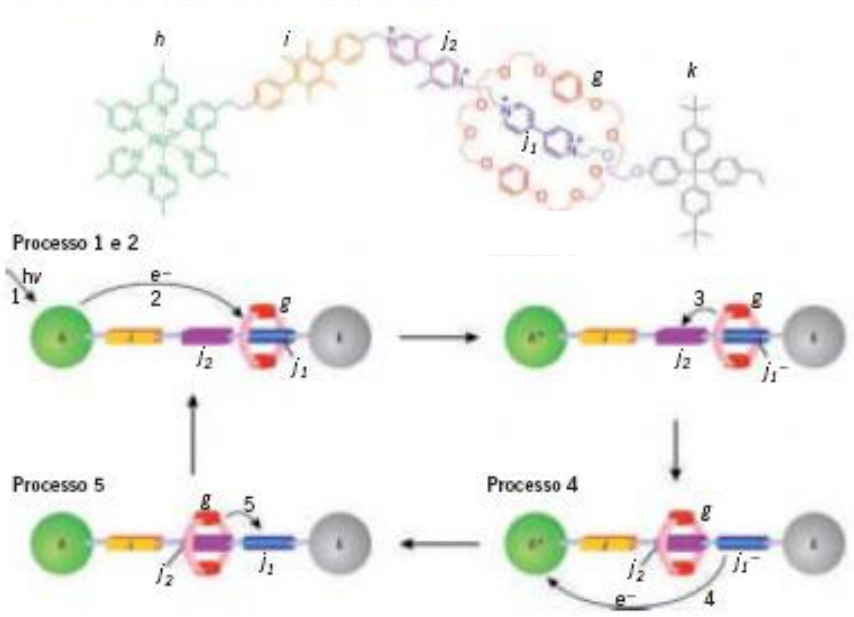

Figure 34. A four-stroke engine based on rotaxane.

The architecture of the system is such that following a light pulse, through a four-stage process, an alternate movement of the ring along the thread from right to left and back again is triggered without waste products production differently to the previous case. In particular, the initial situation of the system is one in which *g* ring surrounds j_1 unit, that is a better electron-acceptor than j_2. Following light excitation of ruthenium complex *h,* occurs in

the system, a series of movements that can be described very schematically in this way:

a) destabilization of initial structure: following the absorption of light (process 1) is obtained an excited state of *h,* which transfers an electron to *j*1 station (process 2) surrounded by *g* ring. Following this electronic transfer j_1 station loses its electron acceptor characteristics of and no longer interacts with *g*;

b) ring shift: failing its interaction with *j*1, *g* ring moves (process 3) and switches to the station *j*2 with which it is able to interact;

c) electronic *reset*: at this point a opposite process brings an electron from destabilized j_1 station, no longer surrounded by *g*, to ruthenium complex that had initially transferred (process 4), in this way, electron acceptor character of j_1 station which is thus resumed;

d) nuclear reset: following electronic reset, *g* ring comes back to j_1 station (process 5), restoring structure.

Going on the same level of structural complexity, a very interesting example of molecular device is the Stoddart shuttle shown in Figure 35 as a prototype of a pH-dependent structure. It is a linear shuttle of nanometric size incorporating, in a macrocycle of bis piridyne units, an axle with a benzidine and alkoxy-phenolic site. Electrons poorness of the macrocycle makes its favorable placement near benzidine site; however, lowering the pH with trifluoroacetic acid, the protonation of amino groups leads migration to bis-phenol station.

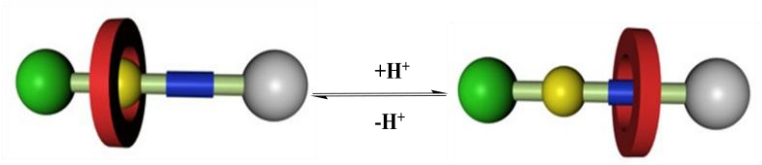

Figura 35. Diagram of a pH dependent molecular shuttle.

This process is also capable of activation by a mono-electron electrochemical oxidation. Sauvage developed and realized a similar device using oxidation by electrolysis of copper from (I) to (II), coordinating a phenanthroline macrocycle along an axle with phenanthroline and tris-pyridine sites. Balzani demonstrated the ability to power photochemically it.

Rotors.[48] Rotary movements are accessible with catenane species. In a catenane, structural changes caused by rotation of one ring with respect to the other can be clearly evidenced when one of the two rings contains two non-equivalent units. A bis-pyridinium cyclophane and a crown ether, integrated with a porphyrin ring, make up a motor that, at suitable pH, in acetonitrile rotates at 1500 Hz. [49] The same mobile unit can be disposed on a crown ether integrated with a tetra-tiafulvalene ring, whose driving force can be also of electrochemical nature (**Figure 36**).

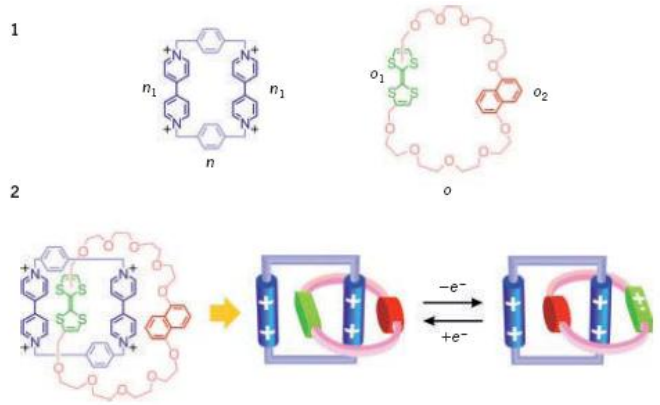

Figura 36. Redox controlled ring rotation in a catenane containing a non-symmetric ring

[48] *Ibid.*, 3376.
[49] V. Balzani, A. Credi, G. Mattersteig, O. A. Matthews, F. M. Raymo, J. F. Stoddart, M. Venturi, A.J. P. White, D. J. Williams, *J. Org. Chem.* **2000**, *65*, 1924.

Artificial myofibrils.[50] Molecular muscles, that convert chemical electrochemical and photochemical energy into mechanical work have attracted the attention of scientists working in the field of nanotechnology and rotaxanes are turning out very versatile in this regard. An example is the dibenzo[24]crown-[8] ether penetrated by an axle with secondary dialkylammonium sites and N,N'-dialkyl-4,4'-bipyridine. The device is controlled by pH value of environment.

Molecular Elevator.[51] From the fusion of three crown ethers with an aromatic bridging unit a tritopic receptor (platform) has been obtained, which is able to recognize a tris-benzyl-ammonium salt (**Figure 37**). Climbs and descents of the platform are regulated by acid. The authors estimated that the force expressed by the device is around 200 pN for a movement of about 0.7 nm.

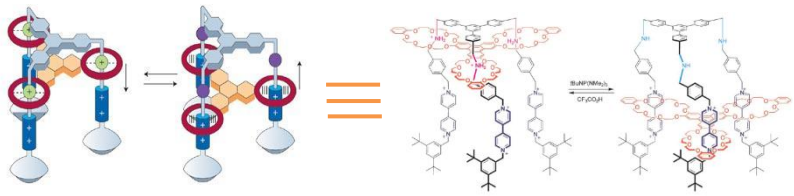

Figura 37. The molecular elevator of Stoddart and Balzani in a graphical representation.

[50] J. Wu, K. Leung, D. Benitez, J.-Y. Han, S. J. Cantrill, L. Fang, J. F. Stoddart, *Angew. Chem. Int. Ed*., **2008**, *47*, 7470.
[51] J. D. Badjic, V. Balzani, A. Credi, S. Silvi, J. Frazer Stoddart, *Science*, **2004**, *303*, 1845.

1.4.2 Rotaxanes and catenanes in nanotechnology.

Over the last years, the scientific and technological world saw a continuous and intensive development of the so-called "nanotechnology", considered by many to be the engine of a new industrial revolution of the twenty-first century.

In current terminology the suffix “nano” is used to indicate materials and structures in which at least one dimension is less than 100 nm, but in reality Nanotechnology is a multidisciplinary field which goes back to theories and techniques developed in various scientific fields ranging from physics, to chemistry, to biology and material sciences, and to mathematics, directed to produce materials, components and devices at the molecular scale and then with dimensions on the order of nanometers.

Figure 38. Structure of the bistable [2]rotaxane used in the crossbar memory and SEMs of the nanowire crossbar memory

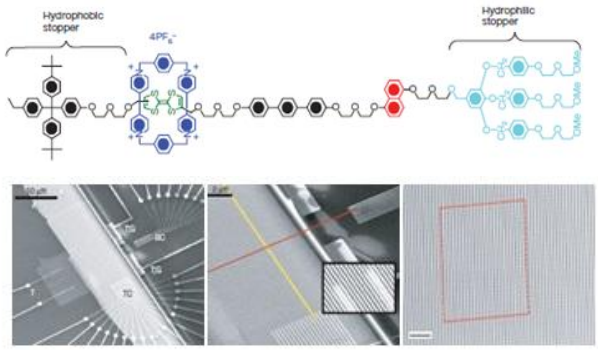

Particularly interesting in this field is the use of rotaxanes as a data storage elements in an electronic molecular 160 Kbit memory[52] built with a density of di 10^{11} bit/cm^2 (**Figura 38**).

Another example of application in molecular electronics involves the use of catenanes to build integrated circuits (**Figura 39**).[53] Here, in fact, a layer of bistable [2]catenane, self-assembled on a particular support, acts as the junction between two electrodes.

Figure 39. Molecular junction constituted by a layer of bistable [2] catenanes.

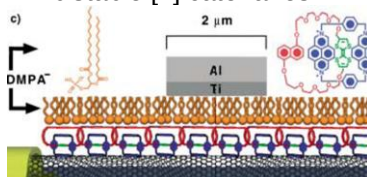

Particularly symbolic is, however, the use of a rotaxane system as controller in a small molecular carrier.[54] In particular, a film of silica was used as a solid support to connect a rotaxane system to nanoporous silica materials that can accommodate small organic molecules. In the interlocked system the cyclic unit can assume, as a function of an appropriate stimulus, different positions with respect to the linear unit. Thus, it plays a crucial role in the release and transport of small molecules (**Figure 40**).

[52] J. E. Green, J. Wook Choi, A. Boukai, Y. Bunimovich, E. Johnston-Halperin, E. DeIonno, Y. Luo, B. A. Sheriff, K. Xu, Y. S. Shin, H.-R. Tseng, J. F. Stoddart, J. R. Heath *Nature* **2007**, *445*, 414.
[53] M. R. Diehl, D. W. Steuerman H. R. Tseng, S. A. Vignon, A. Star, P. C. Celestre, J. F. Stoddart, J. R. Heath, *Chem. Phys. Chem.*, **2003**, *4*, 1335.
[54] M. W. Ambrogio, C. R. Thomas, Y.-L. Zhao, J. I. Zink, J. F. Stoddart *Acc. Chem. Res.* **2011**, *44*, 903.

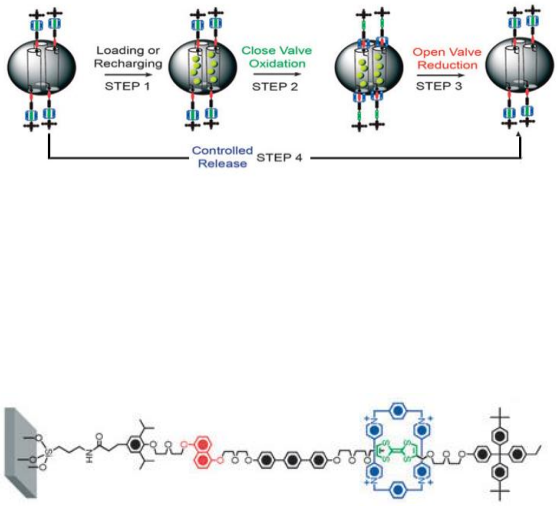

Figura 40. Schematic representation of a molecular carrier and bistable [2]rotaxane structure

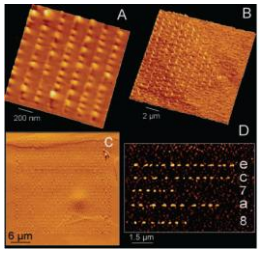

Figure 41. AFM image on the writing on a rotaxane film

A final application is a demonstration of the important connection/transduction of molecular properties to the macroscopic world. In particular, Leigh and coworkers [55] have reported an example of supramolecular writing in which instead of using the usual magnetic support, the writing takes place on a surface covered with a thin film of rotaxanes

[55] M. Cavallini, F. Biscarini, S. Leo´, F. Zerbetto, G. Bottari, D. A. Leigh *Science*, **2003**, *299*, 531.

(**Figure 41**). The authors observed that by applying to the rotaxane film an external perturbation through an atomic force microscope, the interaction between the tip and the thin film causes a "spontaneous" alignment of the molecules at the touched points', thus creating chains of "nano-balls' of 20-40 nanometers in diameter separated by 100 nanometers. The patterns thus obtained are permanently stable. There are three fundamental advantages with respect to the usual magnetic support: 1) the small dimensions of “nano-balls” which allow a higher density of information storage; 2) the absolute precision of patterm reproduction; 3) the unrequired planarity of the support. This latter can open up the way to three-dimensional flexible and complex devices with unlimited possibilities.

CHAPTER II

CHAPTER II

2.1 Complex Topologies based on Calixarenes

Chemical reaction of molecules in specific and selective ways forms the basis of the living world. Taking clue from this, chemists have shifted their focus from molecular chemistry to supramolecular chemistry. In the majority of cases, the supramolecular architecture is constructed through selective host-guest interactions.[56] During the molecular evolution of biological system, the highly selective complexation process between the *host* and the *guest* must have played a central role. This attribute of biological life was mimicked in synthetic chemistry which later came to be known as the *host-guest* chemistry. A molecular complex is composed of at least one host and one guest components. The host is an organic molecule or ion whose binding sites converge. The guest is an organic molecule or ion or metal ion whose binding sites diverge.[57]

The complexes of the host-guest chemistry are held together in unique structural relationship by forces other than those of covalent nature. Before the accidental discovery of crown ethers[58] by Pedersen, the word "supramolecule" was not commonly used; but along with cyclodextrins[59] the crown ethers were also included as another family of hosts. Later came the discovery of **calixarenes**,[60] which became the third generation of

[56] Lehn, JM. *Supramolecular Chemistry.* Weinheim, Germany: Springer; **1995**.
[57] Cram DJ, Cram JM. Design of complexes between synthetic hosts and organic guests. *Accounts of Chemical Research.* **1978**,*11*(1), 8.
[58]Lehn, J.-M. "*Supramolecular Chemistry - Scope and Perspective: Molecules, Supermolecules and Molecular Devices (Nobel Lecture)*" *Angew. Chem. Int. Ed.* **1988**, *27*, 89.
[59] .Shinkai S., *Calixarenes—the third generation of supramolecules*, *Tetrahedron,* **1993**, ***49****(*40), 8933.
[60] Gutsche CD, Dhawan B, No KH, Muthukrishnan R. Calixarenes. 4. The synthesis,characterization, and properties of the calixarenes from *p-tert*-butylphenol. *Journal of the American Chemical Society.* 1981;**103**(13):3782

supramolecules. All coexist under the title of supramolecules as well as host-guest chemistry.

There were and there are a good number of research groups in the field of calixarene chemistry whose work has already generated hundreds of original journal articles, extensive literature reviews and monographs[61] in supramolecular chemistry. Although worked upon by many before his arrival in this field, the credit of naming this class of compounds goes to C. D. Gutsche, who perceived a similarity between the shapes of these cyclic tetramers and a type of Greek vase known as calix crater (**Figure 42**). He suggested the compound to be called **"Calixarene."**

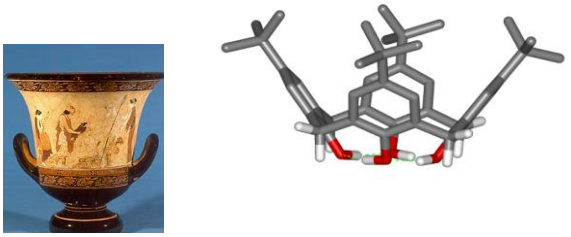

Figure 42. calix crater and *p -terz*-butilcalix[*4*]arene structure

This "crater" or "basket" plays a very important role in shaping the entire architecture of calixarene for its function in host-guest chemistry. With their well organized and preformed cavities, the calixarenes are able to act as

[61] Gutsche, CD. Calixarenes. In: Stoddart J. , editor. *Monographs in Supramolecular Chemistry.* Cambridge, Mass, USA: Royal Society of Chemistry; 1989.

host molecules. Over the years, calixarenes have been frequently employed as platforms that permit the design and synthesis of interesting host compounds. The common convention to refer to calixarene derivatives is to report in square bracket the number *n* of phenolic units involved in the structure: in this way the tetramer will be the calix[4]arene, the pentamer will be the calix[5]arene, etc. (**Figure 43**).

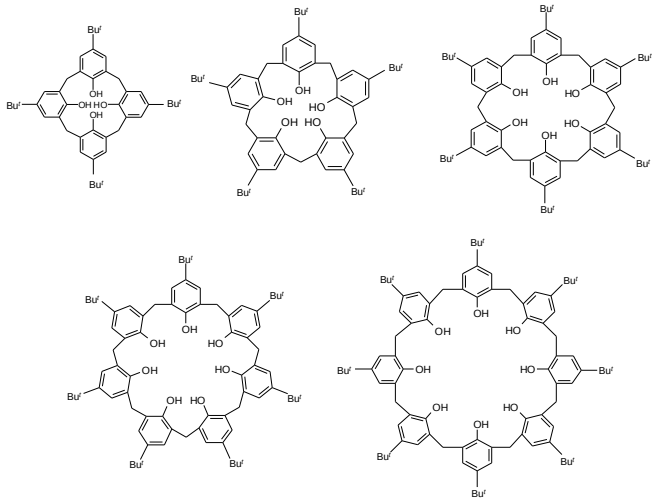

Figure 43. The phenol-derived calixarene family.

Two are the methodologies for synthesizing calix[n]arene macrocycles: the *one-step* synthesis and the *multi-step* approach.[62]

ONE-STEP SYNTHESIS: this field was explored mainly by Gutsche and coworkers. The very early procedures were not reproducible and led to difficulty separable mixtures. In the early 1980s reliable procedures for *p-tert*-butylcalix[4]arene, *p-tert*-butylcalix[6]arene, and *p-tert*-butylcalix[8]arene were introduced. *p-tert*-butylphenol is the eligible starting material for this

[62] Munch, J. H.; Gutsche, C. D. *Org. Synth.* **1990**, *68*, 243.

synthetic approach and the choice of the right catalytic reagent for the condensation between *p-tert*-butylphenol itself and formaldehyde (acidic or basic catalysis) is fundamental:

a) the condensation of the *p-terz*-butylphenol with formahaldehyde using NaOH as the base, followed by dissolution in diphenyl ether, produces *p-tert*-butylcalix[4]arene;[63]
b) the condensation of the *p-tert*-butylphenol with formahaldehyde using KOH as the base, followed by dissolution in xylene, produces *p-tert*-butylcalix[6]arene;[64]
c) the condensation of the *p-tert*-butylphenol with formaldehyde in xylene, using NaOH as the base, produces *p-tert*-butylcalix[8]arene.[62]

The base-induced mechanism of formation of calixarenes has been studied in some details and the most reasonable proposal is that the precursor of any macrocycle is a linear oligomer carrying the appropriate number of aryl moieties.[65]

Furthermore from the acid-catalyzed reaction a number of large calixarenes (n = 9-20) can be isolated. The one-step synthesis is the widest used method to synthesize calixarene compounds.

2. *FRAGMENT CONDENSATION SYNTHESIS*: this approach was studied mainly by Kämmerer and then by Böhmer and co-workers. It is useful when polysubstitued, dissymmetric, asymmetric and bridged structures are desired. The schematic route is to synthesize separately different parts and then to build the calixarene structure using a final reaction.

[63] Gutsche, C. D.; Iqbal, M. *Org. Synth.* **1990**, *59*, 3871.
[64] Gutsche, C. D.; Dhawan, B.; Leonis, M.; Stewart, D. *Org. Synth.* **1990**, *68*, 243.
[65] Gutsche, C. D. in *Encyclopedia of Supramolecular Chemistry*; Atwood, J. L., Steed, J. W., Eds.; Dekker, **2004**, pp 153-160 and references cited therein.

A large number of procedures to obtain calixarene related compounds are also known (oxa-, aza-, thio-, homocalixarenes).[66]

2.2 Supramolecular Properties of Calix[n]arenes

The easy functionalization is the major explanation for the rapid and widely differentiated development of calixarene chemistry.

The *p-tert*-butylphenol unit, in addition to making calixarenes readily available, allows their easy functionalization: the functionalization chemistry of calixarenes follows, in substance, the functionalization chemistry of generic phenols. The –OH at the calixarene lower rim can be converted to a variety of esters and ethers, while the *p-tert*-butyl group at the upper rim can be easily removed and replaced by a wide variety of different groups.

These two ways of functionalization can be carried out separately, and this makes calixarenes more advantageous with respect to other hosts, *e.g.* cyclodextrins.[67]

FUNCTIONALIZATION AT THE LOWER RIM: an *O*-alkylation or an *O*-acylation can be easily realized at the calixarene lower rim. The introduction of these groups can block the macrocycle in specific conformations if the substituents are bulky enough. Conformational properties and easy functionalization make calixarenes an interesting family of macrocycles from the supramolecular point of view.

---

[66] B. Masci, "Homooxa- and homoazacalixarenes", pp. 235–249; b) P. M. Marcos, J. R. Ascenso, J. L. C. Pereira, *Eur. J. Org. Chem.* **2002**, 3034–3041; c) For a report on the binding abilities of dihomooxacalix[4]arene derivatives toward quaternary ammonium ions, see: Masci, B.; Finelli, M.; Varrone, M. *Chem. Eur. J.* **1998,** *4,* 2018 (a) P.D. Beer, P.A. Gale, *Angew. Chem., Int. Ed*., **2001** 40, 486–516; S.E. Matthews, P.D. Beer (Eds.), Calixarenes 2001, Kluwer Academic Publishers, Dordrecht, **2001**, 421; C. Chuit, R.J.P. Corriu, C. Reye, J.C. Young, *Chem. Rev*.,**1993,** *93*, 1371; C. Chuit, R.J.P. Corriu, C. Reye, in: K. Akiba (Ed.), *Chemistry of Hypervalant Compounds*, Wiley-VCH, New York, **1999**, 81;
M. Kira, L.C. Zhang, in: K. Akiba (Ed.), *Chemistry of Hypervalent Compounds*, Wiley-VCH, New York, **1999**, 147.

[67] Gutsche, C. D. *Calixarene 2001*, Asfari, Z.; Böhmer, V.; Harrowfield, J.; Vicens, J., Eds.; Kluwer: Dordrecht, **2001**.

FUNCTIONALIZATION AT THE UPPER RIM: the general way to functionalize the upper (or also called *wide* or *exo*) rim of calixarenes is to use an *electrophilic substitution* approach: the calixarene is able to react as a nucleophile, in virtue of the presence of the activated aromatic rings, with electrophilic agents. For this kind of approach, the *para*-position must be free, and this is easily accomplished by means of a complete or selective de-*tert*-butylation reaction, using $AlCl_3$ as Lewis acid catalyst, in toluene.[68]

Different types of reactions have been carried out using the de-*tert*-butylated product, with the introduction of several functional groups at the upper rim. For example, halogenated derivatives can be obtained through a complete or selective bromination, using NBS in CH_2Cl_2, on a substrate bearing ether moieties at the lower rim.

As receptors, calixarenes are able to conjugate the two fundamental characteristics previously discussed: rigidity and flexibility. A series of books and reviews have been published which discuss in length the use of calixarene derivatives for the recognition of cation, anion, and neutral molecules.[1,3] One of the major factors that have contributed to the proliferation of these research papers is the versatile structure of calixarenes for their use as complexing agents. The almost unlimited possibilities of chemical modification of calixarenes have made them a powerful class of host compounds. Their applications range from selective sensors, for analytical and medical applications, to wastewater decontaminant, to electrodes and membranes. The ability in terms of sensitivity and selectivity of calixarene hosts to discriminate among a group of guests make them a special class in supramolecular chemistry.

The possibility to functionalize calixarenes with alkyl chains of appropriate length or with bridging elements, allows to decrease the conformational mobility of the macrocycles and to increase their *preorganization*, which is

[68] Gutsche, C. D.; Levine, J. A. *J. Am. Chem. Soc.* **1982**, *104*, 2652.

fundamental for a selective molecular recognition process. On the other hand, the rotational freedom allows the conformational changes necessary to accommodate guests in thermodynamically favored events.

The great development of the calixarenes chemistry allows, nowadays, to design receptors for every supramolecular challenge.[69,70,]

Furthermore, the appropriate introduction of functional groups at both rims allows to modulate their solubility in organic or aqueous solvents. For these reasons calixarenes have been used in every field of supramolecular chemistry: supramolecular recognition,[71] self-assembly, crystal-engineering,[72] supramolecular catalysis, etc. They have been used as platforms for the construction of more complex structures or for the realization of supramolecular adducts in solution or solid state.

2.3 Through-the-Annulus Threading of Large Calixarenes Induced by Very Loose Alkylammonium Ion Pairs

As seen above, the most common technique for the construction of interlocked structures is the threading. In contrast with other macrocyclic hosts such as cyclodextrins,[73] crown ethers,[74] and cucurbiturils,[75](**Figure 44a**), which readily give *endo*-complexation with native unsubstituted

[69] Böhmer, V. *Angew. Chem. Int. Ed. Engl.* **1995**, 34, 73.
[70] Ikeda, A.; Shinkai, S. *Chem. Rev.* **1997**, *97*, 1713.
[71] a) Coleman, A. W.; Lazar, A. N.; Da Silva, E. in *Encyclopedia of Supramolecular Chemistry*; Atwood, J. L., Steed, J. W., Eds.; Dekker, **2004**, pp 137-144 and references cited therein. b) Stibor, I.; Lhoták, P. in *Encyclopedia of Supramolecular Chemistry*; Atwood, J. L., Steed, J. W., Eds.; Dekker, **2004**, pp 145-151 and references cited therein.
[72] *Calixarenes in the Nanoworld*, Vicens, J.; Harrowfield, J. Eds.; Springer: Dordrecht, **2007**.
[73] J. Szejtli, *Chem. Rev.* **1998**, *98*, 1743.
[74] G. W. Gokel, *Crown Ethers and Cryptands* The Royal Society of Chemistry, Cambridge, 1991.
[75] J.Lagona, P.Mukhopadhyay,; S.Chakrabarti, L. Isaacs, *Angew. Chem. Int. Ed.* **2005**, *44*, 4844.

derivatives, the threading of larger calix[*n*]arenes (*n* = 6, 7 and 8) (**Figure 9b**) is a rare event. In fact, calixarenes often require an extensive chemical modification to give similar results, and more frequently they act as simple scaffolds to construct podand-like receptors where the calix cavity very often remains unexploited.

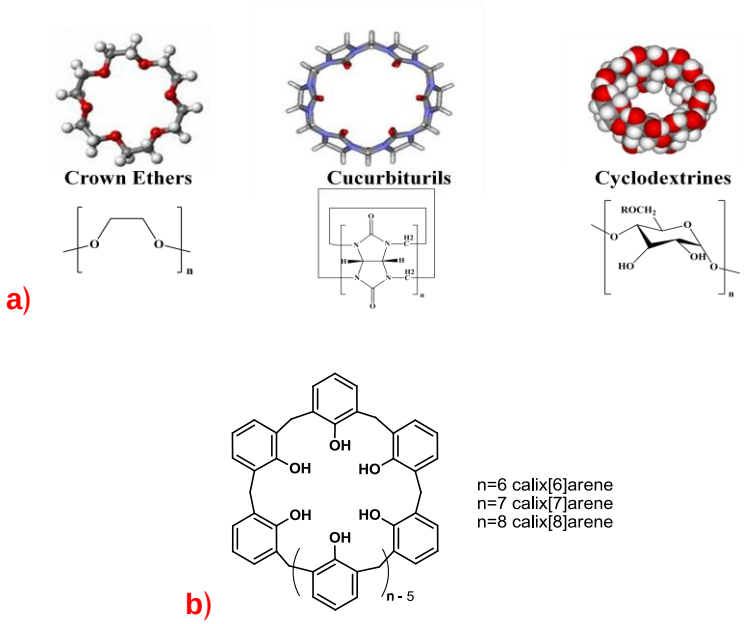

Figure 44. (a) Crown Ethers, Cucurbiturils and Cyclodexstrines; (b) Structure of larger calix[n]arene (n = 6, 7 e 8).

From another point of view, simple ethers of calixarenes can be seen as modified crown ethers, and in principle they should be able to give *endo*-complexation of organic cations in a similar way. Unfortunately, with the notable exception of some calix[5]arene derivatives,[76] simple ethers of

[76] Kogan, K.; Biali, S., *Journal of Organic Chemistry,* **2009**, 74, 7172; Gattuso, G.; Notti, A.; Pappalardo, S; Parisi, M.; Pilati, Tullio; Terraneo, G, *CrystEngComm,* **2012**, *14(8),* 2621; Gattuso, G.; Notti, A.; Pappalardo, A.; Parisi, M. F.; Pisagatti, I; Pappalardo, S; Garozzo, D; Messina, A; Cohen, Y; Slovak, *Journal of Organic Chemistry*, **2008**, 73(18), 7280.

calixarenes do not give such kind of complexation because they are too small in the case of calix[4]arenes or because they are not well preorganized in the case of larger calix[6-8]arenes.

Thus, for example, it is well-known that hexamethoxy-*p*-*tert*-butylcalix[6]arene (**Figure 45**) is conformationally mobile and does not complex halide, hexafluorophosphate, or tetraphenylborate salts of organic dialkylammonium cations.

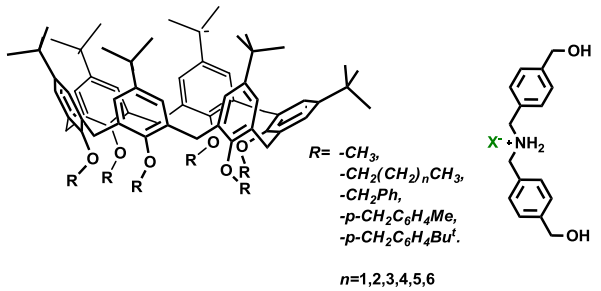

Figura 45. Threading of calix[6]arene derivative.

On the other hand, the *through-the-annulus* threading of dialkylammonium or bipyridium cations to give pseudorotaxane structures, which is very popular with large crown ethers, such as [24]crown-8 or [34]crown-10, is very rare in the calix[n]arene series. In fact, the very few examples regard the threading of viologen derivatives through the annulus of calix[6]arene hosts in wich the anion coordinating ability of their ureido groups is exploited to favor the ion-pair dissociation (**Figure 46**).

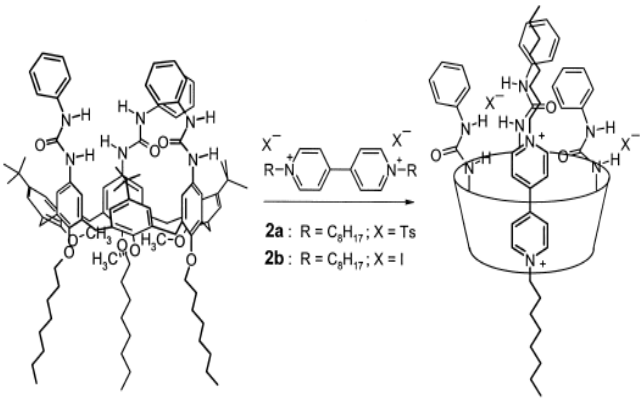

Figura 46. Threading of calix[6]arene derivate.

Instead, no examples of threading through conformationally mobile, larger calix[6-7]arene annuli by dialkylammonium cations were known until the 2010 year.

At that time Gaeta et al[77] introduced an efficient method to obtain *endo*-cavity complexation and *through-the annulus* threading of large calix[6-7]arenes exploiting the inducing effect of a weakly coordinating anion, tetrakis[3,5-bis(trifluoromethyl)phenyl]borate ($TFPB^-$), which is known to be noncoordinating (or very weakly coordinating) to metal ions and therefore is referred to as a "superweak" anion (**Figure 47**).

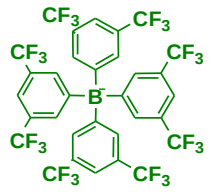

Tetrakis[3,5-bis(triFluoromethyl) Phenyl]Borate ($TFPB^-$)

[77] C. Gaeta, F. Troisi, P. Neri, *Org. Lett.* **2010**, 12, 2092.

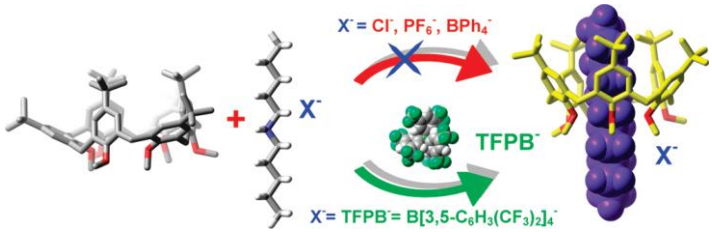

Figure 47. Through-the-Annulus Threading of Calixarenes Induced by Very Loose Alkylammonium Ion Pairs

In particular, they observed that the complexation of a nonsymmetrical alkylbenzylammonium cation (e.g., 3) by hexaalkoxycalix[6]arenes (e.g., 1a) can lead to a preference for the endo-alkyl stereoisomer (3⊂1a) over the endo-benzyl one up to a 30:1 ratio (Figure 48).[77]

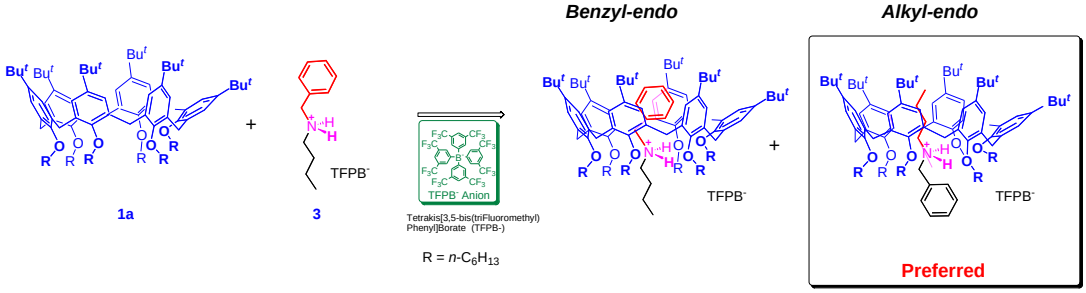

Figure 48. The *endo alkyl p*reference **.**

This approach has been used for the synthesis of [2]rotaxanes,[78] which showed an unprecedented inversion of the wheel orientation. (**Figure 49**)

[78] Pierro, T.; Gaeta, C.; Talotta, C.; Casapullo, A.; Neri, P. *Org. Lett*. **2011**, *13*, 2650.

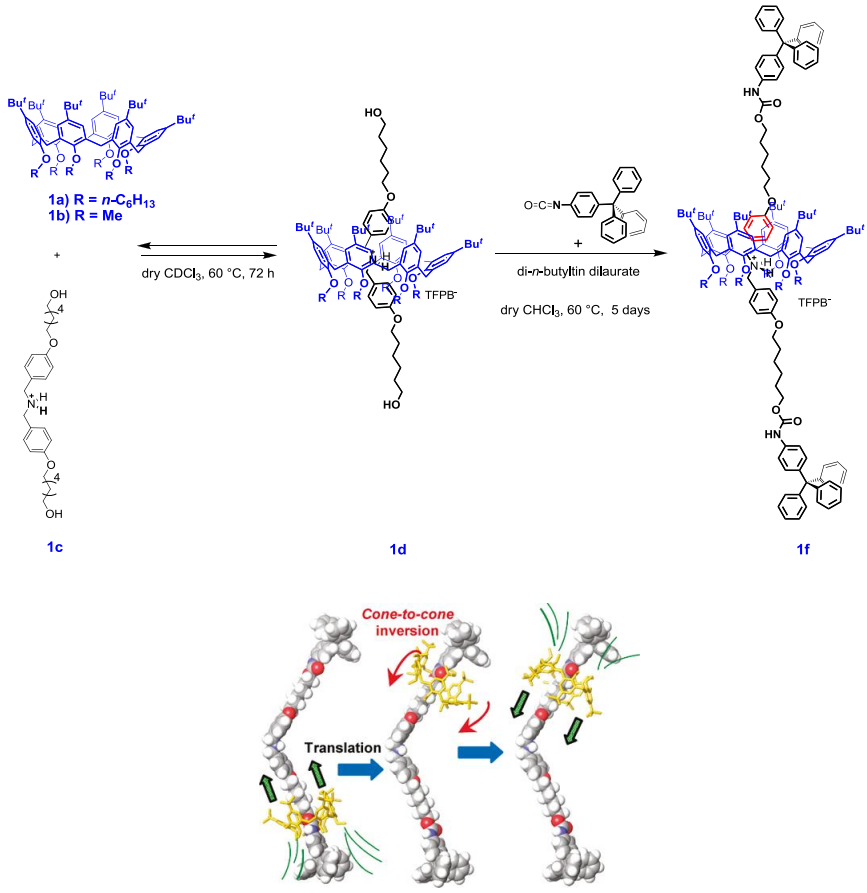

Figure 49. [2]rotaxanes synthesis[78] and its unprecedented inversion of the wheel orientation

Subsequently, on this basis Gaeta and *al* envisioned that the appropriate covalent linkage of two such alkylbenzylammonium recognition motifs could allow good control of the consequent, it was extended to the synthesis of pseudo[3]rotaxane systems in which two calix[6]arene macrocycles are threaded by a bis(benzylalkylammonium) axle.[79]

[79] Talotta, C.; Gaeta, C.; Pierro, T.; Neri, P. *Org. Lett.* **2011**, *13*, 2098.

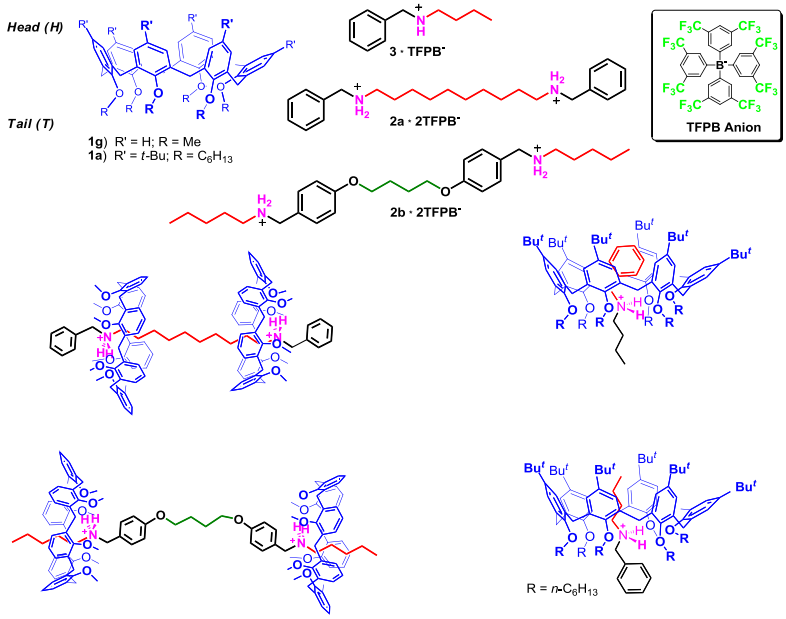

Figure 50. *Through-the-annulus* threading[79] of nonsymmetrical alkylbenzyl ammonium cations by hexaalkoxycalix[6]arene

Because of the three-dimensional non symmetrical nature of the calix[6]arene wheels and on the basis of the above mentioned preference for the *endo*-alkyl complexation by calix[6]arene macrocycles three sequence stereoisomers could be obtained, which were termed as *head-to-head* (H,H), *head-to-tail* (H,T) and *tail-to-tail* (T,T) (**Figure 51**) with rationally designed axles. Taking advantage of these systems, it was possible to obtain the stereoprogrammed synthesis of the first examples of calixarene-based [3]rotaxane architectures. The base-acid treatment demonstrated that these systems act as molecular shuttles, which move on a nanometer scale level.[80]

[80] Talotta, C.; Gaeta, C.; Neri, P. *Org. Lett.* **2012**,.

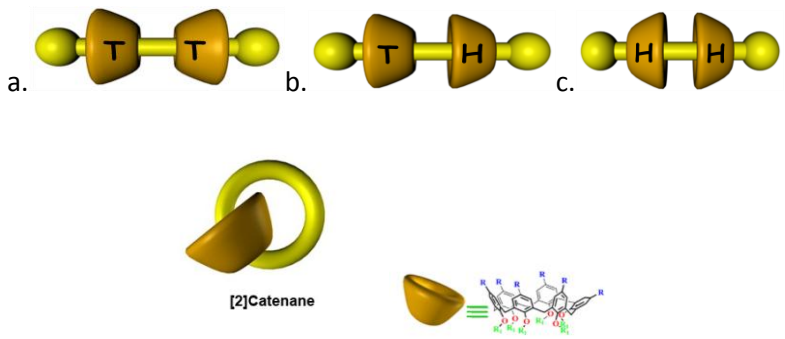

Figure 51. The three stereoisomeric [3]rotaxane structures named ***a.****Tail* to *Tail*, **b.** *Head* to *head*, and ***c.****Head* to *Tail,* **d.** Calix[6]arene-based catenane.

The directionality of the threading and the observed high stereoselection have enabled the synthesis of directional calix[6]arene-based catenane (**Figure 51d.**).

CHAPTER III

3.1 Goal of the research

All the above aspects represent interesting peculiar features of *calixarene threading*, which could be exploited for designing interlocked structures with new properties or functions. The present Ph.D. project was born with the basic logic to exploit the "*superweak anion*" approach for the synthesis and study of supramolecular interpenetrated and interlocked systems that have bis- and tris-calixarenes as cyclic units.

The above mentioned directionality of the threading and the observed high stereoselection have enabled the synthesis of directional double-calix[6]arene-based rotaxane and tris- calix[6]arene-based rotaxane.

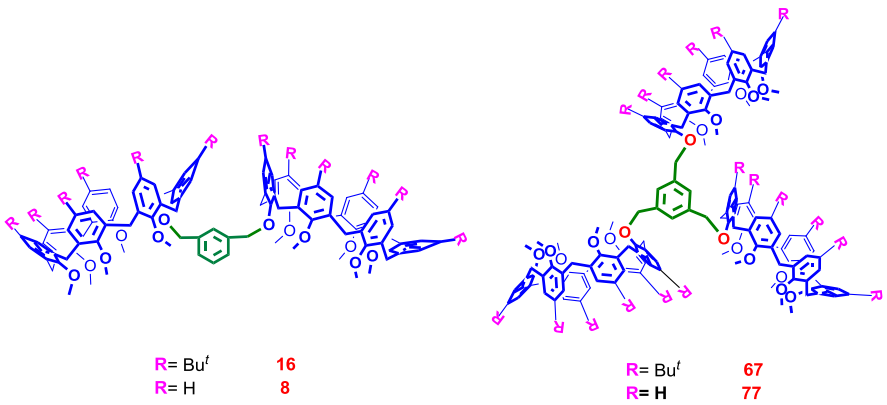

Figure 52. double-calix[6]arene and tris-calix[6]arene structures

Initially, the interest was directed towards the synthesis of a double-calixarene macrocycle, in which two calix-rings are linked to one another by a short *m*-xylylene spacer (**Figure 52**). Afterwards, the attention was

directed to the study of the *threading* of derivatives bearing two or more ammonium units in order to assess whether it is possible to obtain higher order double-threaded-pseudorotaxane systems (**Figure 53**).

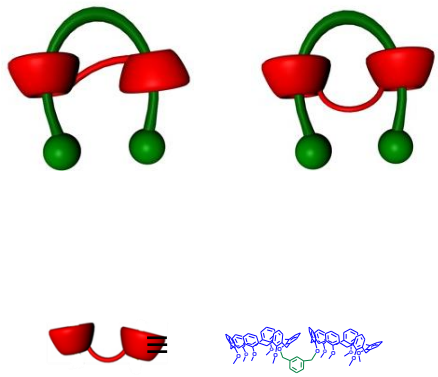

Figure 53. Double-Calixarene-Based Handcuff-Rotaxane

Due to the natural asymmetry of calixarene macrocycle, which possess a lower rim different from the upper rim, it may be particularly interesting to evaluate the possibility to control the formation of adducts bearing a different sequence of *threading* of the cyclic systems with respect to the linear unit.

In fact, the marked *endo*-alkyl preference of calixarene derivatives could play a crucial role for the synthesis of a *double-threaded*-[2]-pseudorotaxane in which the two calix[6]arene wheels have a programmed relative orientation obtained through the rational choice of the threading element.

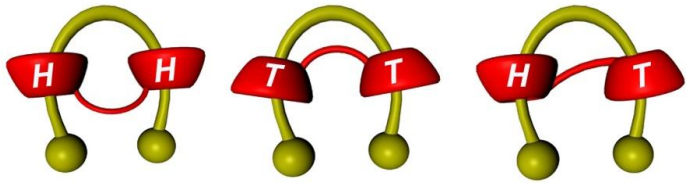

Figure 54. Three stereoisomeric handcuff-pseudo[2]rotaxane structures

It will be also interesting to try to obtain a double-threaded calix[2]catenane system exploiting a macrocyclization reaction of a suitably functionalized double–threaded-pseudorotaxane.(**Figure 55**)

Figure 55. Double-threaded[2]catenane topologies

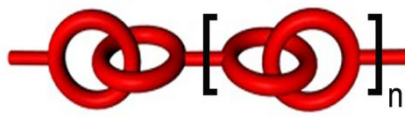

Figure 56. Polymeric double-threaded[2]catenane

Another interesting challenge will concern the study of threading conducted on tritopic receptor with a wide variety of ammonium axles.

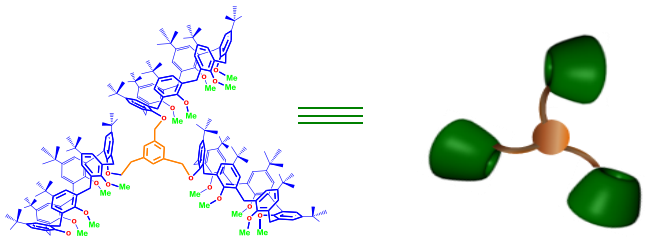

Figure 57. A tritopic receptor

This triple-calixarene receptor could prove incredibly versatile, making accessible several topologies so far never obtained with the cyclophanes, such as triple-threaded [4]rotaxanes and even a triple-threaded [2]catenane.

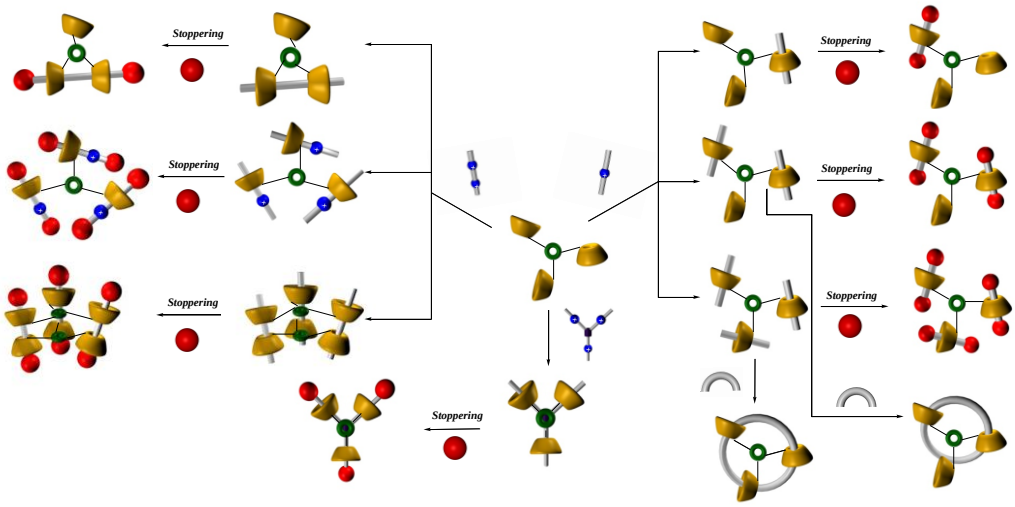

Figure 58. The variety of topological isomers obtainable from a tris-calixarene host.

CHAPTER IV

Threading of a double-calix[6]arene systems with mono-ammonium axles

4.1 Introduction

Rotaxanes and catenanes[81] have gained a prominent position in the field of nanotechnology wherein they have been used as mechanical or electronic molecular devices. In addition, novel and fascinating functions are continuosly emerging for interpenetrated architectures. At this regard, Leigh and coworkers[82] have reported a sequence-specific synthesis of a peptide by a prototype of rotaxane-based artificial ribosome. Rotaxane and catenane architectures can be efficiently obtained through a template-directed threading[83] of a linear axle through a macrocycle to form a pseudorotaxane derivative, which can be considered as the precursor of both rotaxanes and catenanes. At this regards, an early strategy provides the use of dialkylammonium axles and macrocycles such as cyclodextrins,[84] crown ethers[85] and cucurbiturils.[86]

As illustrated in the first section an important contribution to this field of research comes from the work conducted by Neri et *al.*[77] They have introduced an efficient method to obtain *endo*-cavity complexation and *through-the-annulus* threading of large calix[6-7]arenes exploiting the inducing effect of a weakly coordinating anion, tetrakis [3,5-bis (trifluoromethyl) phenyl]borate ($TFPB^-$).

[81] *Molecular Catenanes, Rotaxanes and Knots: A Journey Through the World of Molecular Topology*: Sauvage, J. P.; Dietrich-Buchecker, C., Eds.; Wiley-VCH: Weinheim, 1999.
[82] Lewandowski, B.; De Bo, G.; Ward, J. W.; Papmeyer, M.; Kuschel, S.; Aldegunde, M. J.; Gramlich, P. M. E.; Heckmann, D.; Goldup, S. M.; D'Souza, D. M.; Fernandes, A. E.; Leigh, D. A. *Science*, 2013, *339*, 189.
[83] (a) Zhang, Z.-J.; Han M.; Zhang, H.-Y.; Liu, Y. *Org. Lett.* 2013, *15*, 1698. (b) Frey, J.; Kraus, T.; Heitz, V., Sauvage, J.-P. *Chem. Eur. J.* 2007, *13*, 7584. (c) Balzani, V.; Clemente-León, M.; Credi, A.; Lowe, J. N.; Badjić, J. D., Stoddart, J.F.; Williams, D. J. *Chem. Eur. J.* 2003, *9*, 5348
[84] Szejtli, J. *Chem. Rev.* **1998**, *98*, 1743.
[85] Gokel, G. W. *Crown Ethers and Cryptands: Monographs in Supramolecular Chemistry*; The Royal Society of Chemistry: Cambridge, UK, 1991.
[86] Lagona, J.; Mukhopadhyay, P.; Chakrabarti, S.; Isaacs, L. *Angew. Chem. Int. Ed.* **2005**, *44*, 4844.

From their studies they have deduced a sort of “molecular code” which has been used to develop an integrative self-sorting[87]. This molecular code includes the following stereochemical “*endo*-alkyl rule” (**Figure 59**): "*threading of a directional alkylbenzylammonium axle through a non-tert-butylated hexaalkoxycalix[6]arene occurs with an endo-alkyl preference*".[86a]

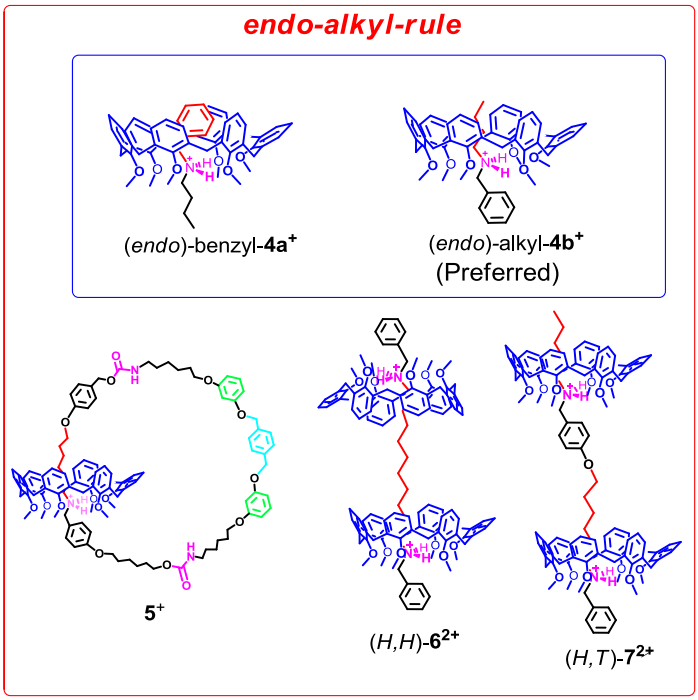

Figure 59. The *endo-alkyl rule*:[86a] "*threading of a directional alkylbenzylammonium axle through a non-tert-butylated hexaalkoxycalix[6]arene occurs with an endo-alkyl preference.*"

On the basis of the *endo-alkyl rule* the first example of oriented calix[2]catenane **5**$^{+}$ has been obtained,[87] after macrocyclization, by using a directional alkylbenzylammonium axle. Encoding the *endo-alkyl rule* on a bis(benzylalkylammonium) axle two calix[6]arene directional wheels can be ordered in the right stereosequence (e.g.: (*H,H*)-**6**$^{2+}$ and (*T,T*)-**7**$^{2+}$) to obtain stereoisomeric pseudo[3]rotaxane architectures.[86b]

[87] C.Talotta, C. Gaeta, Q. Zhenhui, C.A. Schalley, P. Neri Angew. Chem. Int. Ed. Engl. 2013, 52, 7437

With regard to hosts with multiple cavities or rings, spectacular interpenetrated architectures have been obtained by double-threading of dialkylammonium axles through covalently linked macrocycle derivatives[88] (e.g.: double-crown ethers, double-cucurbiturils or double-cyclodextrins). In particular, non-trivial "handcuff" catenane[89] architectures have been reported in which two flat crown-rings, rigidly linked to one another, were threaded with a bis(ammonium) axle to perform a double-leg elevator (**Figure C**).

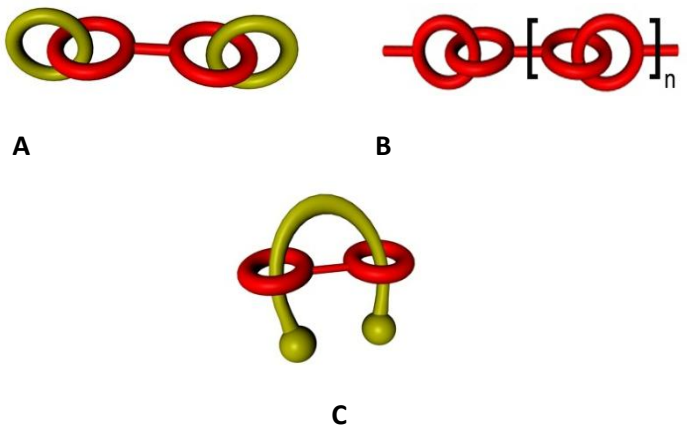

Figure 60. Schematic representation of the currently known prototypical examples of handcuff-derived architectures (**A-C**)

With respect to the use of flat macrocycles in **C** (Figure **60**), a major synthetic challenge is represented by the use of three-dimensional nonsymmetrical rings (directional wheels), such as double-calixarene **8**

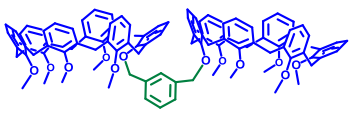

8

because of the inherent difficulty in controlling the stereochemistry of the entire system.[90] In

[88] Badjić, J. D.; Balzani, V.; Credi, A.; Silvi, S.; Stoddart, J. F. *Science* **2004**, *303,* 1845.
[89] (a)Evans, N. H.; Serpell, C. J.; Beer, P. D., *Angew. Chem. Int. Ed.* **2011**, *50*, 2507. (b) Zhang, Z.-J.; Han M.; Zhang, H.-Y.; Liu, Y. *Org. Lett.* **2013**, *15*, 1698;
[90] (a) Talotta, C.; Gaeta, C.; Pierro, T.; Neri, P. *Org. Lett.* **2011**, *13*, 2098–2101; (b) Talotta, C.; Gaeta, C.; Neri, P. *Org. Lett.* **2012**, *14*, 3104.

fact, their threading abilities with dialkylammonium axles has remained unexplored (**Figure 61)**.

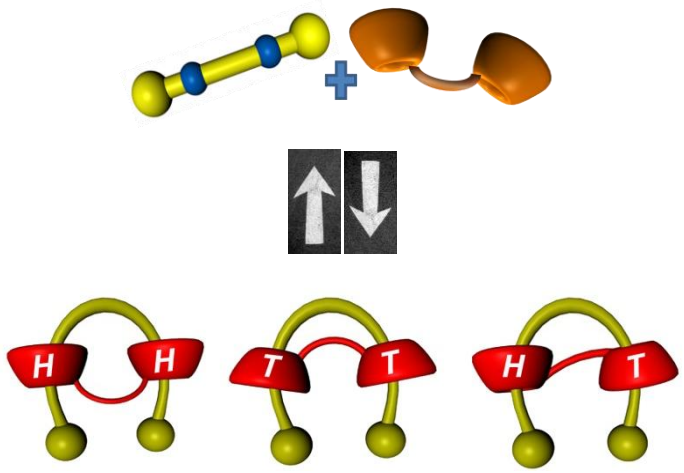

Figure 61. Stereoisomeric oriented handcuff (pseudo)-[2]rotaxanes

4.2. Synthesis of double-calix[6]arene derivative 12.

Double-calix[6]arene **12** was synthesized exploiting the reaction sequence shown in **Scheme 1.** In particular, *p*-H-calix[6]arene **8** was monobenzylated with benzyl bromide in the presence of potassium carbonate as the base in refluxing dry CH_3CN to give mono-benzyl ether **9** (83%) after usual work-up. Compound **9** was smoothly hexamethylated by treatment with MeI in acetone in the presence of Cs_2CO_3 as the base to give **10** in 91% yield. Removal of the benzyl groups of **10** was easily accomplished by hydrogenolysis (H_2, Pd/C) to give pentamethoxy-calix[6]arene-mono-ol **11** in 51% yield. Finally, treatment of 2 equiv of **11** with 1 equiv of 1,3-bis(bromomethyl)benzene in dry THF/DMF (at reflux) in the presence of

NaH as the base afforded double-calix[6]arene derivative **12** in 33% yield, after purification by column chromatography.

Compounds **9**, **10**, **11** and **12** were fully characterized by ^{1}H NMR, ^{13}C NMR, and ESI(+) MS spectra. Regarding double-calix[6]arene **12** its ^{1}H and ^{13}C NMR data, acquired at room temperature, were fully consistent with its molecular symmetry. In particular, three singlets were presents at 2.92, 3.11 and 3.17 ppm relative to OMe groups, while three singlets were presents at 3.92, 3.97 and 4.00 ppm relative to $ArCH_2Ar$ protons (**Figure 62**). In fact, compounds **12** is conformationally mobile and gives rise to sharp signals for the three symmetry related $ArCH_2Ar$ groups groups. This is due to the small dimension of both the methoxy groups at the lower rim and the *p*-H "substituents" at the upper rim, which allow the *through-the-annulus* passage of both rims.[91] Finally, a singlet was present at 4.84 ppm in the ^{1}H NMR spectrum (**Figure 62**) of **12** relative to the OCH_2 protons of the *m*-xylylene bridge.

[91] It is well known that methoxy-*p*-H-calix[6]arene derivatives are conformationally mobile systems, see: Gutsche, C. D.; Bauer, L. J. *J. Am. Chem. Soc.* **1985**, *107*, 6052−6059. In fact, it is known that the blockage of the *O-through-the-annulus* route requires *p*-substituted benzyl groups at the lower rim (Kanamathareddy, S.; Gutsche, C. D. *J. Org. Chem.* **1994**, *59*, 3871), while substituents larger than *t*-Bu groups are required to block the "*p-position-through-the-annulus*" route: Otsuka, H.; Araki, K.; Shinkai, S. *Chem. Exp*. **1993**, *8*, 479−482. van Duynhoven, J. P. M.; Janssen, R. G.; Verboom, W.; Franken, S. M.; Casnati, A.; Pochini, A.; Ungaro, R.; de Mendoza, J.; Nieto, P. M.; Prados, P.; Reinhoudt, D. N. *J. Am. Chem. Soc.* **1994**, *116*, 5814.

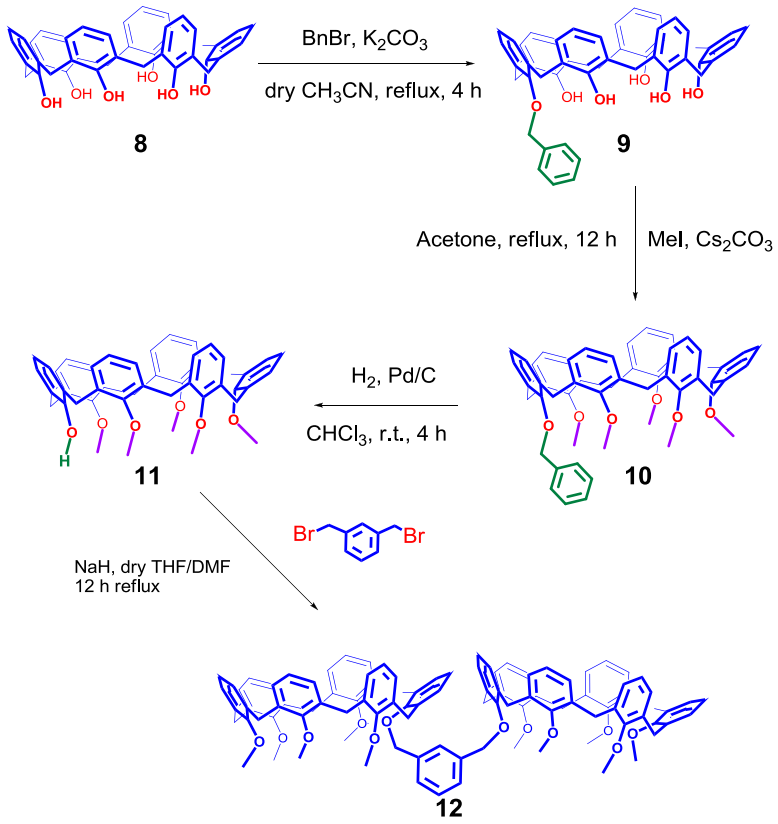

Scheme 1. Synthesis of double-calix[6]arene derivative **12**

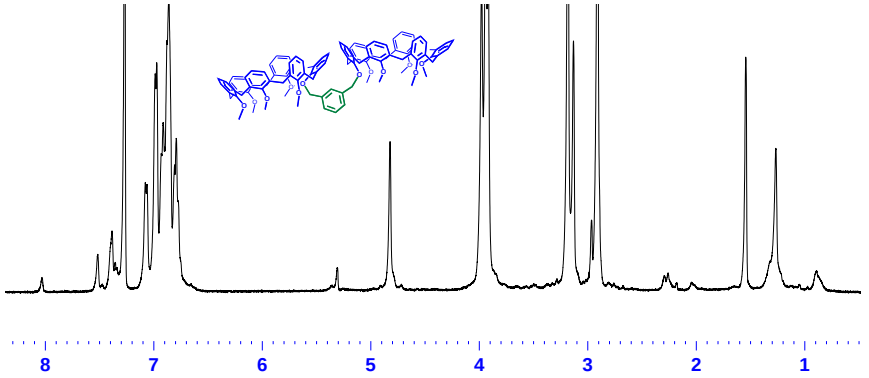

Figure 62. ^{1}H NMR spectrum (400 MHz, $CDCl_3$, 298 K) of double-calixarene derivative **12**

4.3 Threading studies of 8 with mono-ammonium axles: double-threaded pseudo[2]rotaxanes 14 and 18

The synthesized derivative **8** was then used to study the threading with mono-ammonium axles $\mathbf{2}^{+}$, $\mathbf{3}^{+}$ and $\mathbf{4}^{+}$ (**Figure 63**).

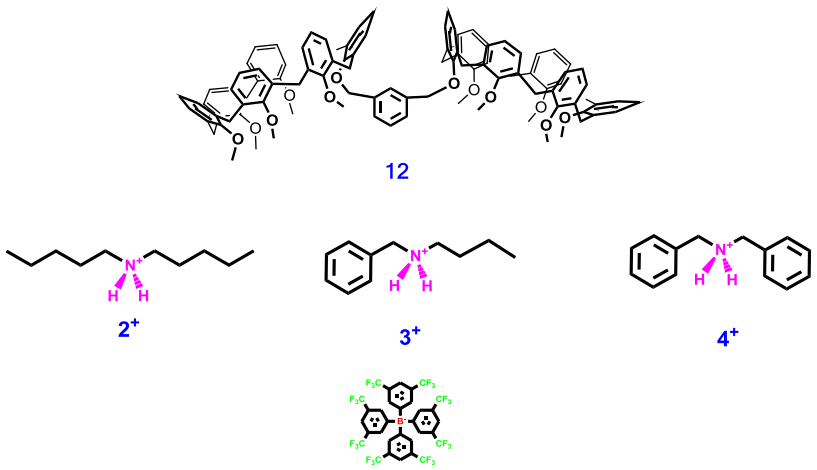

Figure 63. Linear mono-ammonium systems and double–calixarene host

4.3.1 *Threading of double-calix[6]arene 12 with* di-*n*-*pentylammonium axle* 2^+

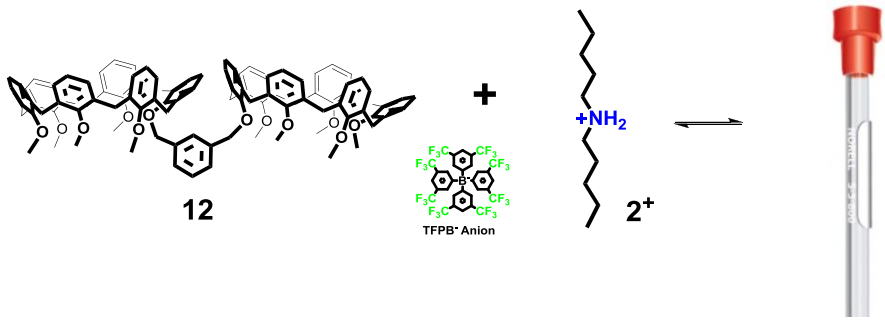

Figure 64. Schematic representation of Directional threading of **12** with the di-*n*-pentylammonium axle $\mathbf{2^+}$.

Interestingly, the addition of di-*n*-pentylammonium salt $\mathbf{2^+}\cdot TFPB^-$ to a $CDCl_3$ solution of double-calix[6]arene **12** caused dramatic changes in its ^1H NMR spectrum (**Figure 65**). In fact, upon addition of 1 equivalent of $\mathbf{2^+}\cdot TFPB^-$ salt a new set of signals emerged (**Figure 65c**) due to the formation of the singly threaded pseudo[2]rotaxane ion $\mathbf{2^+}\subset\mathbf{12}$ (**Scheme 2**)**.** Under these conditions (1 equiv of axle $\mathbf{2^+}$), the formation of a singly threaded pseudo[2]rotaxane ion $\mathbf{2^+}\subset\mathbf{12}$ (**Scheme 2**) was ascertained by the ESI(+) mass spectrum that gave a value of 1672.4 *m*/*z* as the base peak (**Figure 65f)**, corresponding to a 1:1 host/guest stoichiometry, in which only one dialkylammonium axle was threaded into one of the two macrocycles of **12.**

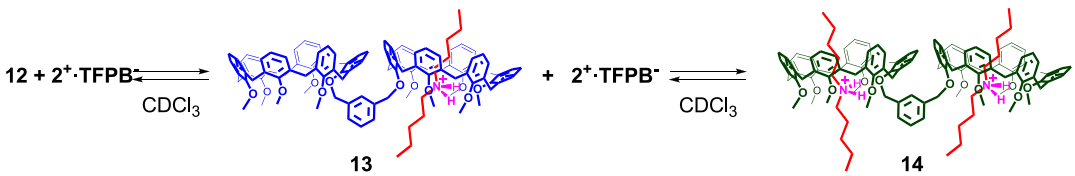

Scheme 2.

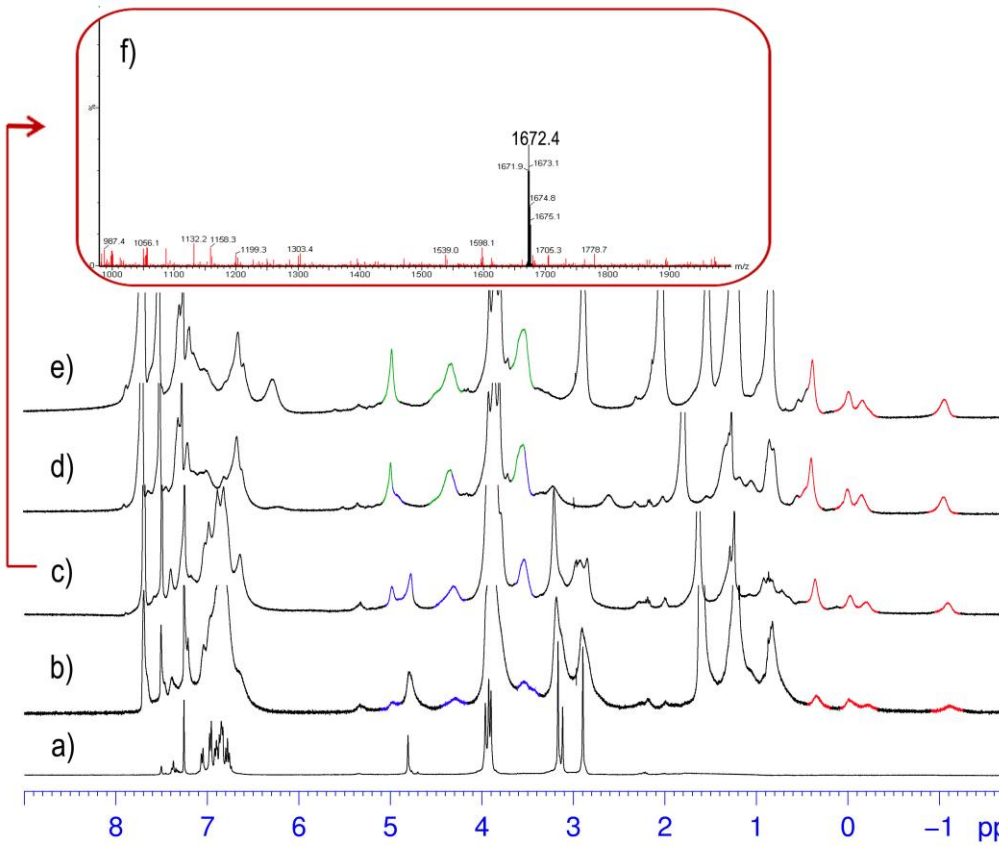

Figure 65. ^{1}H NMR (400 MHz, 298 K, $CDCl_3$) of: a) **8** (aa x10^{-3} M); b) **8** and 0.5 equiv of $\mathbf{2}^{+}$; c) **8** and 1 equiv of $\mathbf{2}^{+}$; d) **8** and 2 equiv of $\mathbf{2}^{+}$; e) **8** and 3 equiv of $\mathbf{2}^{+}$; f) significant portion of the ESI(+) mass spectrum of a mixture of **8** and 1 equiv of $\mathbf{2}^{+}$.

In addition, the appearance of *n*-alkyl resonances in the upfield negative region of the ^{1}H NMR spectrum of the 1:1 mixture of $\mathbf{2}^{+}$ and **12** in $CDCl_3$ and the formation of AX systems for $ArCH_2Ar$ groups corroborate the formation of the pseudo[2]rotaxane.[77] The 1:1 stoichiometry was confirmed by spectral integration. A COSY-45 spectrum ($CDCl_3$, 400 MHz, 298 K) of the 1:1 mixture of thread $\mathbf{2}^{2+}$ and double-calix[6]arene **12** allowed a complete confident assignment of all shielded alkyl resonances. Thus, α protons at −0.02 ppm show a coupling with β methylene group at −1.07 ppm, which presents a cross-peak with γ protons at −0.17 ppm, finally

coupled with δ protons at 0.37 ppm (accidentally isochronous with ε methyl) (**Figure 66**).

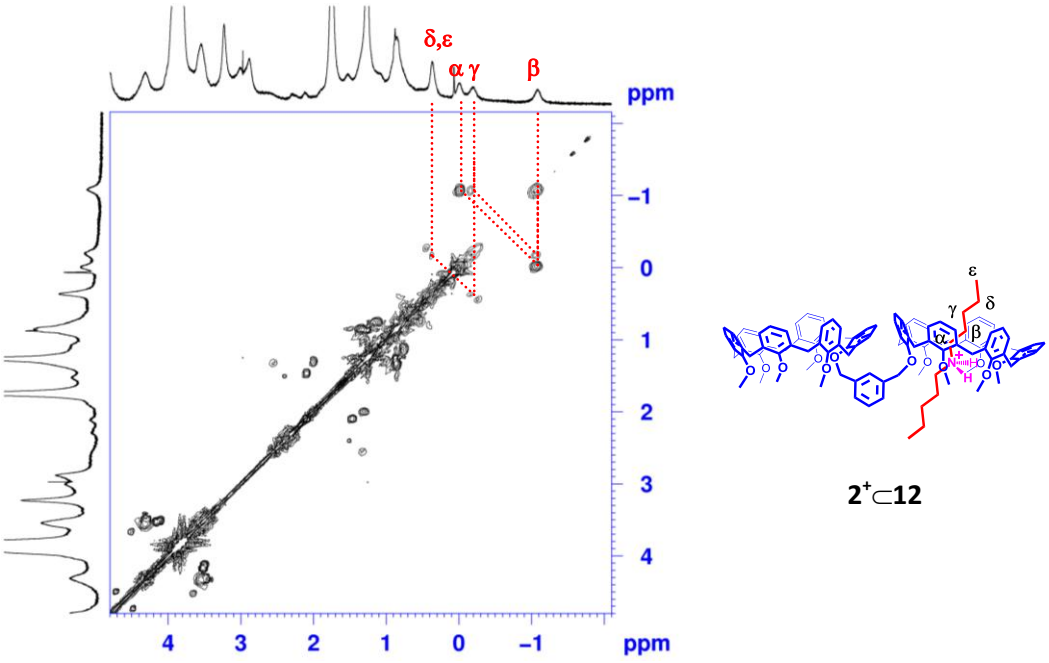

Figure 66. Significant portion of the 2D COSY spectrum (400 MHz, 298 K, $CDCl_3$) of the 1:1 mixture of **12** and **2**$^+$·TFPB$^-$.

Interestingly, a 2D HSQC spectrum (**Figure 67**) revealed the presence of two cross-peaks between two singlets at 4.99 and 4.78 ppm and two pertinent carbon resonances at 75.4 and 74.5 ppm, which can be assigned to OCH_2 groups of the *m*-xylylene bridge. Naturally, these ^1J direct correlations were consistent with a singly-threaded pseudo[2]rotaxane structure.

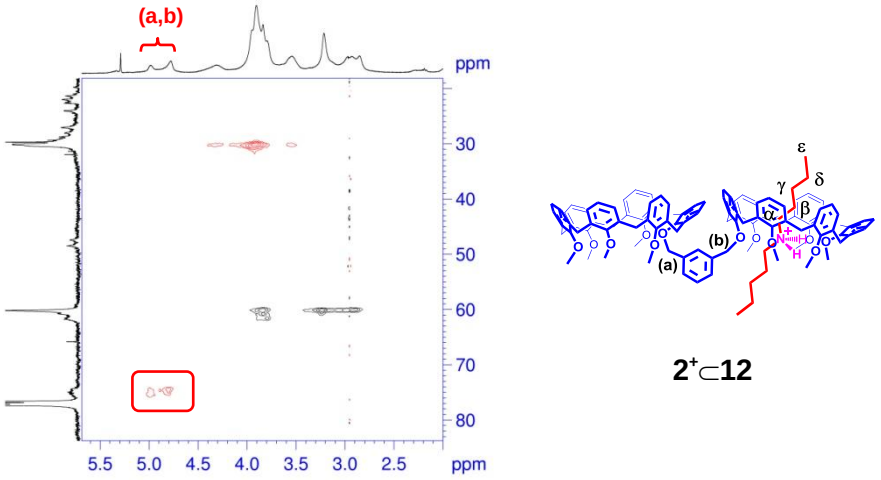

Figure 67. Expansion of the HSQC (400 MHz, 298 K, $CDCl_3$) spectrum of an equimolar solution of $\mathbf{2}^+$ and **12**.

Further addition of 1 equivalent of di-*n*-pentylammonium axle $\mathbf{2}^+$ led to a simplification of the ^{1}H NMR spectrum of the mixture of $\mathbf{2}^+\cdot$TFPB$^-$ and **12** (**Figures 65c-d**). In particular, the appearance of a new singlet at 4.98 ppm (integrating for 4H) relative to OCH_2 groups of the *m*-xylylene bridge, and the presence of three singlets relative to OMe groups were indicative of the formation of a new, higher-symmetry, doubly-threaded pseudo[3]rotaxane $(\mathbf{2}^+)_2\subset\mathbf{12}$ in which two axles $\mathbf{2}^+$ were threaded into the two macrocycles of **12.** This was confirmed by ^{1}H NMR signal integration and by an ESI(+) mass spectrum of a 2:1 mixture of $\mathbf{2}^+\cdot$TFPB$^-$ and **12**, which gave a value of 915.5 *m*/*z* as the base peak, corresponding to a 1:2 host/guest stoichiometry.

DFT calculations at the B3LYP/6-31G* level of theory[92] evidenced strongly stabilizing N-H⋯O hydrogen-bonds (**Figure 68a**) between the

[92] Gaussian 09, Revision **A.1**, Frisch, M. J.; Trucks, G. W.; Schlegel, H. B.; Scuseria, G. E.; Robb, M. A.; Cheeseman, J. R.; Scalmani, G.; Barone, V.; Mennucci, B.; Petersson, G. A.;

ammonium threads and the calix-wheels. Interestingly, the optimized structure of the $(\mathbf{2}^{+})_2 \subset \mathbf{12}$ complex (**Figure 68a**) revealed an approximate C_2 symmetry axis bisecting the *m*-xylyl bridge and an *anti* conformation around the O^{calix}-$CH_2{}^{xylyl}$ bonds of with dihedral angles of 168.2° and 167.2° (**Figure 68**). Consequently, the two calix cavities are diverging with their main axes almost perpendicular. In particular, the two mean planes of the calixarene oxygens form an angle of 60.0°. The preference for the *anti* conformation around the O^{calix}-$CH_2{}^{xylyl}$ bonds was confirmed by molecular dynamics (MD) simulation at 500 K which clearly evidenced that about 48% of the coconformers sampled during the entire MD simulation (20000 ps) showed a dihedral angle in the 150-170° range around the O^{calix}-$CH_2{}^{xylyl}$ bonds (**Figure 68c**).

Nakatsuji, H.; Caricato, M.; Li, X.; Hratchian, H. P.; Izmaylov, A. F.; Bloino, J.; Zheng, G.; Sonnenberg, J. L.; Hada, M.; Ehara, M.; Toyota, K.; Fukuda, R.; Hasegawa, J.; Ishida, M.; Nakajima, T.; Honda, Y.; Kitao, O.; Nakai, H.; Vreven, T.; Montgomery, Jr., J. A.; Peralta, J. E.; Ogliaro, F.; Bearpark, M.; Heyd, J. J.; Brothers, E.; Kudin, K. N.; Staroverov, V. N.; Kobayashi, R.; Normand, J.; Raghavachari, K.; Rendell, A.; Burant, J. C.; Iyengar, S. S.; Tomasi, J.; Cossi, M.; Rega, N.; Millam, J. M.; Klene, M.; Knox, J. E.; Cross, J. B.; Bakken, V.; Adamo, C.; Jaramillo, J.; Gomperts, R.; Stratmann, R. E.; Yazyev, O.; Austin, A. J.; Cammi, R.; Pomelli, C.; Ochterski, J. W.; Martin, R. L.; Morokuma, K.; Zakrzewski, V. G.; Voth, G. A.; Salvador, P.; Dannenberg, J. J.; Dapprich, S.; Daniels, A. D.; Farkas, Ö.; Foresman, J. B.; Ortiz, J. V.; Cioslowski, J.; Fox, D. J. Gaussian, Inc., Wallingford CT, 2009.

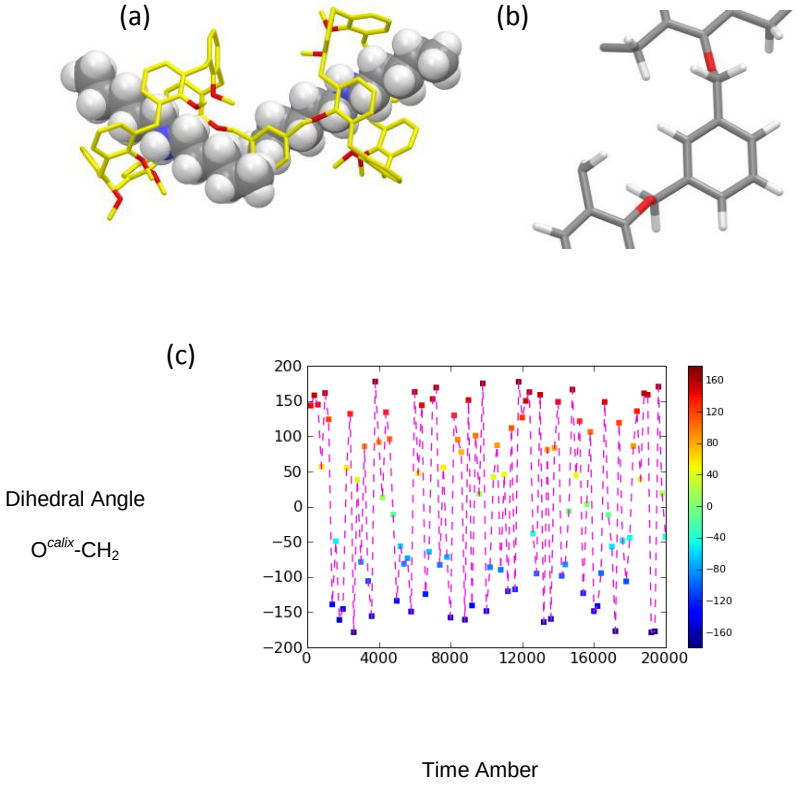

Figure 68. (a) Energy-minimized structures of the $(\mathbf{2}^{+})_2\subset\mathbf{12}$ complex (B3LYP DFT calculation using the 6-31G* basis set). (b) Detailed view of the predicted staggered conformations around O^{calix}-CH_2 bonds of the *m*-xylyl bridge. (c) Variation in the dihedral angle between O^{calix}-CH_2 observed during the MD simulation at 500 K (time given in ps).

The total binding constant (K_{tot}) for $(\mathbf{2}^{+})_2\subset\mathbf{12}$ complex, determined by quantitative ^{1}H NMR analysis of its 2:1 titration mixture in $CDCl_3$ and using tetrachloroethane (TCHE) as internal standard,[93] gave a value $>10^7$ M^{-2}, which was beyond the limit of reliability of the NMR technique. Therefore, in order to have more accurate measurements[94] we decided to evaluate K_{tot} in the presence of a polar competing solvent such as CD_3CN. Thus, in a

[93] 150 and More Basic NMR Experiments: A Practical Course; Braun, S.; Kalinowsky, H.-O.; Berger, S.; Eds.; WILEY-VCH: Weinheim; **1996**, pp. 232.
[94] Fielding, L. *Tetrahedron* **2000**, *56*, 6151.

mixture of $CDCl_3/CD_3CN$ (99/1, *v*/*v*), we were able to measure a value of K_{tot} = 4.4±0.3×10^4 M^{-2} for the $(\mathbf{2}^+)_2\subset\mathbf{12}$ complex by quantitative ^{1}H NMR analysis and using TCHE as internal standard.

4.3.2 Directional threading of double-calix[6]arene 12 with nonsymmetrical n*-butylbenzylammonium axle* 3^+

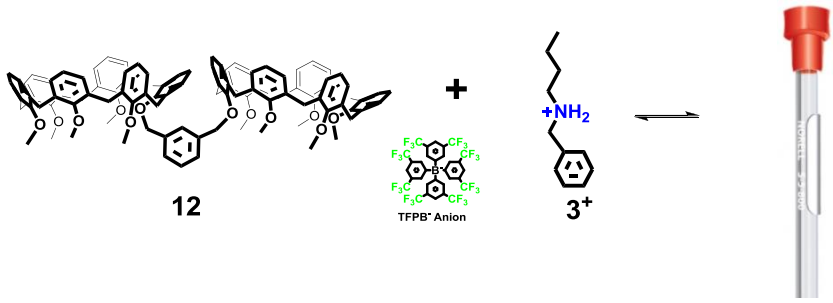

Figure 69. Schematic representation of Directional threading of **12** with the *n*-butylbenzylammonium axle $\mathbf{3}^+$

On the basis of results e decided to verify what happens in the case of double-calix[6]arene host **12**. In fact, the threading of **12** with the *n*-butylbenzylammonium axle $\mathbf{3}^+$ could give rise to three directional double-threaded pseudo[3]rotaxane diastereoisomers with *endo*-alkyl/*endo*-alkyl, *endo*-benzyl/*endo*-alkyl, or *endo*-benzyl/*endo*-benzyl relative orientations (**Figure 71**).

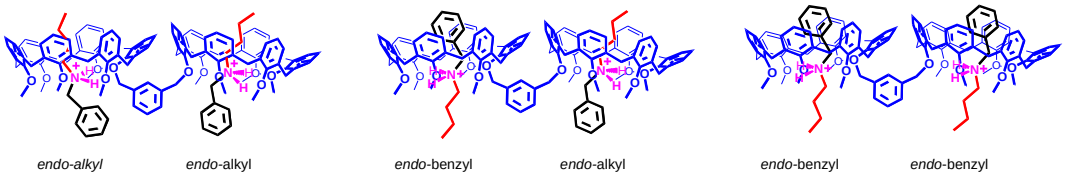

Figure 71. Possible double-threaded pseudo[3]rotaxane stereoisomers by directional threading of **12** with the *n*-butylbenzylammonium axle $\mathbf{3}^+$.

Of course, on the basis of the above discussed *endo*-alkyl rule (**Figure 59**), we expected that the *endo*-alkyl/*endo*-alkyl stereoisomer should be favored. As above, the addition of butylbenzylammonium **3**$^+$ to a solution of **12** in $CDCl_3$ caused significant changes in its ^{1}H NMR spectrum. In particular, 1 equiv of butylbenzylammonium **3**$^+$ led to a new specie corresponding to the singly-threaded complex **3**$^+\subset$**12**, in slow exchange with the free host **12**. The 1:1 host/guest stoichiometry was confirmed by means of ESI(+) MS and integration of ^{1}H NMR signals. In fact, the ESI(+) mass spectrum of a 1:1 mixture of **3**$^+\cdot$TFPB$^-$ and **12** gave a value of 1680.3 *m*/*z* as the base peak (**Figure 70g**), corresponding to a singly threaded pseudo[2]rotaxane ion **3**$^+\subset$**12 (Scheme 3).**

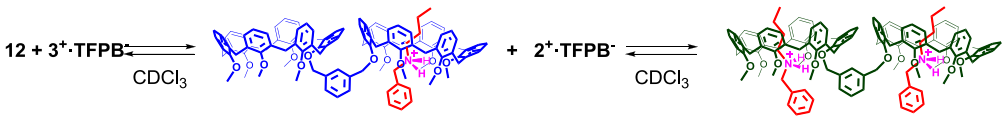

15 **16**

Scheme 3

In analogy to the above discussed **2**$^+\subset$**12** pseudorotaxane, also in this case two singlets at 4.96 and 4.77 ppm relative to the OCH_2 protons of the *m*-xylylene bridge corresponding to the singly-threaded pseudo[2]rotaxane were observed in the ^{1}H NMR spectrum of the 0.75:1 mixture of **3**$^+$ and **12** (**Figure 71d**).

The progressive addition of **3**$^+$ led to the disappearance of these two singlets while a new singlet emerged at 4.96 ppm corresponding to the doubly-threaded pseudo[3]rotaxane (**3**$^+$)$_2\subset$**12**, as confirmed by ESI(+) MS and ^{1}H NMR signal integration.

As concerns the stereochemistry of the threading, the ^{1}H NMR spectra of the 1:1 and 1:2 mixtures of **12** and **3**$^+$ showed typical signatures at highfield negative values (from 1.0 to –1.0 ppm) characteristic of an *endo*-alkyl complexation.[77,80] This result and the absence of shielded

benzylic resonances in the 4–6 ppm region, typical of an *endo*-benzyl complexation, were clear-cut proofs that in both singly- and doubly-threaded pseudorotaxanes an *endo*-alkyl orientation of butylbenzylammonium threads was present.[95] This result demonstrated the validity of the *endo*-alkyl rule also for double-calixarenes and confirmed the possibility to control the directionality of the double-threading in these systems.

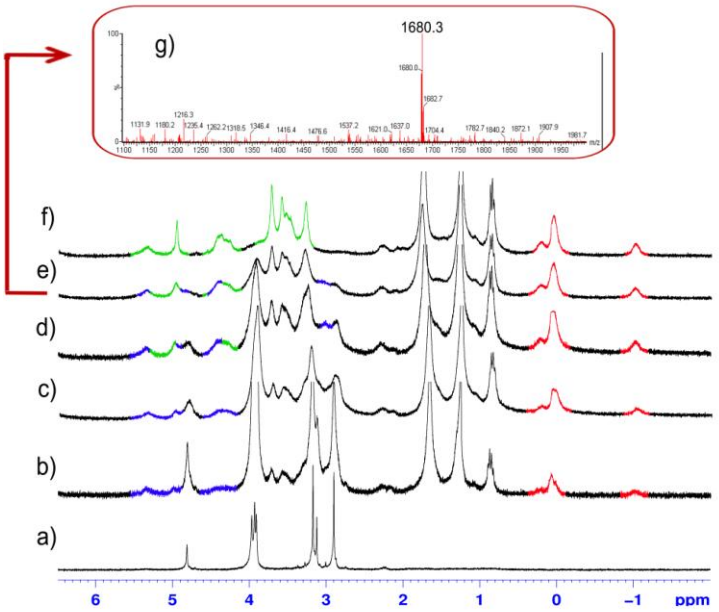

Figure 71. ^{1}H NMR (400 MHz, 298 K, $CDCl_3$) of: a) **12** (aa x10^{-3} M); b) **12** and 0.25 equiv of $\mathbf{3}^{+}$; c) **12** and 0.5 equiv of $\mathbf{3}^{+}$; d) **8** and 0.75 equiv of $\mathbf{3}^{+}$; e) **12** and 1.0 equiv of $\mathbf{3}^{+}$; f)**12** and 2.0 equiv of $\mathbf{3}^{+}$; g) significant portion of the ESI(+) mass spectrum of a mixture of **12** and 1 equiv of $\mathbf{3}^{+}$.

[95] For comprehensive reviews on calixarene macrocycles, see: (a) Gutsche, C. D. *Calixarenes, An Introduction*; Royal Society of Chemistry: Cambridge, UK, 2008, Chapter 5, pp. 116-128. (b) Böhmer, V. *Angew. Chem., Int. Ed. Engl.* **1995**, *34*, 713-745. (c) Gutsche, C. D. *Calixarenes Revisited*; Royal Society of Chemistry: Cambridge, 1998. (d) *Calixarenes 2001*; Asfari, Z.; Böhmer, V.; Harrowfield, J.; Vicens J.; Eds.; Kluwer: Dordrecht, 2001. (e) Böhmer, V. In *The Chemistry of Phenols*; Rappoport, Z., Ed.; Wiley: Chichester, UK, 2003; Chapter 19. (f) *Calixarenes in the Nanoworld*; Vicens J.; Harrowfield, J.; Eds.; Springer, Dordrecht, 2007.

In analogy to the $(\mathbf{2}^{+})_2\subset\mathbf{12}$ complex above described**,** DFT calculations at the B3LYP/6-31G* level of theory[92] also in this case confirmed the presence of stabilizing N-H···O hydrogen-bonds (**Figure 72a**) between the ammonium cations and the calixarene oxygens. The optimized structure of the $(\mathbf{3}^{+})_2\subset\mathbf{12}$ complex (**Figure 72a**) was very similar to that $(\mathbf{2}^{+})_2\subset\mathbf{12}$, showing again an *anti* conformation around O^{calix}-CH_2^{xylyl} bonds with dihedral angles of 162.7° and 166.1°. This conformational preference was confirmed by MD simulation at 500 K, which clearly evidenced that about 46% of the sampled coconformers showed a dihedral angle in the 150-170° range around the O^{calix}-CH_2^{xylyl} bonds (**Figure 72b**).

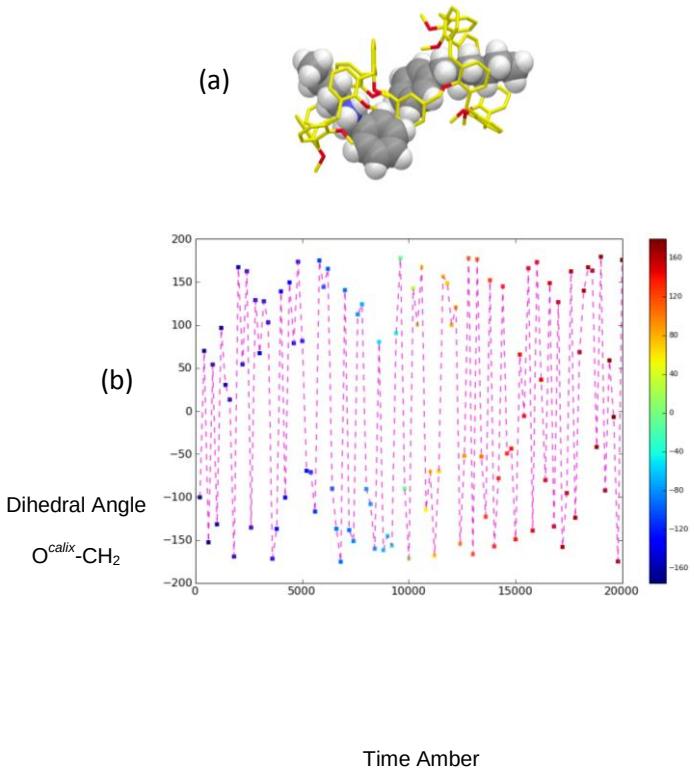

Figure 72. (a) Energy-minimized structures of the $(\mathbf{3}^{+})_2\subset\mathbf{12}$ complex (B3LYP DFT calculation using the 6-31G* basis set). (b) Variation in the dihedral angle between O^{calix}-CH_2 observed during the MD simulation at 500 K (time given in ps).

The extension of DFT calculations to the other *endo*-benzyl/*endo*-alkyl and *endo*-benzyl/*endo*-benzyl orientational isomers of $(\mathbf{3}^{+})_2\subset\mathbf{12}$ (**Figure 73**) confirmed the higher stability of *endo*-alkyl/*endo*-alkyl orientation experimentally evidenced by ^{1}H NMR. In fact, this latter orientation was 3.9 kcal/mol more stable than the *endo*-benzyl/*endo*-alkyl one, which in turn was 4.3 kcal/mol more stable than the *endo*-benzyl/*endo*-benzyl orientational isomer.

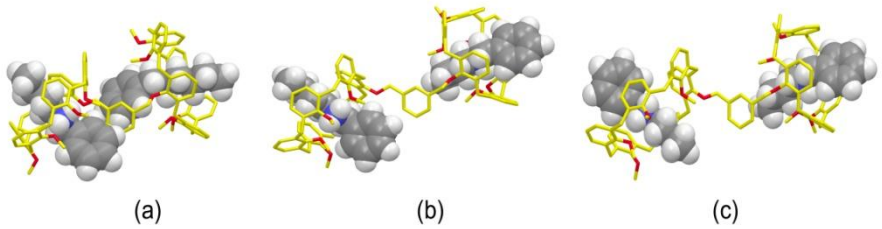

Figure 73. Energy-minimized structures of *endo*-alkyl/*endo*-alkyl (a), *endo*-benzyl/*endo*-alkyl (b) *endo*-benzyl/*endo*-benzyl (c) orientational isomers of pseudo[3]rotaxane $(\mathbf{3}^{+})_2\subset\mathbf{12}$ (B3LYP DFT calculation using the 6-31G* basis set).

As discussed above, also in this case the total binding constant (K_{tot}) of the $(\mathbf{3}^{+})_2\subset\mathbf{12}$ complex was determined by quantitative ^{1}H NMR analysis of its 2:1 titration mixture in $CDCl_3/CD_3CN$ (99/1, *v*/*v*), to give a value of $8.8\pm0.2\times10^4$ M^{-2}. This value is only slightly higher with respect to that found ($4.4\pm0.3\times10^4$ M^{-2}) for dipentylammonium complex $(\mathbf{2}^{+})_2\subset\mathbf{12}$.

In order to further validate the *endo*-alkyl rule we decided to study the threading of double-calix[6]arene **12** with dibenzylammonium axle $\mathbf{4}^{+}$. In particular, the addition of increasing amounts (0.5-1.5 equivalents) of dibenzylammonium salt $\mathbf{4}^{+}\cdot TFPB^{-}$ to a $CDCl_3$ solution of **12 (Scheme 4)** did not caused significant changes in its ^{1}H NMR spectrum. This results and the absence of shielded benzylic resonances in the 4─6 ppm region typical of an *endo*-benzyl complexation, were clear-cut proof that both singly-threaded

and doubly- threaded pseudorotaxane structures were not formed. This indicates that the *endo*-benzyl complexation by double-calix[6]arene **12** is an unfavourable process.

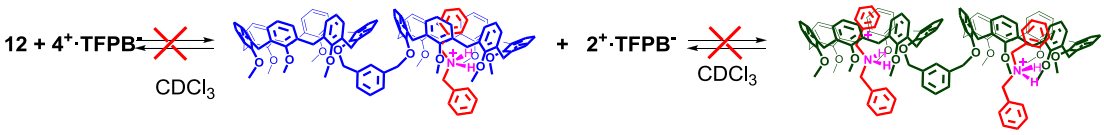

Scheme 4

4.4. Synthesis of double-calix[6]arene derivative 21

As a natural complement to derivative **12**, we decide to synthesize double-calix[6]arene **21** bearing *p-tert*-butyl groups at the upper rim in place of the "*p*-H-substituents" of **12**. The synthesis of **21** was realized by exploiting the reaction sequence shown in **Scheme 5**, very similar to that already described for derivative **12.**

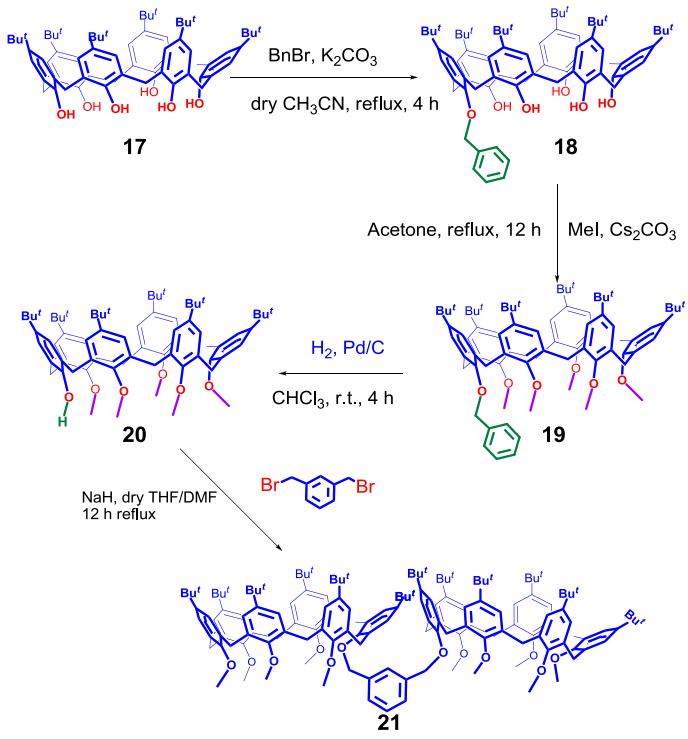

Scheme 5. Synthesis of double-calix[6]arene Derivative **21**

All the compounds **18**, **19**, **20** and **21** were fully characterized by means of ^{1}H NMR, ^{13}C NMR, and ESI(+) MS spectra. Regarding double-calix[6]arene derivative **16**, its ^{1}H and ^{13}C NMR data, acquired at room temperature, were fully consistent with its molecular symmetry. In particular, three singlets were presents at 2.92, 3.11 and 3.17 ppm relative to OMe groups (**Figure 73**). It is interesting to note that the increased steric hindrance to the conformational interconversion[91] generated by the t-Bu groups at the upper rim gives rise to the fine structure of three AX systems for the symmetry related $ArCH_2Ar$ protons [4.50 e 3.58 ppm (J = 14.7 Hz), 4.17 e 4.04 ppm (J

= 14.5 Hz), 3.83 e 3.68 ppm (J = 15.1 Hz)]. Finally, a singlet was present at 4.89 ppm in the ^{1}H NMR spectrum (Figure 74) of **21** relative to OCH_2 protons of the *m*-xylylene bridge.

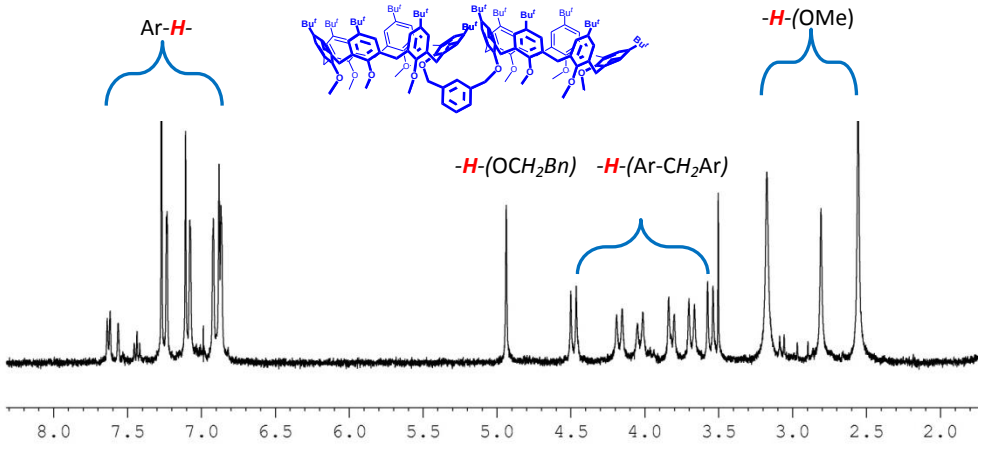

Figure 74. ^{1}H NMR spectrum (400 MHz, $CDCl_3$, 298 K) of double-calixarene derivative **21**

4.5 Threading studies of 21 with mono-ammonium axles: double-threaded pseudo[2]rotaxanes 22 and 23

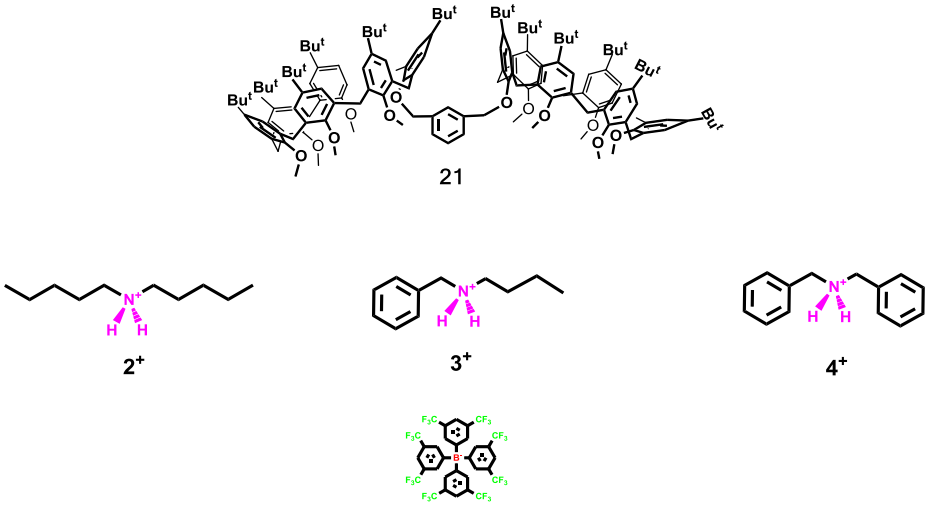

Figure 75. Linear mono-ammonium systems (**2**$^{+}$**, 3**$^{+}$**, 4**$^{+}$) and double–calixarene host **21**

4.5.1 *Threading of double-calix[6]arene 21 with di-*n*-pentylammonium axle 2*$^{+}$

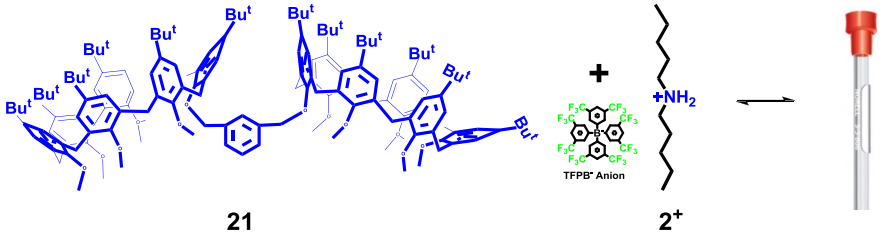

Figure 76. Schematic representation of Directional threading of **21** with the di-*n*-pentylammonium axle **2**$^{+}$.

In analogy to the above discussed $\mathbf{2}^{+}\subset\mathbf{12}$ pseudorotaxane, also in this case two singlets at 4.96 and 4.77 ppm relative to the OCH_2 protons of the *m*-xylylene bridge corresponding to the singly-threaded pseudo[2]rotaxane were observed in the ^{1}H NMR spectrum of the 0.75:1 mixture of $\mathbf{2}^{+}$ and **21** (**Figure 76d**). The progressive addition of $\mathbf{2}^{+}$ led to the disappearance of these two singlets while a new singlet emerged at 4.96 ppm corresponding to the doubly-threaded pseudo[3]rotaxane $(\mathbf{2}^{+})_2\subset\mathbf{21}$, as confirmed by ESI(+) MS and ^{1}H NMR signal integration. (**Figure 76**)

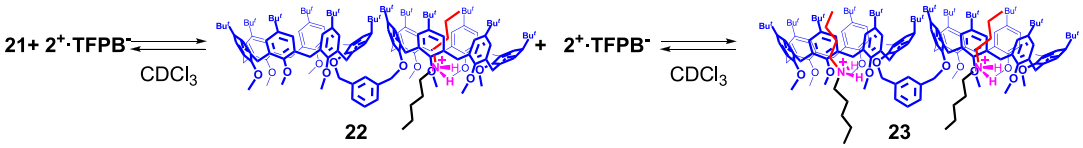

Scheme 6

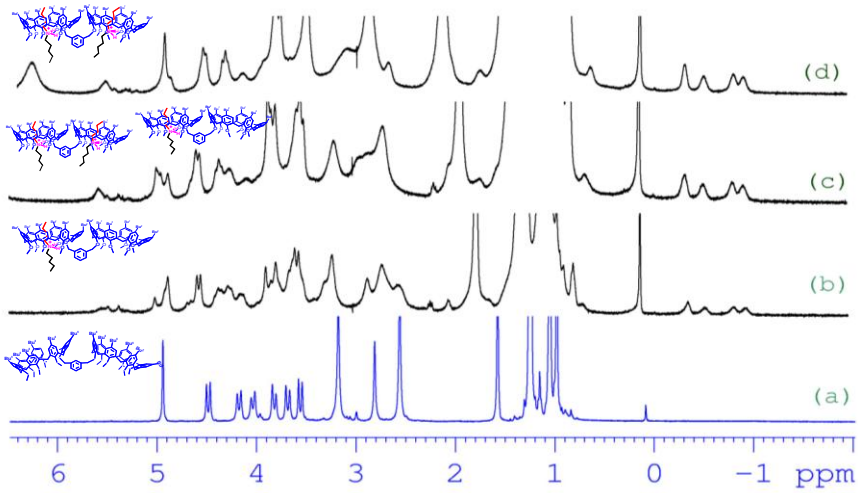

Figure 77. ^{1}H NMR (400 MHz, 298 K, $CDCl_3$) of: a) **21**(aa x10^{-3} M); b) **21** and 1.0 equiv of $\mathbf{2}^{+}$; c) **21** and 2.0 equiv of $\mathbf{2}^{+}$; d) **21** and 5.0 equiv of $\mathbf{2}^{+}$; significant portion of the ESI(+) mass spectrum of a mixture of **16** and 1 equiv of $\mathbf{2}^{+}$.

In addition, the appearance of *n*-alkyl resonances in the upfield negative region of the ^{1}H NMR spectrum of the 1:1 mixture of **2**$^+$ and **21** in $CDCl_3$ and the formation of new AX systems for $ArCH_2Ar$ groups corroborate the formation of the pseudo[2]rotaxane. In addition, the 1:1 stoichiometry was confirmed by spectral integration. A COSY-45 spectrum ($CDCl_3$, 400 MHz, 298 K) of the 1:1 mixture of thread **2**$^{2+}$ and double-calix[6]arene **21** allowed a complete confident assignment of all shielded alkyl resonances. Thus, α protons at −0.02 ppm show a coupling with β methylene group at −1.04 ppm, which presents a cross-peak with γ protons at −0.15 ppm, finally coupled with δ protons at 0.37 ppm (accidentally isochronous with ε methyl) (**Figure 78.**).

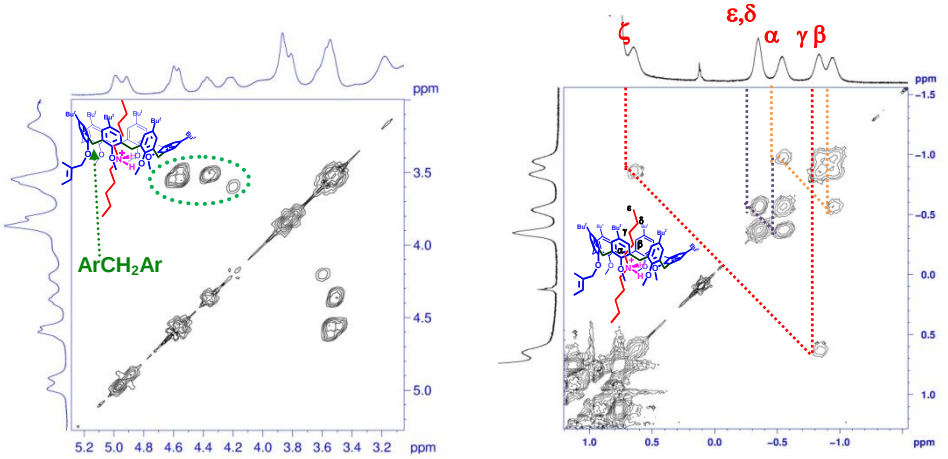

Figure 78. Significant portions of the 2D COSY spectrum (400 MHz, 298 K, $CDCl_3$) of the 1:2 mixture of **21** and **2**$^+$·$TFPB^-$.

4.5.2 Directional threading of double-calix[6]arene 21 with nonsymmetrical n-*butylbenzylammonium axle* 3^+

As illustrated above the “endo-alkyl rule” (**Figure 59**) is also valid for calix[6]arenes bearing the *tert-butyl* groups at the upper rim , consequently it is particularly relevant to verify its validity on double-calix[6]arene host **21.** Thus, in analogy to **12**, the threading of **21** with *n*-butylbenzylammonium axle $\mathbf{3^+}$ could give rise to three directional double-threaded pseudo[3]rotaxane diastereoisomers with *endo*-alkyl/*endo*-alkyl, *endo*-benzyl/*endo*-alkyl, or *endo*-benzyl/*endo*-benzyl relative orientations (**Figure 81**).

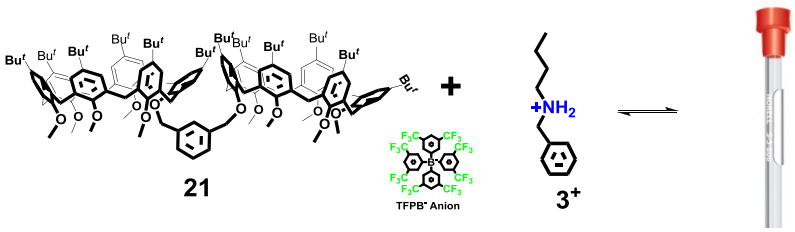

Figure 79. Schematic representation of Directional threading of **21** with the *n*-butylbenzylammonium axle $\mathbf{3^+}$.

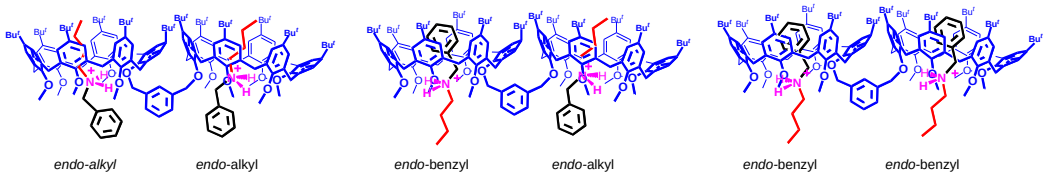

Figure 80. Possible double-threaded pseudo[3]rotaxane stereoisomers by directional threading of **21** with the *n*-butylbenzylammonium axle $\mathbf{3^+}$.

Of course, on the basis of the above discussed *endo*-alkyl rule, we expected that the *endo*-alkyl/*endo*-alkyl stereoisomer should be favored. As above, the addition of butylbenzylammonium $\mathbf{3^+}$ to a solution of **21** in $CDCl_3$

caused significant changes in its ^{1}H NMR spectrum. In particular, 1 equiv of **3**$^+$ led to a new species corresponding to the singly-threaded

complex **3**$^+$⊂**21**, in slow exchange with the free host **21**. The 1:1 host/guest stoichiometry was confirmed by means of ESI(+) MS and integration of ^{1}H NMR signals.

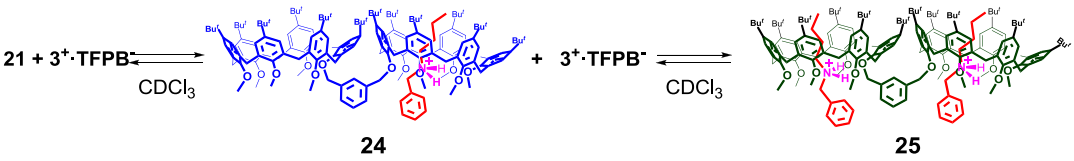

Scheme 7.

In analogy to the above discussed **2**$^+$⊂**12** pseudorotaxane, also in this case two singlets at 4.96 and 4.77 ppm relative to the OCH_2 protons of the *m*-xylylene bridge corresponding to the singly-threaded pseudo[2]rotaxane were observed in the ^{1}H NMR spectrum of the 0.75:1 mixture of **3**$^+$ and **12** (**Figure 70d**). The progressive addition of **3**$^+$ led to the disappearance of these two singlets while a new singlet emerged at 4.96 ppm corresponding to the doubly-threaded pseudo[3]rotaxane (**3**$^+$)$_2$⊂**12**, as confirmed by ESI(+) MS and ^{1}H NMR signal integration.

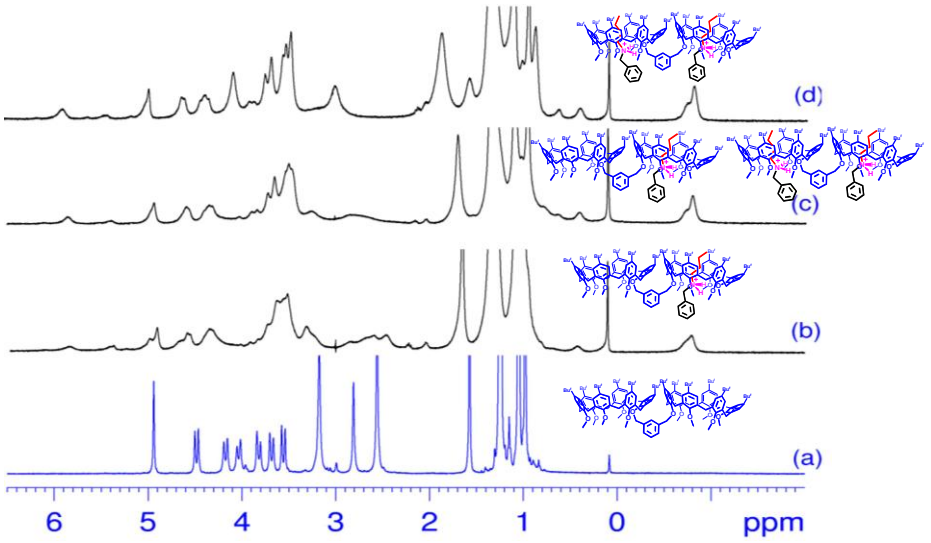

Figure 81. ^{1}H NMR (400 MHz, 298 K, $CDCl_3$) of: a) **21**(aa x10^{-3} M); b) **21** and 1.0 equiv of $\mathbf{3}^{+}$; c) **21** and 2.0 equiv of $\mathbf{3}^{+}$; d) **21** and 5.0 equiv of $\mathbf{3}^{+}$;

As concerns the stereochemistry of the threading, the ^{1}H NMR spectra of the 1:1 and 1:2 mixtures of **21** and $\mathbf{3}^{+}$ showed typical signatures at highfield negative values (from 1.0 to ─1.0 ppm) characteristic of an *endo*-alkyl complexation.[77,80] This result and the absence of shielded benzylic resonances in the 4─6 ppm region, typical of an *endo*-benzyl complexation, were clear-cut proofs that in both singly- and doubly-threaded pseudorotaxanes an *endo*-alkyl orientation of butylbenzylammonium threads was present.[95] This result demonstrated the validity of the *endo*-alkyl rule also for double-calixarenes bearing the t-Bu groups at the upper rim and confirmed the possibility to control the directionality of the double-threading in these systems.

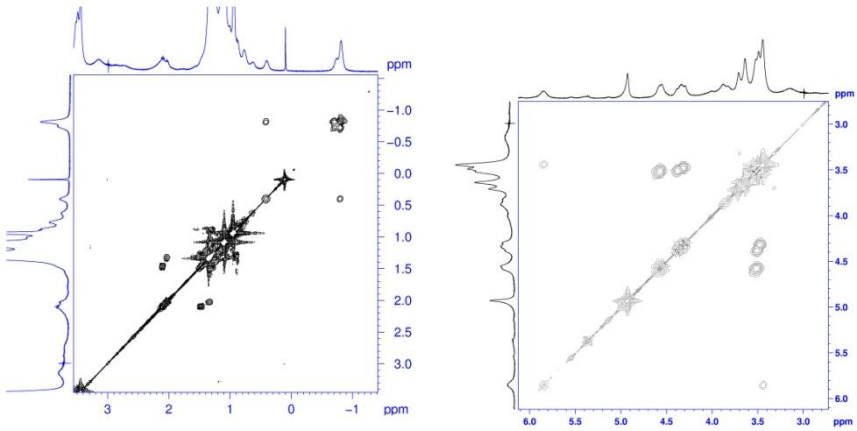

Figure 82. Significant portions of the 2D COSY spectrum (400 MHz, 298 K, $CDCl_3$) of the 1:2 mixture of **21** and **3**$^{+}$·TFPB^{-}.

4.5.3. Threading of double-calix[6]arene 21 with di-benzylammonium axle 4^{+}

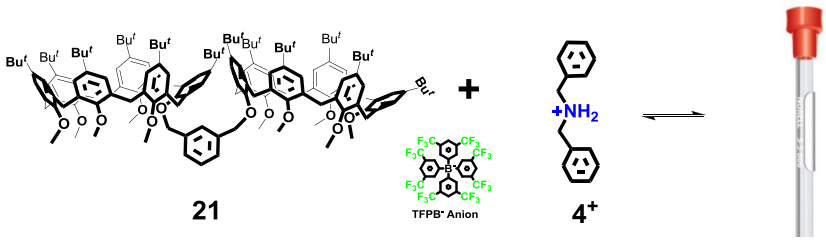

Figure 83. Schematic representation of threading of **21** with the di-benzylammonium axle **4**$^{+}$.

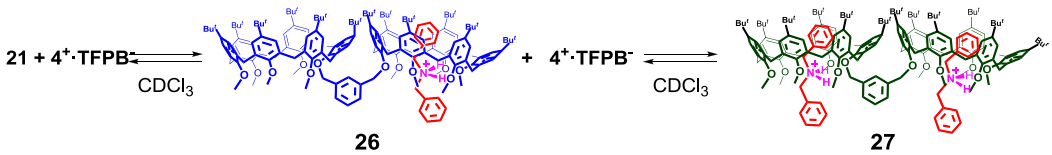

Scheme 8

Additional interesting threading results were obtained with dibenzylammonium salt ($Bn_2NH_2^+$*$TFPB^-$) and *tert-butylated* double-calix[6]arene **21** in $CDCl_3$ (**Scheme 8**). In fact, unlike derivative **12**, the threading of **21** and **4**$^+$·$TFPB^-$ gave rise to *endo*-benzyl complexation.

In particular, the addition of 0.5 equivalents of di-benzylammonium salt **4**$^+$·$TFPB^-$ to a solution of **21** in $CDCl_3$, caused dramatic changes in its ^1H NMR spectrum (**Figure 80)**. A new set of signals emerged (**Figure 80c**) due to the formation of the singly threaded pseudo[2]rotaxane.

Particularly diagnostic was the presence of shielded benzylic resonances in the 4─6 ppm region, related to benzylic *orto, meta e para* protons shielded by calix[6]arene cavity (**Figure on the left)** that were clear-cut proof that a singly-threaded pseudorotaxane structure was formed by *endo*-benzyl complexation.

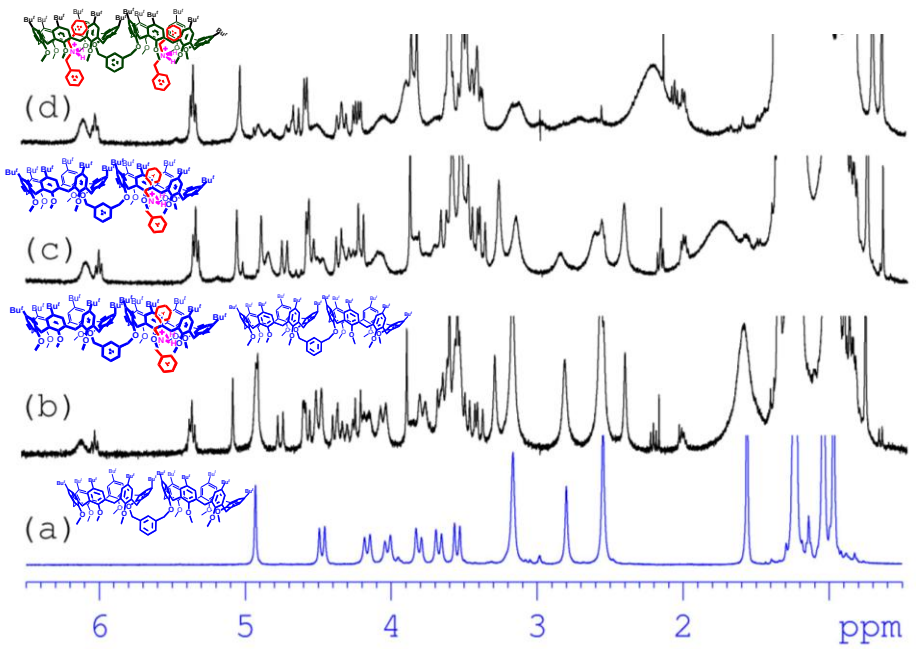

Figure 84. ^{1}H NMR (400 MHz, 298 K, $CDCl_3$) of: a) **21** (aa x10^{-3} M); b) **21** and 0.5 equiv of $\mathbf{4}^{+}$; c) **21** and 1.0 equiv of $\mathbf{4}^{+}$; d) **21** and 2.0 equiv of $\mathbf{4}^{+}$

A further addition of 1 equivalent of di-benzylammonium axle $\mathbf{4}^{+}$ led to a simplification of the ^{1}H NMR spectrum of the mixture of $\mathbf{4}^{+}\cdot TFPB^{-}$ and **21** (**Figures c-d**). In particular, the appearance of a new singlet at 4.98 ppm (integrating for 4H), relative to OCH_2 groups of the *m*-xylylene bridge, and the upfield shift of the three OMe singlets was indicative of the formation of a new, higher-symmetry, doubly-threaded pseudo[3]rotaxan $(\mathbf{4}^{+})_2\subset\mathbf{21}$ in which two axles $\mathbf{4}^{+}$ were threaded into the two macrocycles of **21**

This was confirmed by ^{1}H NMR signal integration and by an ESI(+) mass spectrum of a 2:1 mixture of $\mathbf{4}^{+}\cdot TFPB^{-}$ and **21**, which gave a value of 1290,3 *m*/*z* as the base peak, corresponding to a 1:2 host/guest stoichiometry. A COSY-45 spectrum ($CDCl_3$, 400 MHz, 298 K) allowed a complete confident assignment of all shielded benzyl resonances. Thus, ***ortho*** protons at 4.6 ppm show a coupling with ***meta*** protons at 5.3 ppm, which are coupled to ***para*** ones at 6.0 ppm.

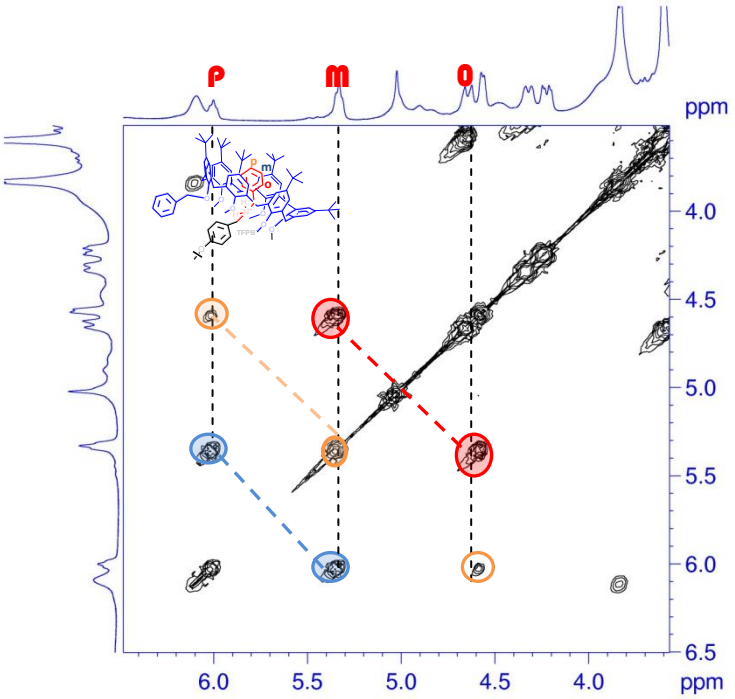

Figure 85. Significant portions of the 2D COSY spectrum (400 MHz, 298 K, $CDCl_3$) of the 1:2 mixture of **21** and **4**$^{+}$·TFPB^{-}.

4.6 Conclusion

In summary, this part of the Ph.D. thesis has been devoted to the threading abilities of double-calix[6]arene hosts **12** and **21** with mono-ammonium axles in the presence of the TFPB superweak anion. ^{1}H NMR and ESI(+) MS spectra evidenced the stepwise formation of singly- and doubly-threaded pseudorotaxane architectures by changing the host/guest stoichiometry from 1:1 to 1:2. The directional threading of nonsymmetrical *n*-butylbenzylammonium axle **3**$^{+}$ with double-calix[6]arene host **12** and **21** occurs with an *endo*-alkyl preference in accordance with the known "*endo*-alkyl rule".

DFT calculations indicated that the lowest-energy structures of the pseudo[3]rotaxane complexes are characterized by an *anti* conformation

around the O^{calix}-CH_2^{bridge} bonds which led to a spatial divergence of the two calix-cavities. Another important aspect concerns the *endo*-benzyl complexation observed only in the case of "*tert*-butylated" double-calix[6]arene **21** to form singly- and doubly-threaded pseudorotaxane architectures.

4.7 Experimental section

ESI(+)-MS measurements were performed on a Micromass Bio-Q triple quadrupole mass spectrometer equipped with electrospray ion source, using $CHCl_3$ as solvent. All chemicals were reagent grade and were used without further purification. When necessary compounds were dried in vacuo over $CaCl_2$. Reaction temperatures were measured externally. Derivative $\mathbf{2}^{+}\cdot TFPB^{-}$[77] , $\mathbf{3}^{+}\cdot TFPB^{-}$[77], and **12**[96] were synthesized according to literature procedures. NMR spectra were recorded on Bruker Avance-400 spectrometer [400 (1H) and 100 MHz (13C)], Bruker Avance-300 spectrometer [300 (1H) and 75 MHz (13C)], or Bruker Avance-250 spectrometer [250 (1H) and 63 MHz (13C)]; chemical shifts are reported relative to the residual solvent peak (CHCl3: δ 7.26, CDCl3: δ 77.23). COSY-45 spectra were taken using a relaxation delay of 2 seconds with 30 scans and 170 increments of 2048 points each. HSQC spectra were performed with gradient selection, sensitivity enhancement, and phase sensitive mode using Echo/Antiecho−TPPI procedure. A typical experiment comprised 20 scans with 113 increments of 2048 points each. Monte Carlo conformational searches (10000 steps) were performed with MacroModel-9/Maestro-4.1 program using $CHCl_3$ as solvent (GB/SA model). MD simulations were performed at T = 500 K, for 20000 ps, using a time step of 1.0 fs.

[96] Ciao, R.; Talotta, C.; Gaeta, C.; Margarucci, L.; Casapullo, A.; Neri, P., *Organic Letters,* 15(22), **2013,** 5694.

4.7.1 Synthesis and characterization of double-calixarene 12.[96]

CHART 1

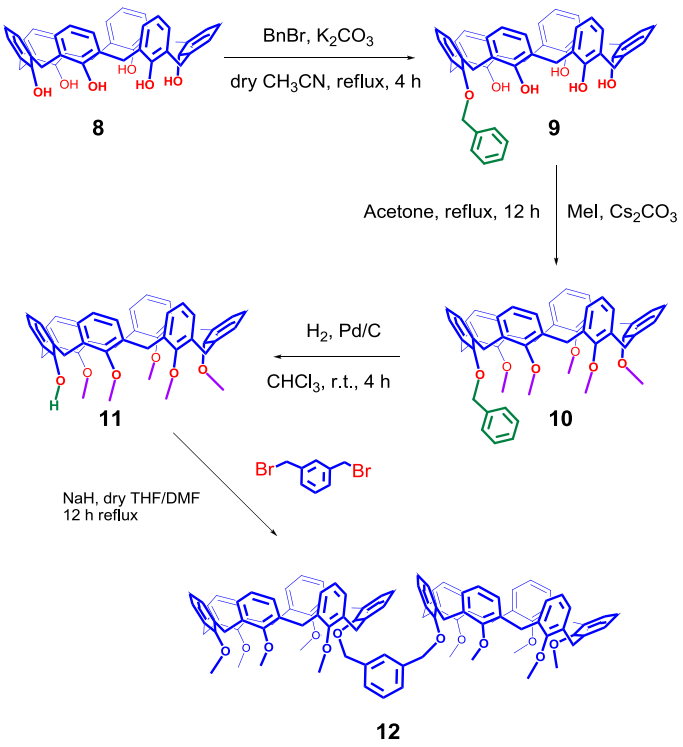

Synthesis of Double-Calix[6]arene 12

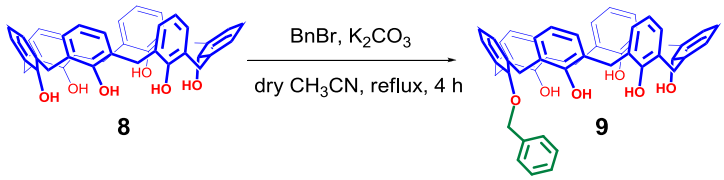

K_2CO_3 (0.94 g, 6.80 mmol) was added, under stirring, to a solution of *p*-H-calix[6]arene **8** (4.00 g, 6.30 mmol) in dry CH_3CN (300 mL). The mixture was kept at reflux under stirring, and after 1 h benzylbromide (0.82 mL, 1.18 g, 6.80 mmol) was added. The reaction was stirred at reflux for 3 h, then the solvent was removed under reduced pressure and the mixture was

partitioned between CH_2Cl_2 and H_2O. The organic layer was washed with 1N HCl (50 mL), brine (50 mL) and dried over Na_2SO_4. The crude product was triturated with methanol, collected by filtration, and dried, to give **9** as a white solid (3.74 g, 5.17 mmol, 76%), which was sufficiently pure for subsequent synthetic manipulations. **ESI(+) MS**: *m*/*z* = 727 (MH^+); **^{1}H NMR** (400 MHz, $CDCl_3$, 323 K): δ 9.68 (s, OH, 2H), 9.58 (s, OH, 1H), 8.66 (s, OH, 2H), 7.72 (br d, ArH, 2H), 7.60 (br t, ArH, 2H), 7.40 (br t, ArH, 1H), 7.11−6.77 (overlapped, ArH, 18H), 5.22 (s, OCH_2Ar, 2H), 4.01 (br s, $ArCH_2Ar$, 4H), 3.92 (s, $ArCH_2Ar$, 4H), 3.71 (s, $ArCH_2Ar$, 4H); **^{13}C NMR** (63 MHz, $CDCl_3$, 298 K): δ 152.6, 151.8, 150.8, 149.4, 136.4, 133.5, 129.7, 129.6, 129.4, 129.2, 129.1, 129.0, 128.7, 128.1, 127.7, 125.7, 122.1, 121.4, 120.8, 77.9, 32.2, 32.1, 32.09; Anal. Calcd for $C_{49}H_{42}O_6$: C, 80.97; H, 5.82. Found: C, 81.05; H, 5.73.

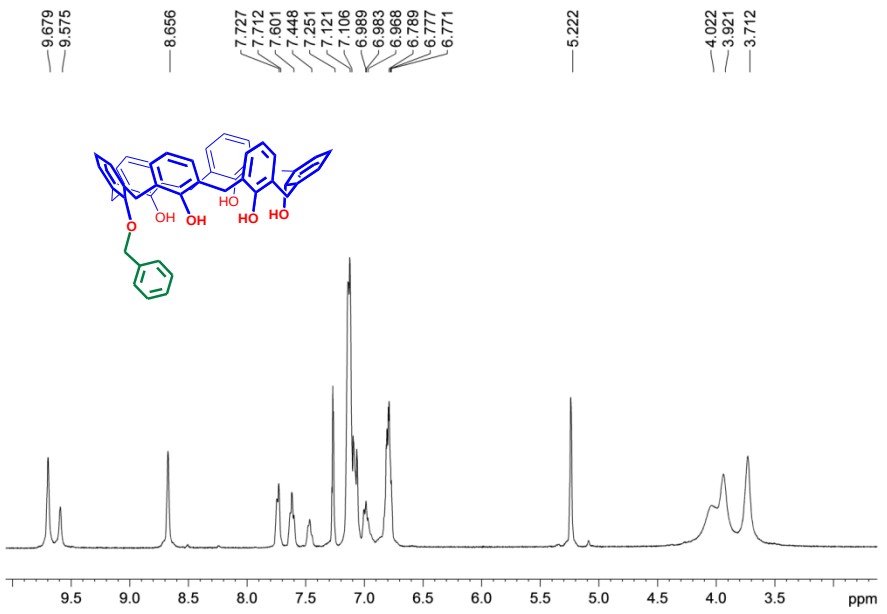

Figure 86. ^{1}H NMR spectrum of derivative **9** (400 MHz, $CDCl_3$, 323 K).

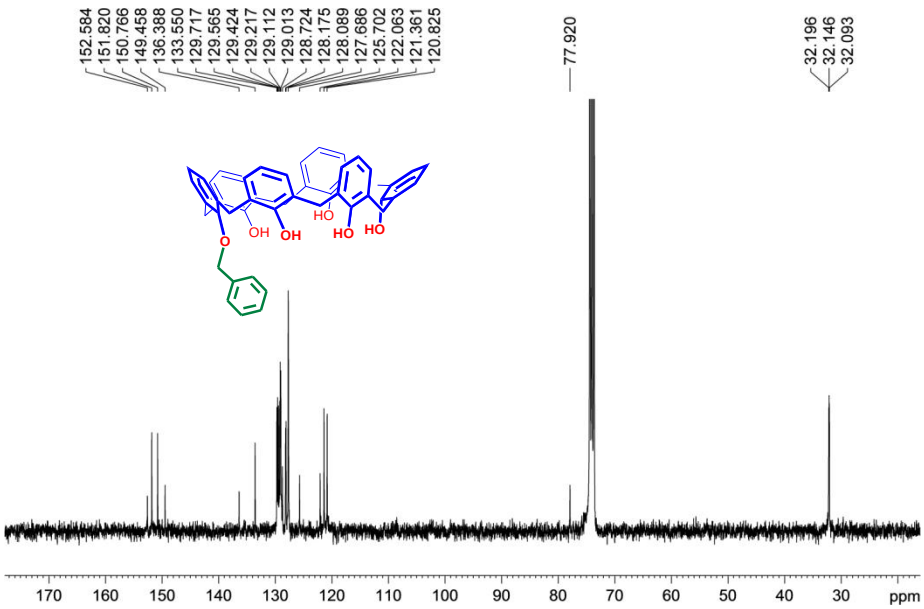

Figure 87. ^{13}C NMR spectrum of derivative **9** (63 MHz, $CDCl_3$, 298 K).

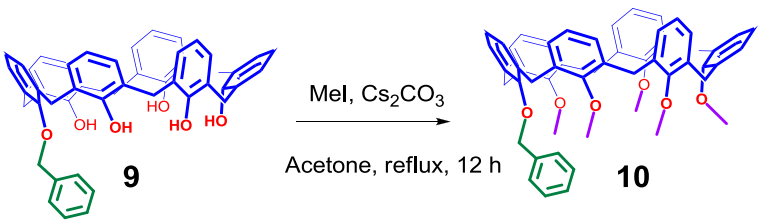

A solution of **9** (3.74 g, 5.17 mmol) in acetone (300 mL) was added of Cs_2CO_3 (15 g, 46 mmol). The mixture was stirred at the reflux temperature for 2 h and then iodomethane (15 g , 6.6 mL, 106 mmol) was added. The reaction mixture was stirred for 12 h under reflux. The solution was concentrated to dryness and the residue was partitioned between 1 N HCl (50 mL) and CH_2Cl_2 (50 mL). The organic phase was washed with water (3×30 mL) and dried over Na_2SO_4. Solvent evaporation under vacuum afforded a crude product that was triturated with methanol, collected by filtration, and dried, to give **10** as a white solid (3.70 g, 4.64 mmol, 90%), which was sufficiently pure for subsequent synthetic manipulations. **ESI(+)**

MS: *m*/*z* 797 (MH^+); **^{1}H NMR** (250 MHz, $CDCl_3$, 298 K) δ: 7.40− 6.79 (overlapped, ArH, 23H), 4.76 (s, OCH_2Ar, 2H), 3.99, 3.97, 3.94 (s, $ArCH_2Ar$, 4H each one), 3.23 (s, OCH_3, 6H), 3.13 (s, OCH_3, 3H), 2.97 (s, OCH_3, 6H); **^{13}C NMR** (63 MHz, $CDCl_3$, 298 K): δ 156.2, 156.1, 154.6, 137.8, 134.9, 134.75, 134.71, 134.58, 134.56, 134.4, 129.8, 129.6, 129.3, 128.9, 128.7, 128.5, 128.3, 127.9, 127.8, 123.8, 123.6, 123.5, 74.9, 60.3, 60.2, 30.6, 30.4, 29.8. Anal. Calcd for $C_{54}H_{52}O_6$: C, 81.38; H, 6.58. Found: C, 81.45; H, 6.49.

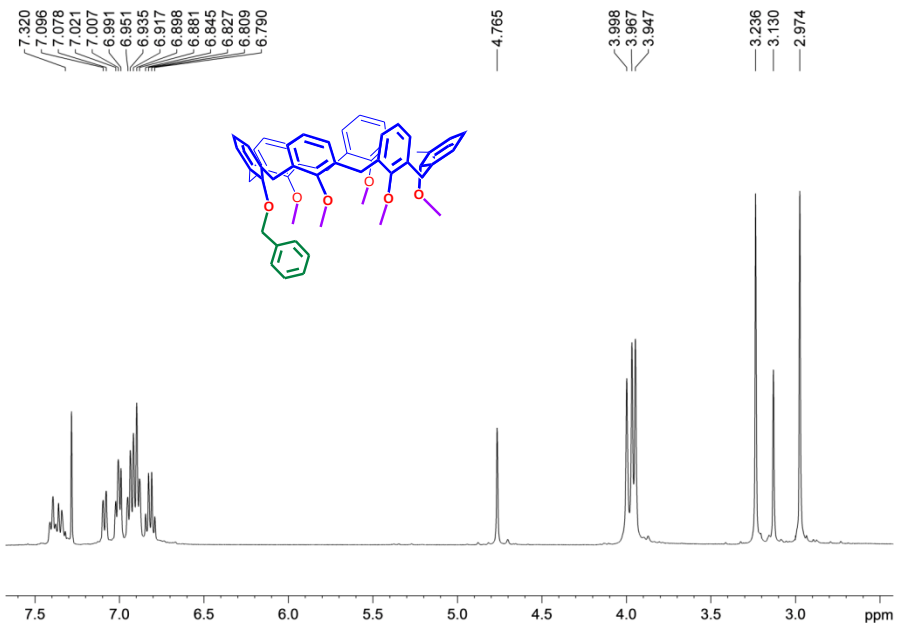

Figure 88. ^{1}H NMR spectrum of derivative **10** (250 MHz, $CDCl_3$, 298 K).

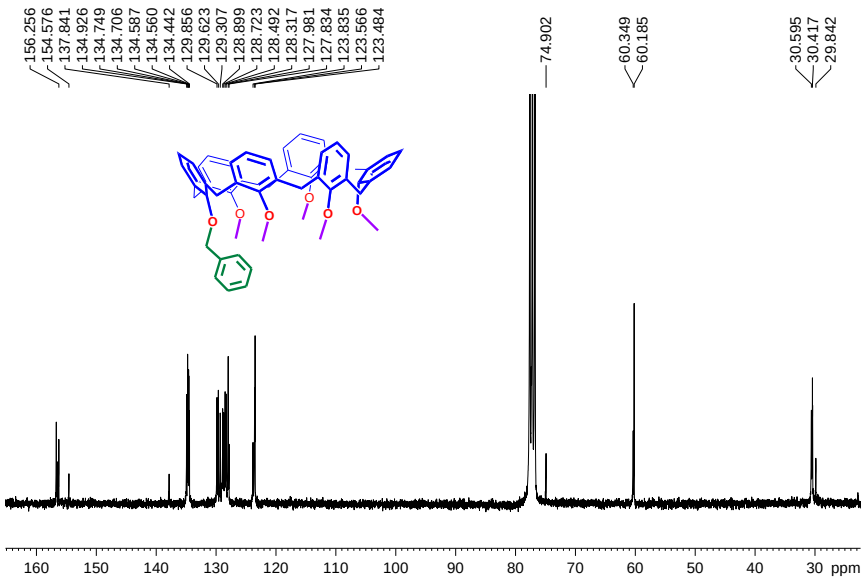

Figure 89. ^{13}C NMR spectrum of derivative **10** (63 MHz, $CDCl_3$, 298 K).

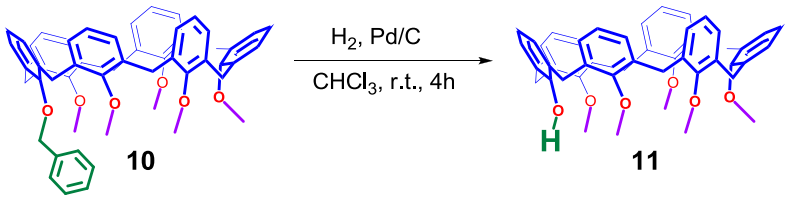

A solution of **10** (3.70 g, 4.64 mmol) in $CHCl_3$ (400 mL) was added of Pd/C (10%) and stirred for 4 h under H_2 at 25 °C. After filtration of the catalyst, the solvent was evaporated to give **11** (1.47 g, 2.07 mmol, 45%). **ESI(+) MS**: *m/z* 707 (MH^+); **^{1}H NMR** (300 MHz, $CDCl_3$, 298 K): δ 7.38 (s, OH, 1H), 7.12−6.72 (overlapped, ArH, 18H), 3.99 (s, $ArCH_2Ar$, 8H), 3.85 (s, $ArCH_2Ar$, 4H),), 3.57 (s, OMe, 3H), 3.34 (s, OMe, 6H), 3.23 (s, OMe, 6H); **^{13}C NMR** (63 MHz, $CDCl_3$, 298 K): δ 156.8, 156.6, 155.1, 152.3, 134.34, 134.32, 134.1, 134.07, 133.4, 129.7, 129.3, 128.9, 127.2, 124.3, 123.5, 123.4, 119.6, 61.0, 60.5, 60.3, 31.4, 31.1, 30.6. Anal. Calcd for $C_{47}H_{46}O_6$: C, 79.86; H, 6.56. Found: C, 79.95; H, 6.45.

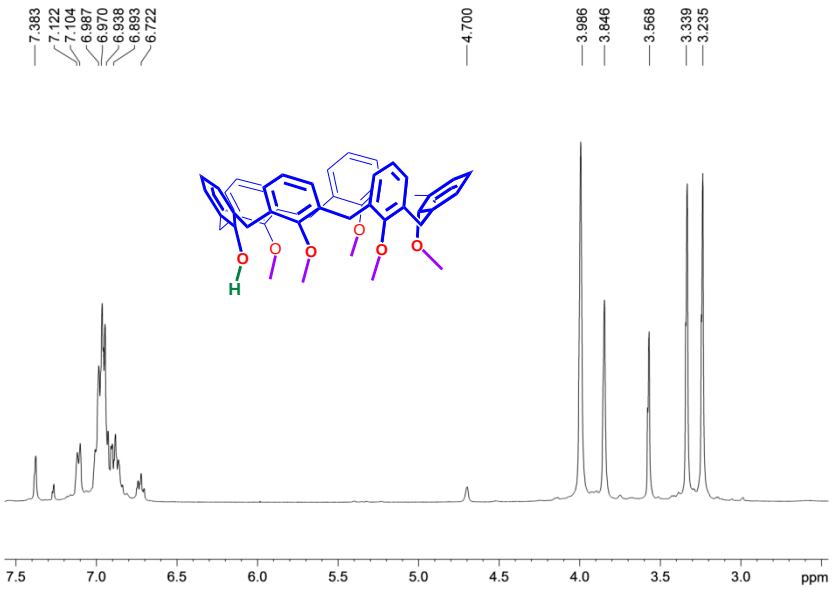

Figure 90. ^{1}H NMR spectrum of derivative **11** (300 MHz, $CDCl_3$, 298 K).

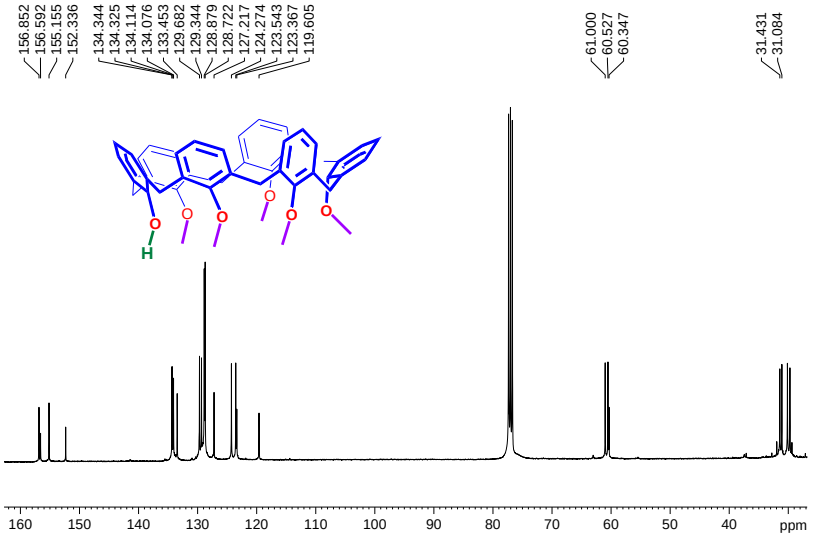

Figure 91. ^{13}C NMR spectrum of derivative **11** (63 MHz, $CDCl_3$, 298 K).

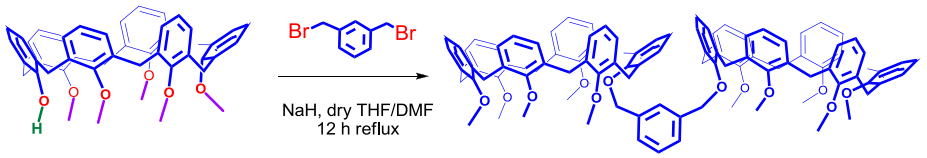

11 **12**

NaH (1.30 g, 54.2 mmol) was added at 0 °C, under stirring, to a solution of derivative **11** (1.47 g, 2.07 mmol) in dry THF/DMF (75 mL, 7/3 *v/v*). The mixture was kept at 25 °C under stirring, and after 1 h, 1,3-bis(bromomethyl)benzene (0.26 g, 0.98 mmol) was added. The reaction was stirred at reflux for 12 h under a nitrogen atmosphere, then the solvent was removed under reduced pressure and the mixture was partitioned between CH_2Cl_2 and H_2O. The organic layer was washed with 1N HCl (50 mL), brine (50 mL), and dried over Na_2SO_4. The crude product was purified by column chromatography (SiO_2; Et_2O/CH_2Cl_2 3/97) to give derivative **12** as a white solid (1.04 g, 0.69 mmol, 33%).

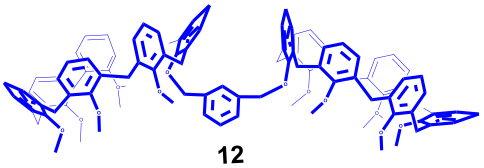

12

ESI(+) MS: *m/z* = 1516 (MH^+); ^{1}H NMR (400 MHz, $CDCl_3$, 298 K): δ 7.06-6.78 (overlapped ArH, 40H), 4.80 (s, OCH_2Ar, 4H), 3.96 (s, $ArCH_2Ar$, 8H), 3.92 (s, $ArCH_2Ar$, 8H), 3.90 (s, $ArCH_2Ar$, 8H), 3.16 (s, OCH_3, 12H), 3.11 (s, OMe, 6H), 2.89 (s, OCH_3, 12H); ^{13}C NMR (75 MHz, $CDCl_3$, 298 K): δ 156.7, 156.6, 156.3, 154.5, 137.9, 134.9, 134.8, 134.7, 134.6, 134.5, 130.0, 129.7, 129.3, 128.9, 128.8, 128.7, 128.2, 127.5, 127.4, 123.6, 74.9, 60.4, 60.2, 30.7, 30.4. Anal. Calcd for $C_{102}H_{98}O_{12}$: C, 80.82; H, 6.52. Found: C, 81.80; H, 6.43.

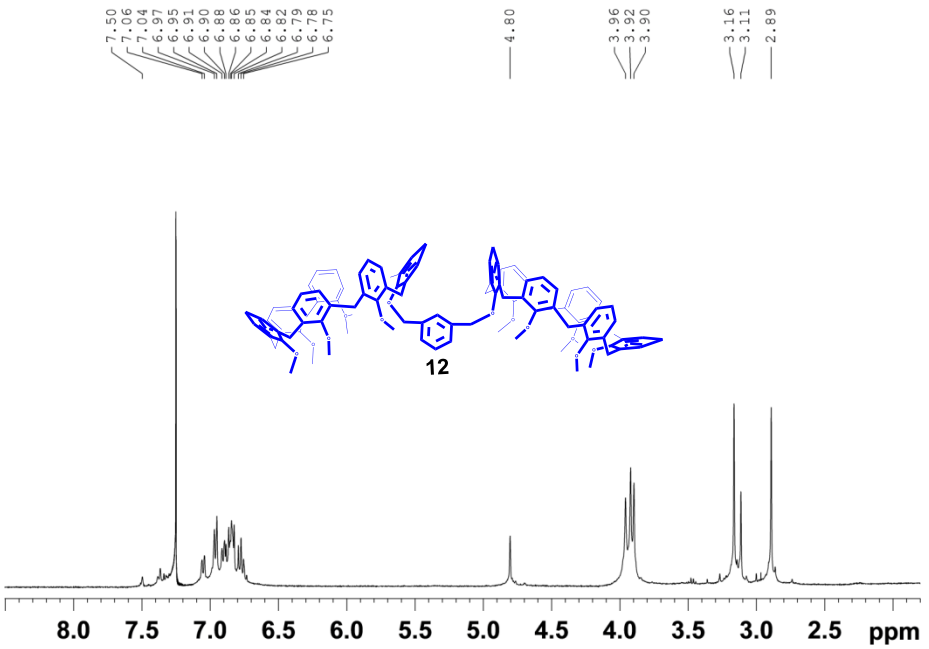

Figure 92. ^{1}H NMR spectrum of derivative **12** (400 MHz, $CDCl_3$, 298 K).

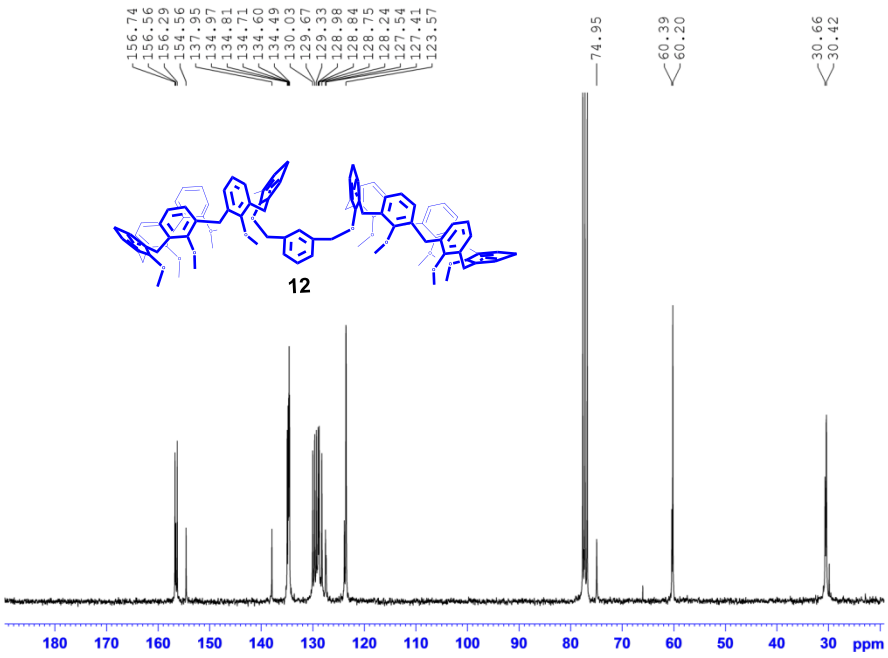

Figure 93. ^{13}C NMR spectrum of derivative **12** (75 MHz, $CDCl_3$, 298 K).

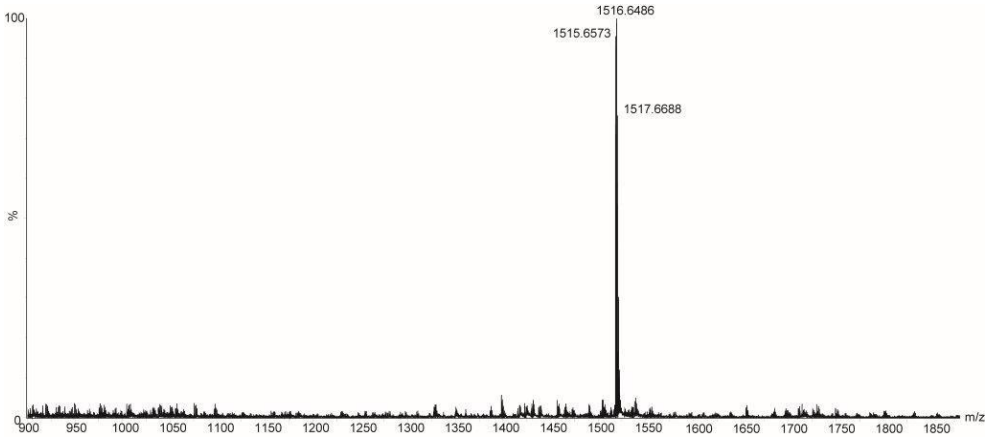

Figure 94. ESI(+) MS spectrum of derivative **12**.

4.7.2 Preparation of singly-threaded pseudo[2]rotaxanes 13,17.

Derivative 13

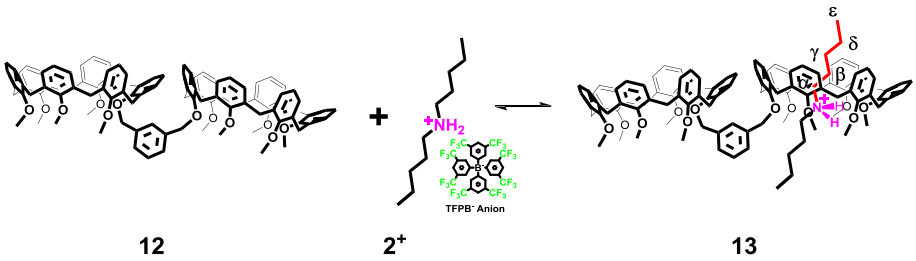

12 **2^+** **13**

Double-calixarene derivative **12** ($1.81 \cdot 10^{-3}$ g, $1.2 \cdot 10^{-3}$ mmol) and the ialkylammonium derivative $\mathbf{2}^+$ ($1.2 \cdot 10^{-3}$ mmol) were dissolved in 0.4 mL of $CDCl_3$ and the mixture was stirred for 5 min at 25 °C. Then, the solution was transferred in a NMR tube for 1D and 2D NMR spectra acquisition. Selected

spectral data for singly threaded pseudo[2]rotaxane ion **2**$^{+}\subset$**12.** ESI(+) MS: *m*/*z* = 1672.4 [**2**$\subset$**12**]$^{+}$. ^{1}H NMR ($CDCl_3$, 400 MHz, 298 K): δ −1.07 [broad, $(CH_2)_\beta$, 2H], −0.17 [broad, $(CH_2)_\gamma$, 2H], −0.02 [broad, $(CH_2)_\alpha$, 2H], 0.37 [broad, $(CH_2)_\delta$ + $(CH_3)_\varepsilon$, 5H], 3.53 and 4.29 (broad overlapped, $ArCH_2Ar$, 24H), 2.87, 2.99, 3.23 (br s, OCH_3, 6H, 3H, 6H), 3.78, 3.84, 3.90 (br s, OCH_3, 3H, 6H, 6H), 4.79 (br s, OCH_2, 2H), 4.98 (br s, OCH_2, 2H), 6.63–6.99 (overlapped, ArH, 40H).

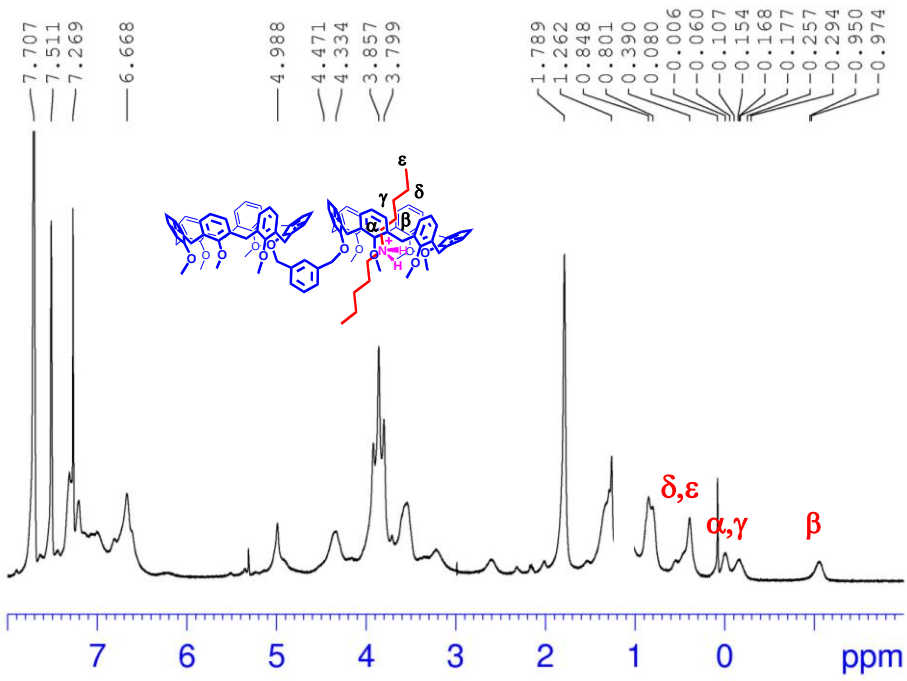

Figure 95. ^{1}H NMR spectrum (400 MHz, 298 K, $CDCl_3$) of the 1:1 mixture of **12** and **2**$^{+}$·$TFPB^{-}$.

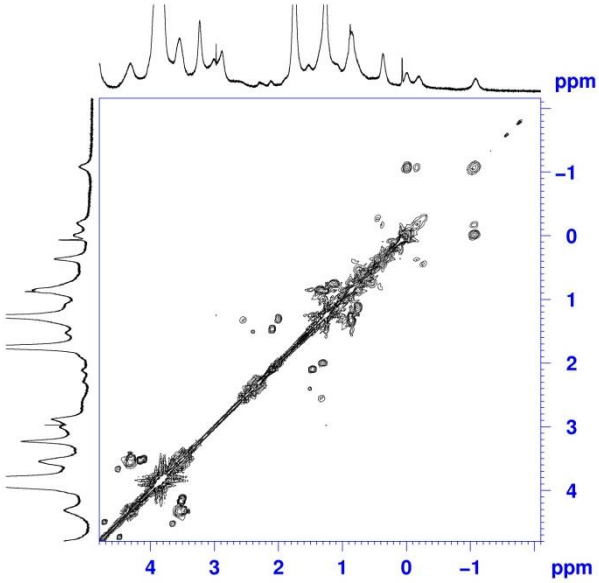

Figure 96. Significant portion of the 2D COSY spectrum (400 MHz, 298 K, $CDCl_3$) of the 1:1 mixture of **12** and **2**$^{+}$·TFPB^{-}.

Derivative 15.

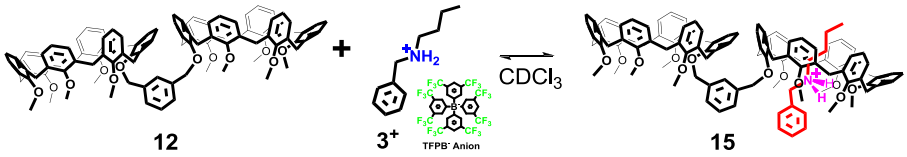

Double-calixarene derivative **12** ($2.0\cdot10^{-3}$ g, $1.3\cdot10^{-3}$ mmol) and the dialkylammonium derivative **3**$^{+}$ ($1.3\cdot10^{-3}$ mmol) were dissolved in 0.5 mL of $CDCl_3$ and the mixture was stirred for 5 min at 25 °C. Then, the solution was transferred in a NMR tube for 1D and 2D NMR spectra acquisition.

ESI(+) MS: *m*/*z* = 1680.3 [**3**⊂**12**]$^{+}$. ^{1}H NMR ($CDCl_3$, 400 MHz, 298 K): δ −1.02 [broad, $(CH_2)_\beta$, 2H], 0.04 [broad, $(CH_2)_\gamma + (CH_3)_\delta$, 5H], 0.22 [broad, $(CH_2)_\alpha$, 2H], 2.30 [broad, ($H_2N^+CH^\alpha_2Ph$), 2H], 2.87−3.93 (broad overlapped OCH_3+ $ArCH_2Ar$, 42H), 4.31−4.41 (broad overlapped, $ArCH_2Ar$, 12H), 4.78

(br s, OCH_2, 2H), 4.98 (br s, OCH_2, 2H), 5.37 (br s, $^+NH_2$, 2H), 6.76–7.40 (overlapped, ArH, 45H).

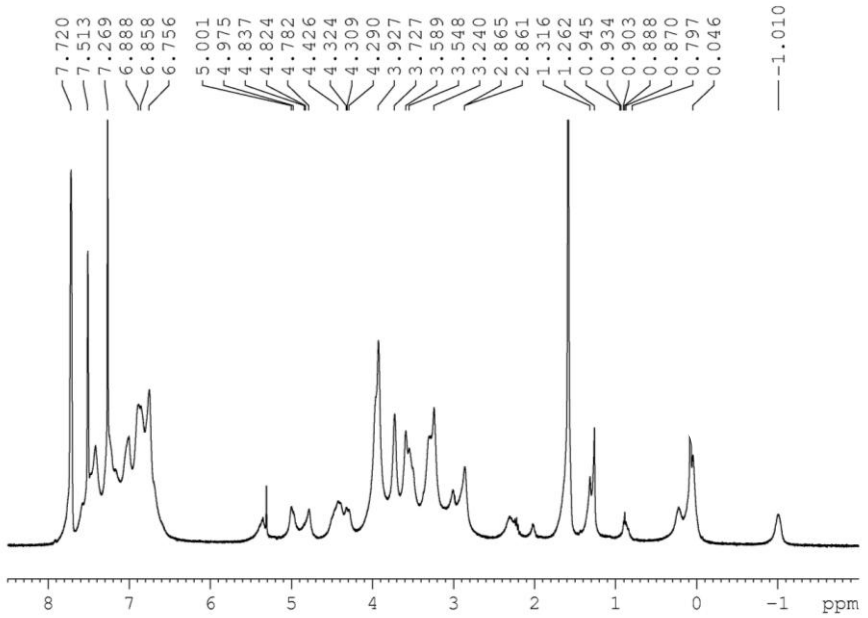

Figure 97. ^1H NMR spectrum (400 MHz, 298 K, $CDCl_3$) of the 1:1 mixture of **12** and **3**$^+$·TFPB$^-$.

4.7.3 Preparation of doubly threaded pseudo[3]rotaxanes 14,16

Derivative 14

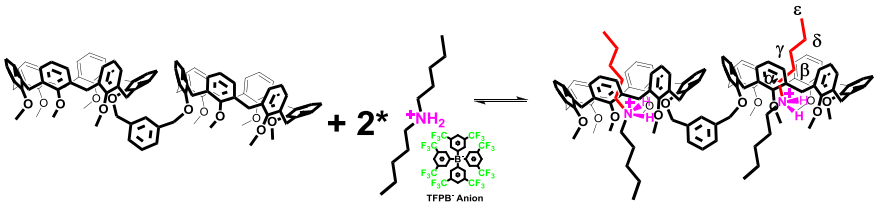

12 **2**$^+$ **14**

Double-calixarene derivative **12** ($1.81 \cdot 10^{-3}$ g, $1.2 \cdot 10^{-3}$ mmol) and the dialkylammonium derivative $\mathbf{2}^{+}$ ($2.4 \cdot 10^{-3}$ mmol) were dissolved in 0.4 mL of $CDCl_3$ and the mixture was stirred for 5 min at 25 °C. Then, the solution was transferred in a NMR tube for 1D and 2D NMR spectra acquisition. ESI(+) MS: *m*/*z* = 915.5 $[(\mathbf{2})_2 \subset \mathbf{12}]^{2+}$. ^{1}H NMR ($CDCl_3$, 400 MHz, 298 K): δ −1.07 [broad, $(CH_2)_\beta$, 4H], −0.18 [broad, $(CH_2)_\gamma$, 4H], −0.01 [broad, $(CH_2)_\alpha$, 4H], 0.39 [broad, $(CH_2)_\delta$ + $(CH_3)_\varepsilon$, 10H], 3.52 and 4.33 (broad, $ArCH_2Ar$, 24H), 3.79, 3.84, 3.91 (br s, OCH_3, 6H, 12H, 12H), 4.98 (br s, OCH_2, 4H), 6.66–7.61 (overlapped, ArH, 40H).

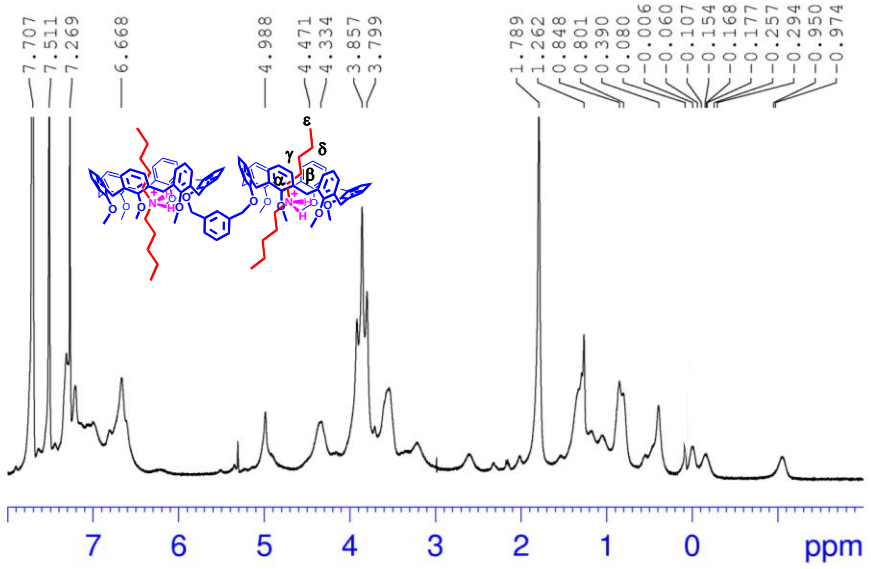

Figure 98. ^{1}H NMR spectrum (400 MHz, 298 K, $CDCl_3$) of the 1:2 mixture of **12** and $\mathbf{2}^{+}\cdot TFPB^{-}$.

Derivative 16

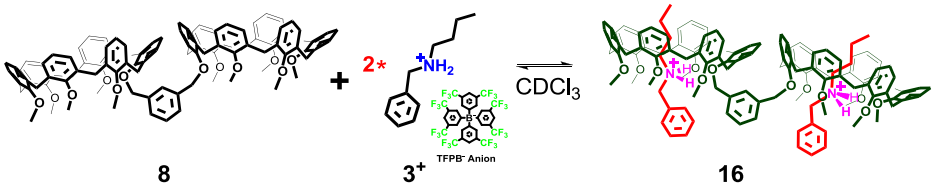

8 **3**$^{+}$ **16**

Double-calixarene derivative **12** ($2.0\cdot10^{-3}$ g, $1.3\cdot10^{-3}$ mmol) and the dialkylammonium derivative **3**$^{+}$ ($2.6\cdot10^{-3}$ mmol) were dissolved in 0.5 mL of $CDCl_3$ and the mixture was stirred for 5 min at 25 °C. Then, the solution was transferred in a NMR tube for 1D and 2D NMR spectra acquisition.

ESI(+) MS: *m*/*z* = 921.5 $[(\mathbf{3})_2\subset\mathbf{12}]^{2+}$. ^{1}H NMR ($CDCl_3$, 400 MHz, 298 K): δ −1.01 [broad, $(CH_2)_\beta$, 4H], 0.03 [broad, $(CH_2)_\gamma$ + $(CH_3)_\delta$, 10H], 0.23 [broad, $(CH_2)_\alpha$, 4H], 2.27 [broad, ($^+H_2NCH^\alpha_2Ph$), 4H], 3.28, 3.59, 3.70 (s, OCH_3, 6H, 12H, 12H), 3.50 and 4.44 (broad, $ArCH_2Ar$, 8H), 3.52 and 4.32 (broad, $ArCH_2Ar$, 8H), 3.58 and 4.43 (broad, $ArCH_2Ar$, 8H), 4.97 (br s, OCH_2, 4H), 5.35 (br s, $^+NH_2$, 4H), 6.64─7.59 (overlapped, ArH, 50H).

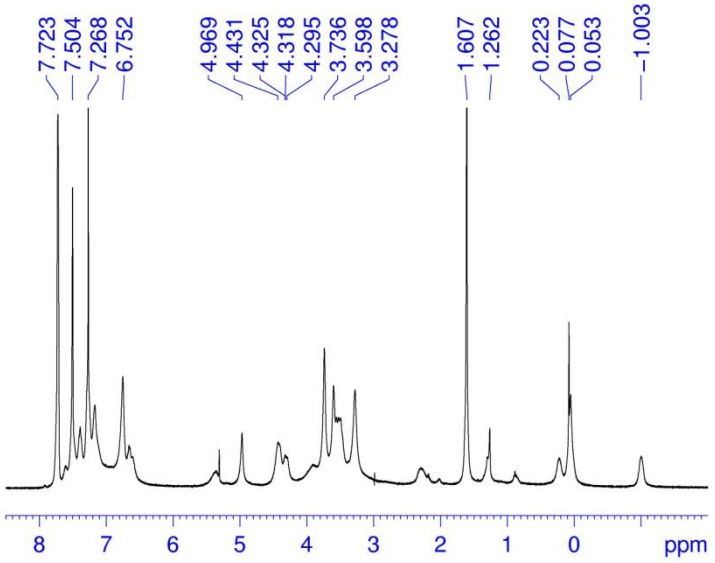

Figure 99. ^{1}H NMR spectrum (400 MHz, 298 K, $CDCl_3$) of the 1:2 mixture of **12** and **3**$^{+}$·TFPB^{-}.

4.7.4 *Synthesis and characterization of double-calixarene 21*

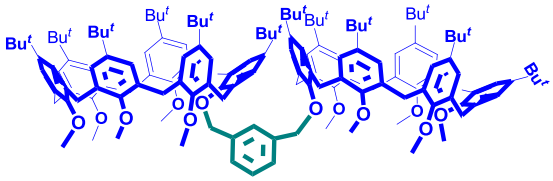

21

Synthesis of Double-Calix[6]arene 21

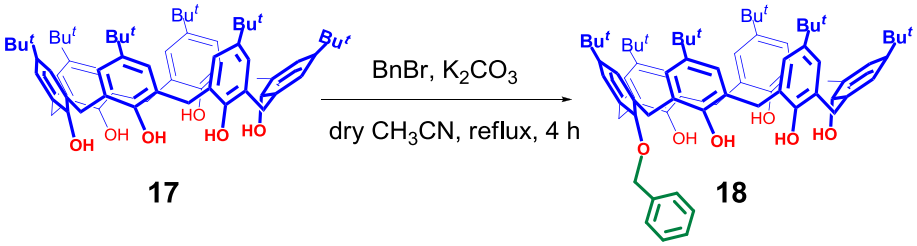

17 **18**

K_2CO_3 (8.0 g, 8.21 mmol) was added, under stirring, to a solution of *p-t-but*-calix[6]arene **17** (1.2 g, 9.0 mmol) in dry CH_3CN (300mL). The mixture was kept at reflux under stirring, and after 1 h benzylbromide (1.1 mL, 9.0 mmol) was added. The reaction was stirred at reflux for 3 h, then the solvent was removed under reduced pressure and the mixture was partitioned between CH_2Cl_2 and H_2O. The organic layer was washed with 1N HCl (100 mL), brine (100 mL) and dried over Na_2SO_4. The crude product was triturated with methanol, collected by filtration, and dried, to give **18** as a white solid (6.7 g, 6.31 mmol, 84%), which was sufficiently pure for subsequent

synthetic manipulations. **ESI(+) MS**: *m*/*z* = 1062 (MH^+); **^{1}HNMR** (250 MHz, $CDCl_3$, 298 K): δ 1.19 (s, C(C*H*$_3$)$_3$, 9H) 1.23 (s, C(C*H*$_3$)$_3$, 9H), 1.29 -1.28 (s, C(C*H*$_3$)$_3$, 36H), 4.02 e 3.39 (AX, ArC*H*$_2$Ar, *J*=13.9 Hz, 4H), 4.27 e 3.56 (AX, ArC*H*$_2$Ar, *J*=14.0 Hz, 4H), 4.45 e 3.54 (AX, ArC*H*$_2$Ar, *J*=13.4 Hz, 4H), 5.21 (s, C*H*$_2$Ar$_{Bn}$, 2H), 7.17-7.09 (overlapped, Ar*H* $_{calix}$, 12H), 7.45 (m, Ar*H* $_{Bn}$, 1H), 7.64 (m, Ar*H* $_{Bn}$, 2H), 7.78 (m, Ar*H* $_{Bn}$, 2H), 9.12 (s, *OH*, 2H), 9.82 (s, *OH*, 1H),10.02 (s, *OH*, 2H),. **^{13}CNMR** (250 MHz, $CDCl_3$, 298 K): δ 31.8 (2), 32.9, 33.5, 34.1, 34.2, 34.5, 78.1, 125.6, 125.9,126.2, 126.4, 126.9, 127.0, 127.2, 127.4, 127.6, 128.6129.3,132.7, 136.6, 143.1, 143.7, 144.6, 146.7, 148.3, 148.4, 149.4, 149.6,

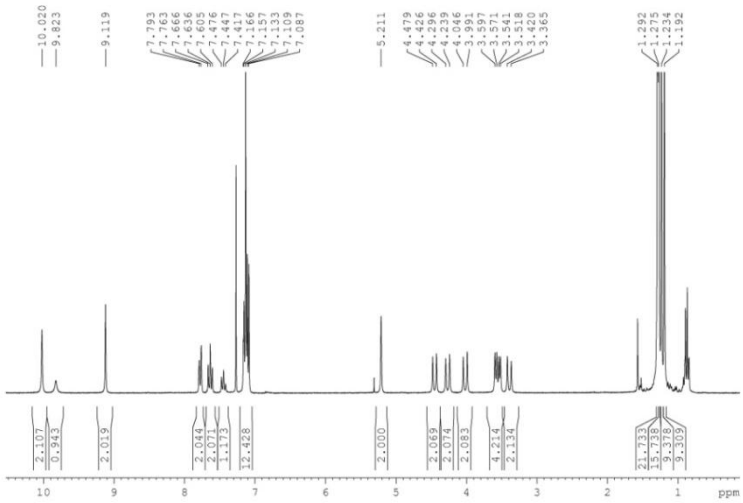

Figura 100. Spectrum ^{1}H NMR of derivative **18** in $CDCl_3$ (250 MHz, 298 K).

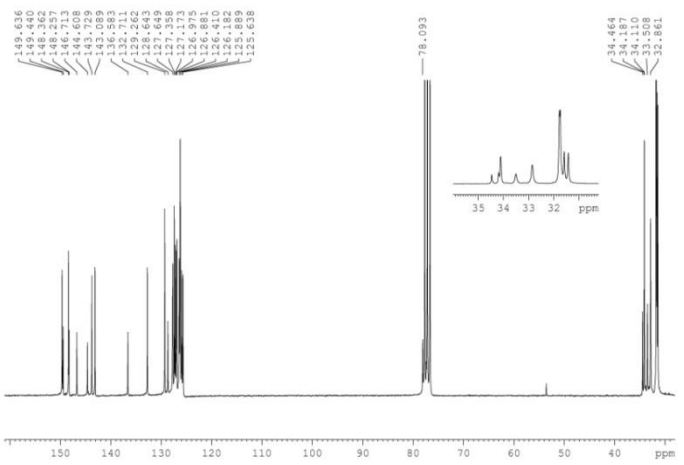

Figura 101. Spectrum ^{13}C NMR del derivato **18** in $CDCl_3$ (250 MHz, 298 K).

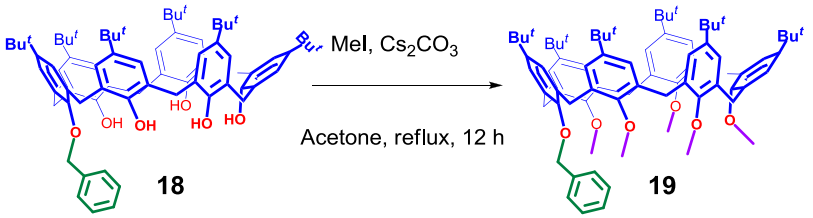

A solution of **18** (6.7 g, 6.31 mmol) in acetone (300 mL) was added of Cs_2CO_3 (18.5 g, 56.8 mmol). The mixture was stirred at the reflux temperature for 2 h and then iodomethane (17.3 g , 7.6 mL, 126.2 mmol) was added. The reaction mixture was stirred for 12 h under reflux. The solution was concentrated to dryness and the residue was partitioned between 1 N HCl (100 mL) and CH_2Cl_2 (100 mL). The organic phase was washed with water (3×90 mL) and dried over Na_2SO_4. Solvent evaporation under vacuum afforded a crude product that was triturated with methanol, collected by filtration, and dried, to give **19** as a white solid (6.03 g, 5.32 mmol, 90%), which was sufficiently pure for subsequent synthetic

manipulations. ESI(+) MS: *m*/*z* 1132 (MH^+); ^{1}HNMR (250 MHz, $CDCl_3$, 298 K): δ 1.03 -0.97 (s, C(CH_3)$_3$, 18H), 1.25 -1.24 (s, C(CH_3)$_3$, 27H), 2.53 (s, OCH_3, 6H), 2.78 (s, OCH_3, 3H), 3.20 (s, OCH_3, 6H), 4.05 e 3.54 (AX, ArCH_2Ar, *J*=14.2Hz, 4H), 4.18 e 3.82 (AX, ArCH_2Ar, *J*=15.3 Hz, 4H), 4.46 e 3.68 (AX, ArCH_2Ar, *J*=14.7 Hz, 4H), 4.88 (s, CH_2Ar$_{Bn}$, 2H), 7.55- 6.9 (overlapped, ArH_{calix} e ArH_{Bn}, 16H); **^{13}CNMR** (250 MHz, $CDCl_3$, 298 K): δ 31.4, 31.5, 31.6, 34.2, 34.3, 60.0, 60.1, 60.2, 74.5, 77.4, 124.7, 125.2, 125.3, 126.9, 127.0, 127.4, 127.9, 128.6, 133.3, 133.4, 133.5, 133.7, 134.0, 138.0, 145.8 (2), 146.0, 152.2, 153.7, 154.4, 154.5.

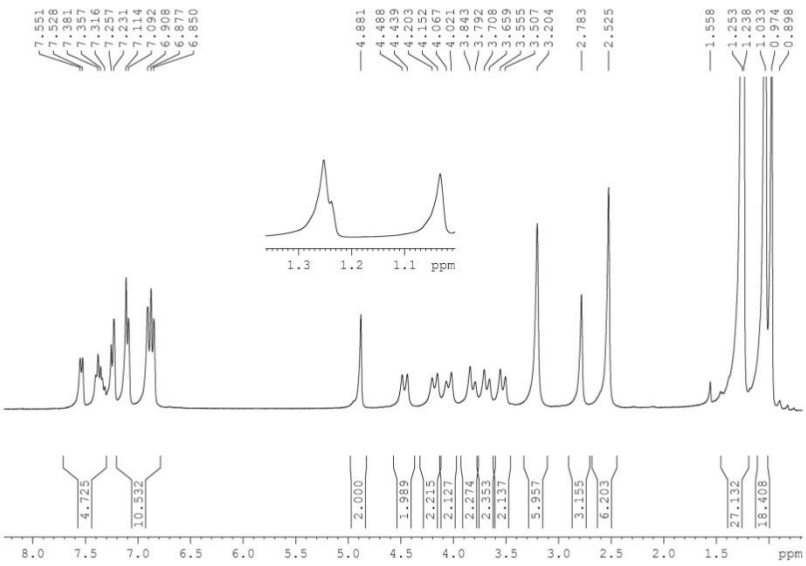

Figura 102. Spectrum ^{1}H NMR of derivative **19** in $CDCl_3$ (250 MHz, 298 K).

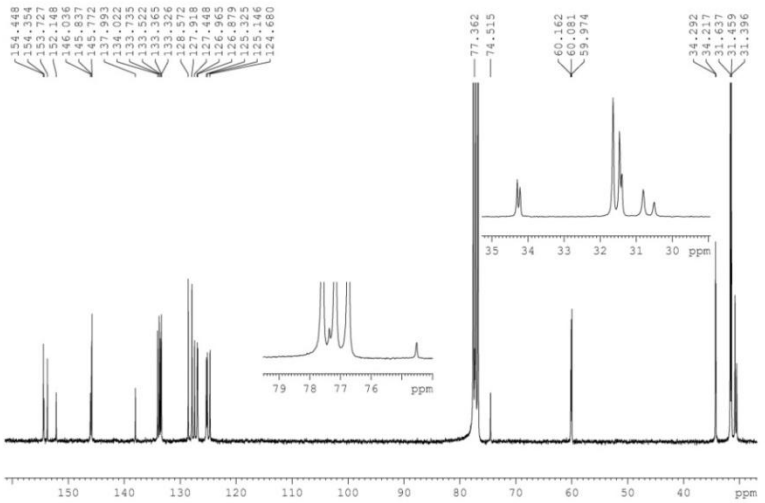

Figura 103. Spectrum ^{13}C NMR of derivative **19** in $CDCl_3$(250 MHz, 298 K).

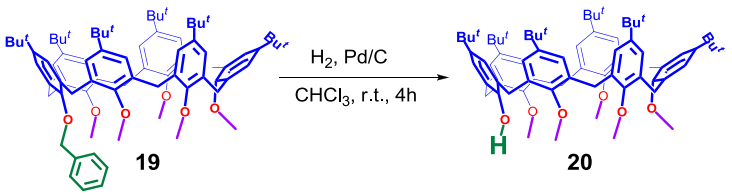

A solution of **19** (6.0 g, 5.32 mmol) in $CHCl_3$ (400 mL) was added of Pd/C (10%) and stirred for 4 h under H_2 at 25 °C. After filtration of the catalyst, the solvent was evaporated to give **20** (5.4 g, 5.23 mmol, 90%). **ESI(+) MS**: *m*/*z* 1032 (MH^+);**^{1}HNMR** (250 MHz, $CDCl_3$, 298 K): δ 1.12 (s, C(C*H*$_3$)$_3$, 9H) 1.19 - 1.17 (s, C(C*H*$_3$)$_3$, 45H), 3.07 (s, OC*H*$_3$, 12H), 3.52 (s, OC*H*$_3$, 3H), 3.82 (broad, ArC*H*$_2$Ar, 4H), 3.97 e 3.94 (broad, ArC*H*$_2$Ar, 8H), 6.80 (s, Ar*H*$_{calix}$, 2H), 6.89 (s, Ar*H*$_{calix}$, 2H), 7.04- 7.01 (overlapped, Ar*H*$_{calix}$, 6H), 7.12- 7.11 (overlapped, Ar*H*$_{calix}$, 2H), 7.38 (s, O*H*),.**^{13}CNMR** (250 MHz, $CDCl_3$, 298 K): δ 31.4, 31.6 (2), 34.1, 34.2, 34.4, 60.8, 61.1, 77.5, 124.9, 125.6, 125.9, 126.3, 126.5, 126.7, 127.3, 132.8, 133.4, 133.6, 133.9, 142.2, 145.3, 146.0, 146.7, 149.7, 153.3, 154.2, 154.6.

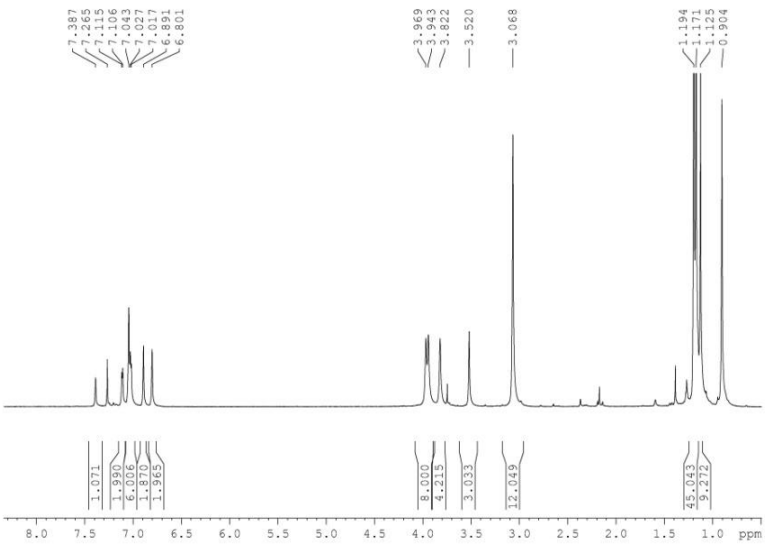

Figura 104. Spectrum ^{1}H NMR of derivative **20** in $CDCl_3$ (400 MHz, 298 K).

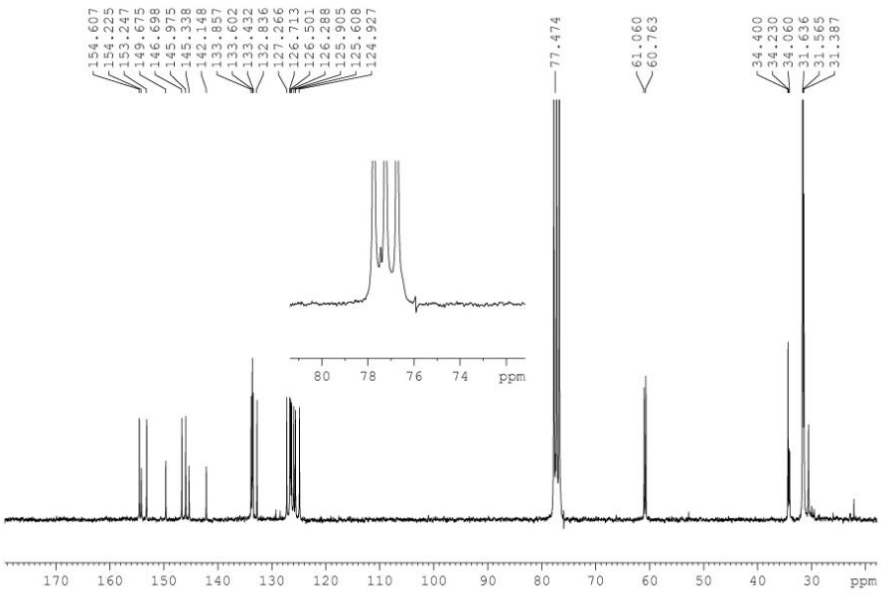

Figura 105. Spectrum ^{13}C NMR of derivative **20** in $CDCl_3$ (250 MHz, 298 K).

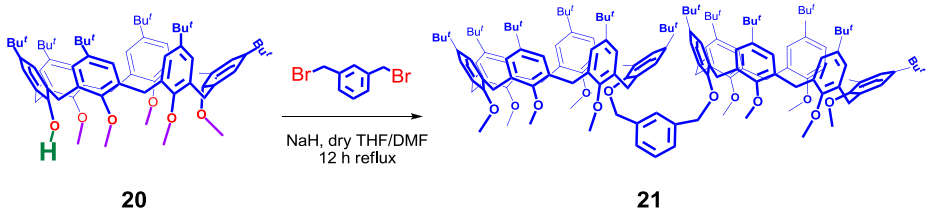

20 **21**

NaH (1.30 g, 54.2 mmol) was added at 0 °C, under stirring, to a solution of derivative **20** (1.47 g, 2.07 mmol) in dry THF/DMF (75 mL, 7/3 *v/v*). The mixture was kept at 25 °C under stirring, and after 1 h, 1,3-bis(bromomethyl)benzene (0.26 g, 0.98 mmol) was added. The reaction was stirred at reflux for 12 h under a nitrogen atmosphere, then the solvent was removed under reduced pressure and the mixture was partitioned between CH_2Cl_2 and H_2O. The organic layer was washed with 1N HCl (50 mL), brine (50 mL), and dried over Na_2SO_4. The crude product was purified by column chromatography (SiO_2; Et_2O/CH_2Cl_2 3/97) to give derivative **21** as a white solid (1.04 g, 0.69 mmol, 80%). **ESI(+) MS**: *m/z* 2188 (MH^+) (**Figure 107**); **^{1}HNMR** (400 MHz, $CDCl_3$, 298 K): δ 1.07 (s, C(C*H*$_3$)$_3$, 36H), 1.24 (2) (overlapped C(C*H*$_3$)$_3$, 54H), 2.58 (s, OC*H*$_3$, 18H), 2.82 (s, OC*H*$_3$, 9H), 3.15 (s, OC*H*$_3$, 18H), 3.83 e 3.68 (AX, ArC*H*$_2$Ar, *J*=15.1Hz, 6H), 4.17 - 4.04 (AX, ArC*H*$_2$Ar, *J*=14.5Hz, 6H), 4.50 - 3.58 (AX, ArC*H*$_2$Ar, *J*=14.7Hz, 6H), 5.06 (s, Ar*H* $_{Bn}$,6H), 6.94 – 6.87 (overlapped, Ar*H*$_{calix}$, 18H), 7.11 - 7.06 (overlapped Ar*H*$_{calix}$, 12H), 7.28 - 7.26 (overlapped Ar*H*$_{calix}$, 6H), 7.78 (s, Ar*H,* 3H); **^{13}CNMR** (250 MHz, $CDCl_3$, 298 K): δ 14.4, 22.7, 30.6, 30.8, 31.5 (2), 31.7(2), 31.8, 34.3 (2), 60.0, 60.2, 74.8, 75.9, 77.5, 124.8, 125.3, 125.5, 126.9, 127.5, 133.4, 133.6, 133.7, 133.9, 134.1, 138.8, 145.7, 145.9, 152.4, 153.9, 154.4, 154.5.

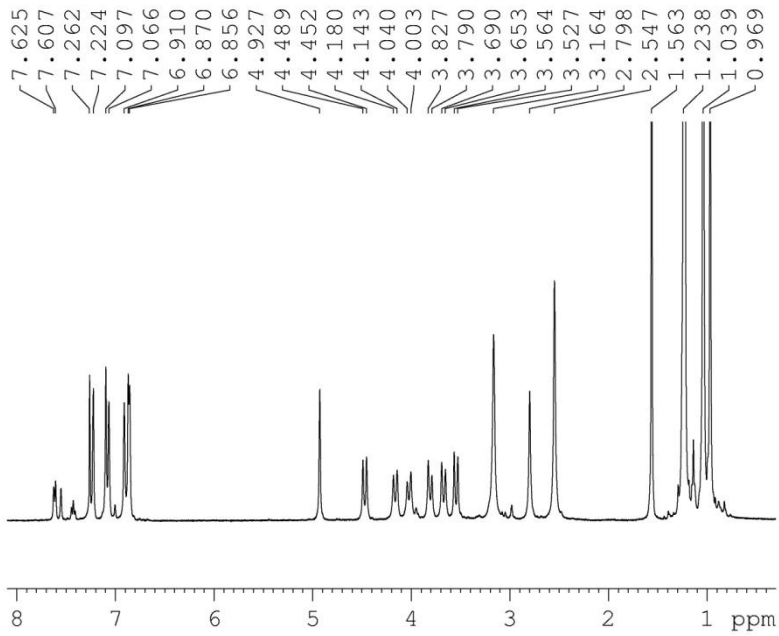

Figura 106. Spectrum ^{1}H NMR of derivative **21** in $CDCl_3$ (250 MHz, 298 K).

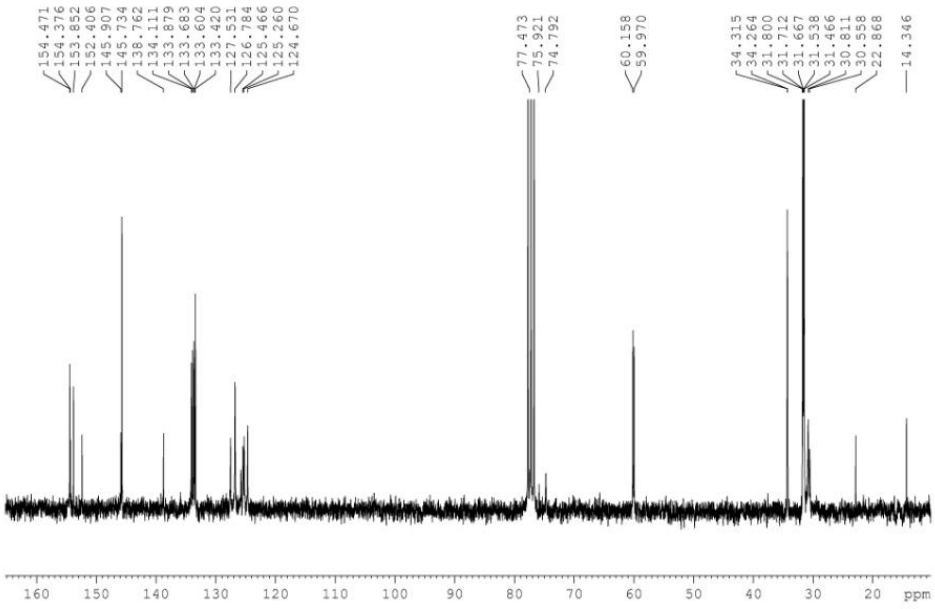

Figura 107. Spectrum ^{13}C NMR of derivative **21** in $CDCl_3$ (250 MHz, 298 K).

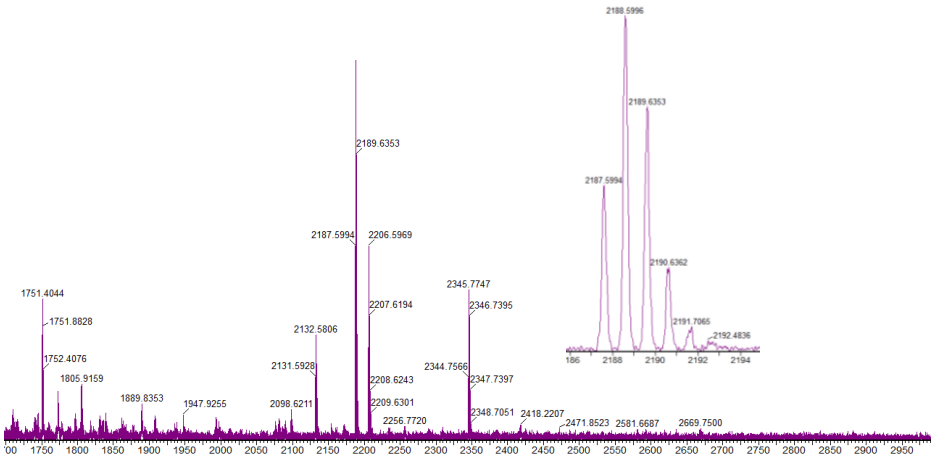

Figure108. ESI(+) MS spectrum of derivative **21**.

4.7.5 Preparation of singly-threaded pseudo[2]rotaxanes 22, 24, 26.

Derivative 22

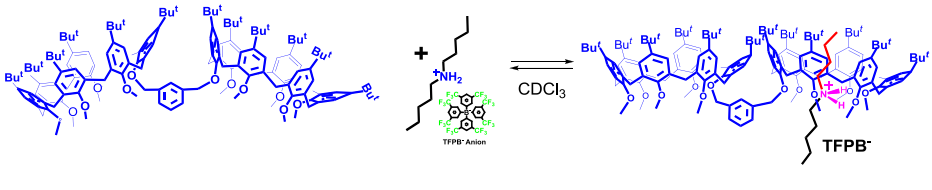

21 **2**$^{+}$ **22**

Double-calixarene derivative **21** ($2.0 \cdot 10^{-3}$ g, $0.91 \cdot 10^{-3}$ mmol) and the dialkylammonium derivative **2**$^{+}$ ($0.91 \cdot 10^{-3}$ mmol) were dissolved in 0.4 mL of

$CDCl_3$ and the mixture was stirred for 5 min at 25 °C. Then, the solution was transferred in a NMR tube for 1D and 2D NMR spectra acquisition. Selected spectral data for singly threaded pseudo[2]rotaxane ion **2**$^+$⊂**21.** ESI(+) MS: *m*/*z* = 2344.3 [**2**⊂**21**]$^+$. ^{1}H NMR ($CDCl_3$, 400 MHz, 298 K): δ −1.00 [broad, $(CH_2)_\beta$, 2H], −0.88 [broad, $(CH_2)_\gamma$, 2H], −0.52 [broad, $(CH_2)_\alpha$, 2H], -0.41 [broad, $(CH_2)_\delta$ + $(CH_3)_\varepsilon$, 5H], 3.18 and 4.24 (broad overlapped, $ArCH_2Ar$, 24H), 3.20, 3.54, 3.76 (br s, OCH_3, 6H, 3H, 6H), 3.78, 3.84, 3.90 (br s, OCH_3, 3H, 6H, 6H), 4.79 (br s, OCH_2, 2H), 4.85 (br s, OCH_2, 2H), 6.86–7.20 (overlapped, ArH, 40H).

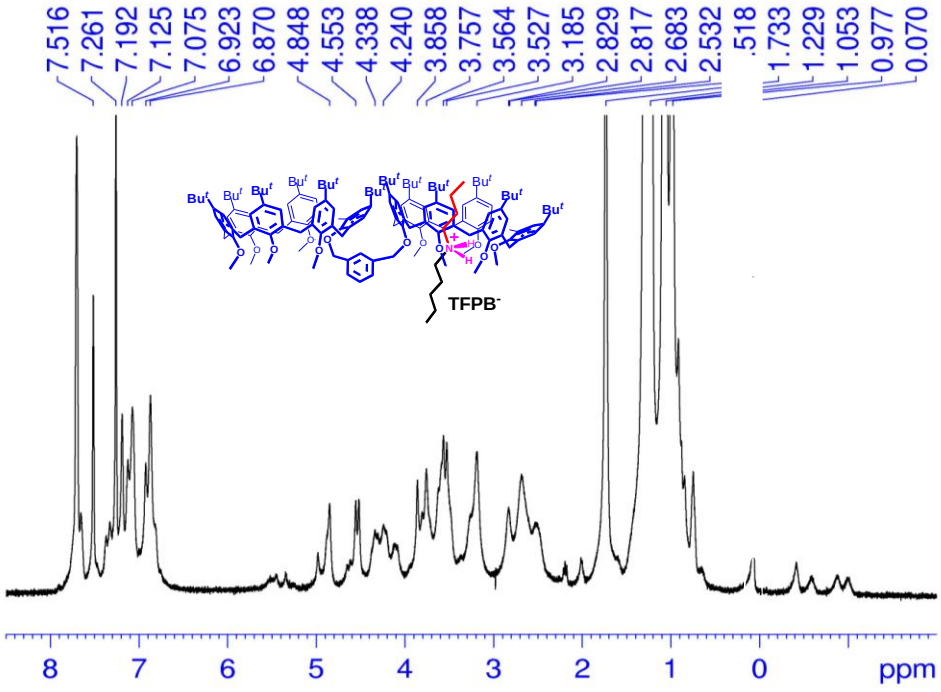

Figure 109. ^{1}H NMR spectrum (400 MHz, 298 K, $CDCl_3$) of the 1:1 mixture of **21** and **2**$^+$·TFPB$^-$.

Derivative 24

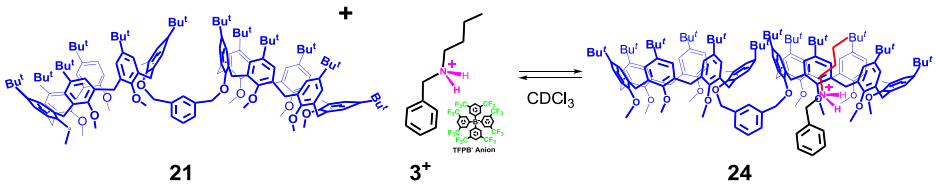

21 **3**$^{+}$ **24**

Double-calixarene derivative **21** ($2.0\cdot10^{-3}$ g, $0.91\cdot10^{-3}$ mmol) and the dialkylammonium derivative **3**$^{+}$ ($0.91\cdot10^{-3}$ mmol) were dissolved in 0.5 mL of $CDCl_3$ and the mixture was stirred for 5 min at 25 °C. Then, the solution was transferred in a NMR tube for 1D and 2D NMR spectra acquisition.

ESI(+) MS: *m*/*z* = 2350.3 [**3**⊂**21**]$^{+}$. ^{1}H NMR ($CDCl_3$, 400 MHz, 298 K): δ −1.02 [broad, $(CH_2)_\beta$, 2H], 0.04 [broad, $(CH_2)_\gamma + (CH_3)_\delta$, 5H], 0.22 [broad, $(CH_2)_\alpha$, 2H], 2.30 [broad, ($H_2N^+CH^\alpha_2Ph$), 2H], 2.87−3.93 (broad overlapped OCH_3+ $ArCH_2Ar$, 42H), 4.31−4.41 (broad overlapped, $ArCH_2Ar$, 12H), 4.78 (br s, OCH_2, 2H), 4.98 (br s, OCH_2, 2H), 5.37 (br s, $^{+}NH_2$, 2H), 6.76–7.40 (overlapped, ArH, 45H).

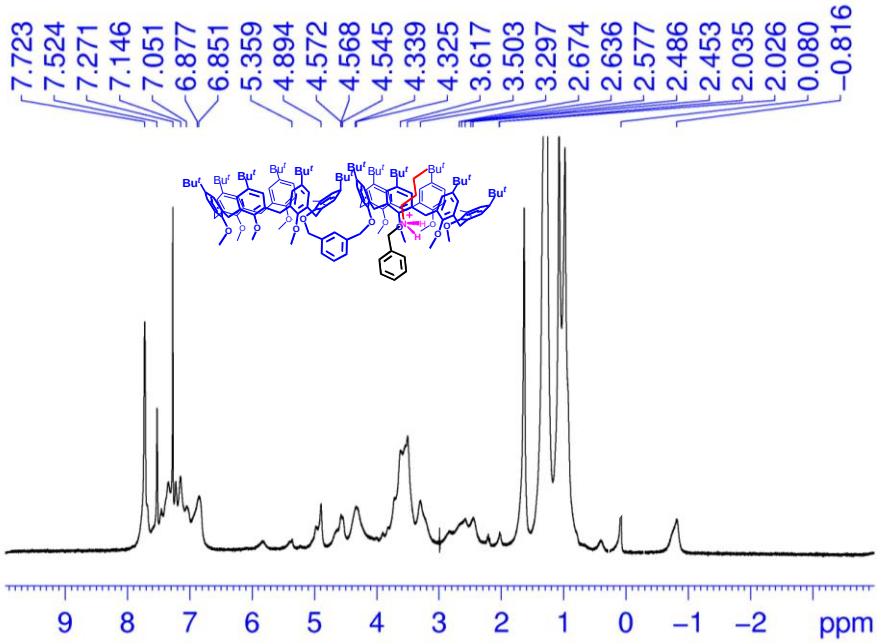

Figure 110. ^{1}H NMR spectrum (400 MHz, 298 K, $CDCl_3$) of the 1:1 mixture of **21** and **3**$^{+}$·TFPB^{-}.

Derivative 26

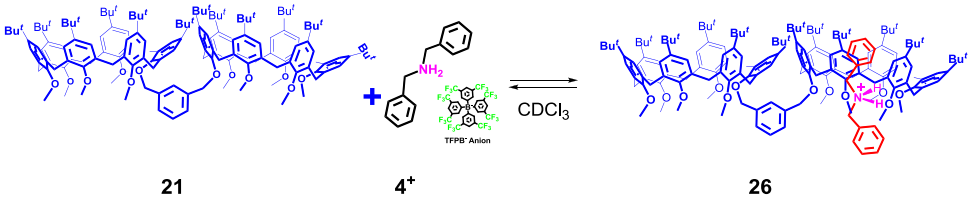

21 **4**$^{+}$ **26**

Double-calixarene derivative **21** ($2.0\cdot10^{-3}$ g, $0.91\cdot10^{-3}$ mmol) and the dibenzylammonium derivative **3**$^{+}$ ($1.3\cdot10^{-3}$ mmol) were dissolved in 0.5 mL of $CDCl_3$ and the mixture was stirred for 5 min at 25 °C. Then, the solution was transferred in a NMR tube for 1D and 2D NMR spectra acquisition.

^{1}H NMR (400 MHz, $CDCl_3$, 298 K): δ 1.04 [s, $(CH_3)_3C$-, 45H], 1.28 [s, $(CH_3)_3C$-, 45H], 1.38 [m, $(CH_2)_r$, 2H)], 1.53 [m, $(OCH_2)_j$, 2H], 1.61 [m, $(OCH_2)_x$, 2H], 3.45 and 4.39 (AX, $ArCH_2Ar$, 12H, J = 12.0 Hz), 3.75 [s, OCH_3, 15H], 3.75 [s, OCH_3, 15H], 4.01and 4.51 (d, ArH_r, 2H, J = 8.0 Hz), 5.07 [s, $(OCH_2)_s$, 4H,), 4.78 (d, ArH_o, J= 8.0 Hz, 1H), 5.33 (dd, ArH_m, J_1=J_2=7.6 Hz, 4H), 5.98 (t, ArH_p, J_1 = 7.6 Hz, 2H), 6.11 (*broad*, NH_2^+, 2H), 7.14-7.30 (*overlapped*, Ar*H*, 52H), 7.50 (s, ArH_{TFPB}, 4H), 7.71 (t, ArH_{TFPB}, 8H, J = 4.0 Hz), 7.83 (d, ArH_n, 2H, J = 8.0 Hz);

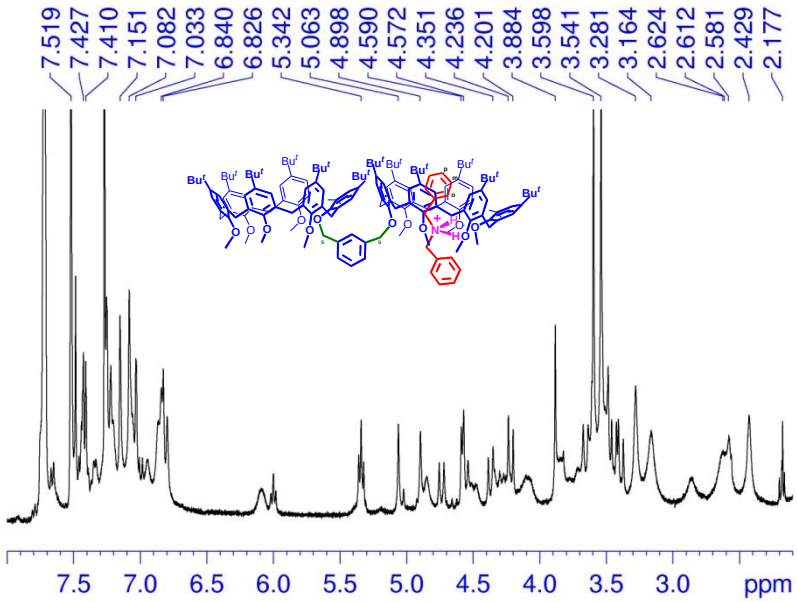

Figure 111. ^{1}H NMR spectrum (400 MHz, 298 K, $CDCl_3$) of the 1:1 mixture of **21** and **4**$^{+}$·TFPB^{-}.

4.7.6 Preparation of doubly-threaded pseudo[3]rotaxanes 23, 25, 27

Derivative 23

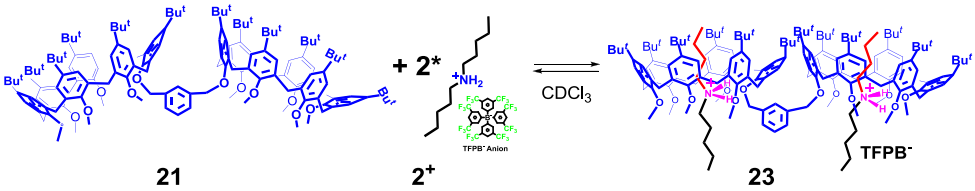

21 **2**$^{+}$ **23**

Double-calixarene derivative **21** ($2.0\cdot10^{-3}$ g, $0.91\cdot10^{-3}$ mmol) and the dialkylammonium derivative **2**$^{+}$ ($2.4\cdot10^{-3}$ mmol) were dissolved in 0.4 mL of

$CDCl_3$ and the mixture was stirred for 5 min at 25 °C. Then, the solution was transferred in a NMR tube for 1D and 2D NMR spectra acquisition. ESI(+) MS: *m*/*z* = 1248.33 $[(\mathbf{2})_2 \subset \mathbf{21}]^{2+}$. ^{1}H NMR ($CDCl_3$, 400 MHz, 298 K): δ −1.07 [broad, $(CH_2)_\beta$, 4H], −0.18 [broad, $(CH_2)_\gamma$, 4H], −0.01 [broad, $(CH_2)_\alpha$, 4H], 0.39 [broad, $(CH_2)_\delta$ + $(CH_3)_\varepsilon$, 10H], 1.15 (s, Bu^t, 90H), 3.52 and 4.33 (broad, $ArCH_2Ar$, 24H), 3.79, 3.84, 3.91 (br s, OCH_3, 6H, 12H, 12H), 4.98 (br s, OCH_2, 4H), 6.66─7.61 (overlapped, ArH, 40H).

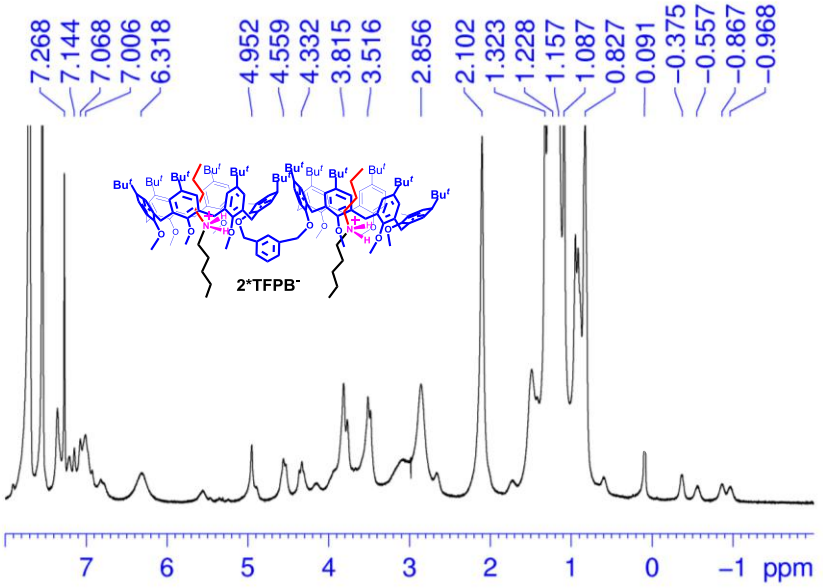

Figure 112. ^{1}H NMR spectrum (400 MHz, 298 K, $CDCl_3$) of the 1:2 mixture of **21** and $\mathbf{2}^+ \cdot TFPB^-$.

Derivative 25

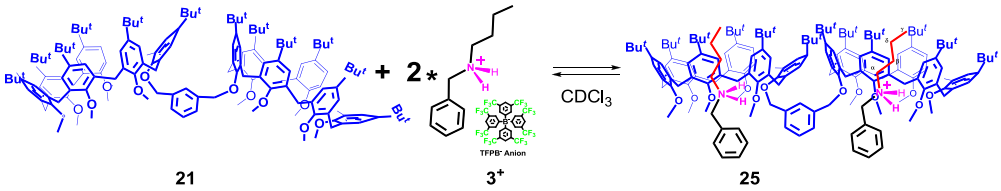

21 3^+ 25

Double-calixarene derivative **21** ($2.0\cdot10^{-3}$ g, $0.91\cdot10^{-3}$ mmol) and the dialkylammonium derivative $\mathbf{2}^+$ ($2.4\cdot10^{-3}$ mmol) were dissolved in 0.4 mL of $CDCl_3$ and the mixture was stirred for 5 min at 25 °C. Then, the solution was transferred in a NMR tube for 1D and 2D NMR spectra acquisition. ESI(+) MS: *m*/*z* = 1257 $[(\mathbf{3})_2\subset\mathbf{21}]^{2+}$.

^{1}H NMR ($CDCl_3$, 400 MHz, 298 K): δ −1.01 [broad, $(CH_2)_\beta$, 4H], 0.03 [broad, $(CH_2)_\gamma$ + $(CH_3)_\delta$, 10H], 0.23 [broad, $(CH_2)_\alpha$, 4H], 1.67(s, Bu^t, 90H), 2.27 [broad, ($^+H_2NCH^\alpha{}_2Ph$), 4H], 3.28, 3.59, 3.70 (s, OCH_3, 6H, 12H, 12H), 3.50 and 4.44 (broad, $ArCH_2Ar$, 8H), 3.52 and 4.32 (broad, $ArCH_2Ar$, 8H), 3.58 and 4.43 (broad, $ArCH_2Ar$, 8H), 4.97 (br s, OCH_2, 4H), 5.35 (br s, $^+NH_2$, 4H), 6.64─7.59 (overlapped, ArH, 50H).

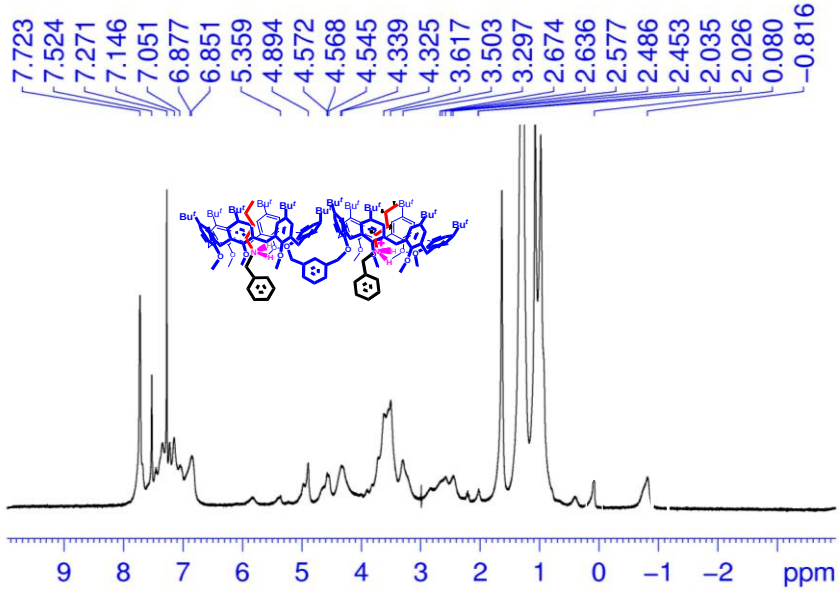

Figure 113. ^{1}H NMR spectrum (400 MHz, 298 K, $CDCl_3$) of the 1:2 mixture of **21** and **3**$^{+}$·TFPB^{-}.

Derivative 27

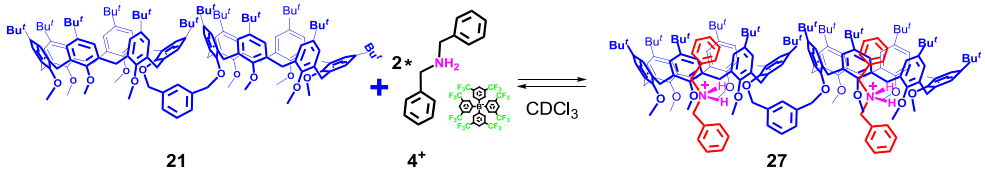

Double-calixarene derivative **21** ($2.0\cdot10^{-3}$ g, $0.91\cdot10^{-3}$ mmol) and the dibenzylammonium derivative **4**$^{+}$ ($2.4\cdot10^{-3}$ mmol) were dissolved in 0.5 mL of $CDCl_3$ and the mixture was stirred for 5 min at 25 °C. Then, the solution was transferred in a NMR tube for 1D and 2D NMR spectra acquisition. ESI(+) MS: *m*/*z* =1290.3 $[(\mathbf{4})_2\subset\mathbf{21}]^{2+}$.

δ1.17 (s, Bu^{t}, 90H), 1.45 [(CH_2)$_{d}$, 4H], 2.94 [(CH_2)$_{f}$, 4H], 3.51 and 4.40 (AX, ArCH_2Ar, *J* =13.6 Hz, 12H each), 3.86 (s, OCH_3, 36H), 4.67 (d, ArH_o, *J*= 8.0 Hz, 2H), 5.34 (dd, ArH_m, J_1=J_2=7.6 Hz, 4H), 5.40 [s (OCH_2)$_s$], 6.01 (t, ArH_p, J_1 = 7.6 Hz, 4H), 6.09 (*broad*, NH_2^+, 4H), 7.01 (s, ArH_{calix}, 24H), 7.48 (s, ArH_{TFPB}^-, 8H), 7.71 (ArH_{TFPB}^-, 16H).

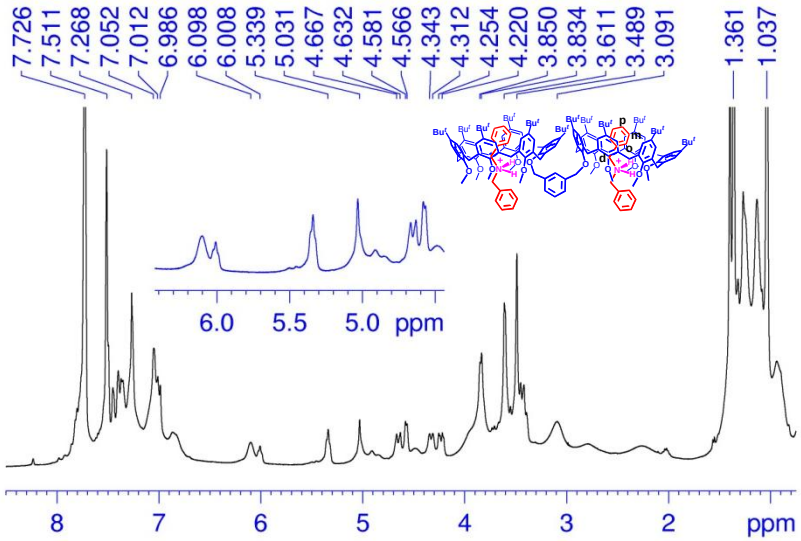

Figure 114. ^{1}H NMR spectrum (400 MHz, 298 K, $CDCl_3$) of the 1:2 mixture of **21** and **4**$^{+}$·TFPB^{-}.

4.7.7 Determination of K_{ass} values of $(2^{+})_2\subset$**12** *and* $(3^{+})_2\subset$**12** *complexes by quantitative ^{1}H NMR analysis*

The samples were prepared by dissolving **8**(1.24×10^{-3} mmol) and the appropriate alkylammonium guest **2**$^{+}$ or **3**$^{+}$(2.48×10^{-3} mmol) in $CDCl_3$ (0.4 mL) containing 1 μL of 1,1,2,2-tetrachloroethane (d = 1.59 g/mL) as internal standard. The complex concentration [complex] was evaluated by integration of the ^{1}H NMR signal of C*H*Cl_2CHCl_2 vs the shielded signals at negative values of the guest molecule. The following equation was used to obtain the moles of the complex:

$$\frac{G_a}{G_b} = \frac{F_a}{F_b} \times \frac{N_b}{N_a} \times \frac{M_a}{M_b}$$

Where:

G_a = grams of 1,1,2,2-tetrachloroethane; G_b= grams of complex

F_a and F_b = areas of the signals of 1,1,2,2-tetrachloroethane and shielded signal of the guest

N_a and N_b = numbers of nuclei which cause the signals (N_a for 1,1,2,2-tetrachloroethane; N_b for guest)

M_a and M_b = molecular masses of 1,1,2,2-tetrachloroethane (a) and complex (b)

CHAPTER V

Stereo-Programmed Synthesis of

Calixarene-Based Handcuff Rotaxanes

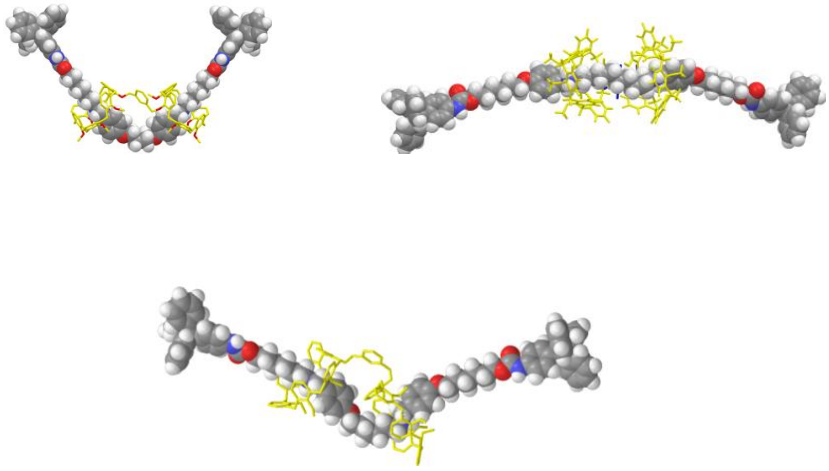

5.1 *Introduction*

In the last decade, macrocyclic hosts with multiple cavities or multiple recognition sites have attracted increasing attention because they are particularly useful for developing non-trivial interlocked architectures.[20]
At this regards, handcuff-like systems in which two interpenetrated rings are linked to one another, represent a significative synthetic challenge.[97] Based on the template-direct threading[98,20] of linear axles through double-macrocycles, spectacular handcuff-like architectures have been reported to date, which shows interesting properties and functions.
In 1993 Stoddart[99] and coworkers reported the first example of handcuff architecture **B** (**Figure 116**), which was followed by the similar [2]catenane polymer **C.**[100] Successively, Becher[101] reported the handcuff architecture **D**, in which two connected macrocycles were threaded through the same large ring to form an handcuff [3]catenane. A similar topology was built later by Sauvage[102] in 2005 through the template effect of Cu(I) and recently by Beer[103] through an anion templation. In 2000 Vögtle[104] and coworkers

[97] Zhang, Z.-J.; Han M.; Zhang, H.-Y.; Liu, Y. *Org. Lett.* **2013**, *15*, 1698−1701; (b) Geng, J.; Biedermann, F.; Zayed, J. M.; Tian, F.; Scherman, O. A. *Macromolecules* **2011**, *44*, 4276–4281; (c) Guo, J.-B.; Xiang, J.-F.; Chen, C.-F. *Eur. J. Org. Chem.* **2010**, 5056–5062; (d) Han, T.; Chen, C.−F. *J. Org. Chem.* **2008**, *73*, 7735–7742; (e) Frey, J.; Kraus, T.; Heitz, V., Sauvage, J.-P. *Chem. Eur. J.* **2007**, *13*, 7584 –7594; (f) Frey, J.; Kraus, T.; Heitz, V., Sauvage, J.-P. *Chem. Commun*. **2005**, *13*, 5310 –5312; (g) Badjić, J. D.; Balzani, V.; Stoddart, J. F.; Silvi, S.; Stoddart, J. F. *Science* **2004**, *303,* 1845−1849; (h) Balzani, V.; Clemente-León, M.; Credi, A.; Lowe, J. N.; Badjić, J. D., Stoddart, J. F.; Williams, D. J. *Chem. Eur. J.* **2003**, *9*, 5348−5360.
[98](a) Hoss, R.; Vögtle, F. *Angew. Chem., Int. Ed. Engl.* **1994**, *33*, 375−384. (b) *Templated Organic Synthesis*; Diederich, F., Stang, P. J.; Eds.; Wiley-VCH: Weinheim, 1999.
[99] Ashton, P. R.; Reder, A. S.; Spencer N. ; Stoddart, J. F. *J. Am. Chem. Soc.,* **1993**, *115*, 5286.
[100] (a) Badjić, J. D.; Balzani, V.; Credi, A.; Silvi, S.; Stoddart, J. F. *Science* **2004**, *303,* 1845−1849. (b) Evans, N. H.; Serpell, C. J.; Beer, P. D., *Angew. Chem. Int. Ed.* **2011**, *50,* 2507−2510. (c) Zhang, Z.-J.; Han M.; Zhang, H.-Y.; Liu, Y. *Org. Lett.* **2013**, *15,* 1698.
[101] Li, Z.-T.; Becher, J. *Chem. Commun.,* **1996**, *5*, 639.
[102] Frey, J.; Kraus, T.; Heitz, V.; Sauvage, J.-P. *Chem. Commun*., **2005**, 5310. Frey, J.; Kraus, T.; Heitz, V.; Sauvage, J.-P. *Chem. Eur. J.* **2007**, 13, 7584.
[103] Evans, N. H.; Serpell, C. J.; Beer, P. D., *Angew. Chem. Int. Ed.* **2011**, *50*, 2507.
[104] Reuter, C.; Mohry, A.; Sobansky, A.; Vögtle, F. *Chem. Eur. J.*, **2000**, *6*, 1674.

reported a molecular ‘‘pretzelane’’ **A** (**Figure 115)** in which the two rings of a [2]catenane were bridged with a short spacer.

Regarding the handcuff [3]rotaxane architecture **E** (**Figura 115**), recently an example has been reported[2a] in which two flat crown-rings, rigidly linked to one another, were threaded with a bis(ammonium)axle to give a double-leg elevator.

With respect to the use of flat macrocycles in **E** (**Figure 115**), an increased synthetic challenge is represented by the use of three-dimensional nonsymmetrical rings (directional wheels), such as double-calixarene **8** (**Figure 48**), because of the inherent difficulty in controlling the stereochemistry of the entire system.[79] In fact, the synthesis of an handcuff-rotaxane by threading **12** with a bis(ammonium) axle could give rise to three stereoisomeric handcuff pseudo[2]rotaxane structures, in which the calix-wheels could show three different relative orientations, *head-to-head* (H,H), *head-to-tail* (H,T), and *tail-to-tail* (T,T), represented by **F−H** in **Figure 115**.

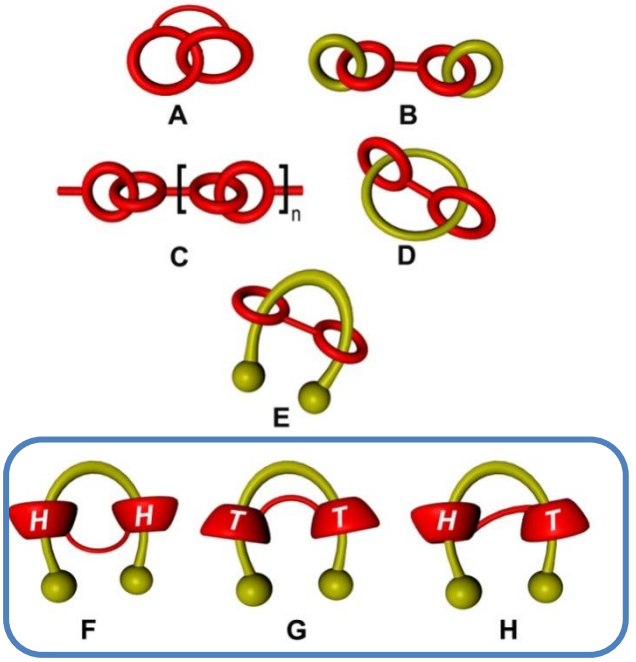

Figure 115. Cartoon representations of handcuff-like systems.

The control of the relative orientation of the two directional wheels along bis(alkylbenzylammonium) threads could be obtained on the basis of the previously reported "*endo-alkyl rule*".[77] This control was already realized by Gaeta *et al.* in the stereo-programmed direct synthesis of calixarene-based pseudo[3]rotaxanes[80] (**Figure 116**).

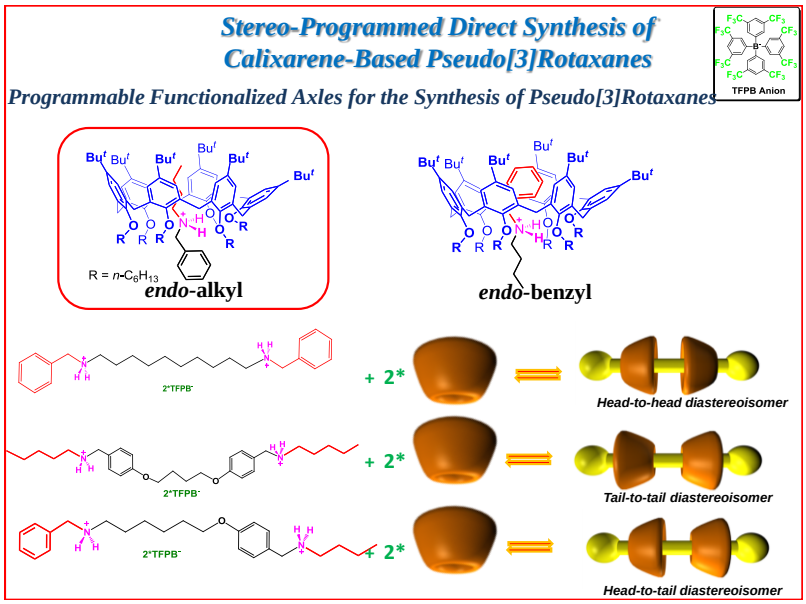

Figure 116. Stereo-programmed direct synthesis of calixarene-based pseudo[3]rotaxanes[80]

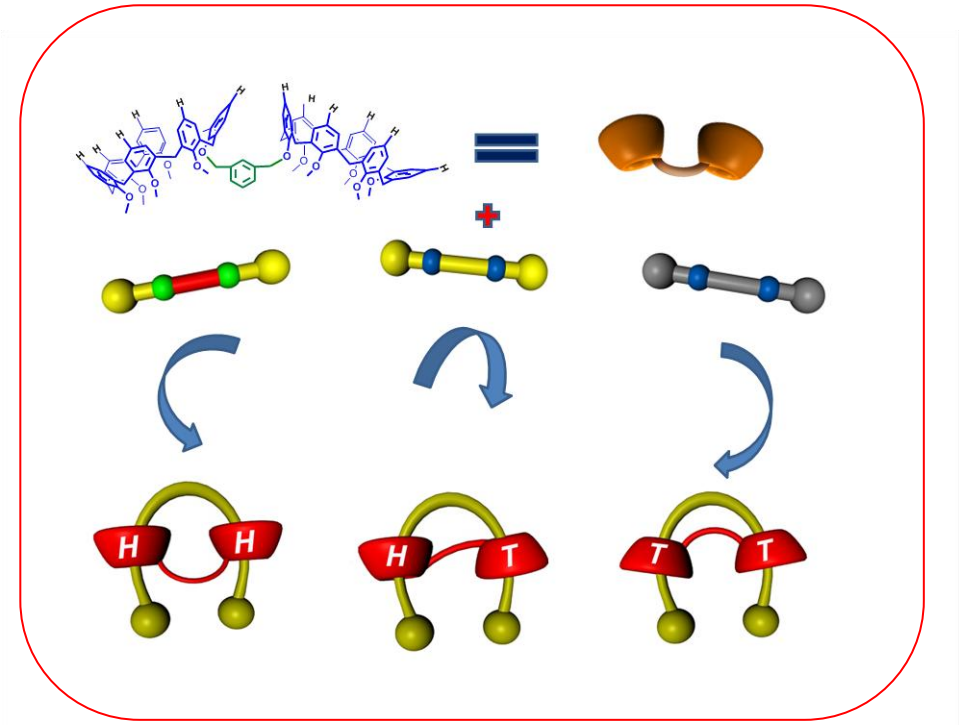

Figure 117. Handcuff-rotaxanes based on threading of the double-calix[6]arene derivative **12** with a rationally controlled way designed bis(ammonium) axles .

It is obvious that to obtain handcuff rotaxanes with different orientation of the calix-wheels you must rely on an appropriate design of the threading element (**Figure 117**).

In fact, the suitable choice of the alkyl-benzyl sequence along bis(benzylalkylammonium) axles in conjunction with the above mentioned *endo*-alkyl rule could drive the stereochemistry of the rotaxane adducts. Thus, two calix[6]arene directional wheels can be ordered in the right stereo-sequence by their *through-the-annulus* threading (**Figure 117**).

Thus, as a first step, we have designed three axles in which the appropriate covalent linkage of two alkylbenzylammonium recognition motifs could have a good control of the consequent sequence stereoisomerism (**Figure 118**).

Thus, the specific stereosequences of handcuff pseudo[2]rotaxanes (*T,T*)-**12⊂28,** (*H,H*)-**12⊂33** and (*H,T*)-**12⊂38** (**Figure 118**) could be obtained. The introduction of appropriate stoppers would lead to handcuff [2]rotaxane structures with a programmed orientation of the calix-wheels.

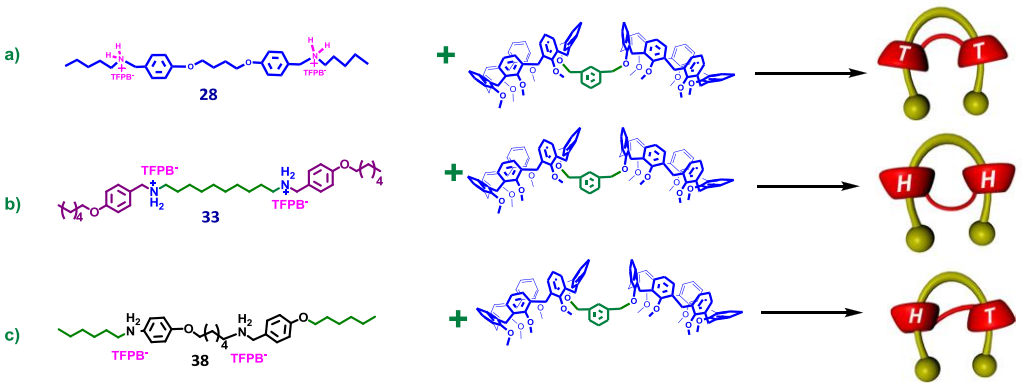

Figure 118. Predicted **s**equence stereoisomerism in handcuff pseudo[2]rotaxane by threading with rationally designed bis(benzylalkylammonium) axles (**28**, **33**, **38**).

5.2 Stereo-programmed synthesis of *(T,T)*-handcuff [2]rotaxane

5.2.1 Stereo-programmed formation of a *(T,T)*-handcuff pseudo[2]rotaxane (29)

In order to prepare a handcuff-pseudo-[2]rotaxane with a programmed *tail-to-tail* stereosequence, we decided to connect two alkylbenzylammonium moieties by the benzyl ends to give the thread $\mathbf{28}^{2+}$ exposing alkyl chains at the terminations [**Figure 118 a**)]. On the basis of the *endo-alkyl rule*, the threading of $\mathbf{28}^{2+}$ with **12** should result in a *tail-to-tail* orientation of the calix-wheels of **12** and thus in a *tail-to-tail* handcuff pseudo[2]rotaxane.

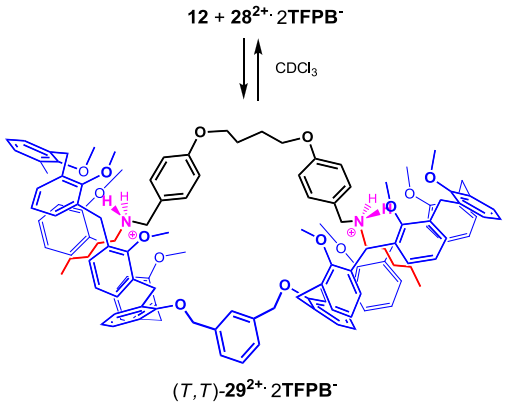

Scheme 9. Stereo-programmed handcuff-threading of **12** with $\mathbf{28^{2+}}$ to give (*T,T*)-handcuff-pseudo[2]rotaxane $\mathbf{29^{2+}}$.

Therefore, the TFPB[105] salt of $\mathbf{28^{2+}}$ was equilibrated with double-calix[6]arene **12** (**Scheme 9**). Then, the formation of handcuff pseudo[3]rotaxane architecture $\mathbf{29^{2+}}$ was confirmed by 1D and 2D NMR spectroscopy and ESI(+) mass spectrum. In particular, the ^{1}H NMR spectrum ($CDCl_3$, 400 MHz, 298 K) of a 1:1 mixture (**Figure 119b**) of TFPB salt of dicationic thread $\mathbf{28^{2+}}$ and double-calix[6]arene **12** (**Scheme 9**) showed a typical signature at highfield negative values (from 1.0 to −1.0 ppm, see **Figure 119b**) characteristic of an *endo*-complexation of the alkyl chains shielded by calixarene aromatic rings. This result and the absence of shielded benzylic resonances in the 4−6 ppm region, typical of *endo*-benzyl complexation,[77,80] were a clear-cut proof that *tail*-to-*tail* (*T,T*)-handcuff pseudo[3]rotaxane $\mathbf{29^{2+}}$ (**Scheme 9**) had been stereo-selectively formed. This result indicates that the presence of a short *m*-xylylene spacer between the two calix-wheels of **12** does not generate any abnormal stereo-sequence of the directional wheels with respect to that expected by the *endo-alkyl rule*.

[105] For a review on superweak anion $TFPB^-$: Strauss, S. H. *Chem Rev.* **1993**, *93*, 927.

The formation of the handcuff pseudo[3]rotaxane **29**$^{2+}$ was confirmed by a prominent peak at 980.3 *m*/*z* in the ESI(+) mass spectrum in **Figure 120**, corresponding to the doubly-charged molecular ion **29**$^{2+}$. In fact, as showed in the expansion of ESI mass spectrum (**Figure 120 inset**), the Δ spacing of 0.5 *m*/*z* between the peaks in the isotopic envelop solely accounts for a doubly-charged species of **29**$^{2+}$**,** excluding architectures with higher charges, such as a cyclic or square-type supramolecular architecture **A** or an undefined supramolecular oligomer or polymer **B**

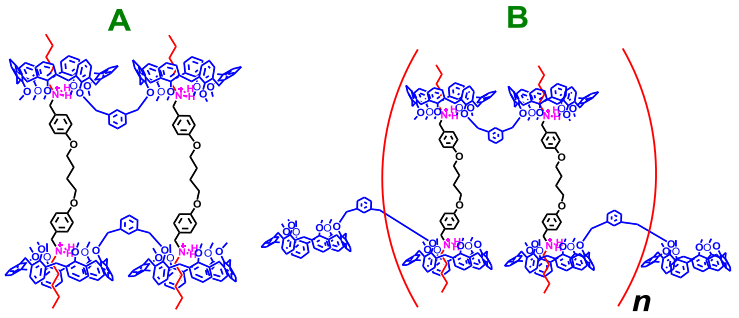

A COSY-45 spectrum ($CDCl_3$, 400 MHz, 298 K) of the 1:1 mixture of thread **28**$^{2+}$ and double-calix[6]arene **12** (**Figure 121**) allowed a complete confident assignment of all shielded alkyl resonances. Thus, α protons at 0.17 ppm, shows a coupling with β methylene group at −0.96 ppm, which presents a cross-peak with γ protons at −0.03 ppm, finally coupled with δ methyl at 0.39 ppm, which was coupled with ε protons at 0.40 ppm (**Figure 121 right**).

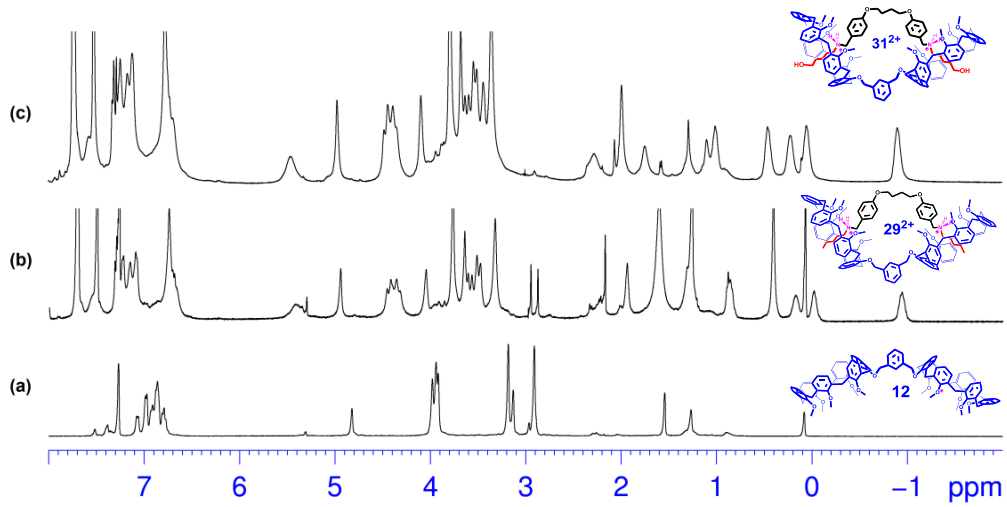

Figure 119. ^{1}H NMR spectra (400 MHz, $CDCl_3$, 298 K) of: (a) **12**, (b) an equimolar mixture (3 mM) of **12** and **28**$^{2+}$· 2TFPB^{-}, (c) an equimolar mixture (3 mM) of **12** and **31**$^{2+}$· 2TFPB^{-}.

In addition, the $ArCH_2Ar$ region (3−5 ppm, **Figure 121 left**) of the COSY-45 spectrum revealed the presence of three AX systems at 4.43/3.58, 4.38/3.49 and 4.31/3.49 ppm relative to calixarene $ArCH_2Ar$ groups. Furthermore, the corresponding ^{1}H NMR spectrum showed three singlets in a 2:1:2 ratio at 3.77, 3.63 and 3.33 ppm, relative to OMe groups, and a singlet a 4.95 ppm relative to oxymethylene groups of the *m*-xylylene bridge. These data were in accordance with the presence of a symmetry plane bisecting the *m*-xylylene bridge and the 1,4-diphenoxybutane chain, which is only possible in the case of a handcuff-threading of **12**.

The presence of well-defined AX systems for $ArCH_2Ar$ groups in the COSY-45 spectrum in **Figure 121 (left)**, is a clear indication that the thread **29**$^{2+}$ gave a *through-the-annulus*-threading with double-calix[6]arene **12** in $CDCl_3$. In fact, the $ArCH_2Ar$ protons appear as singlets for the conformationally mobile free host **12** (see ^{1}H NMR spectrum of **12** in **Figure 120a**), whereas they give rise to a couple of doublets (AX system) when the wheel is conformationally blocked by pseudorotaxane formation.

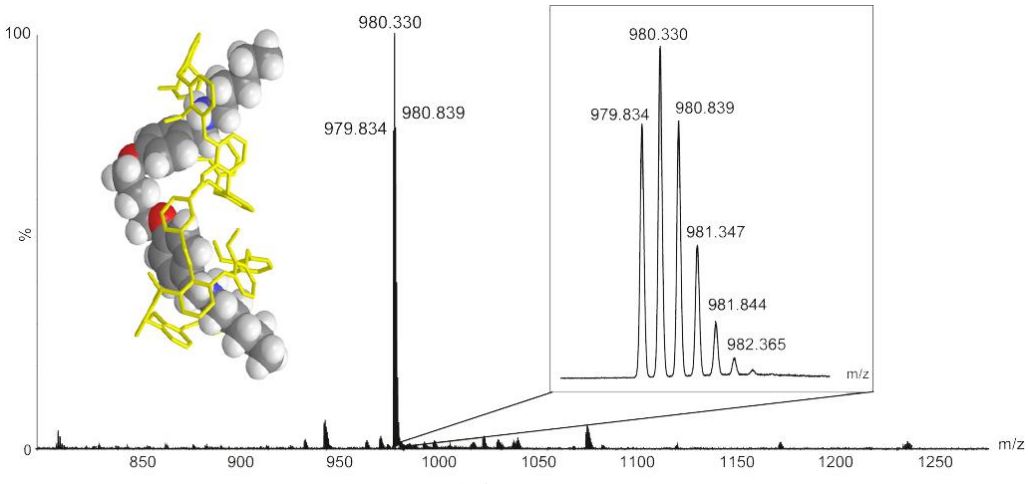

Figure 120. ESI(+) mass spectrum of (*T,T*)-**29**$^{2+}$ and its AMBER energy-minimized structure (inset).

The preference for *tail*-to-*tail* stereo-sequence of two wheels of **12** along thread **29**$^{2+}$ was also confirmed by molecular mechanics calculations[10617] (AMBER force field, $CHCl_3$, GB/SA model solvent), which indicated the (*T,T*)-**29**$^{2+}$ stereoisomer as the lowest in energy with respect to (*H,T*) and (*H,H*) ones (**Figure 123**). Molecular mechanics calculations revealed that a folding of the thread **28**$^{2+}$ is required to simultaneously thread the two calix-wheels of **12**. Thus, the folded conformation adopted by **29**$^{2+}$ in (*T,T*)-handcuff pseudo[2]rotaxane **29**$^{2+}$ was characterized by unfavorable gauche conformations around the O(1)-C(1) and C(2)-C(3) bonds of the central 1,4-diphenoxybutane fragment (**Figures 123 and 124**). The dihedral angles around O(1)-C(1) and C(2)-C(3) bonds are 65° and 78°, respectively (see **Figure 125c**).

[106] MacroModel-9.0/Maestro-4.1 program: Mohamadi, F.; Richards, N. G.; Guida, W. C.; Liskamp, R.; Lipton, M.; Caufield, C.; Chang, G.; Hendrickson, T.; Still, W. C. *J. Comput. Chem*. **1990**, *11*, 440–467.

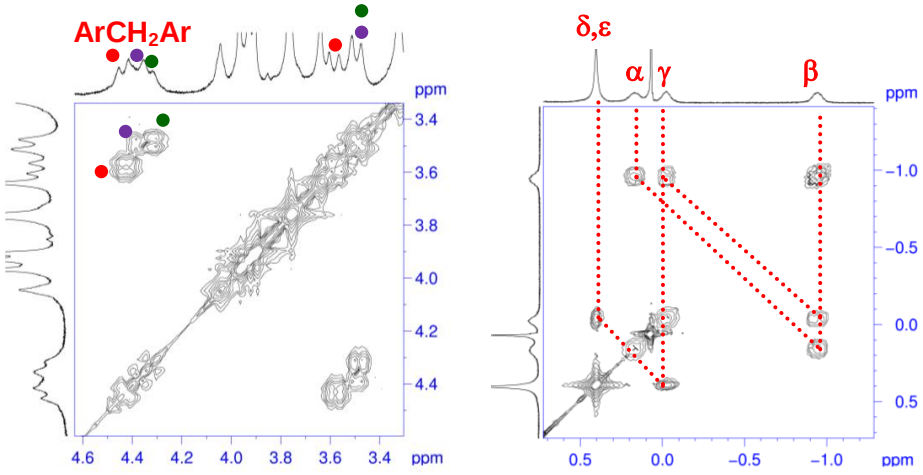

Figure 121. Expansions of 2D COSY-45 spectrum (400 MHz, $CDCl_3$, 298 K) of an equimolar mixture (3 mM) of **12** and **28**$^{2+}$· 2TFPB^{-}.

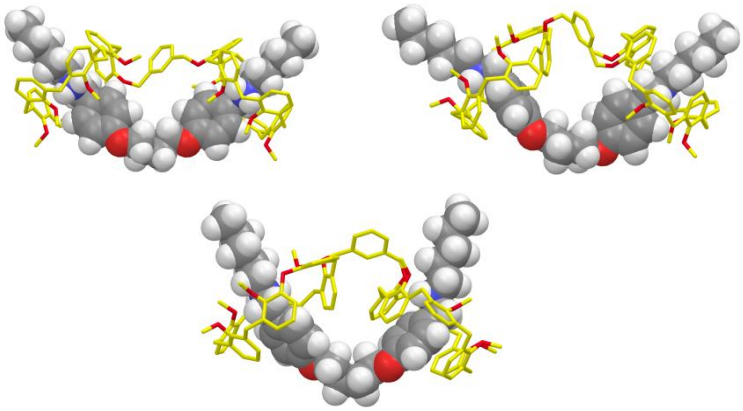

Figure 122. Lowest energy structure of three possible handcuff-pseudo[2]rotaxane **29**$^{2+}$ (from left to right: *T,T*; *H,T* and *H,H*) found by Monte Carlo conformational search (10000 steps, MacroModel V. 9.0, AMBER force field).

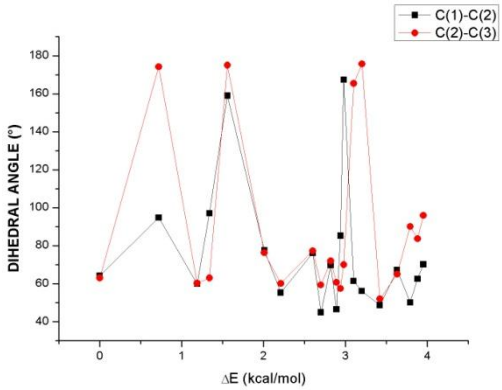

Figure 123. Dihedral angle values (°) around C(1)-C(2) and C(2)-C(3) bonds measured for the SA structures of (*T,T*)-**29**$^{2+}$ in the 4 kcal/mol lowest energy window. The structures are ranked according to their energy difference (ΔE) with respect to the lowest minimum one (0.0 kcal/mol).

Molecular Dynamics (MD) simulation at 500 K clearly showed that about 55% of the coconformers sampled during the entire MD simulation (20000 ps) showed a dihedral angle in the 65-80° range around the O-C bond (**Figure 124**). Analogous results were obtained upon sampling the dihedral angle between C(2)-C(3) bond (**Figure 124**). In fact, about 69% of the coconformers sampled during the entire MD simulation (20000 ps) showed a dihedral angle in the 65-90° range.

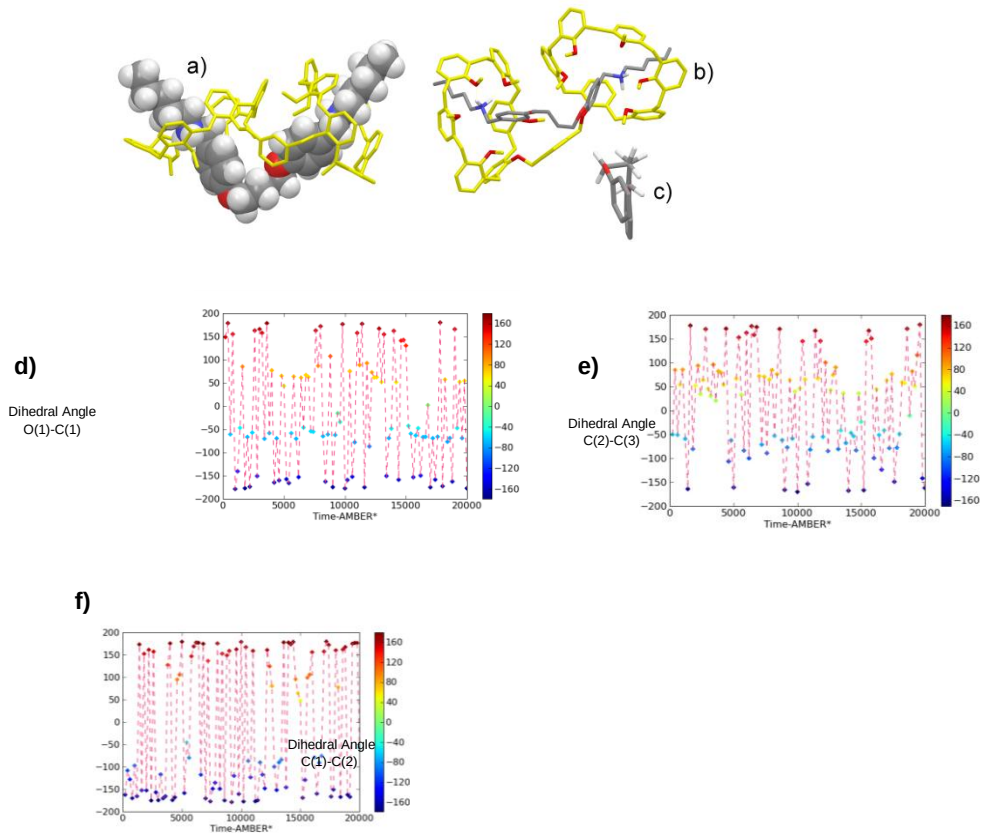

Figure 124. **(a-c)** Snapshot from an MD simulation of (*T,T*)-handcuff-pseudo[2]rotaxane **29**$^{2+}$ illustrating the thread **28**$^{2+}$ in an folded conformation. **(d-e)** Variation in the dihedral angle between O(1)-C(1), C(2)-C(3) and C(1)-C(2) observed during the MD simulation at 500 K.

This situation is resembling those observed by Rebek,[107] in the encapsulation of long alkanes in a coiled form inside a self-assembled capsule, and recently by us,[10815f] in the *endo*-complexation of large di-*n*-alkylammonium cations inside the narrow cavity of 18-membered dihomooxacalix[4]arene ring. In analogy to those complexes, in the present

[107] (a) Scarso, A.; Trembleu, L.; Rebek, J. Jr. *Angew. Chem. Int. Ed. Engl.* **2003**, *42*, 5499-5502;(b) Scarso, A.; Trembleu, L.; Rebek, J. Jr. *J. Am. Chem. Soc.* **2004**, *126*, 13512-13518.
[108] Gaeta, C.; Talotta, C.; Farina, F.; Teixeira, F. A.; Marcos, P. A.; Ascenso, J. R.; Neri, P. *J. Org. Chem.* **2012**, *77*, 10285−10293.

case the energy loss due to the folding of the thread to a less stable form is counterbalanced by the gain of H-bonds due to the threading of the calix[6]-cavities.

The apparent total association constant (Ktot = K1×K2 = 1.6±0.3 × 10^3, percentage of formation 58%) for complex (*T,T*)-**29^{2+}** was determined by integration of ^{1}HNMR spectrum of its 1:1 titration mixture in $CDCl_3$ which showed slowly exchanging signals for both the free and complexed guest.

5.2.2 Stereo-programmed synthesis of (T,T)-handcuff [2]rotaxane 32^{2+}

In order to obtain a handcuff [2]rotaxane architecture we attempted the handcuff-threading of derivative **12** with axle **30^{2+}** encoding alkyl chains at the terminations and bearing two terminal OH groups, which are derivatizable with a trityl-bearing isocyanate as the stoppering reagent (**Scheme 10**).[80]

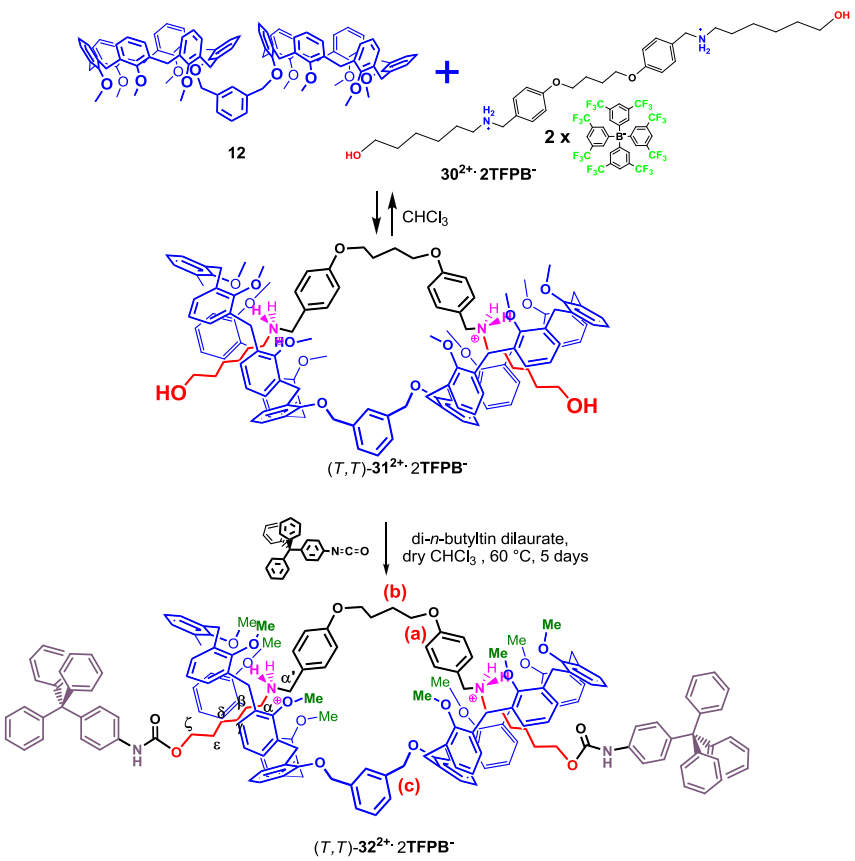

Scheme 10. *Synthesis of the first example of a calix[6]arene-based handcuff [2]rotaxane*

Therefore, the TFPB salt of **30**$^{2+}$ was equilibrated with double-calix[6]arene **12** to give (*T,T*)-handcuff pseudo[2]rotaxane **31**$^{2+}$ (**Scheme 10**).

The ^{1}H NMR spectrum (**Figure 118c**) of a 1:1 mixture of TFPB salt of dicationic **30**$^{2+}$ and double-calix[6]arene **12** in $CDCl_3$ showed a typical signature at highfield and negative values (from 1.0 to −1.0 ppm) characteristic of an *endo*-complexation of the alkyl chains shielded by calixarene aromatic rings.

As above, the absence of shielded benzylic resonances in the 4-6 ppm region, typical of *endo*-benzyl complexation, were a clear-cut proof that *tail-*

to-tail handcuff pseudo[2]rotaxane **31**$^{2+}$ had been stereoselectively formed. Again, the validity of the *endo-alkyl rule* is confirmed. As above, a COSY-45 spectrum allowed a complete confident assignment of all *n*-alkyl resonances of the axle of (*T,T*)-handcuff pseudo[2]rotaxane **31**$^{2+}$. Thus, one strongly shielded chain inside the cavity was observed, with ζ, ε, δ, γ, β, and α protons resonating at 3.43, 1.00, 0.45, 0.04, −0.92 and - 0.23 ppm, respectively while three $ArCH_2Ar$ AX systems were observed at 4.44/3.60, 4.42/3.52 and 4.34/3.50 ppm.

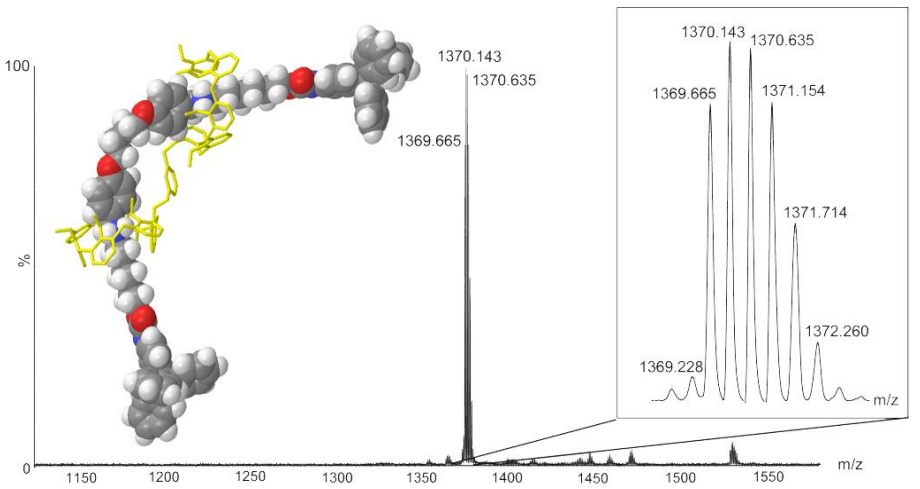

Figure 125. ESI(+) mass spectrum of (*T,T*)-**31**$^{2+}$ and its AMBER energy-minimized structure (inset).

This pseudorotaxane was then stoppered by reaction with 4-tritylphenyl isocyanate to give the first example of calixarene-based handcuff [2]rotaxane (*T,T*)-**32**$^{2+}$ in 65% yield (**Scheme 9**). The formation of (*T,T*)-**32**$^{2+}$ was confirmed by a prominent peak at 1370.1 m/z in the ESI(+) mass spectrum (**Figure 125**) corresponding to the doubly-charged supramolecular ion. The *tail-to-tail* stereosequence of the two calix-wheels in the precursor (*T,T*)-handcuff pseudo[2]rotaxane **29**$^{2+}$ was retained after the stoppering

reaction as evidenced by the ^{1}H NMR spectrum (**Figure 126a**) of (*T,T*)-**32**$^{2+}$ in $CDCl_3$, which showed a typical signature at highfield values (from 1.0 to −1.0 ppm) and no resonances in the 4-6 ppm region. As above the COSY-45 spectrum (**Figure 127**) ($CDCl_3$, 400 MHz, 298 K) of (*T,T*)-**32**$^{2+}$ in $CDCl_3$ allowed a complete confident assignment of all shielded alkyl resonances.

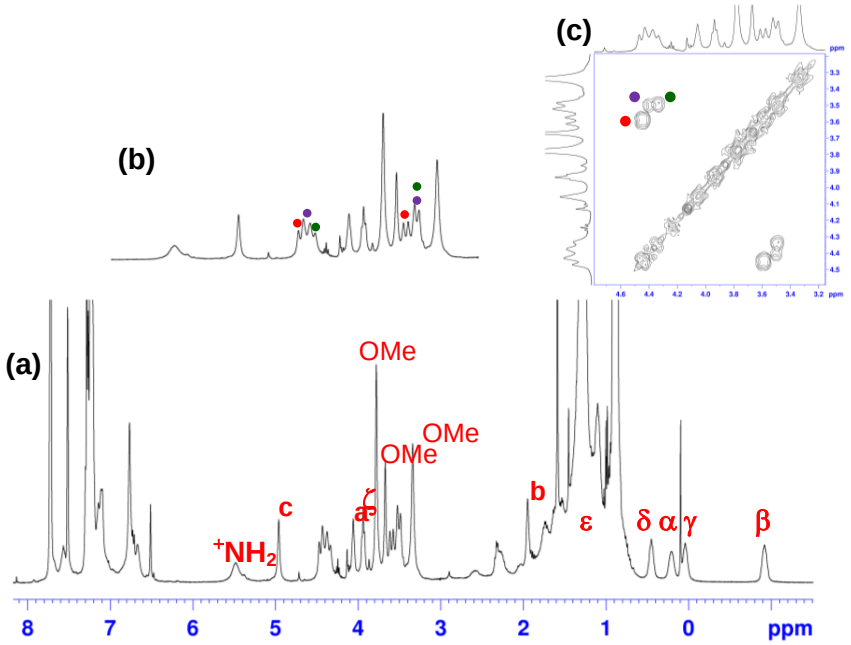

Figure 126. (a) ^{1}H NMR spectrum (400 MHz, $CDCl_3$, 298 K) of handcuff-[2]rotaxane (*T,T*)-**32**$^{2+}$ · 2TFPB$^-$. (b) Expansion of the methylene region of the ^{1}H NMR spectrum of (*T,T*)-**32**$^{2+}$. (c) Expansion of the methylene region of the 2D COSY-45 spectrum of (*T,T*)-**32**$^{2+}$.

Thus, α protons at 0.21 ppm, shows a coupling with β methylene group at −0.92 ppm, which presents a cross-peak with γ protons at 0.04 ppm, finally coupled with δ methylene at 0.44 ppm which was coupled with ε protons at 1.11 ppm that shows a coupling with δmethylene at 3.91 ppm.

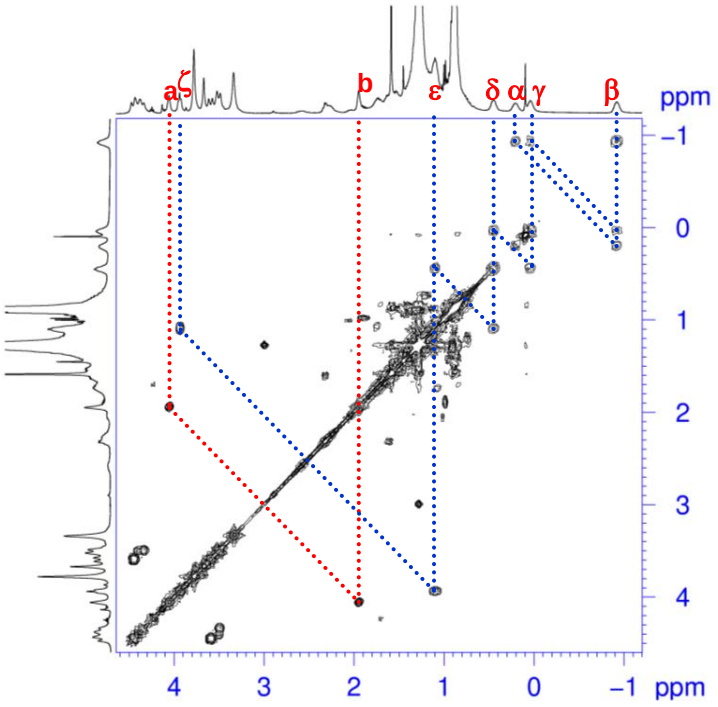

Figure 127. Expansions of 2D COSY-45 spectrum (400 MHz, $CDCl_3$, 298 K) of the (*T,T*)-handcuff-[2]rotaxane **32**$^{2+}$.

Analogously to handcuff-architectures (*T,T*)-**29**$^{2+}$ and (*T,T*)-**31**$^{2+}$ above described, the $ArCH_2Ar$ region (3−5 ppm) of the COSY-45 spectrum (**Figure 127c**) ($CDCl_3$, 400 MHz, 298 K) of (*T,T*)-**32**$^{2+}$, revealed the presence of three AX systems at 4.45/3.60, 4.41/3.50 and 4.34/3.49 ppm relative to calixarene $ArCH_2Ar$ groups, while its ^{1}H NMR spectrum showed three singlets in a 2:2:1 ratio at 3.78, 3.67 and 3.34 ppm relative to OMe groups and a singlet a 4.96 ppm relative to oxymethylene groups of the *m*-xylylene bridge. As above molecular mechanics calculations (AMBER force field, $CHCl_3$, GB/SA model solvent) indicated a folded conformation of the thread in handcuff rotaxane (*T,T*)-**32**$^{2+}$ (**Figure 129**).

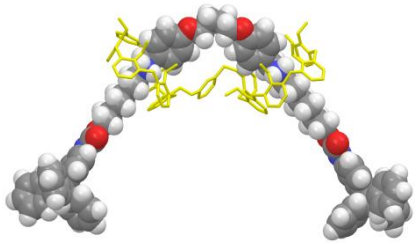

Figure 128. Lowest energy structure of the (*T,T*)-handcuff-pseudo[2]rotaxane **32**$^{2+}$ found by Monte Carlo conformational search (10000 steps, MacroModel V. 9.0, AMBER force field).

5.3 Stereo-programmed synthesis of *(H,H)*-handucff [2]rotaxane

5.3.1 Stereo-programmed formation of *(H,H)*-handcuff pseudo[2]rotaxane 34^{2+}

The logical extension of the above approach was the preparation of a handcuff pseudo-[2]rotaxane with a programmed *head-to-head* stereosequence. For this purpose, we decided to connect two alkylbenzylammonium moieties by the alkyl ends to give thread **33**$^{2+}$ **(Figure 119b)** exposing benzyl chains at the terminations (**Scheme 11**).

On the basis of the *endo-alkyl rule*, we expected that the threading of **12** with **33**$^{2+}$ should result in a *head-to-head* orientation of the calix-wheels of **12**.

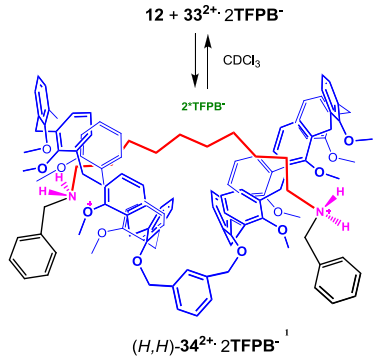

Scheme 11. Stereo-programmed handcuff-threading of **12** with **33**$^{2+}$to give (*H,H*)-handcuff-pseudo[2rotaxane **34**$^{2+}$.

Therefore, the TFPB[109] salt of **33**$^{2+}$ was equilibrated with double-calix[6]arene derivative **12** (**Scheme 9**). Then, the formation of handcuff-pseudo[2]rotaxane architecture **33**$^{2+}$ was confirmed by 1D and 2D NMR spectroscopy and ESI(+) mass spectrum.3

In particular, the ^{1}H NMR spectrum ($CDCl_3$, 400 MHz, 298 K) of a 1:1 mixture (**Figure 130b**) of **33**$^{2+}$ and **12** (**Scheme 11**) showed a typical signature at highfield negative values (from 1.0 to −1.0 ppm, see **Figure 130b**) characteristic of an *endo*-complexation of the alkyl chains shielded by calixarene aromatic rings. This result and the absence of shielded benzylic resonances in the 4−6 ppm region, typical of *endo*-benzyl complexation,[77,80,] were a clear-cut proof that *head*-to-*head* (*H,H*)-handcuff pseudo[2]rotaxane **34**$^{2+}$ (**Scheme 11**) had been stereo-selectively formed. This result confirms once more the scarce influence of the short *m*-xylylene spacer with respect to the *endo-alkyl rule*. The formation of the handcuff pseudo[3]rotaxane **34**$^{2+}$ was confirmed by a prominent peak at 935.3 *m*/*z* in the ESI(+) mass spectrum (**Figure 132)** corresponding to the doubly-charged ion.

[109] For a review on superweak anion $TFPB^-$: Strauss, S. H. *Chem Rev.* **1993**, *93*, 927.

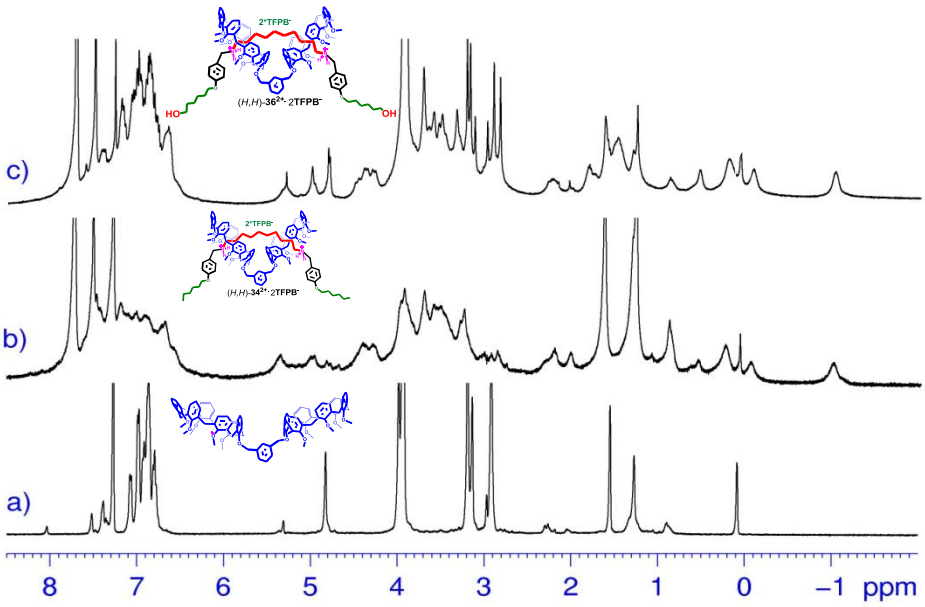

Figure 129. ^{1}H NMR spectra (400 MHz, $CDCl_3$, 298 K) of: (a) **12**, (b) an equimolar mixture (3 mM) of **12** and **33**$^{2+}$· 2TFPB^{-}, (c) an equimolar mixture (3 mM) of **12** and **36**$^{2+}$· 2TFPB^{-}.

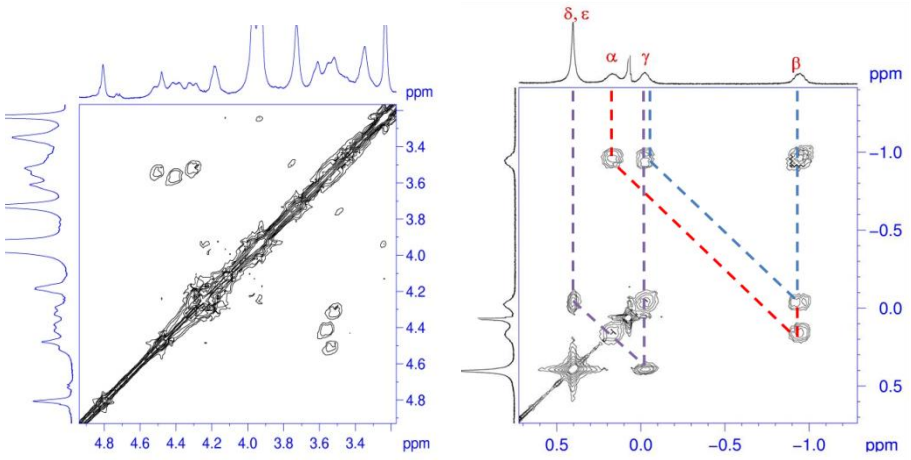

Figure 130. Expansions of 2D COSY-45 spectrum (400 MHz, $CDCl_3$, 298 K) of an equimolar mixture (3 mM) of **12** and **33**$^{2+}$· 2TFPB^{-}.

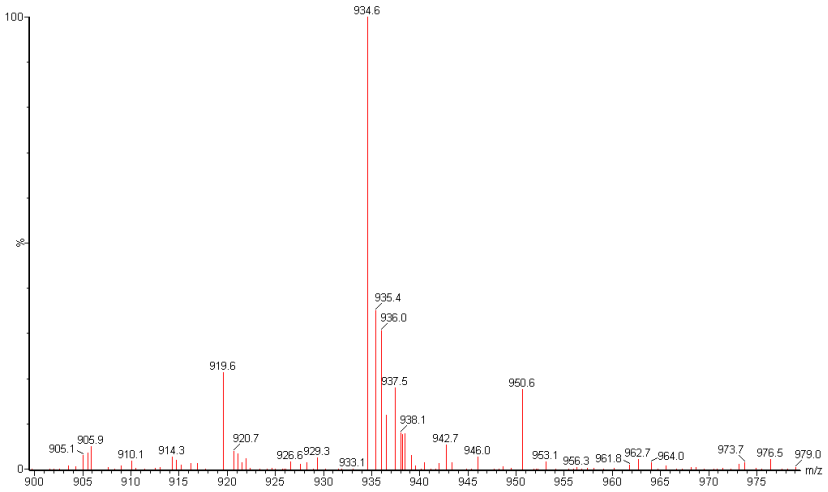

Figure 131. ESI(+) mass spectrum of doubly-charged (*H,H*)-handcuff-pseudo[2]rotaxane **34**$^{2+}$

5.3.2 Stereo-programmed synthesis of (H,H)-handcuff-[2]rotaxane **37**$^{2+}$

In order to obtain a handcuff [2]rotaxane architecture we attempted the handcuff-threading of derivative **12** with axle **35**$^{2+}$ encoding inner alkyl chains and bearing two terminal OH groups, which are derivatizable with a trityl-bearing isocyanate as the stoppering reagent (**Scheme 12**).[80]

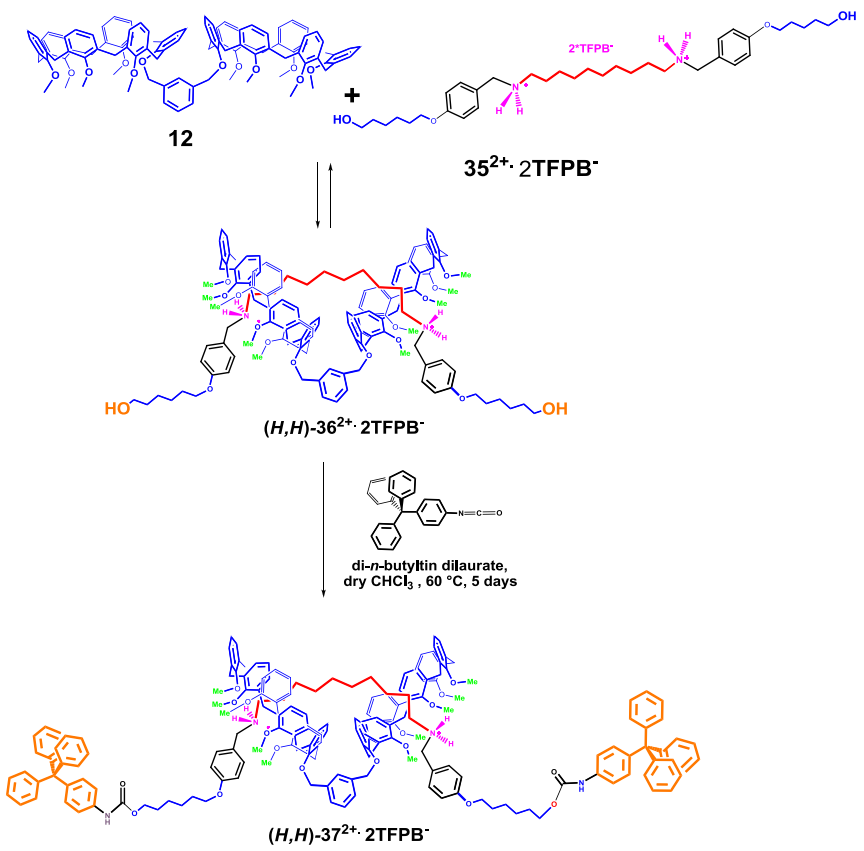

Scheme 12. *Synthesis of double-calix[6]arene-based-(H,H)-handcuff-[2]rotaxane.*

Therefore, the TFPB salt of **35**$^{2+}$ was equilibrated with double-calix[6]arene **12** to give (*H,H*)-handcuff pseudo[2]rotaxane **36**$^{2+}$ (**Scheme 12**). The ^{1}H NMR spectrum (**Figure 130c**) of a 1:1 mixture of **35**$^{2+}$ and **12** in $CDCl_3$ showed a typical signature at highfield and negative values (from 1.0 to −1.0 ppm) characteristic of an *endo*-complexation of the alkyl chains shielded by calixarene aromatic rings.

As above, the absence of shielded benzylic resonances in the 4-6 ppm region, typical of *endo*-benzyl complexation, were a clear-cut proof that *tail-to-tail* (*H,H*)-handcuff pseudo[2]rotaxane **36**$^{2+}$ had been stereoselectively formed.

Again, the validity of our *endo-alkyl rule* is confirmed. As above, a COSY-45 spectrum allowed a complete confident assignment of all *n*-alkyl resonances of the axle of (*H,H*)-handcuff-pseudo[2]rotaxane **36**$^{2+}$. Thus, one strongly shielded chain inside the cavity was observed, with ε, δ, γ, β, and α protons resonating at 1.00, 0.45, 0.04, −0.92 and 0.23 ppm, respectively, while three $ArCH_2Ar$ AX systems was observed at 4.54/3.70, 4.42/3.52 and 4.34/3.50 ppm.

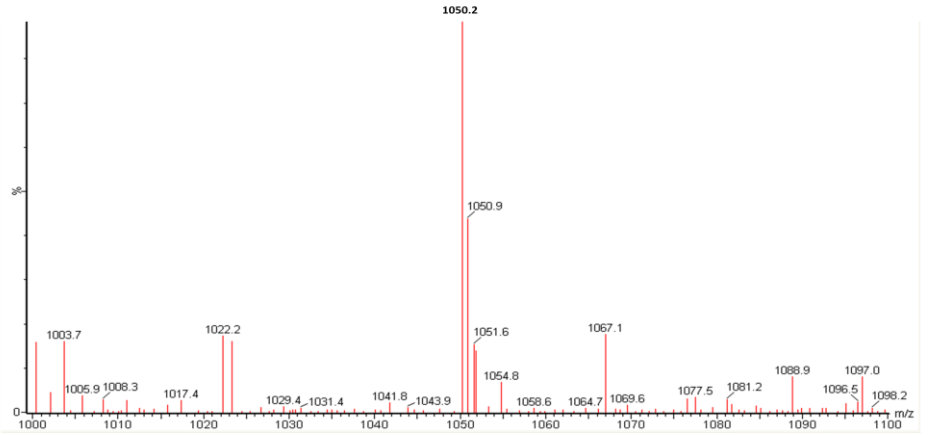

Figure 132. ESI(+) mass spectrum of doubly-charged (*H,H*)-handcuff-pseudo[3]rotaxane **36**$^{2+}$

This pseudorotaxane was then stoppered by reaction with 4-tritylphenyl isocyanate to give handcuff [2]rotaxane (*H,H*)-**37**$^{2+}$ in 35% yield (**Scheme 12**). The formation of (*H,H*)-**37**$^{2+}$ was confirmed by a prominent peak at 1370.1 m/z in the ESI(+) mass spectrum in **Figure 134**, corresponding to the doubly-charged supramolecular ion. The *head-to-head* stereosequence of the two calix-wheels in the precursor (*H,H*)-handcuff pseudo[2]rotaxane **36**$^{2+}$ was retained after the stoppering reaction as evidenced by ^{1}H NMR spectrum (**Figure 135a**) of (*H,H*)-**37**$^{2+}$ in $CDCl_3$, which showed a typical signature at highfield values (from 1.0 to −1.0 ppm) and no resonances in the 4-6 ppm region. As above the COSY-45 spectrum (**Figure 136**) ($CDCl_3$,

400 MHz, 298 K) of (*H,H*)-**37**$^{2+}$ in $CDCl_3$ allowed a complete confident assignment of all shielded alkyl resonances.

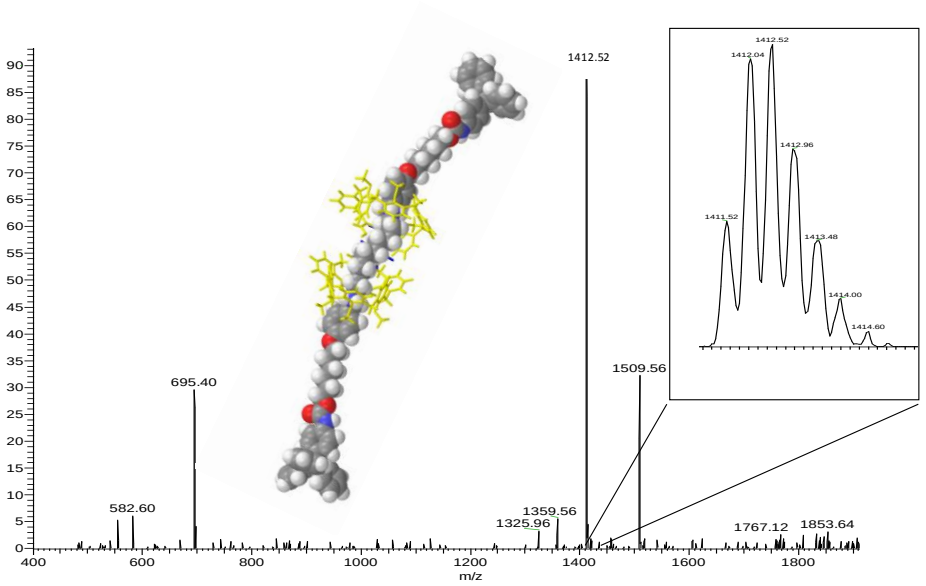

Figure 133. ESI(+) mass spectrum of (*H,H*)-**37**$^{2+}$ and its AMBER energy-minimized structure (inset).

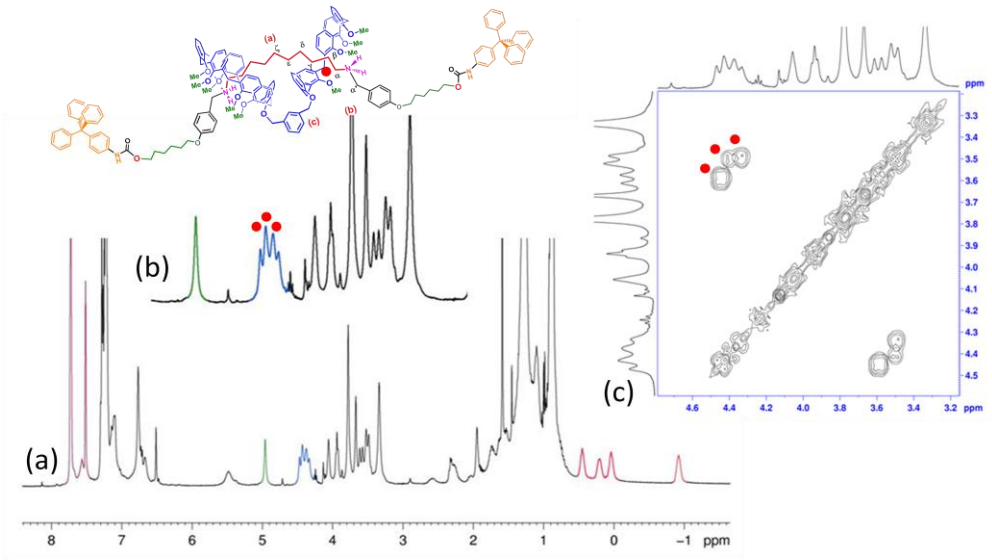

Figure 134. (a) ^{1}H NMR spectrum (400 MHz, $CDCl_3$, 298 K) of handcuff-[2]rotaxane (*H,H*)-**37**$^{2+}$ · 2TFPB^{-} (b) Expansion of the methylene region of the ^{1}H NMR spectrum of (*H,H)*-**37**$^{2+}$and (c) Expansion of methylene region of the 2D COSY-45 spectrum of (*H,H*)-**37**$^{2+}$

Thus, α protons at 0.19 ppm, shows a coupling with β methylene group at −0.99 ppm, which presents a cross-peak with γ protons at 0.04 ppm, finally coupled with δ methylene at 0.44 ppm which was coupled with ε protons at 1.11 ppm.

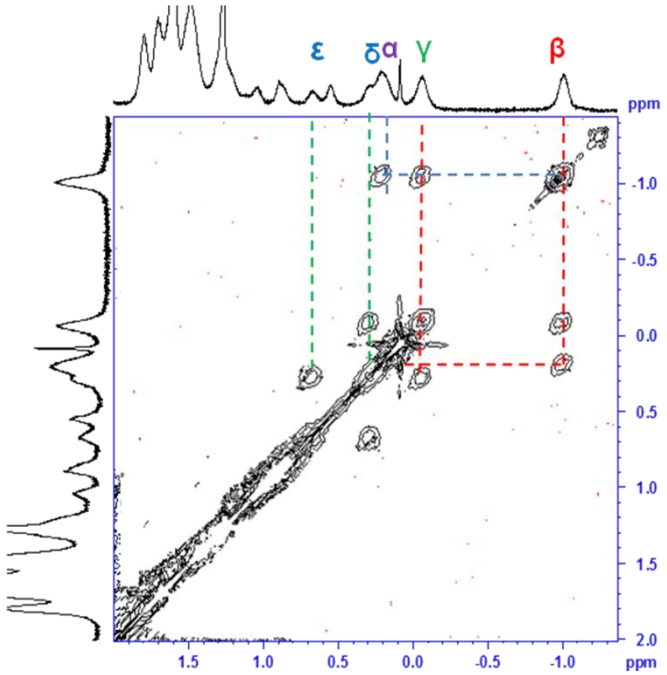

Figure 135. Expansions of 2D COSY-45 spectrum (400 MHz, $CDCl_3$, 298 K) of the (*H,H*)-handcuff-[2]rotaxane **37**$^{2+}$.

Analogously to handcuff-architectures (*H,H*)-**34**$^{2+}$ and (*H,H*)-**36**$^{2+}$ above described the $ArCH_2Ar$ region (3−5 ppm) of the COSY-45 spectrum (**Figure 135c**) ($CDCl_3$, 400 MHz, 298 K) of (*H,H*)-**37**$^{2+}$, revealed the presence of three AX systems at 4.45/3.60, 4.41/3.50 and 4.34/3.49 ppm relative to calixarene $ArCH_2Ar$ groups, while the ^{1}H NMR spectrum of (*H,H*)-**37**$^{2+}$ in $CDCl_3$, showed three singlets in a 2:2:1 ratio at 3.78, 3.67 and 3.34 ppm relative to OMe groups and a singlet a 4.96 ppm relative to methylene groups of the *m*-xylylene bridge.

The stereochemical preference was also confirmed by molecular mechanics calculations[110](AMBER force field, $CHCl_3$, GB/SA model solvent), that

[110] MacroModel-9.0/Maestro-4.1 program: Mohamadi, F.; Richards, N. G.; Guida, W. C.; Liskamp, R.; Lipton, M.; Caufield,C.; Chang,G.; Hendrickson, T.; Still, W. C. *J. Comput. Chem*. **1990**, *11*, 440.

indicates an folded conformation of the thread in handcuff-rotaxane (*H,H*)-**37**$^{2+}$ (**Figure 136**).

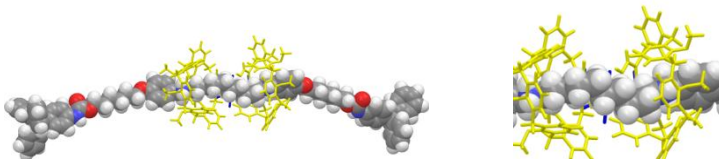

Figure 136. Lowest energy structure of the (*H,H*)-handcuff- [2]rotaxane **37**$^{2+}$ found by Monte Carlo conformational search (10000 steps, MacroModel V. 9.0, AMBER force field) on the left and its expansion on the right

5.4 Stereo-programmed synthesis of a *(H,T)*-handcuff [2]rotaxane

5.4.1 Stereo-programmed synthesis of *(H,T)*-handcuff pseudo[2]rotaxane 39^{2+}

The most natural conclusion of the above approach was the preparation of a handcuff pseudo[2]rotaxane with a programmed *head-to-tail* stereosequence. For this purpose it was very interesting to design an asymmetric axle in which there was both one inner and one outer alkyl chain to allow the *head-to-tail* stereosequence.

At this regard we decided to connect an outer alkylbenzylammonium moiety to a inner ones to give thread **38**$^{2+}$ bearing an alkyl and a benzyl unit at the two extremities (**Scheme 13**).

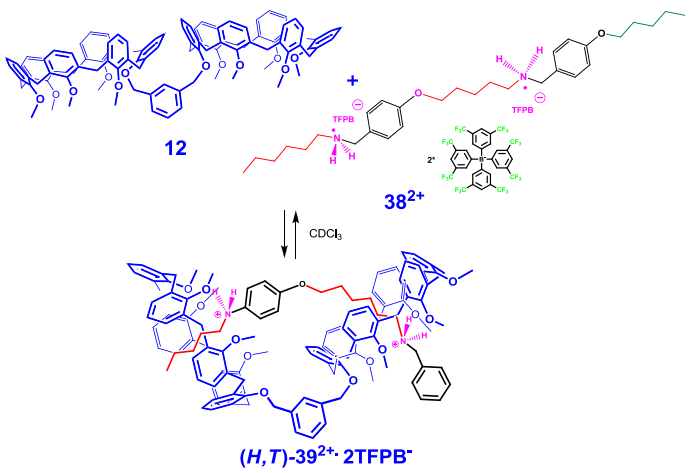

Scheme 13. Stereo-programmed handcuff-threading of **12** with **38**$^{2+}$to give (*H,T*)-handcuff-pseudo[2rotaxane **39**$^{2+}$.

To verify the predicted stereochemical outcome, the TFPB[111] salt of **38**$^{2+}$ was equilibrated with double-calix[6]arene **12** (**Scheme 13**). Then, the formation of the handcuff pseudo[2]rotaxane architecture **39**$^{2+}$ was confirmed by 1D and 2D NMR spectroscopy and ESI(+) mass spectrum.

As expected, the ^{1}H NMR spectrum ($CDCl_3$, 400 MHz, 298 K), of a 1:1 mixture (**Figure 137b**) of **38**$^{2+}$ and **12** (**Scheme 13**) showed a typical signature at highfield negative values (from 1.0 to −1.0 ppm, see **Figure 137b**) characteristic of an *endo*-complexation. This result and the absence of shielded benzylic resonances were a clear-cut proof that *head*-to-*tail* handcuff pseudo[2]rotaxane **39**$^{2+}$ (**Scheme 13**) had been stereo-selectively formed. This formation was confirmed by a prominent peak at 1022 *m/z* in the ESI(+) mass spectrum corresponding to the doubly-charged **39**$^{2+}$ ion.

[111] For a review on superweak anion $TFPB^-$: Strauss, S. H. *Chem Rev.* **1993**, *93*, 927.

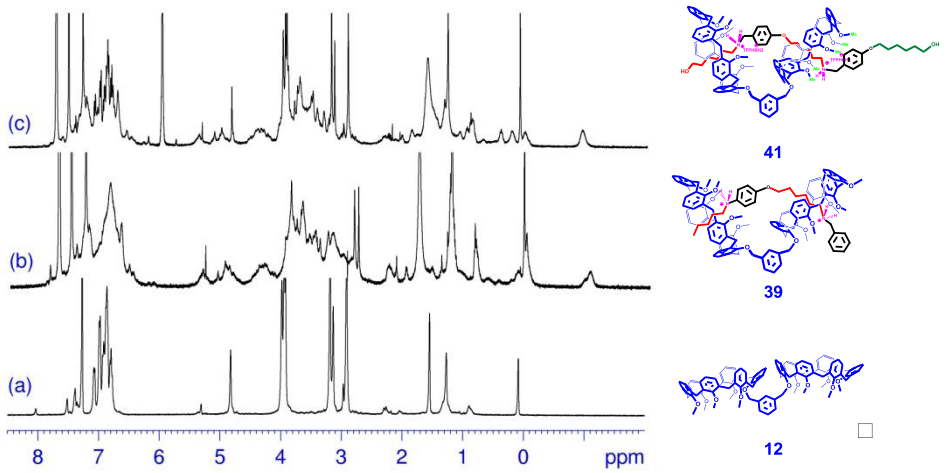

Figure 137. ^{1}H NMR spectra (400 MHz, $CDCl_3$, 298 K) of: (a) **12**, (b) an equimolar mixture (3 mM) of **8** and $\mathbf{38}^{2+}\cdot 2TFPB^{-}$, (c) an equimolar mixture (3 mM) of **12** and $\mathbf{40}^{2+}\cdot 2TFPB^{-}$.

5.4.2 Stereo-programmed synthesis of (H,T)-handcuff [2]rotaxane 42

In order to obtain the corresponding handcuff [2]rotaxane architecture, we decided to study the handcuff-threading of derivative **12** with axle $\mathbf{40}^{2+}$ encoding the same elements of $\mathbf{38}^{2+}$ and bearing two terminal derivatizable OH groups, (**Scheme 14**).[80] Since axle $\mathbf{40}^{2+}$ was unknown, we decided to synthesize it with the synthetic route reported in **Scheme 14.**

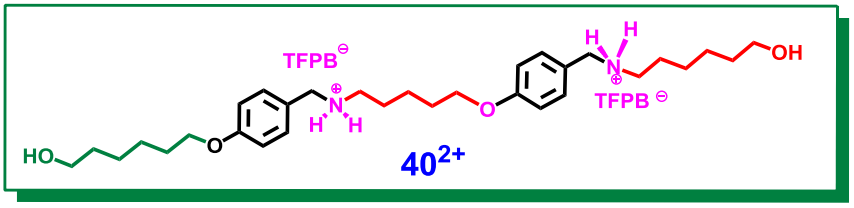

Thread $\mathbf{40}^{2+}$(**Scheme 14**) was obtained by following a six step sequence with the isolation and characterization of five intermediates. The sequence started with the Gabriel synthesis that involved the alkylation of potassium

phthalimide **43** with the 1,6-dibromohexane **44** in DMF^{dry} at reflux for 48 hours, to give derivative **45** with a 87.4% yield.

Compound **45** was then involved in a nucleophilic substitution with *p*-cyanophenol **46**, which led to the formation of compound **47**. The reaction was carried out in acetonitrile in the presence of potassium carbonate to generate the nucleophilic agent, the phenoxide anion. The protected amino function of **47** was then released with *hydrazine* under an Argon atmosphere to obtain the cyano-ammina **48** with a 90% yield. This derivative is a key intermediate, the central building block for the construction of the bis-ammonium axle.

The coupling of derivative **48** with aldehyde **49**, followed by an in-situ imine reduction with sodium borohydride in anhydrous methanol, led to the formation of a secondary amine **50** with a yield higher than 90%.

The next step involved the reduction of the cyano-group of **50** to aldehyde **51** with Adams's catalyst. The subsequent treatment with hydrochloric acid allowed the isolation of chlorohydrate **52.** The latter derivative was then involved in another amination reaction through the coupling with 1-ammino-6-hexanol **53**, followed by imine reduction, to lead to the formation of the second secondary amine function of **54.** This was then treated with 37% HCl to obtain the bis-chloride **55.** The last step involved an ion-exchange reaction by treatment of this bis-chloride with the sodium salt of TFPB, to give derivative $\mathbf{40^{2+}}$.

All synthetic intermediates were isolated and fully characterized by mass spectrometry and NMR spectroscopy.

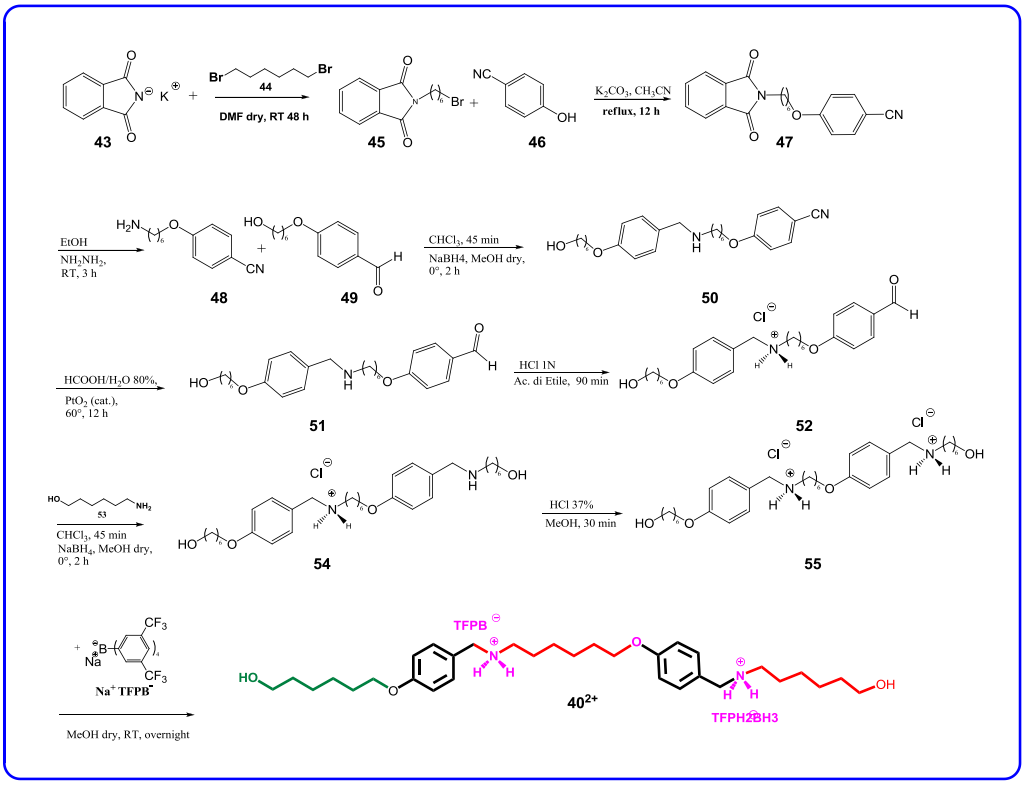

Scheme 14. synthesis of thread **40^{2+}**

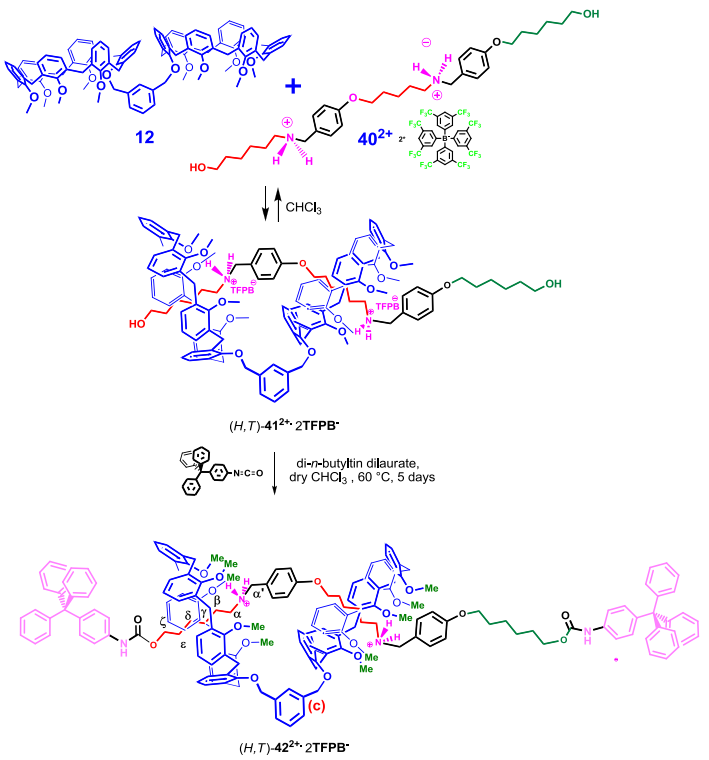

Scheme 15. *Synthesis of the first example of (H,T)double-calix[6]arene-based handcuff-[2]rotaxane* ***42***

The TFPB salt of $\mathbf{40^{2+}}$ was equilibrated with double-calix[6]arene **12** to give (*T,H*)-handcuff pseudo[2]rotaxane $\mathbf{41^{2+}}$ (**Scheme 15**). The ^{1}H NMR spectrum (**Figure 137c**) of a 1:1 mixture of $\mathbf{40^{2+}}$ and **12** in $CDCl_3$ showed a typical signature at highfield and negative values (from 1.0 to −1.0 ppm) characteristic of an *endo*-complexation of the alkyl chains. As in the previous instances, this and the absence of shielded benzylic resonances were a clear evidence that *head-to-tail* handcuff pseudo[2]rotaxane $\mathbf{41^{2+}}$ had been stereoselectively formed. Again, the validity of our *endo-alkyl rule* is confirmed. As above, a COSY-45 spectrum allowed a complete confident assignment of all *n*-alkyl resonances of the axle of $\mathbf{40^{2+}}$. Thus, two different, strongly shielded chains inside the cavity were now observed; the

asymmetry of the system was reflected in the presence of six $ArCH_2Ar$ AX systems three each at 4.45/3.62 4.44/3.60, 4.42/3.52, 4.40/3.57, 4.38/355, 4.36/3.524, .34/3.50 ppm, respectively.(**Figure 137**)

Head-to-tail handcuff pseudo[2]rotaxane **41** was then stoppered by reaction with 4-tritylphenyl isocyanate to give handcuff [2]rotaxane (*H,T*)-**42** in 60% yield (**Scheme 15**). The formation of (*H,T*)-**42** was confirmed by a prominent peak at 1370.1 m/z in the ESI(+) mass spectrum (**Figure 138**) corresponding to the doubly-charged supramolecular ion.

The *head-to-tail* stereosequence of the two calix-wheels was evidenced by a ^1H NMR spectrum (**Figure 139**) of (*H,T*)-**42** in $CDCl_3$, which showed a typical signature at highfield values (from 1.0 to −1.0 ppm) and no resonances in the 4-6 ppm region. As above the COSY-45 spectrum (**Figure 140**) in $CDCl_3$ allowed a complete confident assignment of all shielded alkyl resonances. In particular the asymmetry of the system is evident by the presence of six AX systems, related to $ArCH_2Ar$ groups, as it is well documented by the 2D-COSY spectrum (**Figure 140b**).

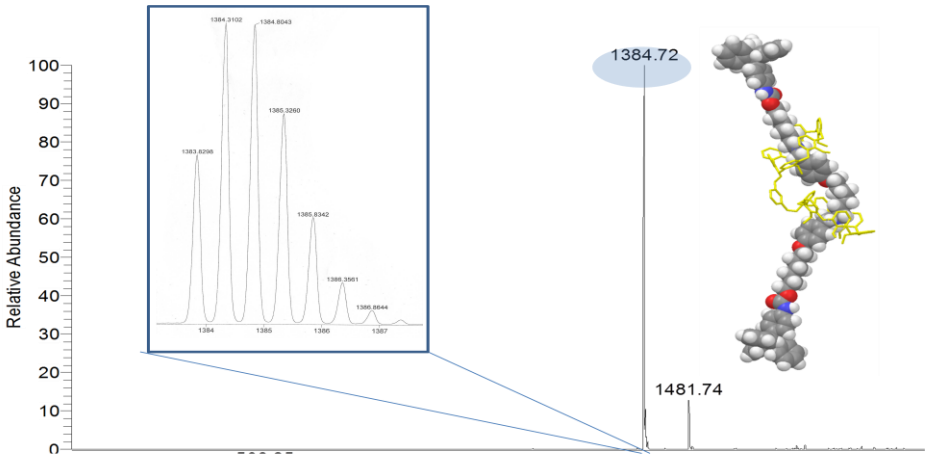

Figure 138. ESI(+) mass spectrum of (*H,T*)-$\mathbf{42}^{2+}$ and its AMBER energy-minimized structure (inset).

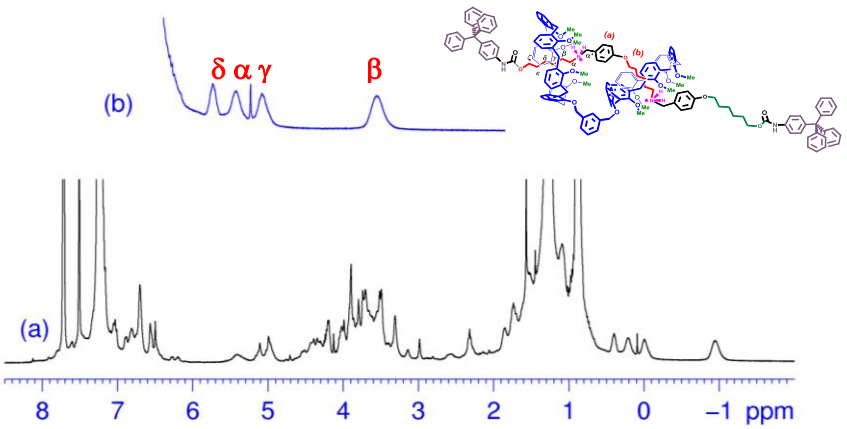

Figure 139. (a) ^{1}H NMR spectrum (400 MHz, $CDCl_3$, 298 K) of handcuff-[2]rotaxane (*H,T*)-**42**$^{2+}$· 2TFPB^{-}. (b) Expansion of the negative region of the ^{1}H NMR spectrum of (*H,T*)-**42**.

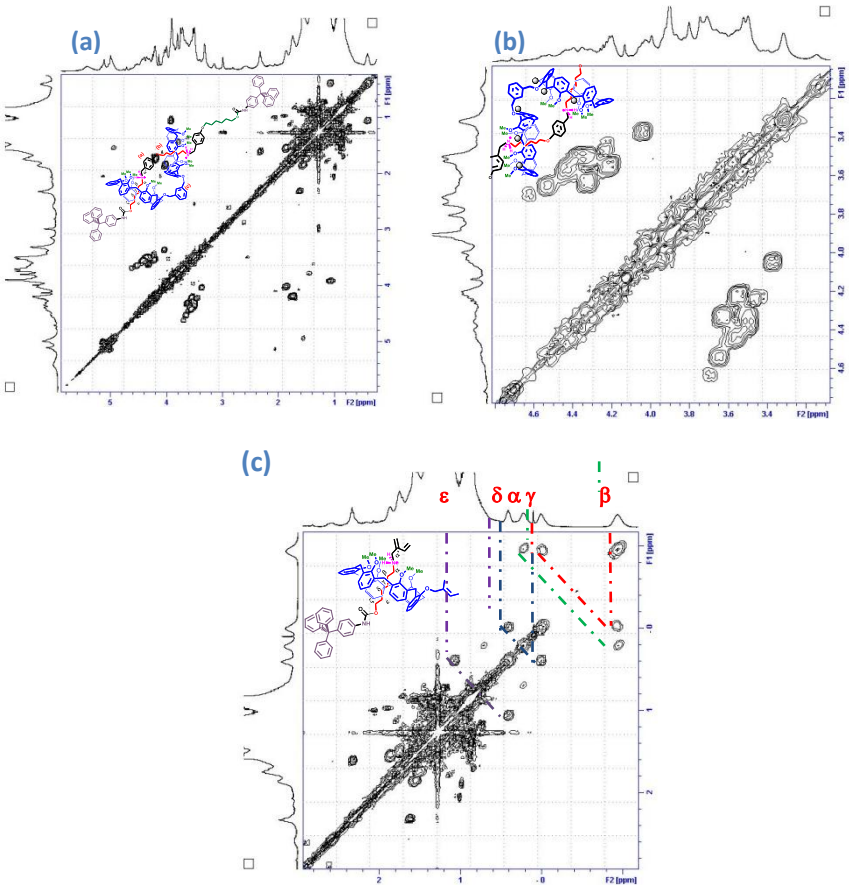

Figure 140. (a) 2D COSY-45 spectrum (400 MHz, $CDCl_3$, 298 K) of the (*H,T*)-handcuff-[2]rotaxane **42**; (b) Expansions of 2D COSY-45 spectrum of methykene region of the (*H,T*)-handcuff-[2]rotaxane **42**; (c) Expansions of 2D COSY-45 spectrum of negative region of the (*H,T*)-handcuff-[2]rotaxane **42**

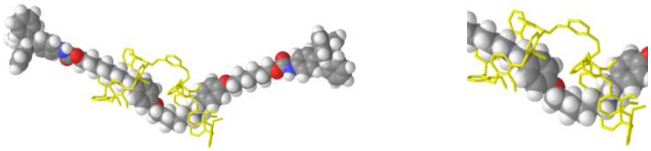

Figure 141. Lowest energy structures of the (*H,T*)-handcuff- [2]rotaxane **42** found by Monte Carlo conformational search (10000 steps, MacroModel V. 9.0, AMBER force field).

5.5 EXPERIMENTAL SECTION

GENERAL COMMENTS

ESI(+)-MS measurements were performed on a Micromass Bio-Q triple quadrupole mass spectrometer equipped with electrospray ion source, using a mixture of H_2O/CH_3CN (1:1) and 5% HCOOH as solvent. Flash chromatography was performed on Merck silica gel (60, 40-63 μm). All chemicals were reagent grade and were used without further purification. Anhydrous solvents were purchased from Aldrich. When necessary compounds were dried *in vacuo* over $CaCl_2$. Reaction temperatures were measured externally. Reactions were monitored by TLC on Merck silica gel plates (0.25 mm) and visualized by UV light, or by sprying with H_2SO_4-$Ce(SO_4)_2$ or phosphomolybdic acid. Sodium tetrakis[3,5-bis(trifluoromethyl)phenyl]borate[112], was synthesized according to literature procedures.

NMR spectra were recorded on a Bruker Avance-400 spectrometer [400 (^{1}H) and 100 MHz (^{13}C)], Bruker Avance-300 spectrometer [300 (^{1}H) and 75 MHz (^{13}C)], or Bruker Avance-250 spectrometer [250 (^{1}H) and 63 MHz (^{13}C)]; chemical shifts are reported relative to the residual solvent peak ($C\mathit{H}Cl_3$: δ 7.26, $\mathit{C}DCl_3$: δ 77.23; $C_6\mathit{H}_5C\mathit{H}_3$: δ 7.09, 7.00, 6.98, 2.09, $\mathit{C}_6D_5\mathit{C}D_3$: δ 137.9, 129.2, 128.3 125.5, 20.4; $CD_3O\mathit{H}$: δ 4.87, $\mathit{C}D_3OD$: δ 49.0; THF-d_8: 3.58, 1.73). Standard pulse programs, provided by the manufacturer, were used for 2D COSY and 2D ROESY experiments. Monte Carlo conformational searches (10000 steps) were performed with MacroModel-

[112] Nishida, H.; Takada, N.; Yoshimura, M.; Sonoda, T.; Kobayashi, H. *Bull. Chem. Soc. Jpn.* **1984**, *57*, 2600.

9/Maestro-4.1[113] program using OPLS force-field and $CHCl_3$ solvent (GB/SA model).

5.5.1 Preparation of handcuff pseudo[2]rotaxane (*T,T*)-29^{2+}

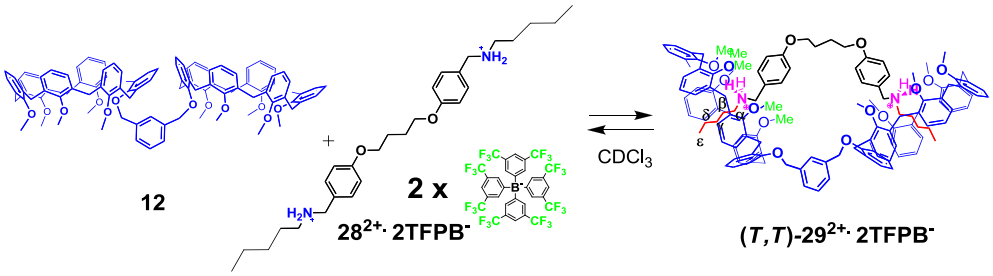

Scheme 16. Formation of handcuff pseudo[2]rotaxane (*T,T*)-$\mathbf{29}^{2+}$·2TFPB^{-}.

Double-calixarene derivative **12** ($1.81 \cdot 10^{-3}$ g, $1.2 \cdot 10^{-3}$ mmol) and derivative $\mathbf{28}^{2+}$ ($2.60 \cdot 10^{-3}$ g, $1.2 \cdot 10^{-3}$ mmol) were dissolved in 0.4 mL of $CDCl_3$ and the mixture was stirred for 5 min at 25 °C. Then, the solution was transferred in a NMR tube for 1D and 2D NMR spectra acquisition.

[113] MacroModel- 9.0/Maestro-4.1 program: Mohamadi, F.; Richards, N. G.; Guida, W. C.; Liskamp, R.; Lipton, M.; Caufield,C.; Chang,G.; Hendrickson, T.; Still, W. C. *J. Comput. Chem*. **1990**, *11*, 440

2D COSY-45 Spectrum of handcuff pseudo[2]rotaxane (*T,T*)-29^{2+}

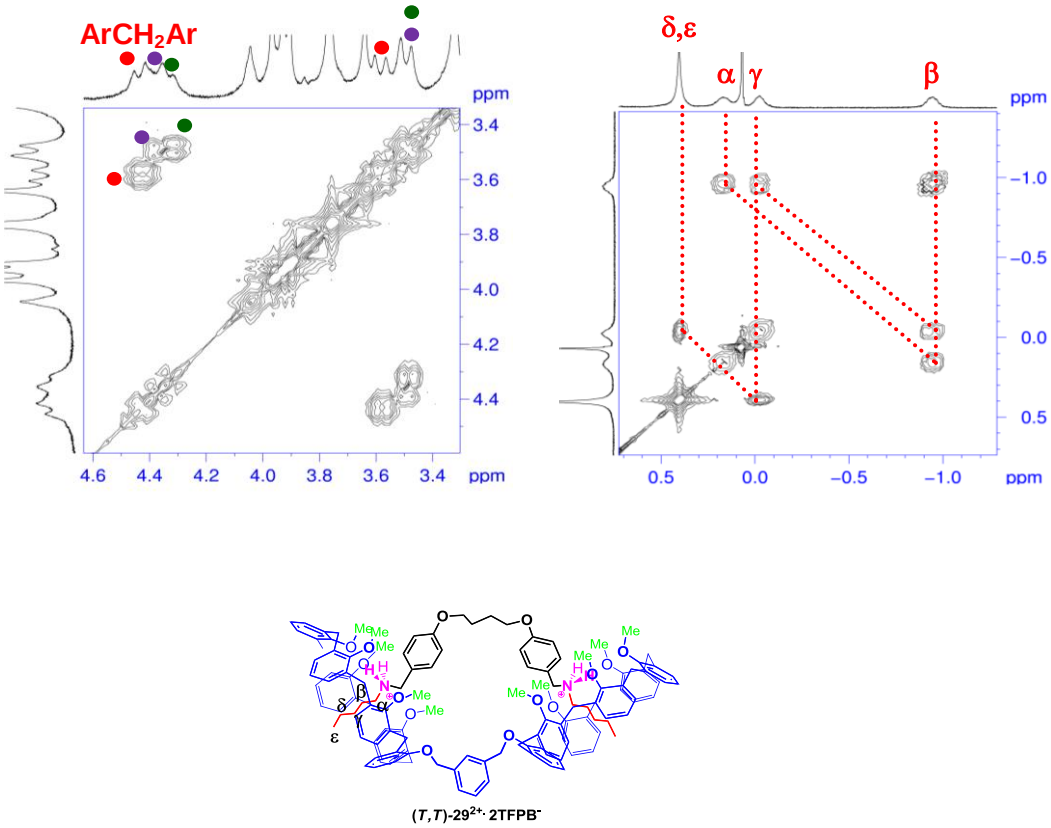

Figure 142. Relevant portions of the 2D COSY spectrum (400 MHz, $CDCl_3$, 298 K) of handcuff pseudo[2]rotaxane (*T,T*)-**29**$^{2+}$·2TFPB^{-}.

5.5.2. Preparation of handcuff pseudo[2]rotaxane (*T,T*)-31^{2+}

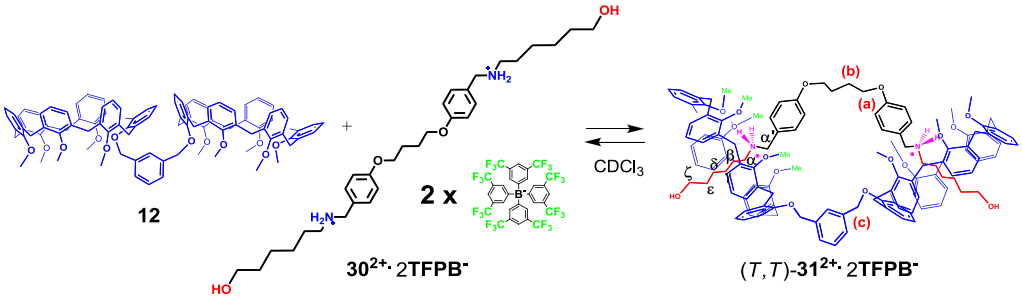

Scheme 17. Formation of handcuff pseudo[2]rotaxane (*T,T*)-**31**$^{2+}$·2TFPB^{-}.

Double-calixarene derivative **12** ($1.81\cdot10^{-3}$ g, $1.2\cdot10^{-3}$ mmol) and derivative **30**$^{2+}$ ($2.67\cdot10^{-3}$ g, $1.2\cdot10^{-3}$ mmol) were dissolved in 0.4 mL of $CDCl_3$ and the mixture was stirred for 5 min at 25 °C. Then, the solution was transferred in a NMR tube for 1D and 2D NMR spectra acquisition.

2D COSY-45 Spectrum of handcuff pseudo[2]rotaxane (*T,T*)-31^{2+}

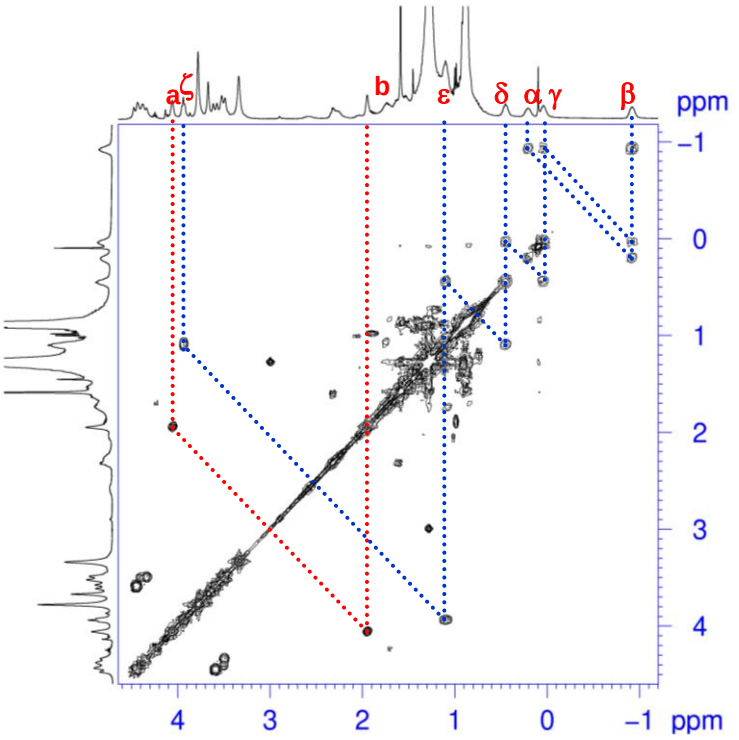

Figure 143. Relevant portion of the 2D COSY spectrum (400 MHz, $CDCl_3$, 298 K) of handcuff pseudo[2]rotaxane (*T,T*)-**31**$^{2+}$·2TFPB^{-}.

5.5.3. Synthesis of Handcuff [2]Rotaxane (*T,T*)-32^{2+}

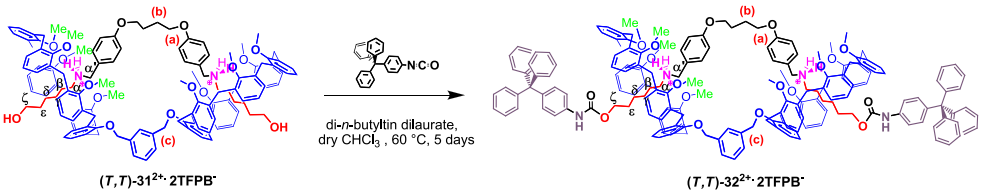

Scheme 18. Synthesis of handcuff [2]rotaxane (*T,T*)-**30**$^{2+}$·2TFPB^{-}.

Di-*n*-butyltin dilaurate (3 drops) was added to a solution of **30**$^{2+}$ (0.18 mmol, 0.41 g) and **12** (0.11 mmol, 0.17 g) in dry $CHCl_3$ (12 mL) at room temperature, and subsequently, 4-triphenylmethylphenylisocyanate (0.083 g, 0.230 mmol) was added. The reaction was kept under stirring at 60 °C for 5 days. The crude product was purified by column chromatography (SiO_2; hexane/CH_2Cl_2 2/8) to give handcuff rotaxane (*T,T*)−**32**$^{2+}$ as a white solid (0.14 g, 0.031 mmol, 28%). **ESI(+) MS**: *m/z* = 1370 (M^{2+}/2); **^{1}H NMR** (400 MHz, $CDCl_3$, 298 K): δ −0.92 (broad, 4H, CH_2^{β}), 0.04 (broad, 4H, CH_2^{γ}), 0.21 (broad, 4H, CH_2^{α}), 0.44 (broad, 4H, CH_2^{δ}), 1.11 (broad, 4H, CH_2^{ε}), 1.94 (broad, $OCH_2CH_2CH_2CH_2O$, 4H), 2.23 (broad, 4H, $CH_2^{\alpha'}$), 3.49 and 4.34 (AX, $ArCH_2Ar$, 8H), 3.50 and 4.41 (AX, $ArCH_2Ar$, 8H), 3.60 and 4.45 (AX, $ArCH_2Ar$, 8H), 3.34, 3.67 and 3.78 (s, OMe, 12, 6 and 12H respectively), 3.91 (broad, 4H, CH_2^{ζ}), 4.05 (broad, $OCH_2CH_2CH_2CH_2O$, 4H), 4.96 (s, $OCH_2^{m\text{-}xylenyl}$, 4H), 5.48 (broad, $^+NH_2$, 4H), 6.77−7.28 (overlapped, 88H, ArH+NHCO), 7.52 [s, 8H, $(ArH)^{TFPB\text{-}}$], 7.72 [s, 16H, $(ArH)^{TFPB\text{-}}$]; ^{13}C NMR (100 MHz, $CDCl_3$, 298 K): δ 24.5, 29.9, 64.7, 117.6, 120.7, 123.4, 126.1, 127.7, 131.3, 134.9, 135.1, 142.5, 146.9, 161.1, 161.6, 162.1. Anal. Calcd for $C_{248}H_{210}B_2F_{48}N_4O_{18}$: C, 66.67; H, 4.74. Found: C, 66.75; H, 4.67.86.

1D and 2D NMR Spectra of Handcuff [2]Rotaxane (*T,T*)-32^{2+}

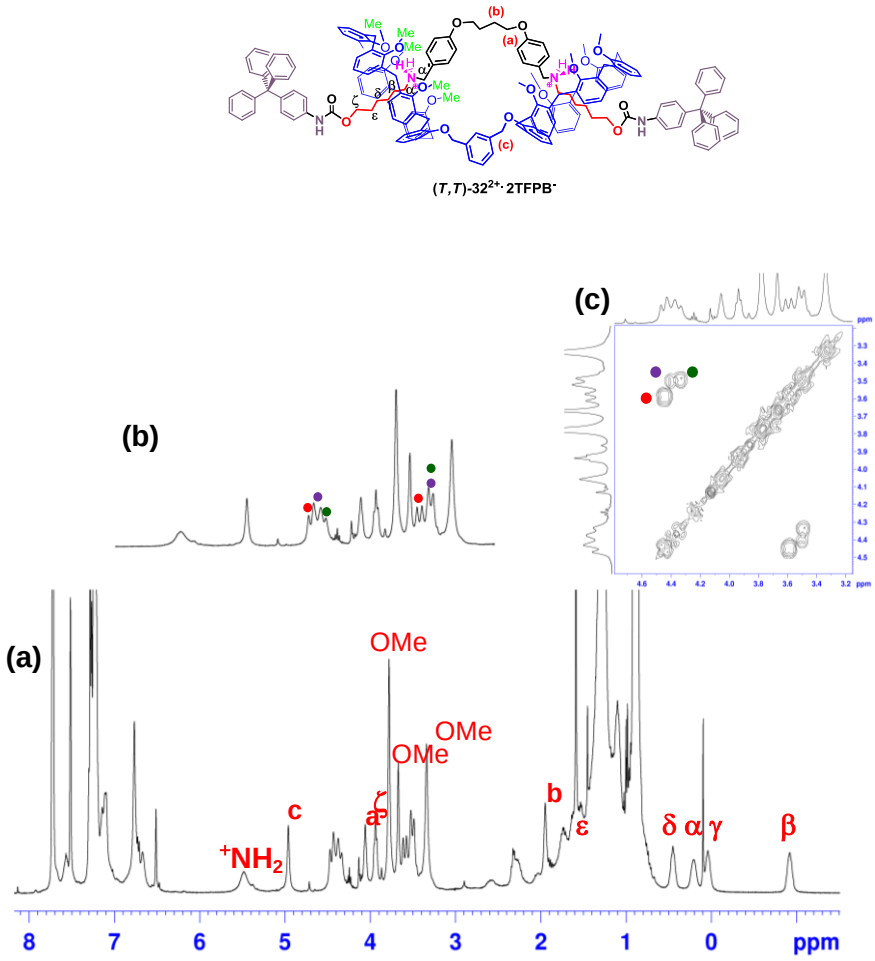

Figure 144. (a) ^{1}H NMR spectrum (400 MHz, $CDCl_3$, 298 K) of handcuff [2]rotaxane (*T,T*)-**32**$^{2+}$ · 2TFPB^{-}. (b) Expansion of the methylene region of the ^{1}H NMR spectrum of (*T,T*)-**32**$^{2+}$. (c) Expansion of the methylene region of the 2D COSY-45 spectrum of (*T,T*)-**32**$^{2+}$.

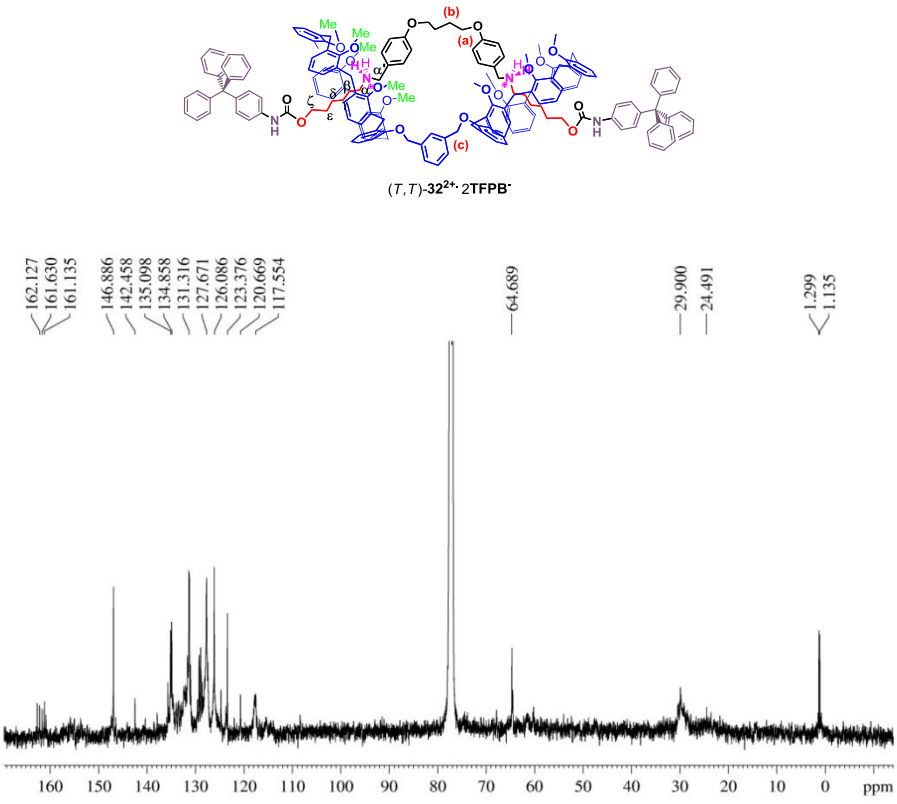

Figure 145. ^{13}C NMR spectrum (100 MHz, $CDCl_3$, 298 K) of handcuff [2]rotaxane (*T,T*)-**32^{2+}.**

2D COSY-45 Spectrum of handcuff [2]rotaxane (*T*,*T*)-32^{2+}

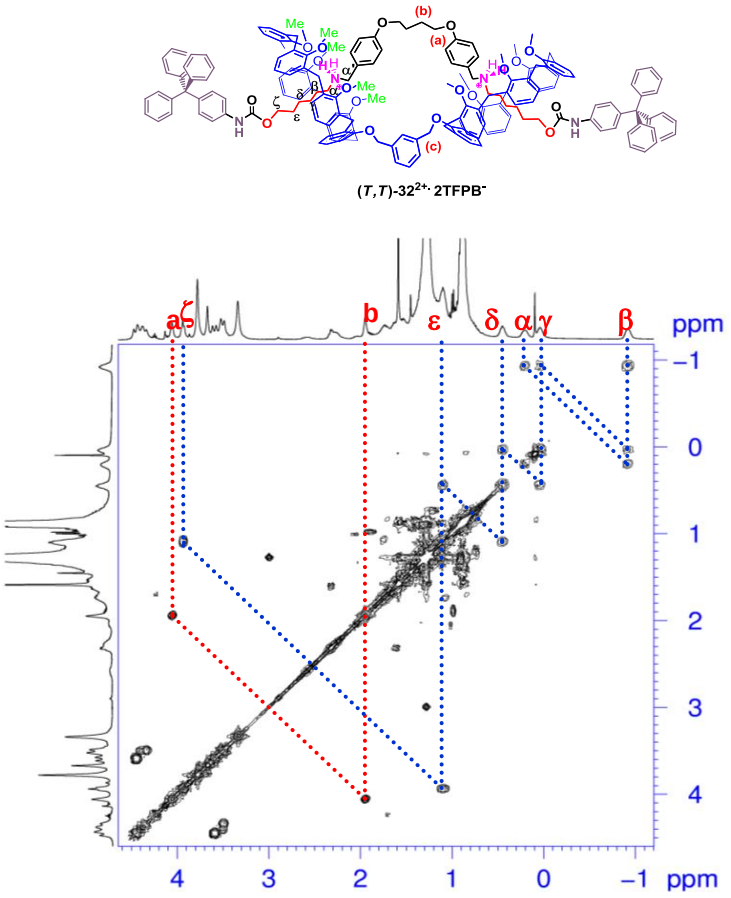

Figure 146. Relevant portion of the 2D COSY spectrum (400 MHz, $CDCl_3$, 298 K) of handcuff -[2]rotaxane (*T*,*T*)-**32**$^{2+}$·2TFPB^{-}.

5.5.4 Simulated Annealing Experiments on Handcuff pseudo[2]rotaxane (*T,T*)-31^{2+}

Simulated Annealing (SA) experiments performed on pseudo[2]rotaxane (*T,T*)-**31**$^{2+}$ evidenced that about 75% of the coconformers in the 4 kcal/mol lowest energy window (200 independent annealing experiments) showed a dihedral angle in the 42-87° range around the C(1)-C(2) bond (Figure S15, black squares). Analogously, about 85% of the same structures gave a C(2)-C(3) dihedral angle in the 50-75° range (**Figure 148**, red circles).

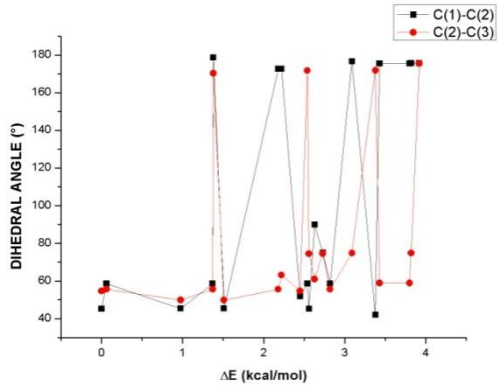

Figure 147. Dihedral angle values (°) around C(1)-C(2) and C(2)-C(3) bonds measured for the SA structures of (*T,T*)-**36**$^{2+}$ in the 4 kcal/mol lowest energy window. The structures are ranked according to their energy difference (ΔE) with respect to the lowest minimum one (0.0 kcal/mol).

5.5.5 Simulated Annealing Experiments on handcuff [2]rotaxane (*T,T*)-32^{2+}

Analogously to pseudorotaxane (*T,T*)-**31**$^{2+}$, SA experiments performed on (*T,T*)-**32**$^{2+}$ evidenced that about 65% of the coconformers in the 4 kcal/mol lowest energy window (200 independent experiments) showed a dihedral angle in the

45-70° range around the C(1)-C(2) bond (**Figure 149,** black squares). Analogously, about 50% of the same structures gave a C(2)-C(3) dihedral angle in the 59-84° range (**Figure 149**, red circles).

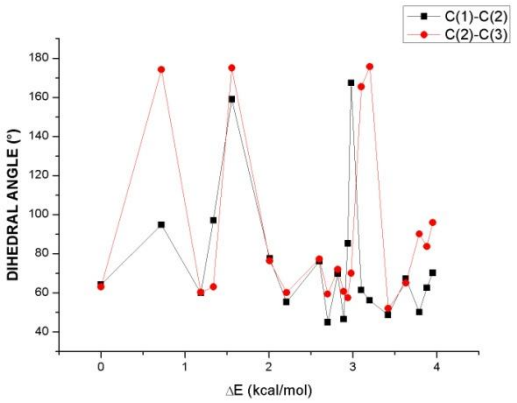

Figure 148. Dihedral angle values (°) around C(1)-C(2) and C(2)-C(3) bonds measured for the SA structures of (*T,T*)-**30**$^{2+}$ in the 4 kcal/mol lowest energy window. The structures are ranked according to their energy difference (ΔE) with respect to the lowest minimum one (0.0 kcal/mol).

5.5.6. Preparation of handcuff pseudo[2]rotaxane (*H,H*)-34^{2+}

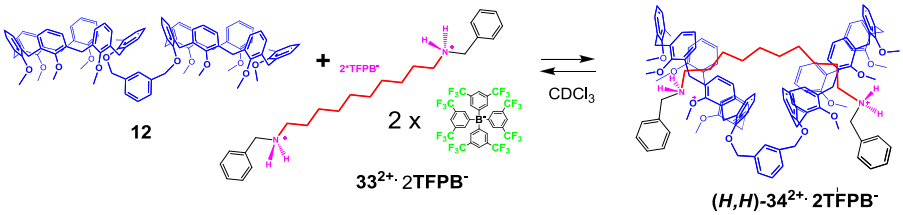

Scheme 19. Formation of handcuff pseudo[2]rotaxane (*H,H*)-**34**$^{2+}$·2TFPB^{-}.

Double-calixarene derivative **12** ($1.89 \cdot 10^{-3}$ g, $1.2 \cdot 10^{-3}$ mmol) and derivative **33**$^{2+}$ ($2.60 \cdot 10^{-3}$ g, $1.25 \cdot 10^{-3}$ mmol) were dissolved in 0.4 mL of $CDCl_3$ and the mixture was stirred for 5 min at 25 °C. Then, the solution was transferred in a NMR tube for 1D and 2D NMR spectra acquisition.

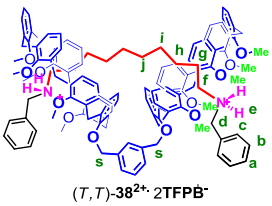

^{1}H NMR (400 MHz, $CDCl_3$, 298 K): δ-0.96 [*broad*, $(CH_2)_g$, 4H], -0.06 [*broad*, $(CH_2)_h$, 4H], 0.22 [*broad*, $(CH_2)_f$ + $(CH_2)_i$, 8H], 0.51 [*broad*, $(CH_2)_j$, 4H], 3.52 and 4.36 (AX, $ArCH_2Ar$, J = 12.6 Hz, 12H), 3.60 (s, OCH_3, 36H), 4.98 (s, $OCH_2^{m\text{-}xylenyl}$, 4H)$_s$ 5.34 [*broad*, $(NH_2^+)_e$, 4H], 6.84-6.95 (overlapped, ArH_{calix} , 36H), 7.49 (s, ArH_{TFPB}^-, 8H), 7.59 (dd, ArH_b, $J_1 = J_2$ = 7.6 Hz, 4H), 7.70 (s, ArH_{TFPB}^-, 16H).

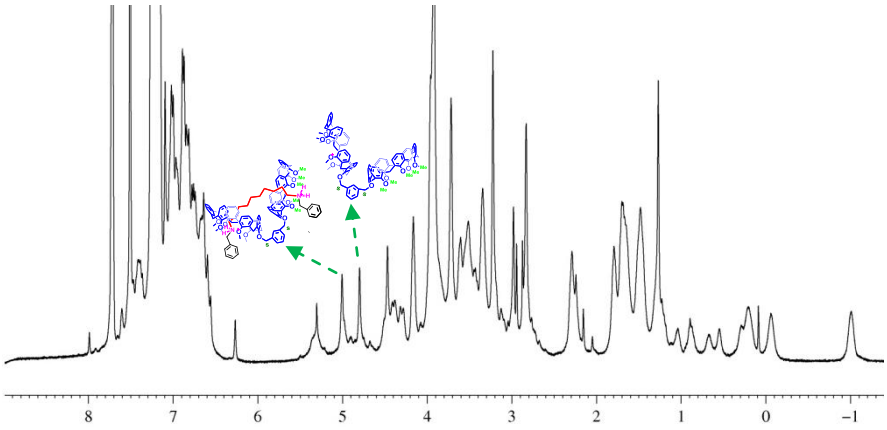

Figure 149. ^{1}H NMR spectrum (400 MHz, $CDCl_3$, 298 K) of handcuff pseudo[2]rotaxane (*H,H*)-**34**$^{2+}$ · 2TFPB$^-$.

2D COSY-45 Spectrum of handcuff pseudo[2]rotaxane (*H,H*)-34^{2+}

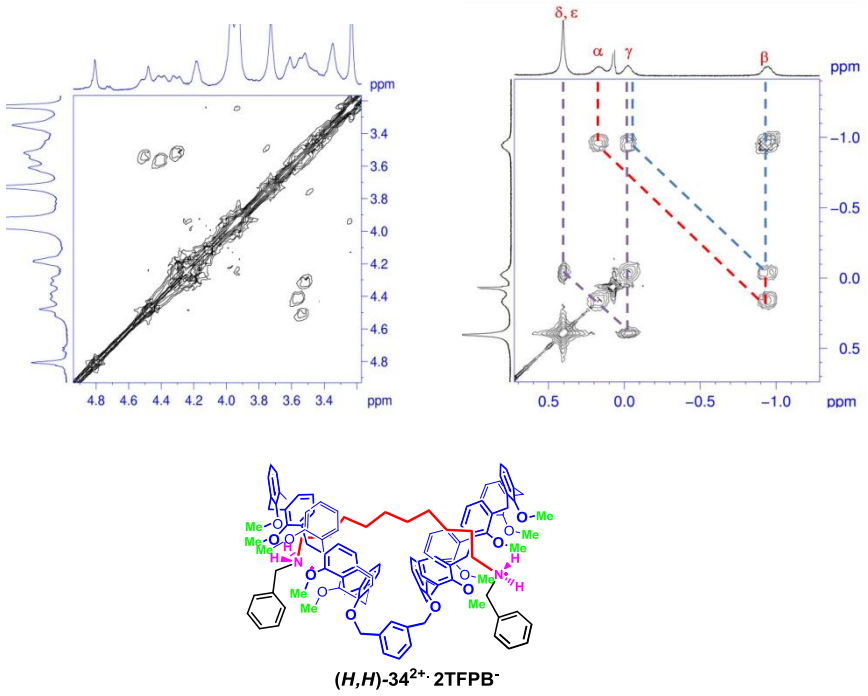

Figure 150. Relevant portions of the 2D COSY spectrum (400 MHz, $CDCl_3$, 298 K) of handcuff pseudo[2]rotaxane (*H,H*)-**34**$^{2+}$·2TFPB$^-$.

5.5.7 Preparation of handcuff pseudo[2]rotaxane (*H,H*)-36^{2+}.

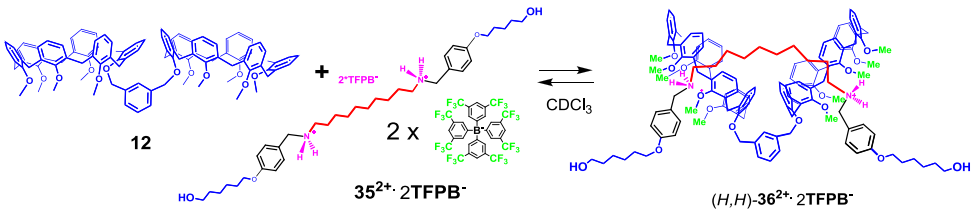

Scheme 20. Formation of handcuff pseudo[2]rotaxane (*H,H*)-**36**$^{2+}$·2TFPB$^-$.

Double-calixarene derivative **12** ($1.89 \cdot 10^{-3}$ g, $1.2 \cdot 10^{-3}$ mmol) and derivative 31^{2+} ($2.67 \cdot 10^{-3}$ g, $1.2 \cdot 10^{-3}$ mmol) were dissolved in 0.4 mL of $CDCl_3$ and the mixture was stirred for 5 min at 25 °C. Then, the solution was transferred in a NMR tube for 1D and 2D NMR spectra acquisition.

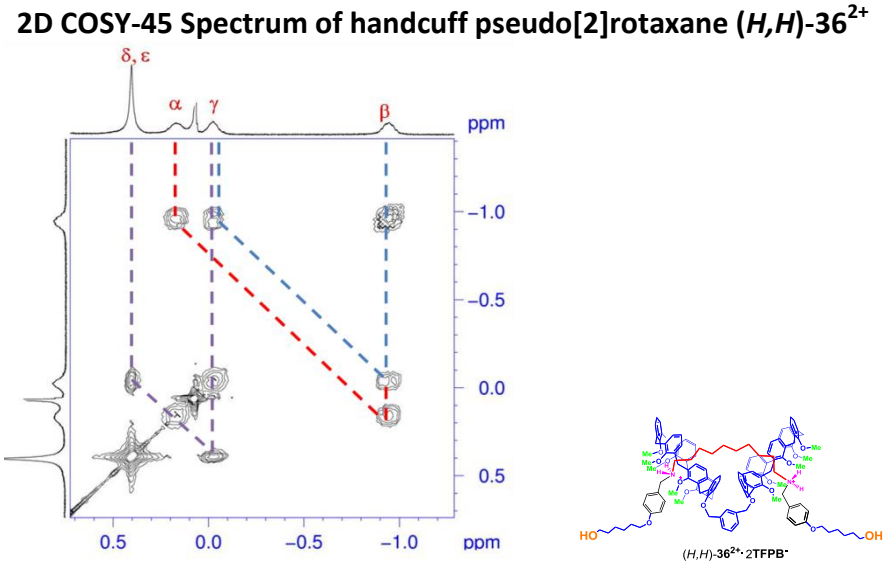

Figure 151. Relevant portion of the 2D COSY spectrum (400 MHz, $CDCl_3$, 298 K) of handcuff pseudo[2]rotaxane (*H,H*)-**36**$^{2+}$·2TFPB$^-$.

5.5.8. Synthesis of Handcuff [2]Rotaxane (*H,H*)-37^{2+}

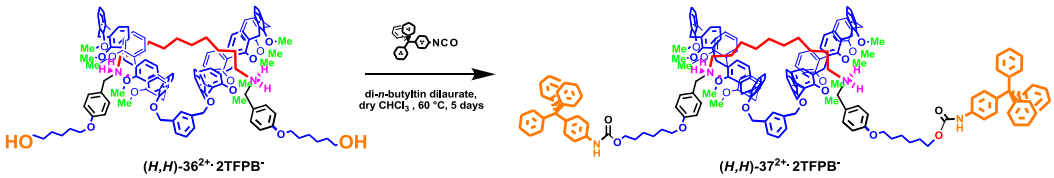

Scheme 21. Synthesis of handcuff [2]rotaxane (*H,H*)-**37**$^{2+}$·2TFPB$^-$.

Di-*n*-butyltin dilaurate (3 drops) was added to a solution of **35**$^{2+}$ (0.18 mmol, 0.41 g) and **12** (0.11 mmol, 0.17 g) in dry $CHCl_3$ (12 mL) at room temperature, and subsequently, 4-triphenylmethylphenylisocyanate (0.083 g, 0.230 mmol) was added. The reaction was kept under stirring at 60 °C for 5 days. The crude product was purified by column chromatography (SiO_2; CH_2Cl_2 100%) to give handcuff rotaxane (*H,H*)**−37**$^{2+}$ as a white solid (0.050 g, 0.035 mmol, 32%).
ESI(+) MS: *m/z* = 1412,82 ($M^{2+}/2$);
^{1}H NMR (400 MHz, $CDCl_3$, 298 K): *δ* −0.92 (broad, 4H, CH_2^{β}), 0.04 (broad, 4H, CH_2^{γ}), 0.21 (broad, 4H, CH_2^{α}), 0.44 (broad, 4H, CH_2^{δ}), 1.11 (broad, 4H, CH_2^{ε}), 1.94 broad, $OCH_2CH_2CH_2CH_2O$, 4H), 2.23 (broad, 4H, $CH_2^{\alpha'}$), 3.49 and 4.34 (AX, $ArCH_2Ar$, 8H), 3.50 and 4.41 (AX, $ArCH_2Ar$, 8H), 3.60 and 4.45 (AX, $ArCH_2Ar$, 8H), 2.84, 3.25 and 3.69 (s, OMe, 12, 6 and 12H respectively), 3.89 (broad, 4H, CH_2^{ζ}), 4.05 (broad, $OCH_2CH_2CH_2CH_2O$, 4H), 4.98 (s, $OCH_2^{m\text{-}xylenyl}$, 4H), 5.48 (broad, $^+NH_2$, 4H), 6.77−7.28 (overlapped, 88H, ArH+NHCO), 7.52 [s, 8H, $(ArH)^{TFPB^-}$], 7.72 [s, 16H, $(ArH)^{TFPB^-}$]; **^{13}C NMR** (100 MHz, $CDCl_3$, 298 K): *δ* 24.5, 29.9, 60.6, 65.1,68.7, 115.6, 118.1, 119.3, 122.9, 124.0, 125.6, 126.4, 127.2, 128.0, 128.4, 129.3,131.4, 131.6, 132.3, 135.0, 161.6, 162.1.

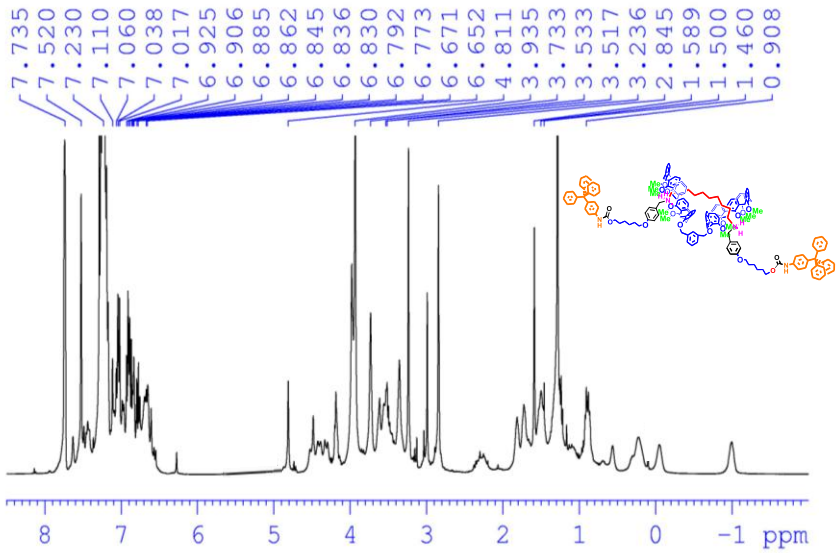

Figure 152. ^{1}H NMR spectrum (400 MHz, $CDCl_3$, 298 K) of handcuff-[2]rotaxane (*H,H*)-**37**$^{2+}$ · 2TFPB^{-}.

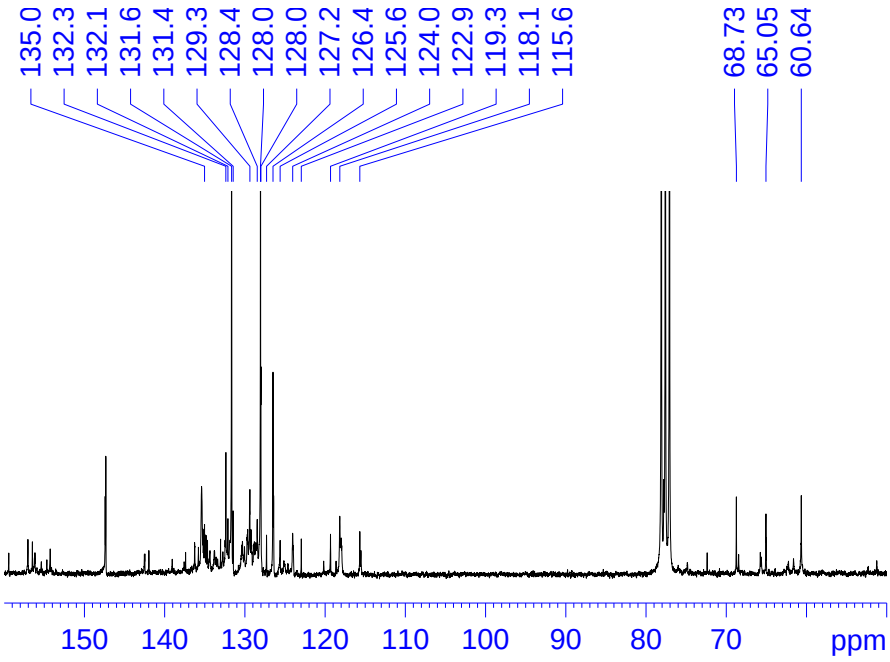

Figure 153. ^{13}C NMR spectrum (100 MHz, $CDCl_3$, 298 K) of handcuff [2]rotaxane (*H,H*)-**37**$^{2+}$.

2D COSY-45 Spectrum of handcuff [2]rotaxane (*H,H*)-37^{2+}

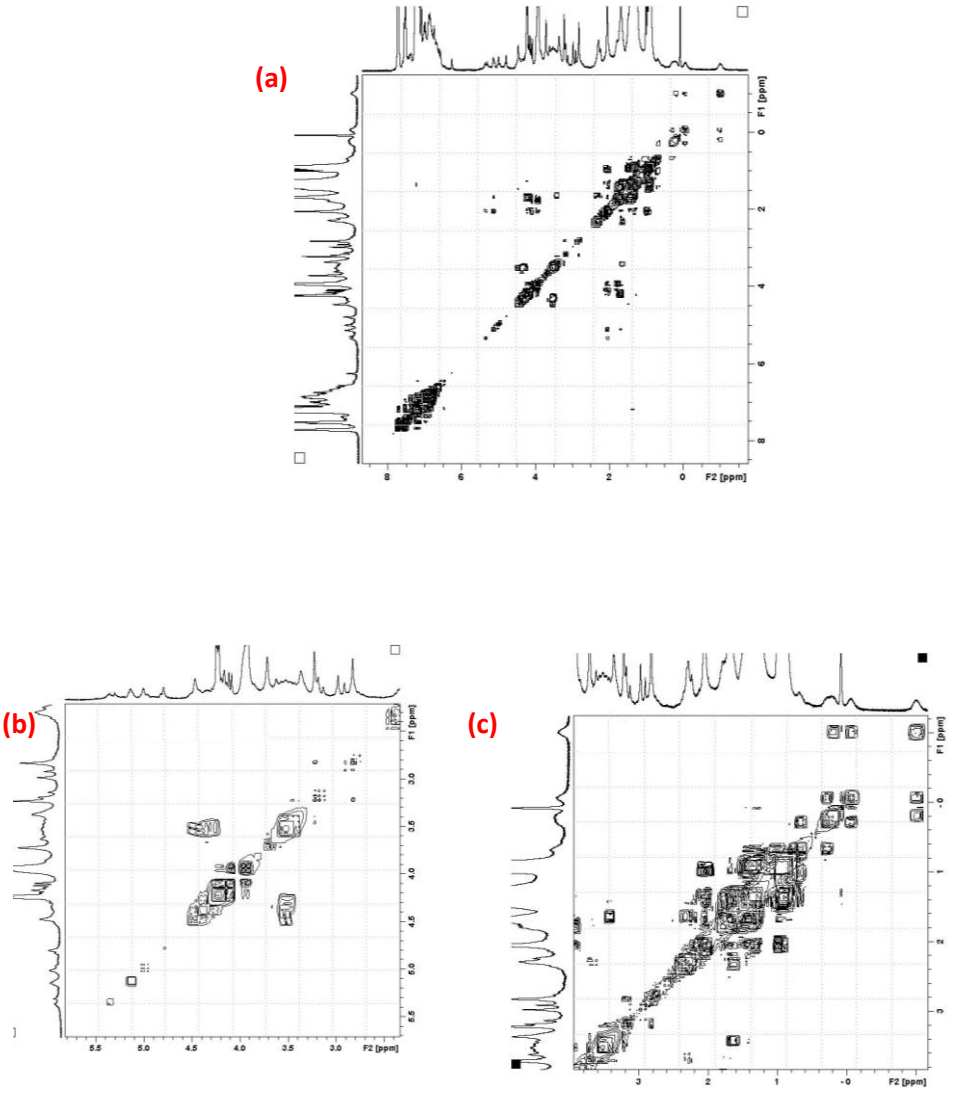

Figure 154. (a) 2D COSY-45 spectrum (400 MHz, $CDCl_3$, 298 K) of Handcuff [2]rotaxane (*H,H*)-**37**$^{2+}$; (b) Expansions of 2D COSY-45 spectrum (400 MHz, $CDCl_3$, 298 K) of methylene region of Handcuff [2]rotaxane (*H,H*)-**37**$^{2+}$;(c)Expansions of 2D COSY-45 spectrum (400 MHz, $CDCl_3$, 298 K) of negative region of Handcuff [2]rotaxane (*H,H*)-**37**$^{2+}$

5.5.9 Preparation of Handcuff Pseudo[2]rotaxane (*H,T*)-39^{2+}.

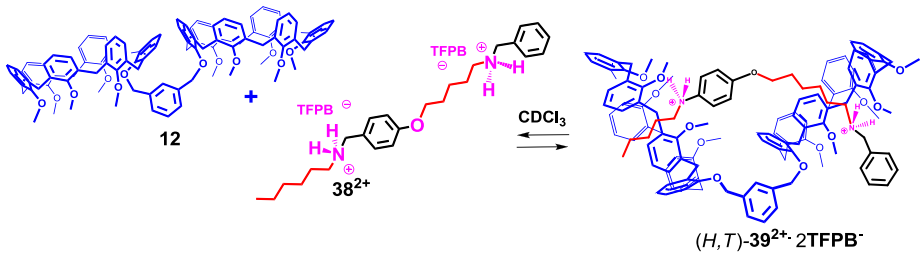

Scheme 22. Formation of handcuff pseudo[2]rotaxane (*H,T*)-$\mathbf{39}^{2+}$·2TFPB$^-$.

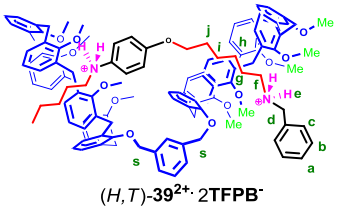

Double-calixarene derivative **12** ($1.89\cdot10^{-3}$ g, $1.2\cdot10^{-3}$ mmol) and derivative $\mathbf{38}^{2+}$ ($2.60\cdot10^{-3}$ g, $1.25\cdot10^{-3}$ mmol) were dissolved in 0.4 mL of $CDCl_3$ and the mixture was stirred for 5 min at 25 °C. Then, the solution was transferred in a NMR tube for 1D and 2D NMR spectra acquisition.

^{1}H NMR (400 MHz, $CDCl_3$, 298 K): δ-0.96 [*broad*, $(CH_2)_g$, 4H], -0.06 [*broad*, $(CH_2)_h$, 4H], 0.22 [*broad*, $(CH_2)_f$ + $(CH_2)_i$, 8H], 0.51 [*broad*, $(CH_2)_j$, 4H], 3.52 and 4.36 (AX, $ArCH_2Ar$, J = 12.6 Hz, 12H), 3.60 (s, OCH_3, 36H), 4.89 (s, $OCH_2^{m\text{-}xylenyl}$, 4H)$_s$ 5.34 [*broad*, $(NH_2^+)_e$, 4H], 6.84-6.95 (overlapped, ArH_{calix} , 36H), 7.49 (s, ArH_{TFPB}^-, 8H), 7.59 (dd, ArH_b, $J_1 = J_2$ = 7.6 Hz, 4H), 7.70 (s, ArH_{TFPB}^-, 16H).

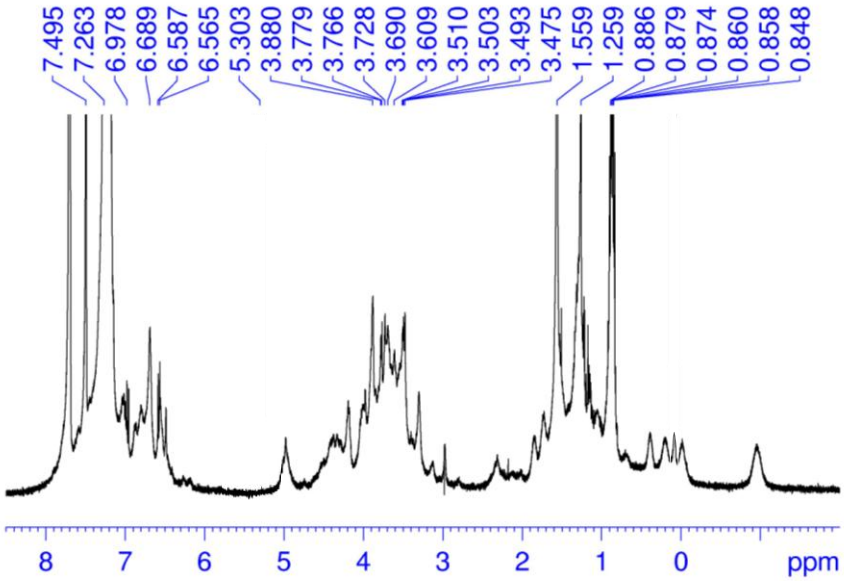

Figure 155. ^{1}H NMR spectrum (400 MHz, $CDCl_3$, 298 K) of handcuff pseudo[2]rotaxane (*H,T*)-**39**$^{2+}$**.**

5.5.10 Synthesis and characterization of thread 40^{2+} and its precursors.

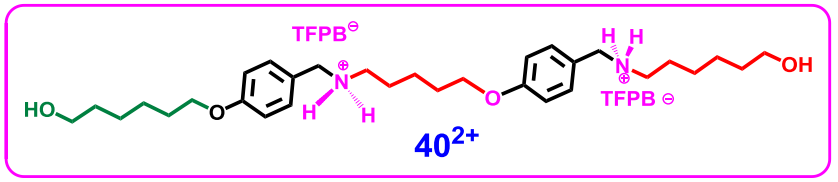

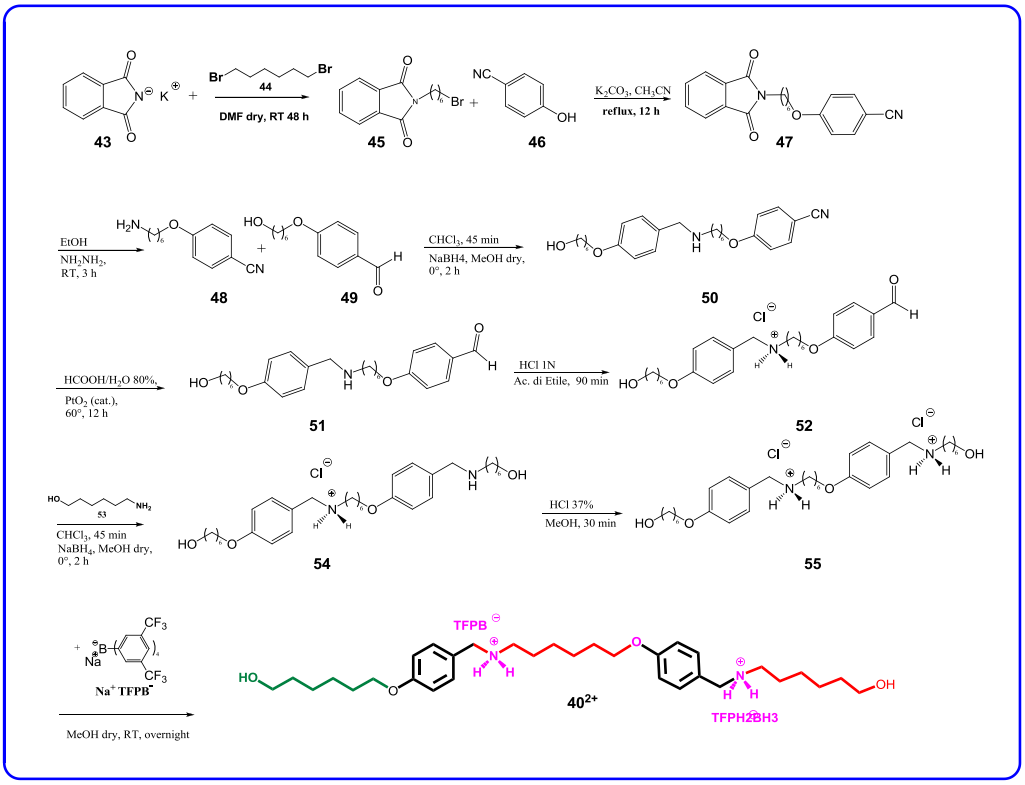

Scheme 23. Thread **40**$^{2+}$ synthesis

Derivative 45

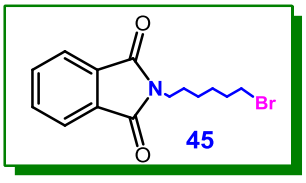

To a suspension of potassium phthalimide **43** (7.5 g, 40.49 mmol) in DMF (300 mL) was added 1,6-dibromohexane **44** (19.75g, 80.98 mmol)**;** The mixture was kept under stirring at room temperature for 48h. KBr was filtered and the product was evaporated under reduced pressure; The crude product was purified by column chromatography (SiO_2 petroleum ether /CH_2Cl_2 50/50 to give derivative **45** as a white solid (10.98 g, 35.40 mmol 87.4%); **^{1}H NMR** (400 MHz, $CDCl_3$, 298 K): δ 7.70 (overlapped, $H_{h,g}$, 4H), 3.66 (*t*, H_a, 2H, J= 7,2 Hz), 3.37 (t, H_f, 2H, J= 6.8 Hz), 1.83 (m, H_b,

2H), 1.67 (m, H_e, 2H), 1.44 (overlapped m, $H_{d,c}$, 4H). **^{13}C NMR** (100 MHz, $CDCl_3$, 298 K): δ 26.2, 27.9, 28.6, 32.8, 33.9, 38.0, 123.4, 132.3, 134.1, 168.6.

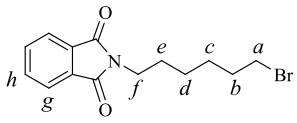

45

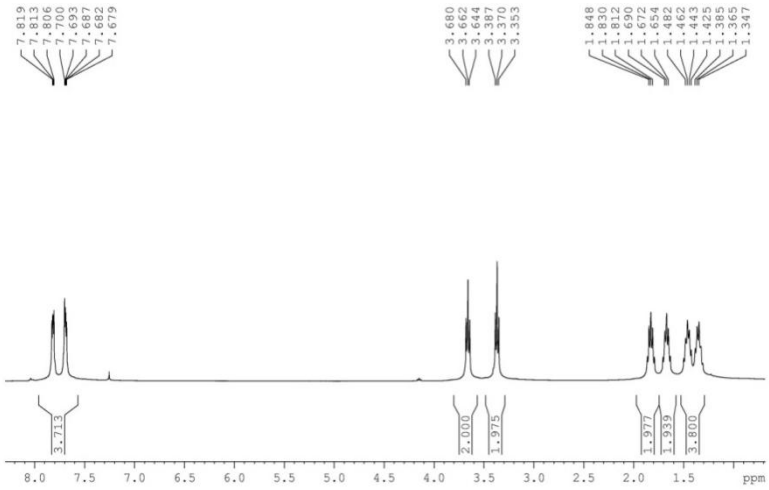

Figura 156. Spectrum ^{1}H NMR of derivative **45** in $CDCl_3$ (400 MHz, 298K)

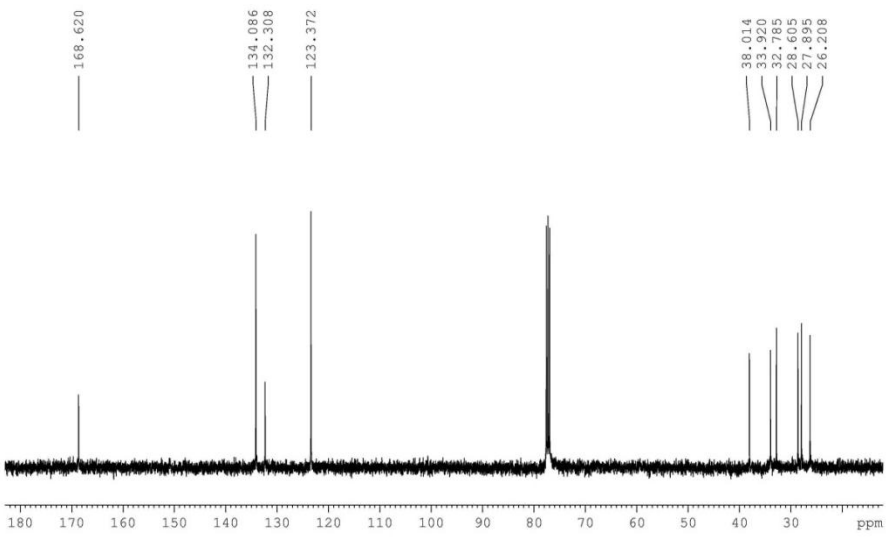

Figura 157. Spectrum ^{13}C NMR of derivative **45** in $CDCl_3$ (65 MHz, 298K)

Derivative 47

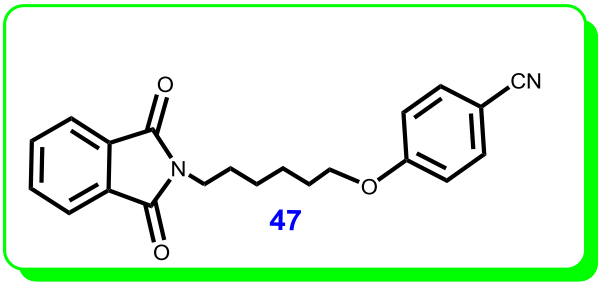

To a solution of cyanophenol **46** (3.84g, 32.2 mmol) in dry CH_3CN (400 mL) was added K_2CO_3 (18.00g, 130.23 mmol). The mixture was refluxed for 1h under N_2. The solution was cooled at room temperature and subsequently, derivative **45** (10 g, 32.25 mmol) was added. The reaction was kept under stirring at 80 °C for 12h, then the solvent was concentrated under reduced pressure. The product was extracted with CH_2Cl_2 (3×80 mL) and the organic layers were collected and dried over $MgSO_4$, filtered and evaporated under reduced pressure to give **47** as a white solid (11.23 g 100%); **^{1}H NMR** ($CDCl_3$,

400 MHz, 298 K): δ 7.82 (overlapped, H_{ab}, 4H), 7.70 (overlapped, H_{j+i}, 4H), 3.97 (t, H_c, 2H, J= 6,3 Hz), 3.69 (t, H_h, 2H, J= 7.0 Hz), 1.79 (m, H_d, 2H), 1.71 (m, H_e, 2H), 1.51 (H_f, 2H), 1.41 (H_g, 2H) .

^{13}C NMR ($CDCl_3$, 250 MHz, 298 K): δ 26.9, 27.87, 29.8, 30.2, 39.2, 60.5, 116.5, 124.6, 135.3.

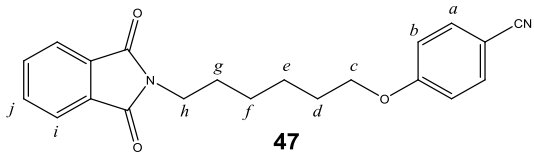

47

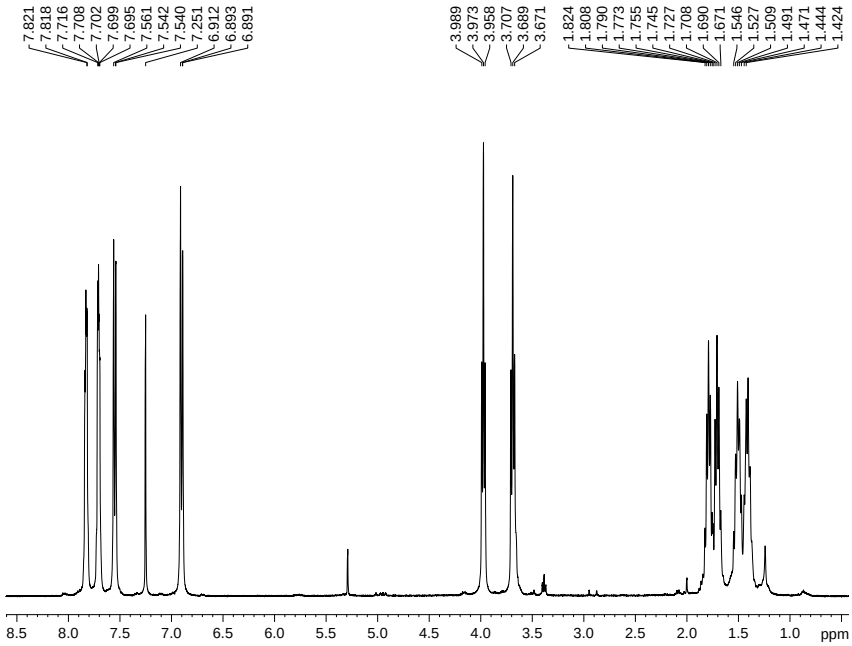

Figura 158. Spectrum ^{1}H NMR of derivative **47** in $CDCl_3$ (400 MHz, 298 K).

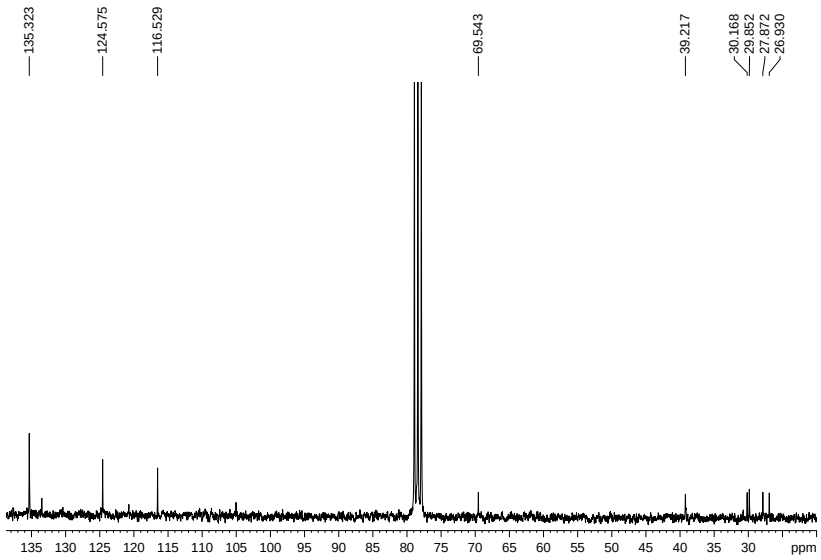

Figura 159. Spectrum in $CDCl_3$ of derivative **47** ^{13}C NMR (65 MHz, 298 K).

Derivative 48

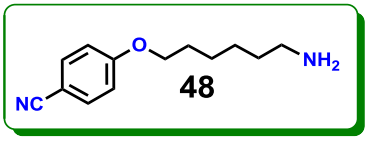

A solution of derivative **47** (5.00 g, 14.36 mmol) and hydrazine (73.3 mmol, 4.6 mL, 50-60% *v*/*v* solution in H_2O) in EtOH (40 mL) was refluxed for 1h under N_2. The solution was cooled at room temperature and H_2O (100 mL) was added. The product was extracted with AcOEt (3×80 mL) and the organic layers were collected and dried over $MgSO_4$, filtered and evaporated under reduced pressure to give **48** as a white solid (2.81 g, 90%). **^{1}H-NMR** ($CDCl_3$, 300 MHz, 298 K): δ 7.58 (H_h, 2H), 6.93 (H_i, 2H), 3.99 (t, H_g, 2H, J= 7,2 Hz), 2.70 (t, H_b, 2H, J= 6.8 Hz), 1.83 (m, H_f, 2H), 1.47 (overlapped, m, H_e+$_{d+c}$, 6H). **^{13}C-NMR** ($CDCl_3$, 300 MHz, 298 K): δ 26.0, 26.8, 33.9, 42.3, 68.5, 103.9, 115.4, 119.5, 134.1, 162.6.

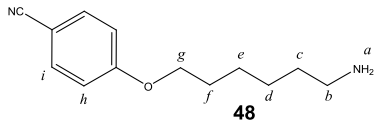

48

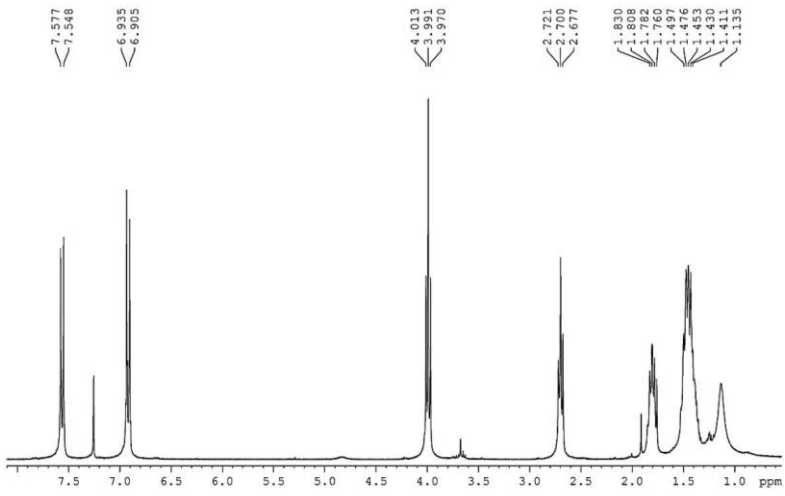

Figura 160. Spectrum ^{1}H NMR of derivative **48** in $CDCl_3$ (300 MHz, 298 K).

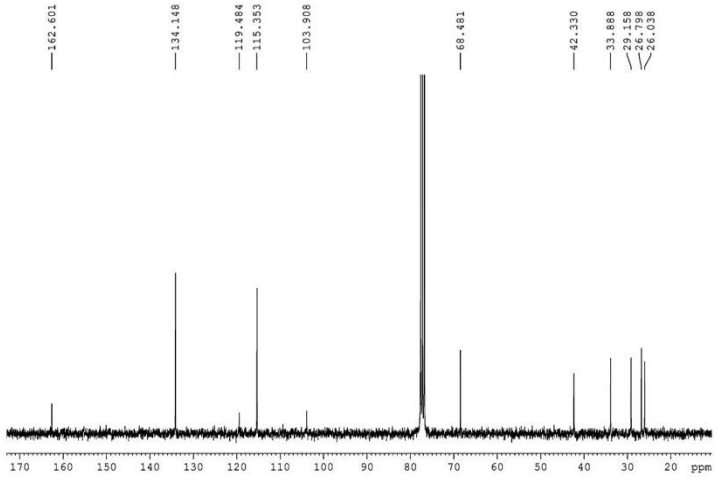

Figura 161. Spectrum in $CDCl_3$ of derivative **48** ^{13}C NMR (65 MHz, 298 K).

Derivative 50

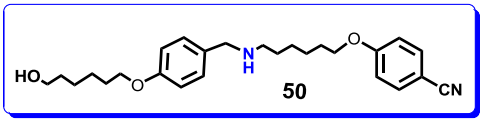

50

A mixture of benzaldehyde **49** (0.071 mL, 0.86 mmol) and derivate **48** (0.13 g, 0.044 mmol,) in $CHCl_3$ (5 mL) was stirred at room temperature for 30 min. The solvent was evaporated under reduced pressure to give the imine intermediate as a yellow oil in a quantitative yield. The imine intermediate was used for the next step without further purification. The imine was dissolved in dry MeOH (20 mL), and $NaBH_4$ (6.15 g, 162.61 mmol) was added at 0 °C and then the mixture was allowed to warm at room temperature. The solution was kept under stirring for 3 h. The solvent was removed under reduced pressure and the residue partitioned between AcOEt (50 mL) and an aqueous saturated solution of $NaHCO_3$ (100 mL). The organic layer was dried over $MgSO_4$ and the solvent was removed under reduced pressure, to give derivative **50** as a white solid (6.63 g, 98%).

^{1}H NMR ($CDCl_3$, 400 MHz, 298 K): δ 7.61 (d, H_r, 2H, J=8.6), 7.26 (H_s, 2H, J=8.4), 6.97 (d, H_h, 2H, J=8.8), 6.89 (H_i, 2H, J=8.5), 4.63 (s, H_j, 2H), 4.03 (t, H_g, 2H, J=6.5), 3.99 (t, H_q, 2H, J=6.54), 3.76 (s, H_a, 1H), 3.67 (t, H_b, 2H, J=6.45), 2.66 (t, H_l, 2H, J=7.3), 2.36 (s, H_k, 1H), 1.87-1.8 (overlapped, m, H_{f+p+c}, 6H), 1.62 (m, H_m, 2H), 1.56-1.43 (overlapped, m, H_e+$_{d+o+n}$, 8H). **^{13}C NMR** ($CDCl_3$, 400 MHz, 298 K): δ 25.7, 25.9, 25.96, 27.1, 28.9, 29.3, 29.8, 32.8, 49.1, 53.4, 62.6, 64.7, 67.9, 68.3, 103.6, 114.4, 115.2, 119.4, 128.6, 129.4, 131.9, 134.0, 158.2, 162.5.

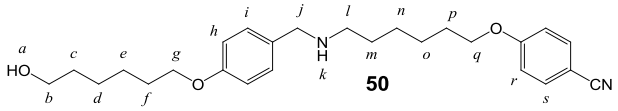

50

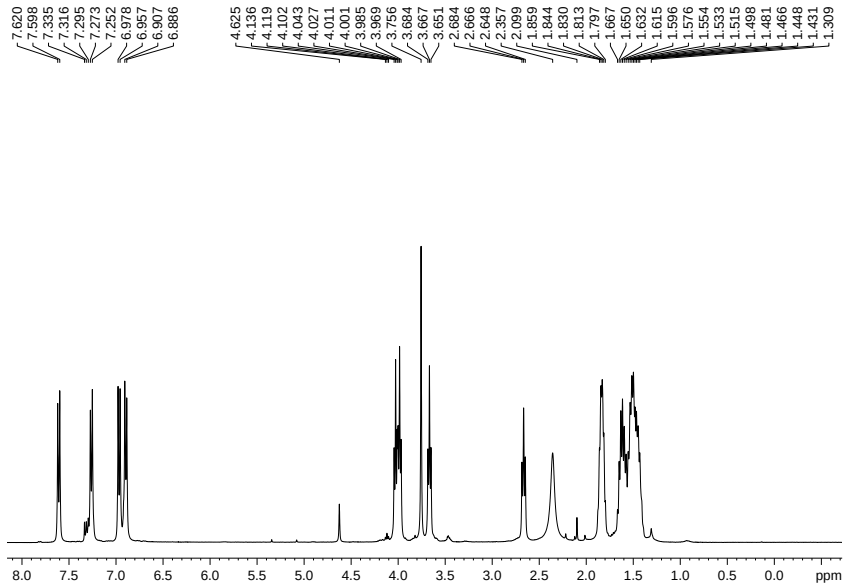

Figura 162. Spectrum ^{1}H NMR of derivative **50** in $CDCl_3$ (400 MHz, 298 K).

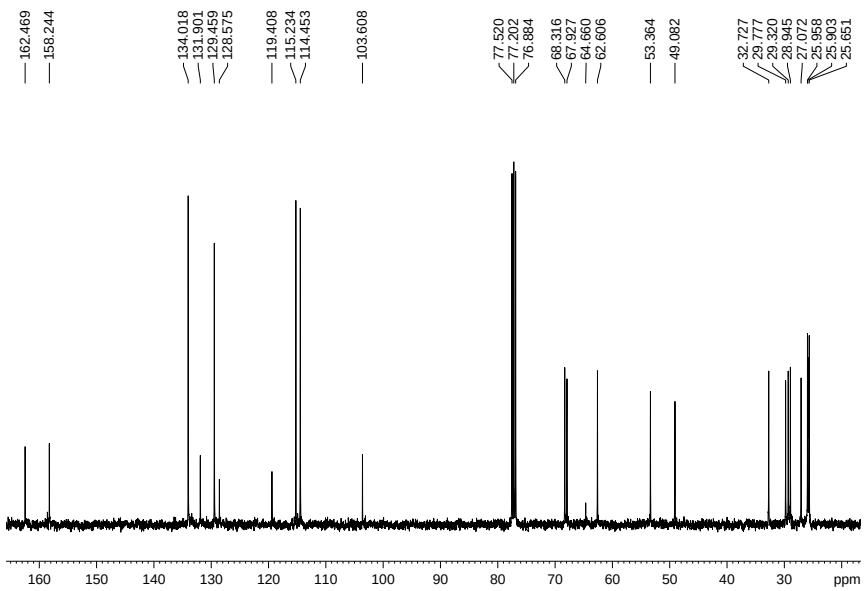

Figura 163. Spectrum ^{13}C NMR of derivative **50** in $CDCl_3$ (100 MHz, 298 K).

Derivative 51

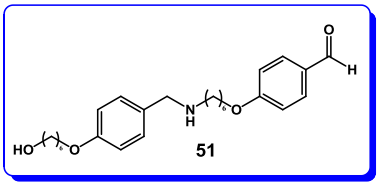

To a solution of derivative **50** (2.57 g, 6.06 mmol) and HCOOH/H_2O (80% *w/w* 116 ml + 34 ml); was added (0.2728 g, 1.20 mmol) and the reaction was stirred at 60°C for 12h. The solution was cooled at room temperature and the catalyst was filtered. The crude product was extracted with AcOEt and the organic layer was dried over $MgSO_4$ and the solvent was removed under reduced pressure, to give derivative **51** (2.00 g, 95%) as a white solid.**^{1}H NMR** ($CDCl_3$, 250 MHz, 298 K): δ 9.85 (s, H_t, 1H), 7.79 (d, H_s, 2H, J=8.9), 7.47 (H_h, 2H, J=8.2), 6.92 (d, H_i, 2H, J=8.5), 6.86 (H_r, 2H, J=8.1), 4.15 (t, H_g, 2H, J=6.6), 3.93 (s, H_a, 1H), 3.99 (t, H_q, 2H, J=6.54), 3.76 (s, H_a, 1H), 3.85 (t, H_g, 2H, J=6.4), 2.66 (t, H_l, 2H, J=7.3), 2.74 (s, H_k, 1H), 1.87-1.8 (overlapped, m, H_{f+p+c}, 6H), 1.62 (m, H_m, 2H), 1.87-1.42 (overlapped, m, $H_{c+f+e+d+m+p+o+n}$, 16H). **^{13}C NMR** ($CDCl_3$, 400 MHz, 298 K): δ 25.5, 25.7, 25.8, 25.8, 26.6, 28.6, 28.9, 29.2, 45.6, 50.1, 64.0, 67.9, 68.1, 114.8, 115.0, 115.3, 121.9, 129.9, 131.9, 132.1, 134.1, 160.0, 161.3, 164.2, 190.9

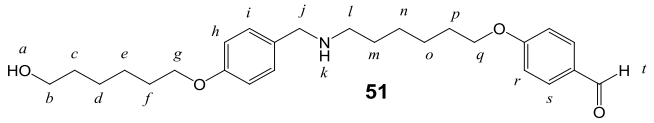

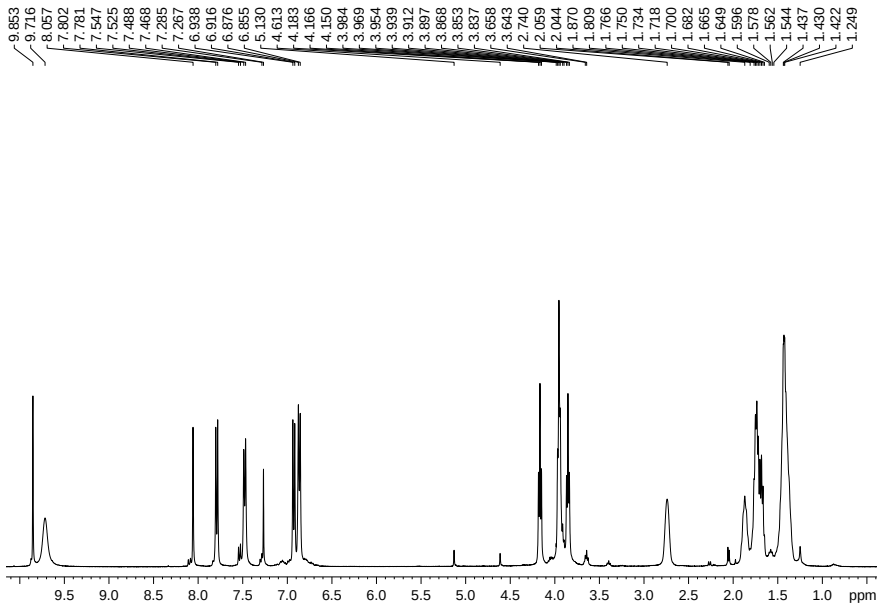

Figure 164. Spectrum ^{1}H NMR of derivative **51** in $CDCl_3$ (250 MHz, 298K)

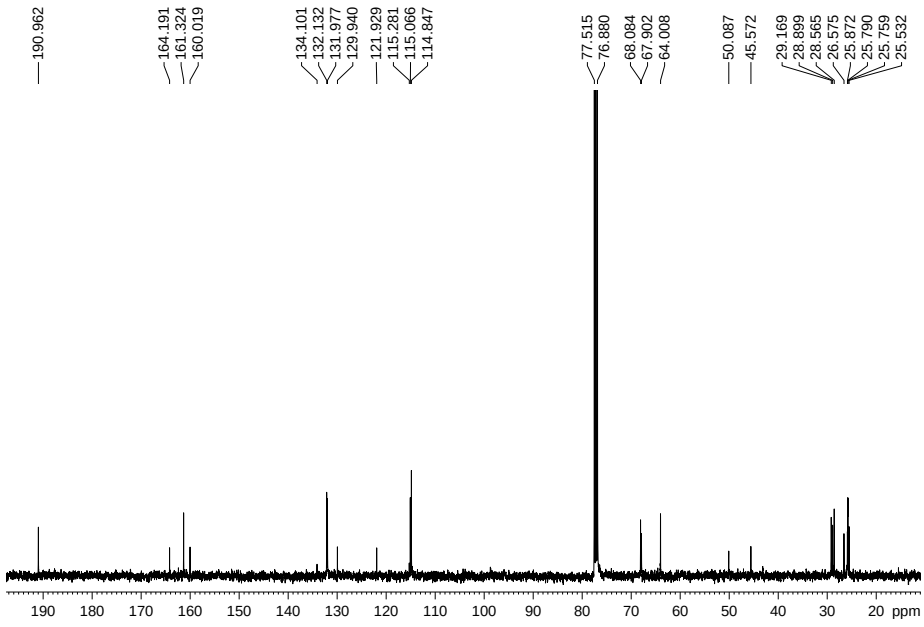

Figure 165. Spectrum ^{13}C NMR of derivative **51** in $CDCl_3$ (100 MHz, 298K)

Derivative 52

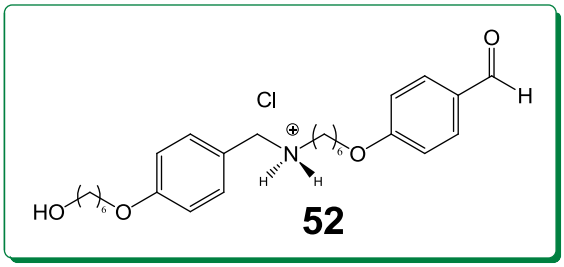

Derivative **51** (0.015 g, 0.035 mmol) was dissolved in Et_2O (20 mL) at room temperature and an aqueous solution of HCl (37% *w/w*, 1 mL) was added dropwise. The mixture was kept under stirring for 30 min, until a white precipitate was formed. The solid was collected by filtration, washed with MeOH (15 mL) and CH3CN (15 mL) and dried under vacuum, to give derivative **58** as a white solid (1.91 g, 4.46 mmol, 73.8%).

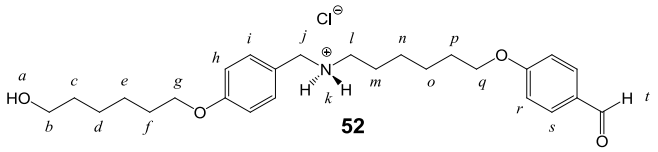

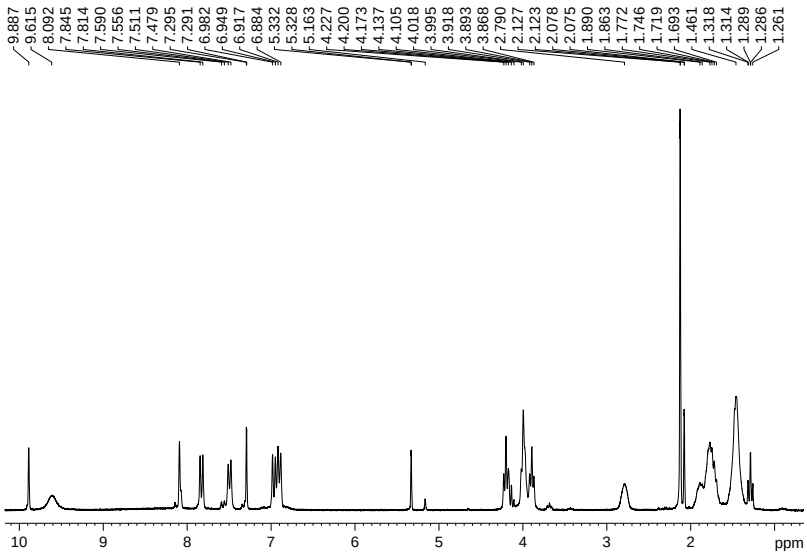

Figure 166. Spectrum ^{1}H NMR of derivative **52** in $CDCl_3$ (250 MHz, 298K)

Derivative 54

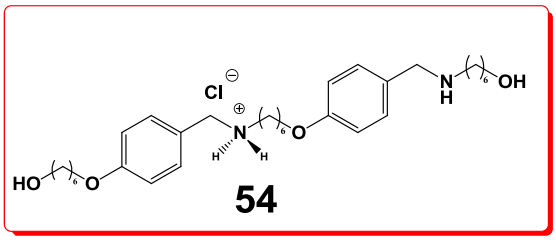

A mixture of derivative **52** (1.5 g, 3.50 mmol) and **53** (0.43 g, 3.61 mmol) in $CHCl_3$ (5 mL) was stirred at room temperature for 30 min. The solvent was evaporated under reduced pressure to give the imine intermediate as a yellow oil in a quantitative yield. The imine intermediate was used for the next step without further purification. The imine was dissolved in dry MeOH (40 mL), and $NaBH_4$ (1.31 g, 35.34 mmol) was added at 0 °C and then the mixture was allowed to warm at room temperature. The solution was kept under stirring for 3 h. The solvent was removed under reduced pressure and the residue partitioned between AcOEt (50 mL) and an aqueous saturated solution of $NaHCO_3$ (100 mL). The organic layer was dried over $MgSO_4$ and the solvent was removed under reduced pressure, to give derivative **54** as a white solid 54.6 % (1 g, 1.77 mmol); **^{1}H NMR** ($CDCl_3$, 400 MHz, 298 K): δ 7.23 (overlapped, H_{h+r}, 4H), 6.87 (overlapped, H_{j+s}, 4H), 3.98-3.92 (overlapped, $H_{a+z''+b+g+q+z'}$, 10H), 3.68-3.61 (overlapped, t, $H_{b+g+q+z'}$, 8H), 2.62 (t, H_l, 2H, J=7.0), 2.18 (s, H_k, 2H), 2.06 (s, H_u, 1H), 1.80-1.26 (overlapped, m, $H_{c+f+n+p+w+z+e}$+$_{d+o+m+y+x}$, 24H). **^{13}C NMR** ($CDCl_3$, 250 MHz, 298 K): δ 26.9, 27.3, 28.5, 30.6, 31.3, 34.0, 50.5, 54.8, 64.2, 69.2, 115.8, 130.0, 130.7, 159.6.

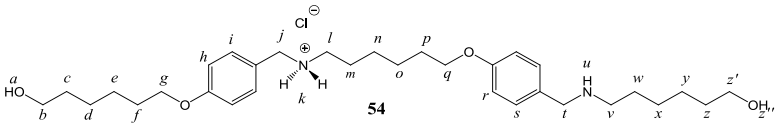

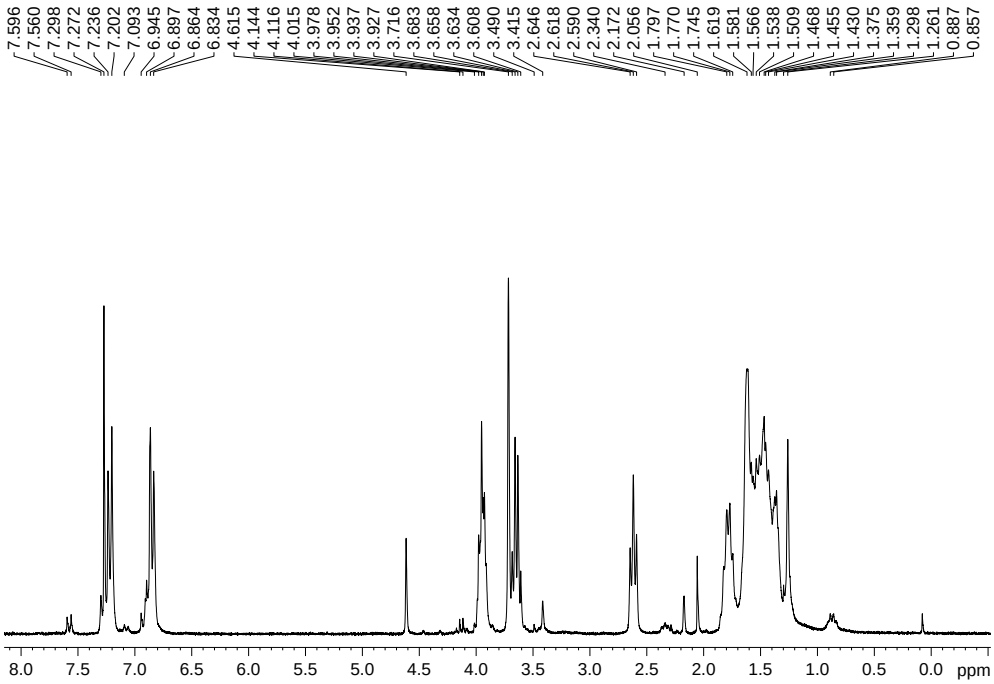

Figura 167. Spectrum ^{1}H NMR of derivative **54** in $CDCl_3$ (250 MHz, 298K)

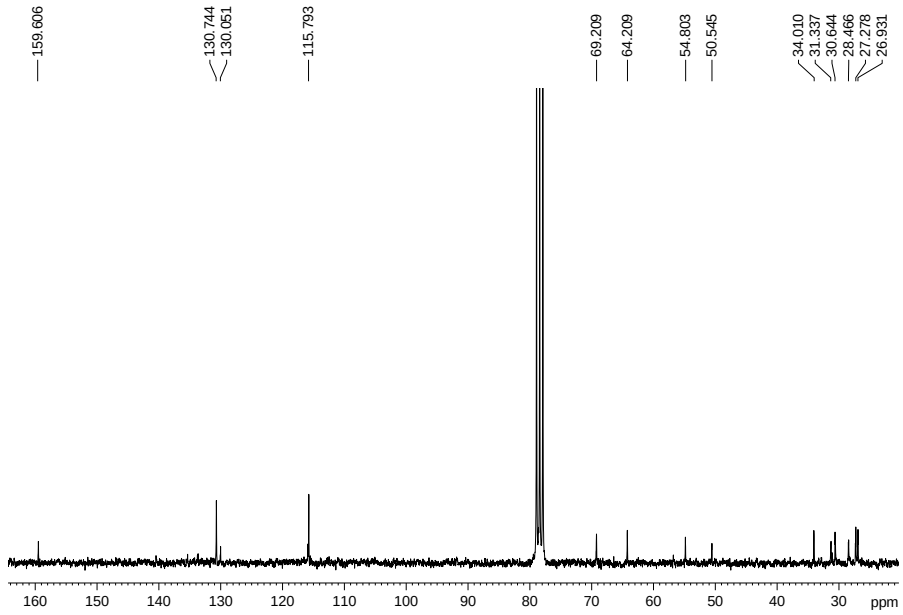

Figura 168. Spectrum ^{13}C NMR of derivative **54** in $CDCl_3$ (250 MHz, 298K

Derivative 55

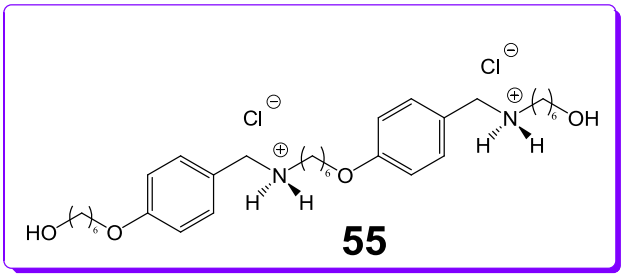

To a solution of derivative **54** (1 g, 1.77 mmol) in MeOH (20 mL) was added dropwise an aqueous solution of HCl (37% *w/w*, 15 mL). The mixture was stirred overnight at 70 °C, then the solvent was concentrated under reduced pressure and the residue partitioned between AcOEt (50 mL) and H_2O (100 mL). The organic layer was dried over $MgSO_4$, filtered and the solvent was removed under reduced pressure, to give derivative **55** as a yellow oil in a quantitative yield (0.6 g, 56.36 %). **^{1}H NMR** ($CDCl_3$, 400 MHz, 298 K): δ 7.40 (overlapped, H_{h+r}, 4H), 6.99 (overlapped, H_{j+s}, 4H), 4.12 (s, $H_{a+z''}$, 2H), 3.99 (overlapped, t, $H_{b+g+q+z'}$, H, J=6.3), 3.56 (t, H_{j+t} , 4H, J=6.6), 3.05-2.98 (overlapped, H_{l+v}, 4H) 2.02 (s, H_{k+u}, 4H), 1.80-1.42 (overlapped, m, $H_{c+f+n+p+w+z+e}$+$_{d+o+m+y+x}$, 24H). **^{13}C NMR** (MeOD, 400 MHz, 298 K): δ 25.5, 25.8, 26.1, 26.2, 26.5, 29.2, 29.4, 32.3, 32.7, 50.9, 61.7, 61.9, 67.8, 67.9, 68.1, 114.4, 115.1, 115.1, 123.3 123.4, 129.8, 131.6, 131.7, 160.6, 160.7.

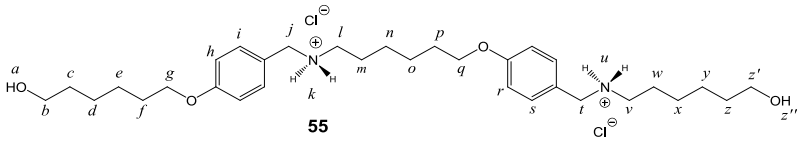

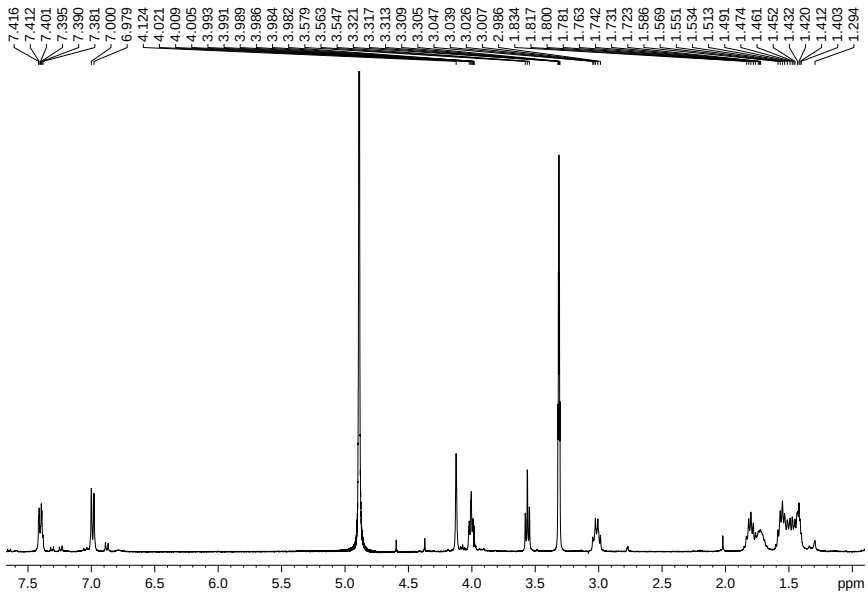

Figura 169. Spectrum ^{1}H NMR of derivative **55** in MeOD (400 MHz, 298K)

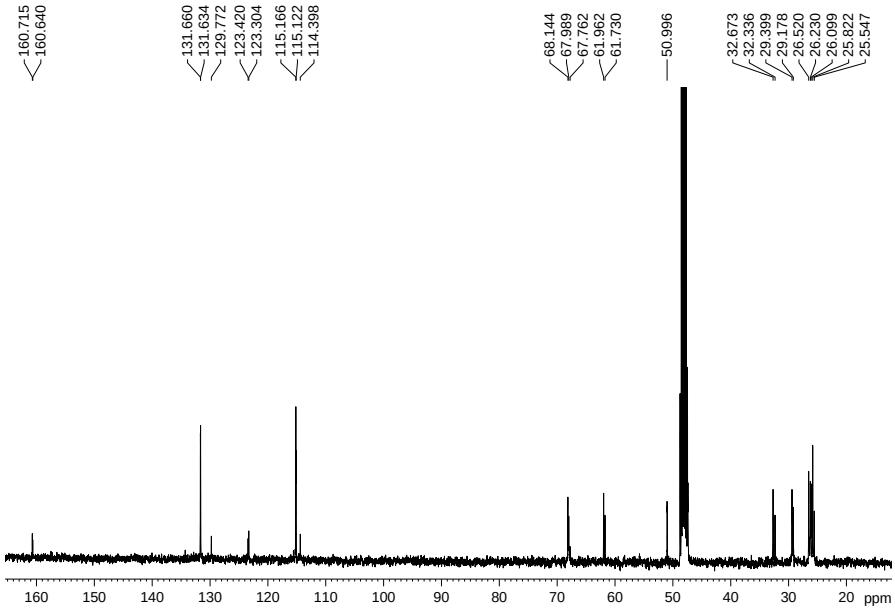

Figura 170. Spectrum ^{13}C NMR of derivative **55** in MeOD (400 MHz, 298K)

Derivative 40^{2+}

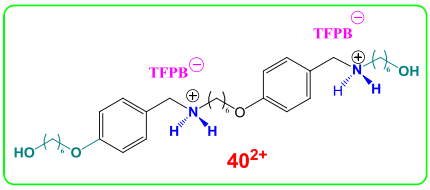

Derivative **55** (0.4 g, 0.67 mmol was dissolved in warm dry MeOH (25 mL), then a solution of sodium tetrakis[3,5-bis(trifluoromethyl)phenyl]borate[4] (1.23 g, 1.39 mmol) in dry MeOH (5 mL) was added. The mixture was kept under stirring overnight in the dark. The solvent was removed and deionized water was added, obtaining a brown precipitate that was filtered off and dried under vacuum for 48 h to give derivative **40^{2+}** as a brown solid (1.23 g, 1.39 mmol, 38%). **^{1}H NMR** ($CDCl_3$, 400 MHz, 298 K): δ 7.59 (s, ArH_{TFPB}, 12H, J=8.6), 7.26 (H_s, 2H, J=8.4), 6.97 (d, H_h, 2H, J=8.8), 6.89 (H_i, 2H, J=8.5), 4.63 (s, H_j, 2H), 4.03 (t, H_g, 2H, J=6.5), 3.99 (t, H_q, 2H, J=6.54), 3.76 (s, H_a, 1H), 3.67 (t, H_b, 2H, J=6.45), 2.66 (t, H_l, 2H, J=7.3), 2.36 (s, H_k, 1H), 1.87-1.8 (overlapped, m, H_{f+p+c}, 6H), 1.62 (m, H_m, 2H), 1.56-1.43 (overlapped, m, H_e+$_{d+o+n}$, 8H). **^{13}C NMR** (MeOD, 400 MHz, 298 K): δ 26.4, 26.7, 26.9, 27.1, 27.3, 30.1, 30.2, 30.6, 33.1, 33.5, 51.9, 62.5, 62.8, 68.8, 69.0, 115.9, 116.1, 118.5, 119.3, 123.6, 124.1, 124.2, 127.9, 129.7, 130.2, 130.6, 131.2, 132.2, 132.4, 135.8, 161.6, 162.4, 163.2, 164.0.

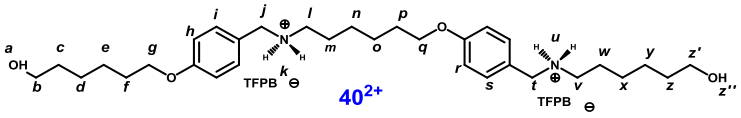

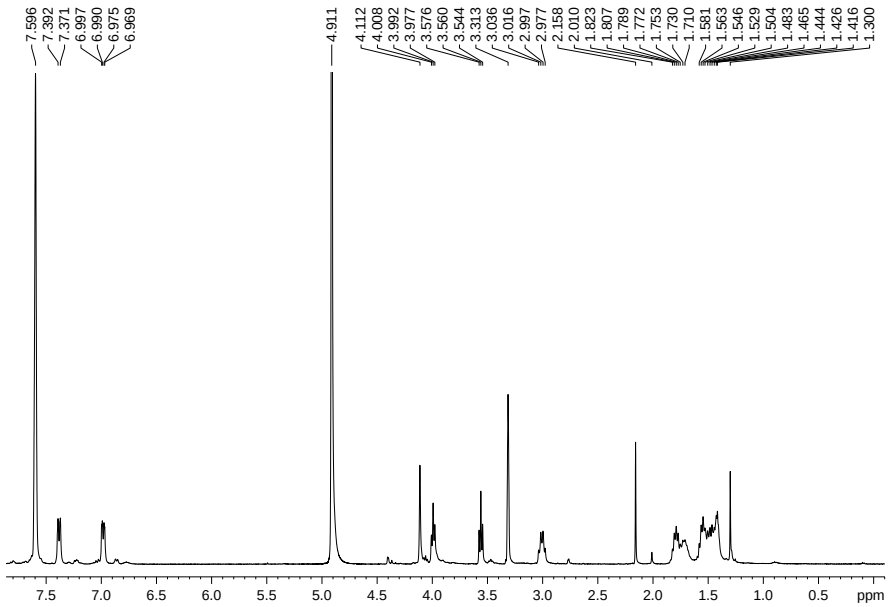

Figura 171. Spectrum ^{1}H NMR of derivative **40** in MeOD(400 MHz, 298K)

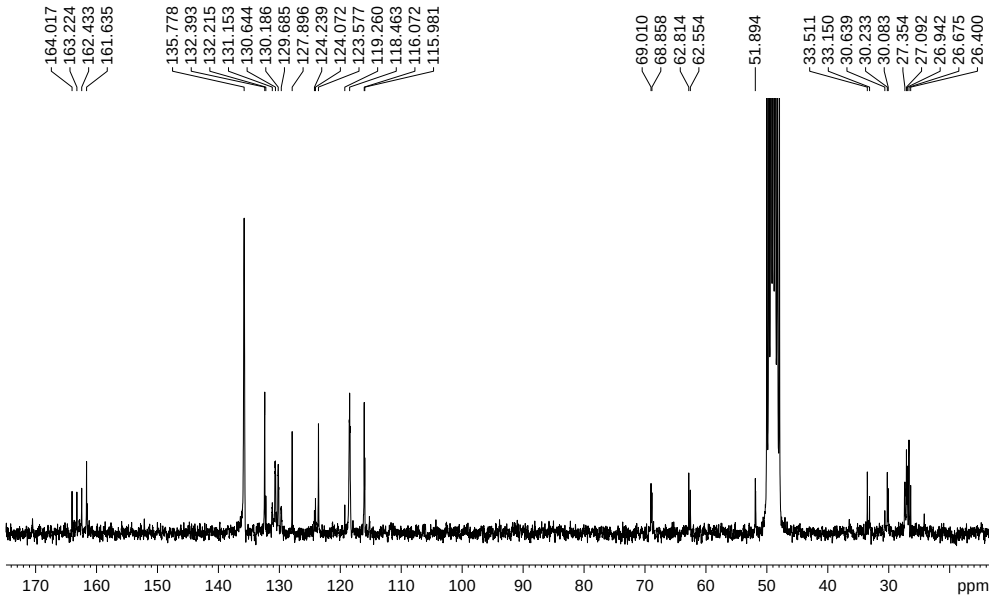

Figura 172. Spectrum ^{13}C NMR of derivative **40^{+}** in MeOD(400 MHz, 298K)

5.5.11 Preparation of handcuff pseudo[2]rotaxane (*H,T*)-41^{+}

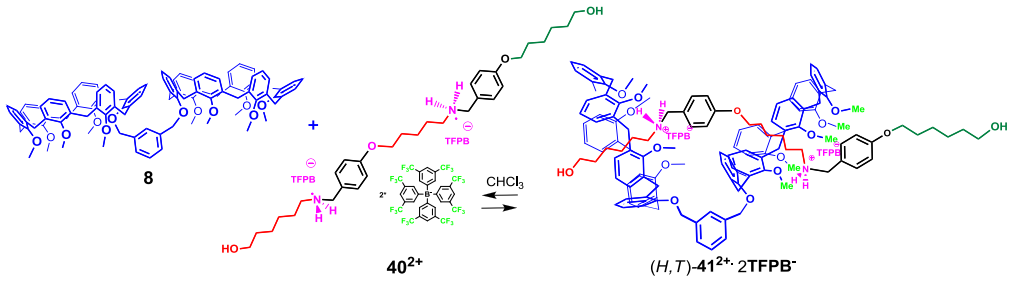

Scheme 23. Formation of handcuff pseudo[2]rotaxane (*H,T*)-**41**$^{2+}$·2TFPB^{-}.

Double-calixarene derivative **12** ($1.81\cdot10^{-3}$ g, $1.2\cdot10^{-3}$ mmol) and derivative **40**$^{2+}$ ($2.67\cdot10^{-3}$ g, $1.2\cdot10^{-3}$ mmol) were dissolved in 0.4 mL of $CDCl_3$ and the mixture was stirred for 5 min at 25 °C. Then, the solution was transferred in a NMR tube for 1D and 2D NMR spectra acquisition.

2D COSY-45 Spectrum of handcuff pseudo[2]rotaxane (*H,T*)-41^{2+}

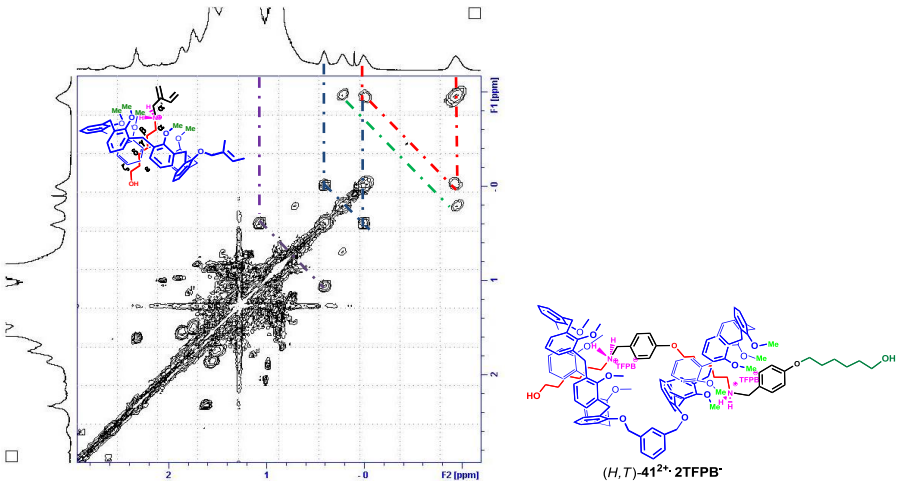

Figure 173. Relevant portion of the 2D COSY spectrum (400 MHz, $CDCl_3$, 298 K) of handcuff pseudo[2]rotaxane (*H,T*)-**41**$^{2+}$·2TFPB^{-}.

5.5.12 Synthesis of handcuff [2]rotaxane (*H,T*)-42^{2+}

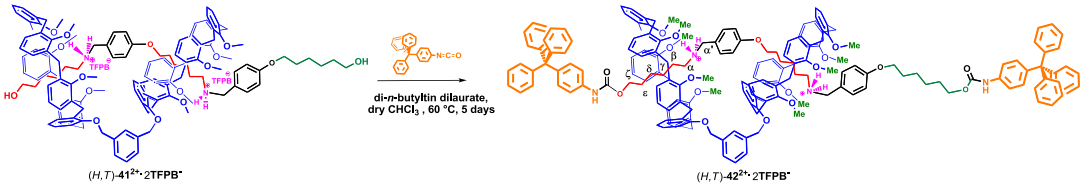

Scheme 24. *Synthesis of the first example of (H,T)double-calix[6]arene-based handcuff-[2]rotaxane* ***42***$^{2+}$

Di-*n*-butyltin dilaurate (3 drops) was added to a solution of **40**$^{2+}$ (0.18 mmol, 0.41 g) and **12** (0.11 mmol, 0.17 g) in dry $CHCl_3$ (12 mL) at room temperature, and subsequently, 4-triphenylmethylphenylisocyanate (0.083 g, 0.230 mmol) was added. The reaction was kept under stirring at 60 °C for 5 days. The crude product was purified by column chromatography (SiO_2; CH_2Cl_2 100%) to give handcuff rotaxane (*H,T*)**−42**$^{2+}$ as a white solid (0.14 g, 0.031 mmol, 27%). **ESI(+) MS**: *m/z* = 1384 (M^{2+}/2); **^{1}H NMR** (400 MHz, $CDCl_3$, 298 K): *δ* −0.67 (broad, 4H, CH_2^{β}), 0.04 (broad, 4H, CH_2^{γ}), 0.21 (broad, 4H, CH_2^{α}), 0.44 (broad, 4H, CH_2^{δ}), 1.11 (broad, 4H, CH_2^{ε}), 1.94 (broad, $OCH_2CH_2CH_2CH_2O$, 4H), 2.23 (broad, 4H, $CH_2^{\alpha'}$), 3.49 and 4.34 (AX, $ArCH_2Ar$, 8H), 3.50 and 4.41 (AX, $ArCH_2Ar$, 8H), 3.60 and 4.45 (AX, $ArCH_2Ar$, 8H), 3.34, 3.67 and 3.78 (s, OMe, 12, 6 and 12H respectively), 3.91 (broad, 4H, CH_2^{ζ}), 4.05 (broad, $OCH_2CH_2CH_2CH_2O$, 4H), 4.96 (s, $OCH_2^{m\text{-}xylenyl}$, 4H), 5.48 (broad, $^+NH_2$, 4H), 6.77−7.28 (overlapped, 88H, ArH+NHCO), 7.52 [s, 8H, $(ArH)^{TFPB^-}$], 7.72 [s, 16H, $(ArH)^{TFPB^-}$]; ^{13}C NMR (100 MHz, $CDCl_3$, 298 K): *δ* 24.5, 29.9, 64.7, 117.6, 120.7, 123.4, 126.1, 127.7, 131.3, 134.9, 135.1, 142.5, 146.9, 161.1, 161.6, 162.1.

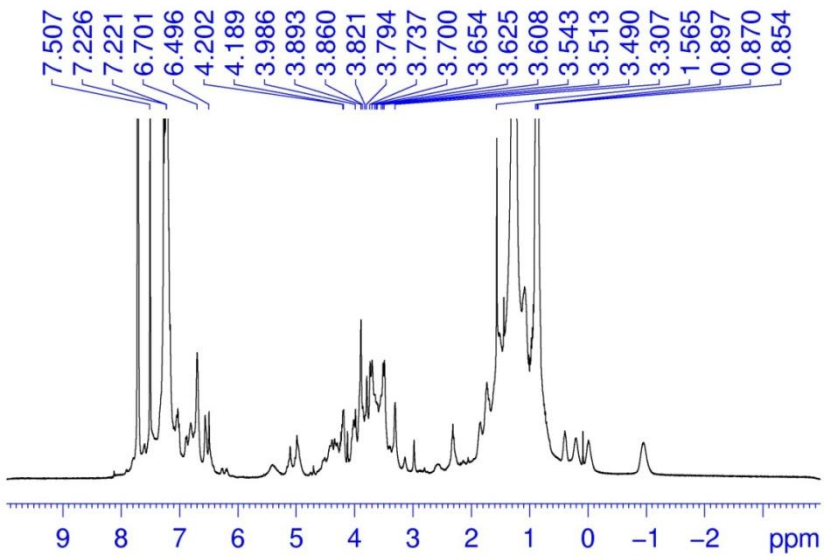

Figure 174. (a) ^{1}H NMR spectrum (400 MHz, $CDCl_3$, 298 K) of handcuff [2]rotaxane (*H,T*)-**42**$^{2+}$ · 2TFPB^{-}.

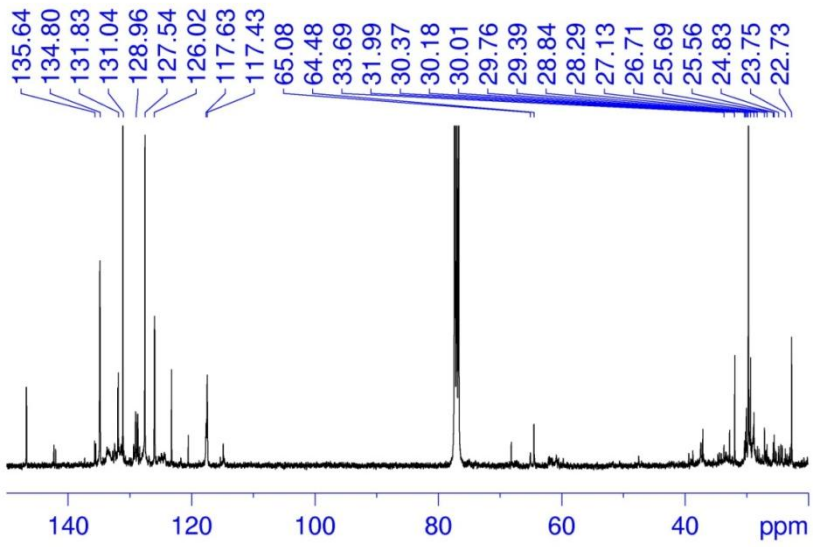

Figure 175 ^{13}C NMR spectrum (100 MHz, $CDCl_3$, 298 K) of handcuff [2]rotaxane (*H,T*)-**42**$^{2+}$.

2D COSY-45 Spectrum of handcuff [2]rotaxane (*H,T*)-42^{2+}

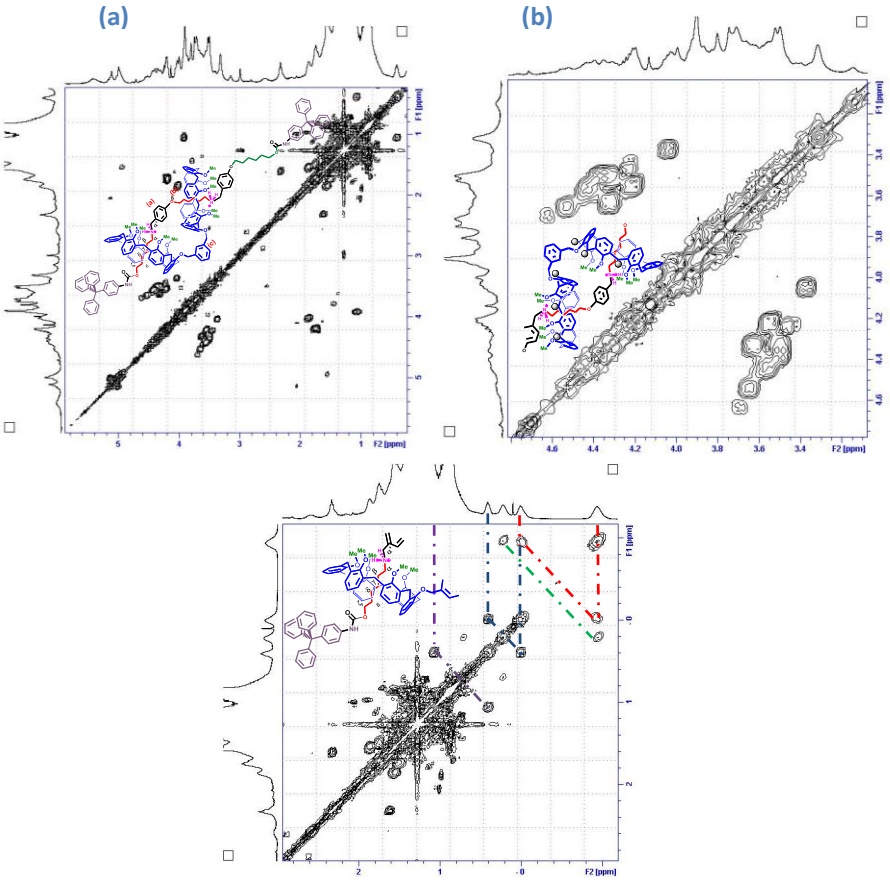

Figure 176 (a) 2D COSY-45 spectrum (400 MHz, $CDCl_3$, 298 K) of handcuff [2]rotaxane (*H,T*)-**42**$^{2+}$; (b) Expansions of 2D COSY-45 spectrum (400 MHz, $CDCl_3$, 298 K) of methylene region of handcuff [2]rotaxane (*H,T*)-**42**$^{2+}$;(c)Expansions of 2D COSY-45 spectrum (400 MHz, $CDCl_3$, 298 K) of negative region of handcuff [2]rotaxane (*H,T*)-**42**$^{2+}$

5.6 *Conclusion*

In conclusion, we have reported here the first examples of calixarene-based handcuff pseudorotaxanes and rotaxanes architectures obtained by *through-the-annulus* threading of a double-calix[6]arene system with a bis-ammonium axle. The relative orientation of the two calix-wheels can be predefined by exploiting the "*endo*-alkyl rule" which controls the directionality of the threading of alkylbenzylammonium axles with calixarene macrocycles.

Thus, following this approach were obtained three examples of beautiful calixarene-based handcuff rotaxane stereoisomers which could be termed as head-to-head (*H,H*), head-to-tail (*H,T*), and tail-to-tail (*T,T*).

Therefore, it is conceivable that the extension of this approach could lead to novel mechanically interlocked architectures with high-order topologies.

CHAPTER VI

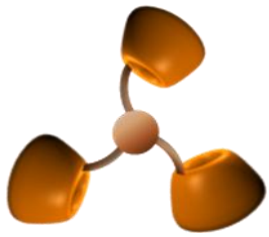

Threading of a *triple-calixarene* host:

"a wealth of new possible architectures"

6.1 Introduction.

In the last 15 years research in the field of artificial molecular machinery has grown exponentially and it has been styimulated by several major scientific breakthroughs. The long been used top-down approach to miniaturization of components was profitably replaced by a (chemical) bottom-up approach.

The latter strategy relies on the control of the self-assembly[20] of molecular components with the aim to construct nanosized molecular devices able to store, process, and interpret information under appropriate external stimuli.[114] Among the possible candidates for bottom-up approach, [*n*]rotaxanes are particularly attractive because of their different, easily accessible co-conformations that make them ideal bi- or multistable systems.

Molecular machines are mechanically interlocked molecules,[20] and they can be considered as topological complex systems able to translocate a macrocyclic component over two or more sites ("stations") under the influence of an external stimulus.[115]

Usually, flat or symmetrical wheels, such as crown ethers,[116] azacyclophanes,[117] cycloamides,[118] or cucurbiturils,[119] are used, which lead to a

---

[114] D. A. Amabilino, J. F. Stoddart, *Chem. Rev.* **1995**, *35*, 1154-1196.

[115] F. M. Raymo, J. F. Stoddart, *Chem. Rev.* **1999**, *99*, 1643-1664; V. Balzani, A. Credi, F. M. Raymo, J. F. Stoddart, *Angew. Chem.* **2000**, *112*, 3486-3531; *Angew. Chem. Int. Ed.* **2000**, *100*, 1789-1816; V. Balzani, A. Credi, M. Venturi, *Molecular Devices and Machines, 2nd ed.,* Wiley-VCH, Weinheim, **2008**; S. Saha, J. F. Stoddart, *Chem. Soc. Rev.* **2007**, *36,* 77-92; E. R. Kay, D. A. Leigh, F. Zerbetto, *Angew. Chem.* **2007**, *119*, 72-196; *Angew. Chem. Int. Ed.* **2007**, *46*, 72.

[116] For recent examples, see: G. J. E. Davidson, S. Sharma, S. J. Loeb, *Angew. Chem.* **2010**, *122*, 5058; *Angew. Chem. Int. Ed.* **2010**, *49*, 4938; E. Busseron, C. Romuald, F. Coutrot, *Chem. Eur. J.* **2010**, *16*, 10062-10073; V. Balzani, M. Clemente-Léon, A. Credi, B. Ferrer, M. Venturi, A. H. Flood, J. F. Stoddart, *Proc. Natl, Acad. Sci. USA* **2006**, *103*, 1178-1183; J. D. Badjic, V. Balzani, A. Credi, S. Silvi, J. F. Stoddart, *Science* **2004**, *303*, 1845; See also, Ref .1, pp. 146-152.

[117] For recent examples, see: A. Coskun, D. C. Friedman, H. Li, K. Patel, H. A. Khatib, J. F. Stoddart, *J. Am. Chem. Soc.* **2009**, *131*, 2493-2495; I. Yoon, D. Benitez, Y.-L. Zhao, O. Š, Miljanić, S.Y. Kim, E. Tkatchouk, K. C.-F. Leung, S. I. Khan, W. A. Goddard ,III, J. F. Stoddart, *Chem. Eur. J.* **2009**, *15*, 1115-1122; L. M. Klivansky, G. Koshkakaryan, D. Cao, Y. Liu, *Angew. Chem.* **2009**, *121*, 4249-4253; *Angew. Chem. Int. Ed.* **2009**, *48*, 1-6; J. O. Jeppesen, J. Perkins, J. Becher, J. F. Stoddart, *Angew. Chem.* **2001**, *113*, 1256-1261; *Angew. Chem. Int. Ed.* **2001**, *40*, 1216-1221; See also, Ref. 1, pp. 153-162.

non-directional shuttling component. Instead the use of three-dimensional nonsymmetrical wheels, such as cyclodextrins[120] or calixarenes,[121] gives rise to directional shuttles with a determined relative orientation of their components and with new related potential properties. However, such systems still remain largely less exploited probably because of the inherent difficulty in controlling their relative orientation.

As above mentioned, concerning the hosts with multiple cavities or rings, spectacular interpenetrated architectures have been obtained by double-threading through systems in which two macrocycles are covalently linked to one another in a handcuff-like fashion[122] [e.g.: double-crown ethers, double-calixarene systems (e.g. **12**)] [96].

However, it would be very attractive to design interpenetrated architectures obtained by threading a triple-host in which three macrocycles are covalently linked to one another by means of an appropriate spacer. To the best of our

---

[118] For recent examples, see: M. R. Panman, P. Bodis, D. J. Shaw, B. H. Bakker, A. C. Newton, E. R. Kay, A. M. Brouwer, W. J. Buma, D. A. Leigh, S. Woutersen, *Science*, 2010, *328*, 1255-1258; A. M. Rijs, N. Sändig, M. N. Blom, J. Oomens, J. S. Hannam, D. A. Leigh, F. Zerbetto, W. J. Buma, *Angew. Chem.* 2010, *122*, 3988-3992; *Angew. Chem. Int. Ed.* 2010, *49*, 3896-3900; M. Alvarez-Pérez, S. M. Goldup, D. A. Leigh, A. M. Z. Slawin, *J. Am. Chem. Soc.* 2008, *130*, 1836-1838; G. Bottari, F. Dehez, D. A. Leigh, P. J. Nash, E. M. Pérez, J. K. Y. Wong, F. Zerbetto, *Angew. Chem.* 2003, *115,* 2398-2402; *Angew. Chem. Int. Ed.* 2003, *42*, 2296-2300; See also, Ref. 1, pp. 177-222.

[119]For recent examples, see: S. Li, D. Taura, A. Hashidzume, A. Harada, *Chem. Asian J.* **2010**, *5*, 2281-2289; A, Harada, A. Hashidzume, H. Yamaguchi, Y. Takashima, *Chem. Rev.* **2009**, *109*, 5974-6023; T. Oshikiri, Y. Takashima, H. Yamaguchi, A. Harada, *Chem. Eur. J.* **2007**, *13*, 7091-7098; G. Wenz, B.-H. Han, A. Müller, *Chem. Rev.* **2006**, *106*, 782-817 and references therein.

[120] For recent examples, see: S. Li, D. Taura, A. Hashidzume, A. Harada, *Chem. Asian J.* **2010**, *5*, 2281-2289; A, Harada, A. Hashidzume, H. Yamaguchi, Y. Takashima, *Chem. Rev.* **2009**, *109*, 5974-6023; T. Oshikiri, Y. Takashima, H. Yamaguchi, A. Harada, *Chem. Eur. J.* **2007**, *13*, 7091-7098; G. Wenz, B.-H. Han, A. Müller, *Chem. Rev.* **2006**, *106*, 782-817 and references therein.

[121] To the best of our knowledge has been reported only one example of calix[6]arene-based rotaxane system in which calix-wheel encircle a viologen axle. In this case no shuttling or inversion motion of the calix-wheel has been evidenced: A. Arduini, R. Ferdani, A. Pochini, A. Secchi, F. Ugozzoli, *Angew. Chem.* **2000**, *112*, 3595–3598; *Angew. Chem. Int. Ed.* **2000**, *39*, 3453–3456.C. D. Gutsche.

[122] (a) Badjić, J. D.; Balzani, V.; Credi, A.; Silvi, S.; Stoddart, J. F. *Science* **2004**, *303,* 1845−1849. (b) Evans, N. H.; Serpell, C. J.; Beer, P. D., *Angew. Chem. Int. Ed.* **2011**, *50*, 2507−2510. (c) Zhang, Z.-J.; Han M.; Zhang, H.-Y.; Liu, Y. *Org. Lett.* **2013**, *15*, 1698−1701.

knowledge, no-examples of threading studies on triple-calixarene systems (e.g. **57**), have been so far reported in the literature. Undoubtedly, the design and synthesis of such a triple-calixarene could represent a new horizon of possible chemical topologies as exemplified by **Figure 177**.

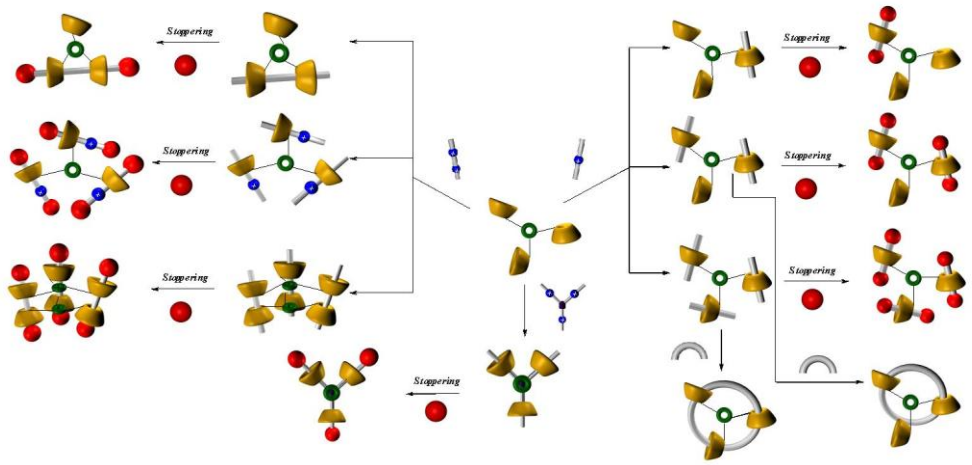

Figure 177. Threading of triple-calixarene hosts with TFPB salts of *n*-alkylammonium cations: horizons of new architectures.

6.2 Synthesis of *tert*-butylated triple-calix[6]arene 57

The tritopic host **57** was designed with the intention to obtain three equivalent recognition sites. Therefore, a bridge with C_3 symmetry and a single kind of macrocyclic unit were chosen for the last step. Of course, this decision is reflected in the high symmetry of the final architecture **57**.

Triple-calix[6]arene **57** was synthesized exploiting the reaction sequence shown in Scheme **25**.[96] In particular, in the key step, pentamethoxy-calix[6]arene-mono-ol **20** was reacted with 1,3,5-tris(bromomethyl)benzene **56**in the presence of NaH to give triple-calix[6]arene **57** in 33% yield.

Compound **57** was fully characterized by means of its ^{1}H NMR, ^{13}C NMR, and ESI(+) MS spectra (**Figure 178**).

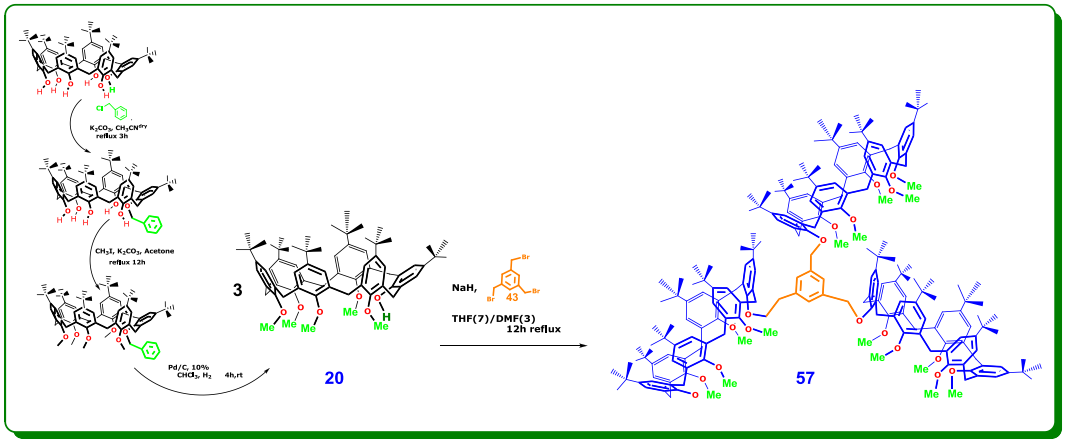

Scheme 25. Synthesis of *tert*-butylated triple-calix[6]arene **57.**

The ^{1}H and ^{13}C NMR data of triple-calix[6]arene **57**, acquired at room temperature, were fully consistent with its molecular symmetry. In particular, three singlets were present in the ^{1}H NMR spectrum (**Figure 176**) at 0.96, 1.07 and 1.29 ppm relative to the four symmetry related *tert-butyl* groups, because of an accidental isochrony. More diagnostic were the three singlets at 2.92, 3.11 and 3.17 ppm (2:1:2) relative to OMe groups. The steric hindrance to conformational interconversion, due to the *t*-Bu groups at the upper-rim, was evident by the three AX systems at 3.58/4.50 ppm (J = 14.7 Hz), 4.17/4.04 ppm (J = 14.5 Hz), and 3.83/3.68 ppm (J = 15.1 Hz). Finally, a singlet was present at 5.05 ppm relative to OCH_2 protons of the bridge.

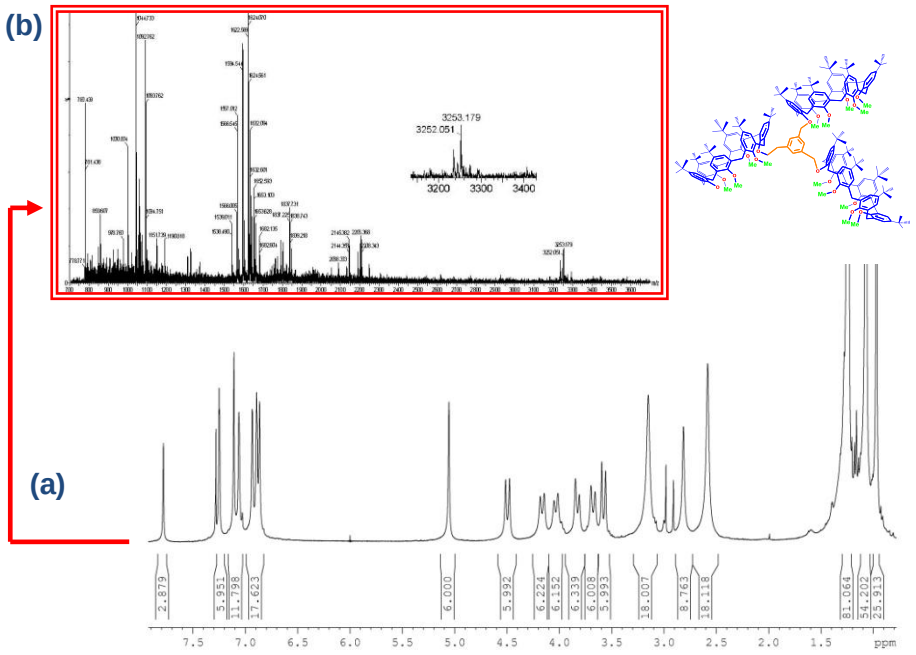

Figure 178. (a) ^{1}H NMR spectrum (400 MHz, $CDCl_3$, 298 K) of tris-calixarene derivative **57; (b)** ESI(+) MS spectra of derivative **57**

6.3 Formation of triply-threaded pseudo[4]rotaxanes

In order to design new topologically complex architectures it is fundamental to know the threading abilities of the new host. Therefore, as a first step we decided to investigate the threading of triple-calix[6]arene derivative **57** with mono-ammonium axles.

It is interesting to note that in this case, three new chemical topologies could be formed. In fact, as showed in **Figure 178,** the threading of triple-calix[6]arene **57** with mono-ammonium axle could give rise to:

1) a singly threaded pseudo[2]rotaxane (**Figure 178a**),
2) a doubly threaded pseudo[3]rotaxane (**Figure 178b**),
3) a triply threaded pseudoro[4]taxane (**Figure 178c**).

Of course, the stoppering of such pseudo[n]rotaxanes would give rise to the corresponding [n]rotaxanes.

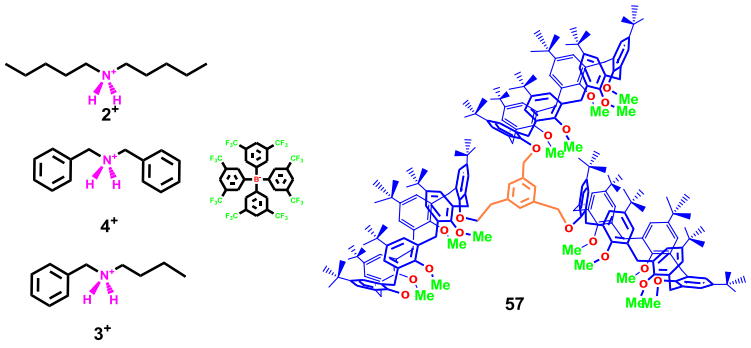

Figure 179. Linear mono-ammonium systems (*left*), triple–calix[6]arene host (*right*)

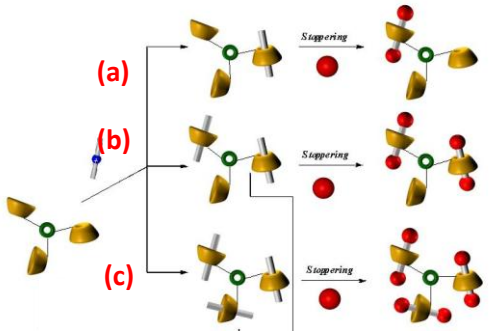

Figure 180. Cartoon rapresentations of the possible topologies obtainable through threading of a triple-calix[6]arene with mono-ammonium axles.

6.3.1 *Threading of triple-calix[6]arene 57 with di-*n*-pentylammonium axle* 2^+

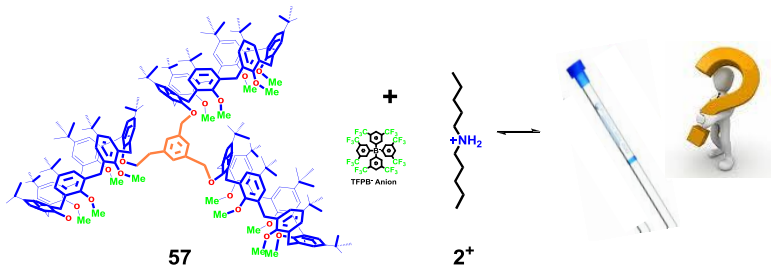

Scheme 26. Schematic representation of Directional threading of **57** with the *di-n-pentyl*ammonium axle $\mathbf{2}^+$.

Interestingly, the addition of di-*n*-pentylammonium salt $\mathbf{2}^+\cdot TFPB^-$ to a $CDCl_3$ solution of triple-calix[6]arene **57** caused the usual changes in its ^1H NMR spectrum (**Figure 179**). In fact, upon addition of 1 equivalent of $\mathbf{2}^+\cdot TFPB^-$ salt a new set of signals emerged (Figure 179b) due to the formation of the singly threaded pseudo[2]rotaxane ion $\mathbf{2}^+\subset\mathbf{57}$ (**Scheme 27**). Under these conditions (1 equiv of axle $\mathbf{2}^+$), the formation of a singly threaded pseudo[2]rotaxane ion $\mathbf{2}^+\subset\mathbf{57}$ (**Scheme 27**) was ascertained by the ESI(+) mass spectrum that gave a value of 3402 *m*/*z* as the base peak, corresponding to a 1:1 host/guest stoichiometry, in which only one dialkylammonium axle was threaded into one of the three macrocycles of **57.**

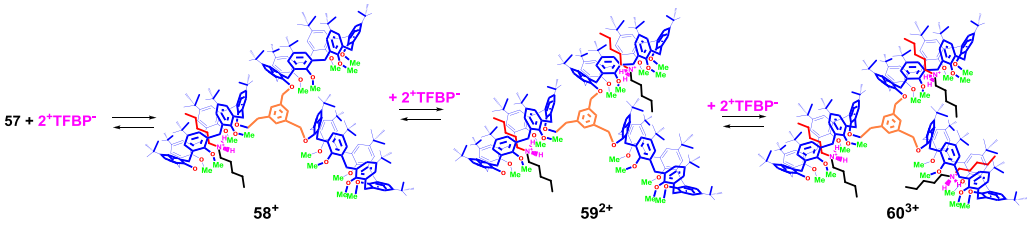

Scheme 27

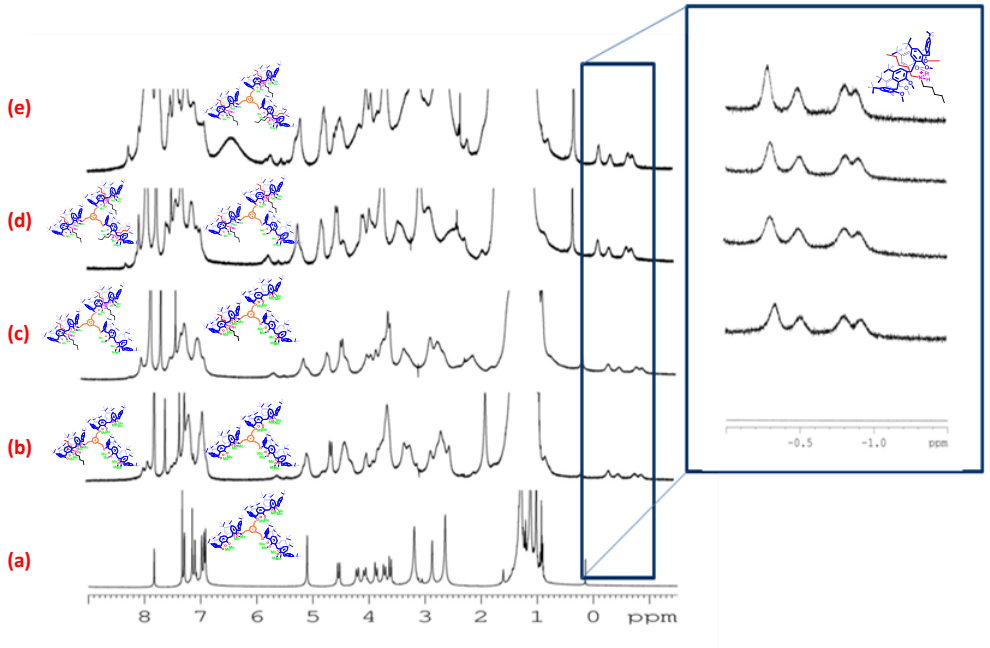

Figure 181. ^{1}H NMR (400 MHz, 298 K, $CDCl_3$) of: a) **57** (aa x10^{-3} M); b) **57** and 1 equiv of $\mathbf{2}^{+}$; c) **57** and 2 equiv of $\mathbf{2}^{+}$; d) **57** and 3 equiv of $\mathbf{2}^{+}$; e) **57** and 8 equiv of $\mathbf{2}^{+}$.

In addition, the appearance of *n*-alkyl resonances in the upfield negative region of the ^{1}H NMR spectrum of the 1:1 mixture of $\mathbf{2}^{+}$ and **57** in $CDCl_3$ corroborates the formation of the pseudo[2]rotaxane.[77] The 1:1 stoichiometry was confirmed by spectral integration. A COSY-45 spectrum of the above 1:1 mixture allowed a complete assignment of all shielded alkyl resonances. Thus, α protons at −0.03 ppm show a coupling with β methylene group at −1.06 ppm, which presents a cross-peak with γ protons at −0.17 ppm, finally coupled with δ protons at 0.37 ppm (accidentally isochronous with ε methyl).

Interestingly, the addition of increasing amounts of di-*n*-pentylammonium axle $\mathbf{2}^{+}$ led to the appearance of new signals attributable to the intermediate formation of pseudo[3]rotaxane which then evolved to pseudo[4]rotaxane (**Figure 179**). The addition of 8 equivalent of $\mathbf{2}^{+}$ led to a

simplification of the ^{1}H NMR spectrum of the mixture of **2**$^+$·TFPB$^-$ and **57** (**Figures 179c-e**). In particular, the appearance of a new singlet at 4.98 ppm integrating for 6H and relative to OCH_2 groups of the bridge, and the presence of three singlets relative to OMe groups were indicative of the prevalence of the higher-symmetry (with respect to singly threaded pseudo[2]rotaxane **2**$^+$⊂**57)** triply threaded pseudo[4]rotaxane (**2**$^+$)$_3$⊂**57** in which three axles **2**$^+$ were threaded into the three subcavities of **57.** Both, ^{1}H NMR signal integration and ESI(+) mass spectrum of 8:1 mixture of **2**$^+$·TFPB$^-$ and **57** gave a value of 1239.6 *m*/*z* as the base peak, corresponding to triply threaded pseudo[4]rotaxane ion (**2**$^+$)$_3$⊂**57** with a 1:3 host/guest stoichiometry.

*6.3.2. Threading of triple-calix[6]arene 57 with di-*benzy*lammonium axle 4*$^+$

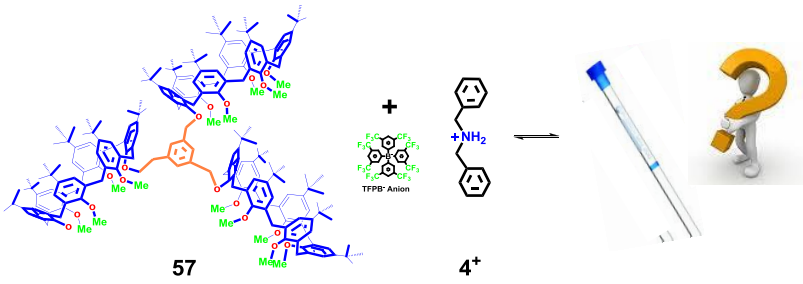

Scheme 28. Schematic representation of threading of **57** with the *di-n-benzyl*ammonium axle **4**$^+$.

Quite interesting was the *through-the-annulus* threading of triple-calix[6]arene **57** with dibenzylammonium axle ($Bn_2NH_2^+$*TFPB$^-$)(**Scheme 28**). In analogy to to the homologue double-calix[6]arene **21,** the *tert-butylated* triple-calix[6]arene **57** gave also rise to *endo*-benzyl complexation. In fact, the addition of 1 equivalent of di-benzylammonium salt **4**$^+$·TFPB$^-$ to a solution of **57** in $CDCl_3$, evidenced the presence of diagnostic shielded benzylic resonances in the 4–6

ppm region of its ^{1}H NMR spectrum (**Figure 180**), typical of *ortho, meta and para protons* (**Figure 182** *on the right* expansion of shielded benzyl region)

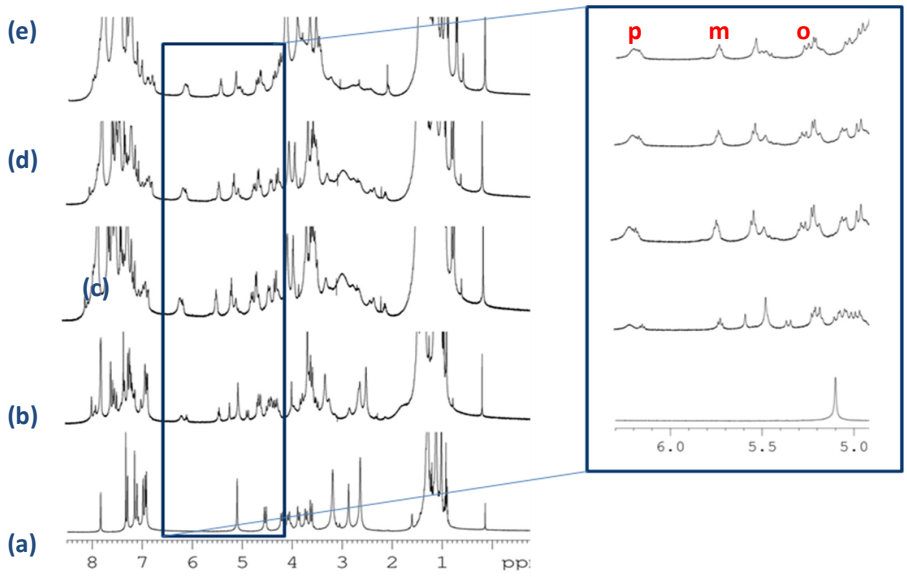

Figure 182. ^{1}H NMR (400 MHz, 298 K, $CDCl_3$) of: a) **57**(aa x10^{-3} M); b) **57** and **1** equiv of $\mathbf{4}^{+}$; c) **57** and 2 equiv of $\mathbf{4}^{+}$; d) **57** and 3 equiv of 4^{+}; e) **57** and 8 equiv of $\mathbf{4}^{+}$: *on the right* expansion of shielded benzyl region.

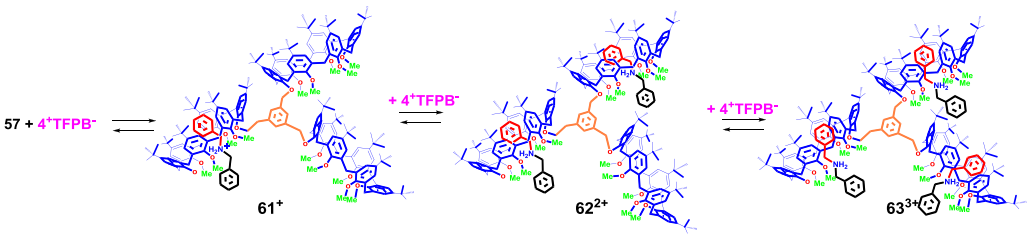

Scheme 29

Further addition of 3 equivalents of di-benzylammonium axle $\mathbf{4}^+$ led to a simplification of the ^{1}H NMR spectrum (**Figure 180** d-e, see in particular the resonance of *para* protons). This was indicative of the formation of a new, higher-symmetry, triple-threaded pseudo[4]rotaxane $(\mathbf{4}^+)_3\subset\mathbf{57}$ in which three axles $\mathbf{4}^+$ were threaded into the three macrocycles of **57.** A confirmation was obtained by ^{1}H NMR signal integration and by an ESI(+) mass spectrum of a 3:1 mixture of $\mathbf{4}^+\cdot$TFPB$^-$ and **57**, which gave a value of 1245,3 *m*/*z* as the base peak, corresponding to a 1:3 host/guest stoichiometry.

6.3.3 Directional threading of triple-calix[6]arene 57 with nonsymmetrical n-*butylbenzylammonium axle* 3^+

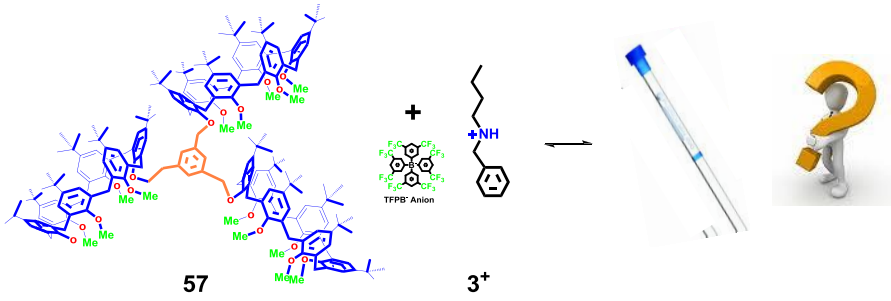

Figure 183. Schematic representation of Directional threading of **57** with the *n*-butylbenzylammonium axle $\mathbf{3}^+$.

As in the case of double calix[6]arene **21 (Figure 82),** the threading of **57** with the *n*-butylbenzylammonium axle **3**$^{+}$ could give rise to four directional triply-threaded pseudo[4]rotaxane diastereoisomers with all possible combination of *endo*-alkyl, or *endo*-benzyl relative orientations (**Figure 184**). Of course, on the basis of the above discussed *endo*-alkyl rule (**Figure 79**), we expected that the triple-*endo*-alkyl stereoisomer should be favored.

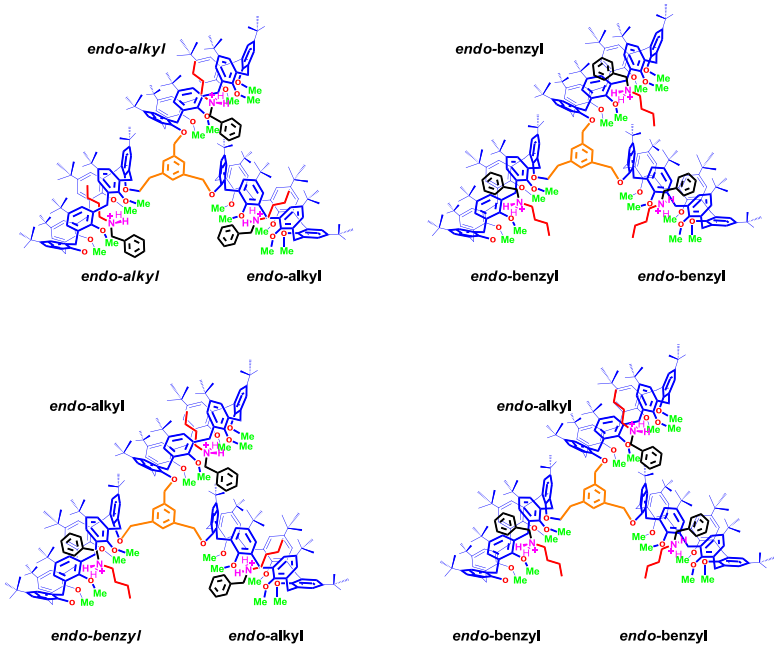

Figure 184. Possible triply-threaded pseudo[4]rotaxane stereoisomers by directional threading of **57** with the *n*-butylbenzylammonium axle **3**$^{+}$.

As above, the addition of butylbenzylammonium **3**$^{+}$ to a solution of **57** in $CDCl_3$ caused the usual changes in its ^{1}H NMR spectrum. As in the previous instances, 1 equiv of guest led to the singly-threaded complex **3**$^{+}\subset$**57** (as confirmed by ESI(+) MS and ^{1}H NMR signal integration. In analogy to the above discussed **2**$^{+}\subset$**57** pseudorotaxane, particularly useful were the singlets

relative to the OCH_2 protons of the bridge, which resonate at 5.02-5.07 ppm (**Figure 185b**). The progressive addition of $\mathbf{3}^+$ led to the emerging of a sole singlet at 5.04 ppm corresponding to the triply-threaded pseudo[4]rotaxane $(\mathbf{3}^+)_3\subset\mathbf{57}$, as confirmed by ESI(+) MS and ^{1}H NMR signal integration.

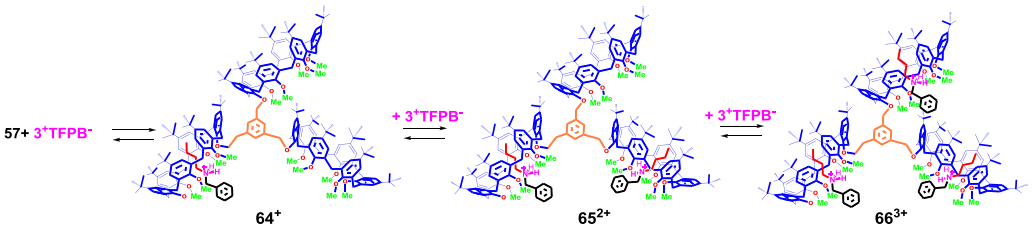

Scheme 30

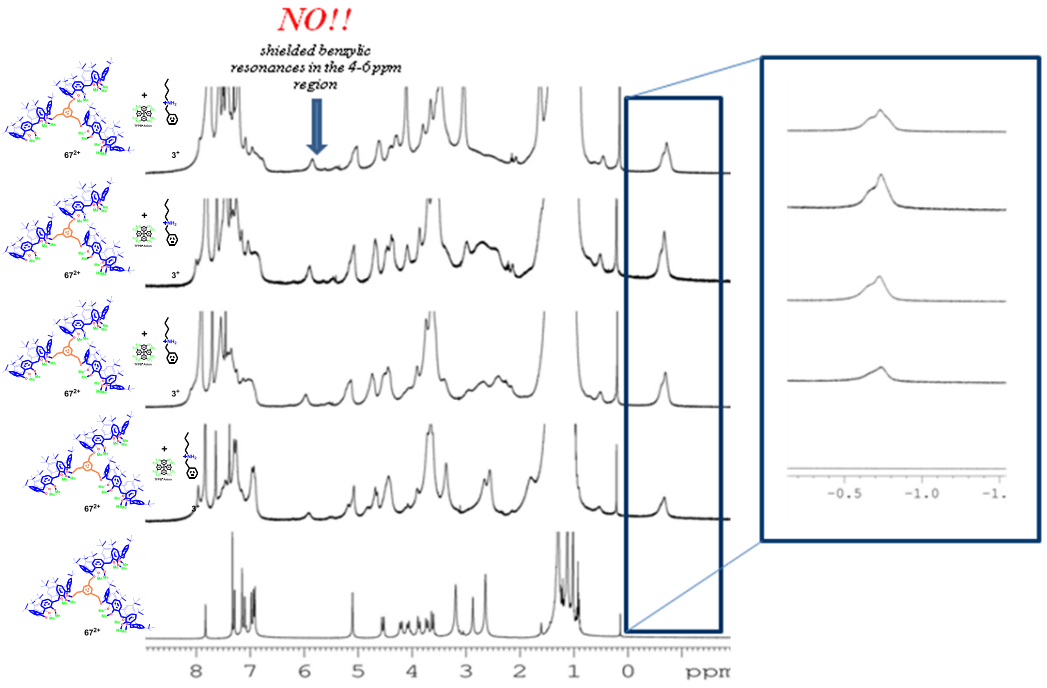

Figure 185. ^{1}H NMR (400 MHz, 298 K, $CDCl_3$) of: a) **57**(aa x10^{-3} M); b) **57** and **1** equiv of $\mathbf{3}^+$; c) **57** and 2 equiv of $\mathbf{3}^+$; d) **56** and 3 equiv of $\mathbf{3}^+$; e) **57** and 8 equiv of $\mathbf{3}^+$: *on the right* expansion of shielded alkyl region.

As concerns the stereochemistry of the threading, the ^{1}H NMR spectra of the mixtures of **57** and **3**$^{+}$ showed typical highfield signals characteristic of an *endo*-alkyl complexation.[77,80] This result in conjunction with the absence of shielded benzylic resonances indicated an *endo*-alkyl orientation of butylbenzylammonium threads in the corresponding pseudorotaxanes.[95] Thus, the validity of the *endo*-alkyl rule is confirmed once again, which would allow to control the threading directionality in interprenetad systems based on such triple-calixarene.

6.4 EXPERIMENTAL SECTION

ESI(+)-MS measurements were performed on a Micromass Bio-Q triple quadrupole mass spectrometer equipped with electrospray ion source, using $CHCl_3$ as solvent. All chemicals were reagent grade and were used without further purification. When necessary compounds were dried in vacuo over $CaCl_2$. Reaction temperatures were measured externally. Derivative **2**$^{+}$·TFPB^{-}[77] , **3**$^{+}$·TFPB^{-} [77], and **12**[123] were synthesized according to literature procedures. NMR spectra were recorded on Bruker Avance-400 spectrometer [400 (1H) and 100 MHz (13C)], Bruker Avance-300 spectrometer [300 (1H) and 75 MHz (13C)], or Bruker Avance-250 spectrometer [250 (1H) and 63 MHz (13C)]; chemical shifts are reported relative to the residual solvent peak (CHCl3: δ 7.26, CDCl3: δ 77.23). COSY-45 spectra were taken using a relaxation delay of 2 seconds with 30 scans and 170 increments of 2048 points each. HSQC spectra were performed with gradient selection, sensitivity enhancement, and phase sensitive mode using Echo/Antiecho−TPPI procedure. A typical experiment comprised 20 scans with 113 increments of 2048 points each. Monte Carlo conformational searches (10000 steps) were performed with MacroModel-9/Maestro-4.1 program using $CHCl_3$ as solvent (GB/SA model). MD simulations were performed at T = 500 K, for 20000 ps, using a time step of 1.0 fs.

[123] Ciao, R.; Talotta, C.; Gaeta, C.; Margarucci, L.; Casapullo, A.; Neri, P., *Organic Letters,* 15(22), **2013,** 5694.

6.4.1 Synthesis of triple *tert-butylated*-calix[6]arene *56*

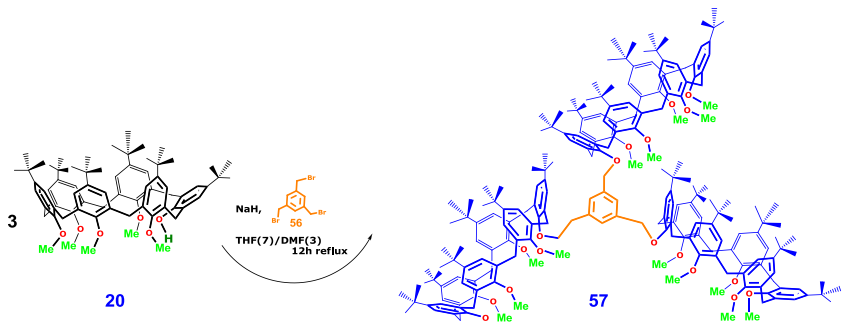

Scheme 31. Synthesis of triple *tert-butylated*- calix[6]arene **57**

NaH (1.05 g, 54.2 mmol) was added at 0 °C, under stirring, to a solution of derivative **20** (3.11, 4.37 mmol) in dry THF/DMF (180 mL, 7/3 *v/v*). The mixture was kept at 25 °C under stirring, and after 1 h, 1,3,5-tris(bromomethyl)benzene **56** (0.36 g, 1.36 mmol) was added. The reaction was stirred at reflux for 24 h under a nitrogen atmosphere, then the solvent was removed under reduced pressure and the mixture was partitioned between CH_2Cl_2 and H_2O. The organic layer was washed with 1N HCl (100 mL), brine (100 mL), and dried over Na_2SO_4. The crude product was purified by column chromatography (SiO_2; Et_2O/CH_2Cl_2 3/97) to give derivative **57** as a white solid (2.22 g, 0.69 mmol, 69%). **ESI(+) MS**: *m/z* 3287.2 (MH^+) .**^{1}HNMR** (400 MHz, $CDCl_3$, 298 K): δ 7.78 (s, Ar*H* *ponte*, 3H), 7.28 - 7.26 (overlapped ArH_{calix}, 6H), 7.11 - 7.06 (overlapped, ArH_{calix}, 12H), 6.94 – 6.87 (overlapped, ArH_{calix}, 18H), 5.06 (s, Ar*H* *Bn*,6H), 4.50 e 3.58 (AX, ArCH_2Ar, *J*=14.7Hz, 12H), 4.17 e 4.04 (AX, ArCH_2Ar, *J*=14.5Hz, 12H), 3.83 e 3.68 (AX, ArCH_2Ar, *J*=15.1Hz, 12H), 3.15 (s, OCH_3, 18H), 2.82 (s, OCH_3, 9H), 2.58 (s, OCH_3, 18H), 1.24 (2) (overlapped, C(CH_3)$_3$, 81H), 1.07 (s, C(CH_3)$_3$, 54H), 0.97 (s, C(CH_3)$_3$, 26H).**^{13}CNMR** (250 MHz, $CDCl_3$, 298 K): δ 154.5, 154.4, 153.9, 152.4,

145.9, 145.7, 138.8, 134.1, 133.9, 133.7, 133.6, 133.4, 127.5, 126.9, 125.5, 125.3, 124.8, 77.5, 75.9, 74.8, 60.2, 60.0, 34.3 (2), 31.8, 31.7(2), 31.5 (2),30.8, 30.6, 22.7, 14.4.

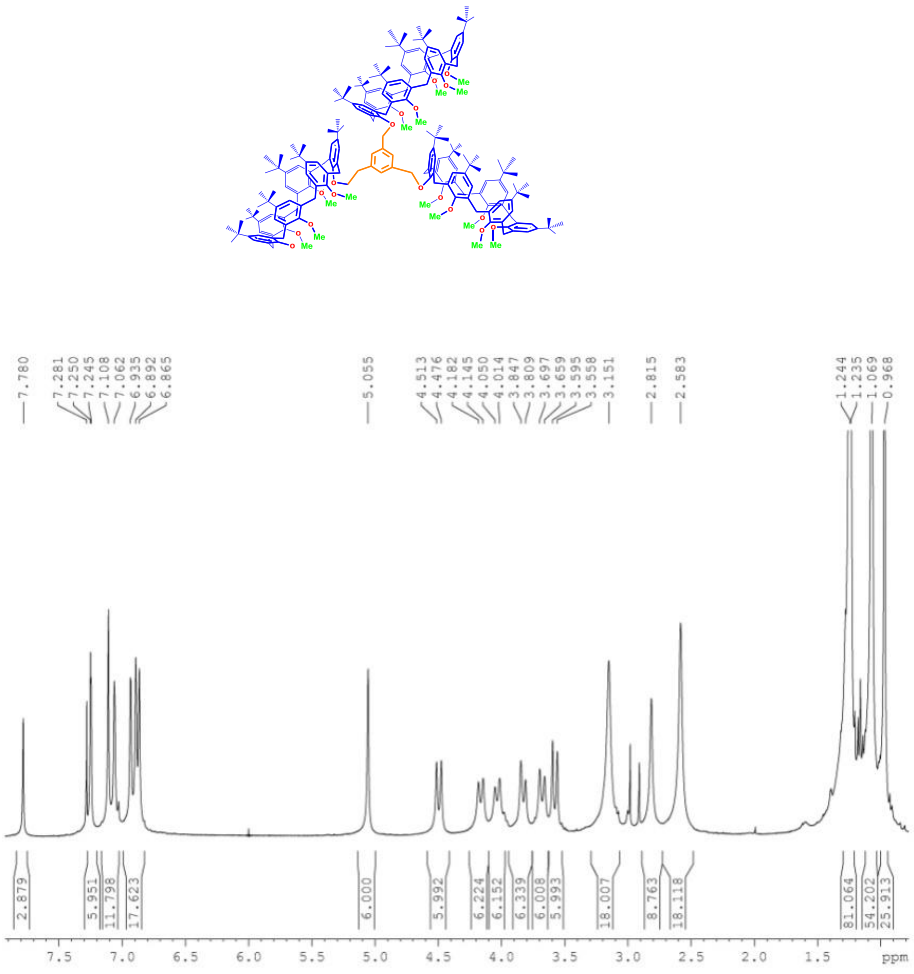

Figura 186 Spectrum ^{1}H NMR of derivative **57** in $CDCl_3$ (400 MHz, 298 K).

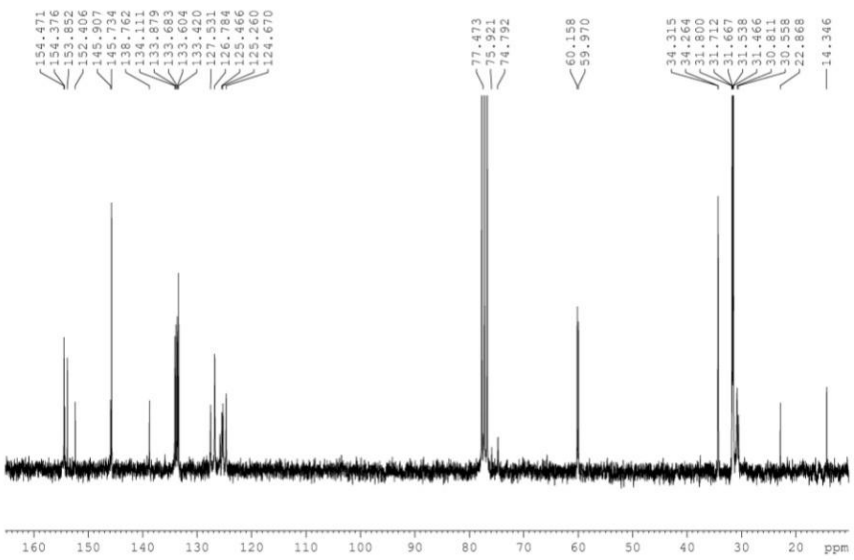

Figura 187. Spectrum ^{13}C NMR of derivative **57** in $CDCl_3$ (250 MHz, 298 K).

6.4.2 Preparation of singly-threaded pseudo[2]rotaxanes 58^+, 61^+ and 64^+

Derivative 58^+

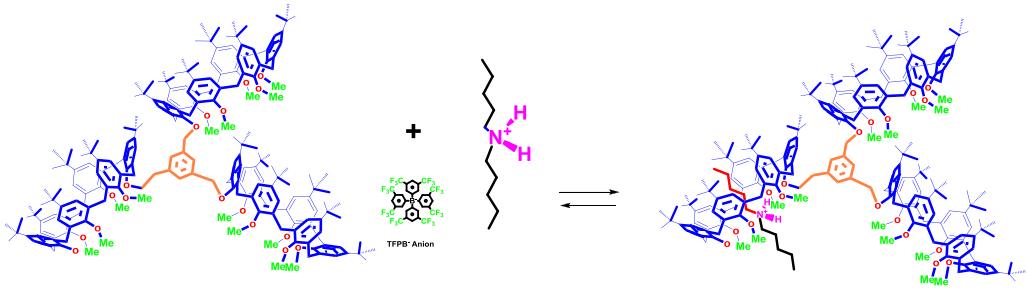

Triple-calixarene derivative **57** ($1.81 \cdot 10^{-3}$ g, $1.2 \cdot 10^{-3}$ mmol) and the di-*n*-pentylammonium derivative $\mathbf{2}^{+}$ ($0.6 \cdot 10^{-3}$ mmol) were dissolved in 0.4 mL of $CDCl_3$ and the mixture was stirred for 5 min at 25 °C. Then, the solution was transferred in a NMR tube for 1D and 2D NMR spectra acquisition. Selected spectral data for singly threaded pseudo[2]rotaxane ion $\mathbf{2}^{+}\subset\mathbf{57}$ ESI(+) MS: *m*/*z* = 3423.4 $[\mathbf{2}\subset\mathbf{57}]^{+}$. ^{1}H NMR ($CDCl_3$, 400 MHz, 298 K): δ −1.07 [broad, $(CH_2)_\beta$, 2H], −0.17 [broad, $(CH_2)_\gamma$, 2H], −0.02 [broad, $(CH_2)_\alpha$, 2H], 0.37 [broad, $(CH_2)_\delta$ + $(CH_3)_\varepsilon$, 5H], 3.53 and 4.29 (broad overlapped, $ArCH_2Ar$, 36H), 2.87, 2.99, 3.23 (br s, OCH_3, 6H, 3H, 6H), 3.78, 3.84, 3.90 (br s, OCH_3, 18H, 9H, 18H), 4.79 (br s, OCH_2, 3H), 4.98 (br s, OCH_2, 3H), 6.63–6.99 (overlapped, ArH, 40H).

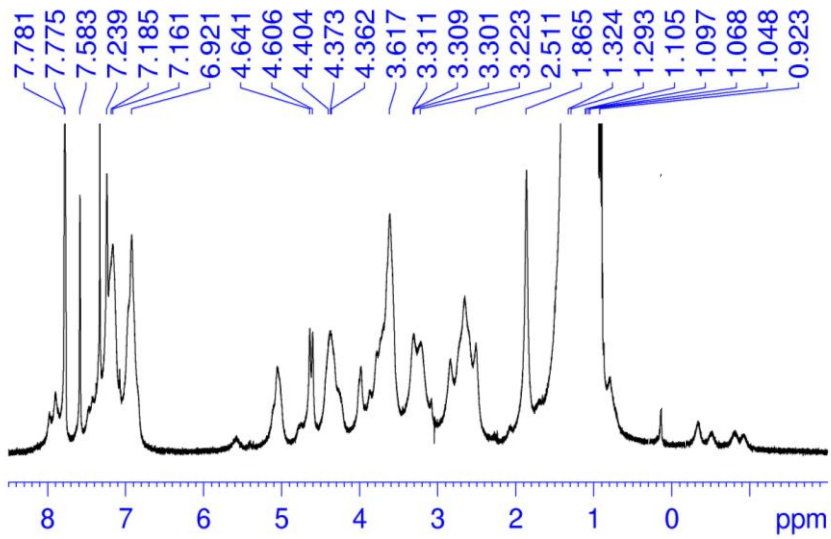

Figure 188. ^{1}H NMR spectrum (400 MHz, 298 K, $CDCl_3$) of the 1:1 mixture of **57** and $\mathbf{3}^{+}\cdot TFPB^{-}$.

Derivative 61^+

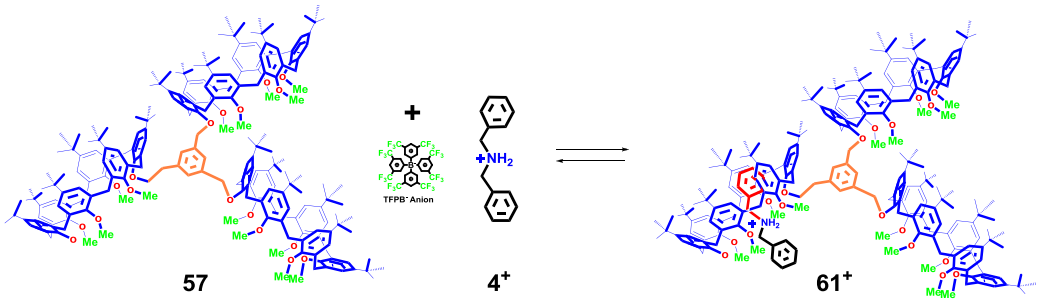

Triple-calixarene derivative **57** ($2.0 \cdot 10^{-3}$ g, $0.91 \cdot 10^{-3}$ mmol) and the dibenzylammonium derivative $\mathbf{3}^+$ ($1.3 \cdot 10^{-3}$ mmol) were dissolved in 0.5 mL of $CDCl_3$ and the mixture was stirred for 5 min at 25 °C. Then, the solution was transferred in a NMR tube for 1D and 2D NMR spectra acquisition.

^{1}H NMR (400 MHz, $CDCl_3$, 298 K): δ 1.04 [s, $(CH_3)_3C$-, 90H], 1.28 [s, $(CH_3)_3C$-, 90H], 1.38 [m, $(CH_2)_r$, 2H)], 1.53 [m, $(OCH_2)_j$, 2H], 1.61 [m, $(OCH_2)_x$, 2H], 3.45 and 4.39 (AX, $ArCH_2Ar$, 12H, J = 12.0 Hz), 3.75 [s, OCH_3, 15H], 3.75 [s, OCH_3, 15H], 4.01and 4.51 (d, ArH_r, 2H, J = 8.0 Hz), 5.07 [s, $(OCH_2)_s$, 6H,), 4.78 (d, ArH_o, J= 8.0 Hz, 1H), 5.33 (dd, ArH_m, J_1=J_2=7.6 Hz, 4H), 5.98 (t, ArH_p, J_1 = 7.6 Hz, 2H), 6.11 (*broad*, NH_2^+, 2H), 7.14-7.30 (*overlapped*, Ar*H*, 52H), 7.50 (s, ArH_{TFPB}, 4H), 7.71 (t, ArH_{TFPB}, 8H, J = 4.0 Hz), 7.83 (d, ArH_n, 2H, J = 8.0 Hz)

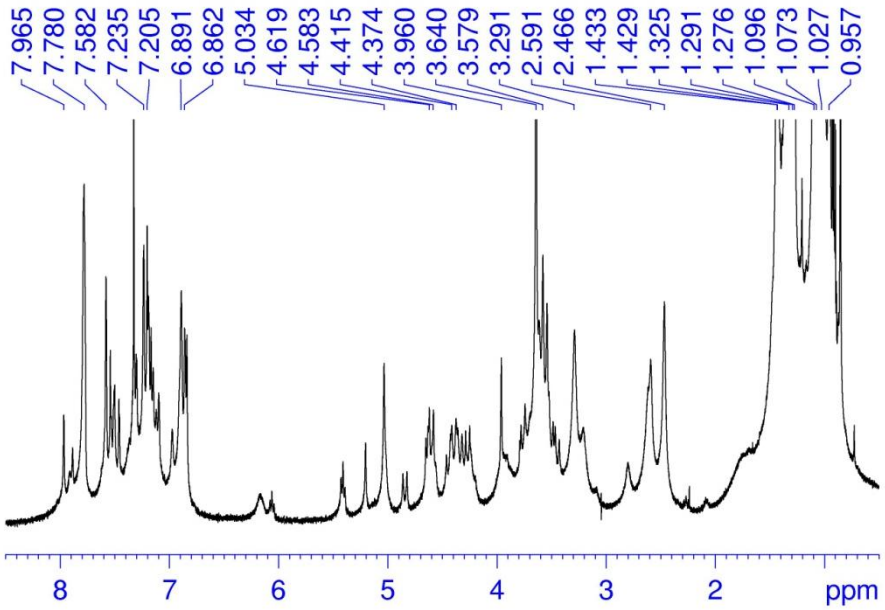

Figure 189. ^{1}H NMR spectrum (400 MHz, 298 K, $CDCl_3$) of the 1:1 mixture of **57** and **3**$^{+}$·TFPB^{-}.

Derivative 64^{+}

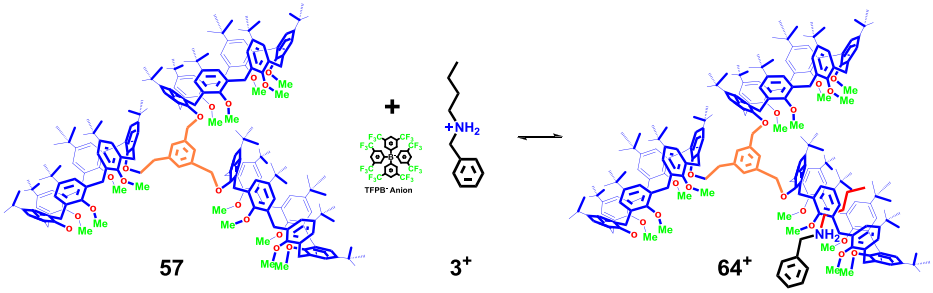

Triple-calixarene derivative **57** ($2.0\cdot10^{-3}$ g, $0.91\cdot10^{-3}$ mmol) and the dialkylammonium derivative **3**$^{+}$ ($0.65\cdot10^{-3}$ mmol) were dissolved in 0.5 mL of $CDCl_3$ and the mixture was stirred for 5 min at 25 °C. Then, the solution was transferred in a NMR tube for 1D and 2D NMR spectra acquisition.

ESI(+) MS: *m*/*z* = 3456 [**3**⊂**57**]$^+$. ^{1}H NMR ($CDCl_3$, 400 MHz, 298 K): δ −1.02 [broad, $(CH_2)_\beta$, 2H], 0.04 [broad, $(CH_2)_\gamma + (CH_3)_\delta$, 5H], 0.22 [broad, $(CH_2)_\alpha$, 2H], 2.30 [broad, ($H_2N^+CH^\alpha{}_2Ph$), 2H], 2.87−3.93 (broad overlapped OCH_3+ $ArCH_2Ar$, 42H), 4.31−4.41 (broad overlapped, $ArCH_2Ar$, 12H), 4.78 (br s, OCH_2, 2H), 4.98 (br s, OCH_2, 2H), 5.37 (br s, $^+NH_2$, 2H), 6.76–7.40 (overlapped, ArH, 45H).

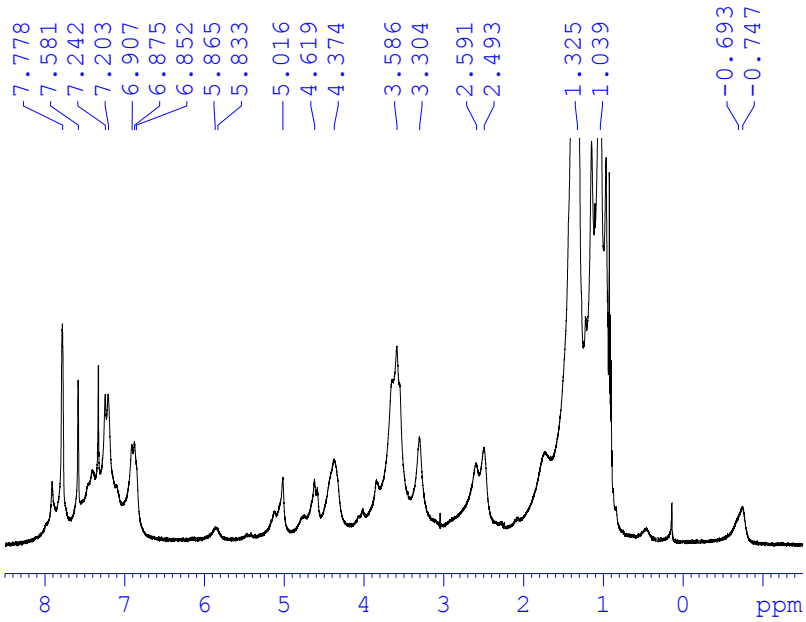

Figure 190. ^{1}H NMR spectrum (400 MHz, 298 K, $CDCl_3$) of the 1:1 mixture of **57** and **3**$^+$·TFPB$^-$.

6.4.3 Preparation of triply-threaded pseudo[4]rotaxanes 60^{3+},63^{3+} and 66^{3+}

Derivative 60^{3+}

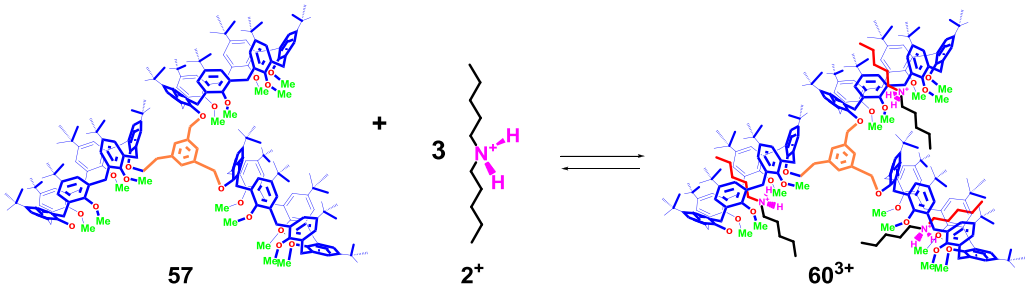

Triple-calixarene derivative **57** ($2.0 \cdot 10^{-3}$ g, $0.91 \cdot 10^{-3}$ mmol) and the di-*n*-pentylammonium derivative $\mathbf{2}^{+}$ ($1.94 \cdot 10^{-3}$ mmol) were dissolved in 0.5 mL of $CDCl_3$ and the mixture was stirred for 5 min at 25 °C. Then, the solution was transferred in a NMR tube for 1D and 2D NMR spectra acquisition. ESI(+) MS: *m*/*z* = 1239,8 $[(\mathbf{2})_3 \subset \mathbf{57}]^{3+}$. ^{1}H NMR ($CDCl_3$, 400 MHz, 298 K): δ −1.07 [broad, $(CH_2)_\beta$, 6H], −0.18 [broad, $(CH_2)_\gamma$, 6H], −0.01 [broad, $(CH_2)_\alpha$, 6H], 0.39 [broad, $(CH_2)_\delta$ + $(CH_3)_\varepsilon$, 15H], 3.52 and 4.33 (broad, $ArCH_2Ar$, 36H), 3.79, 3.84, 3.91 (br s, OCH_3, 9H, 18H, 18H), 4.98 (br s, OCH_2, 6H), 6.66–7.61 (overlapped, ArH, 60H).

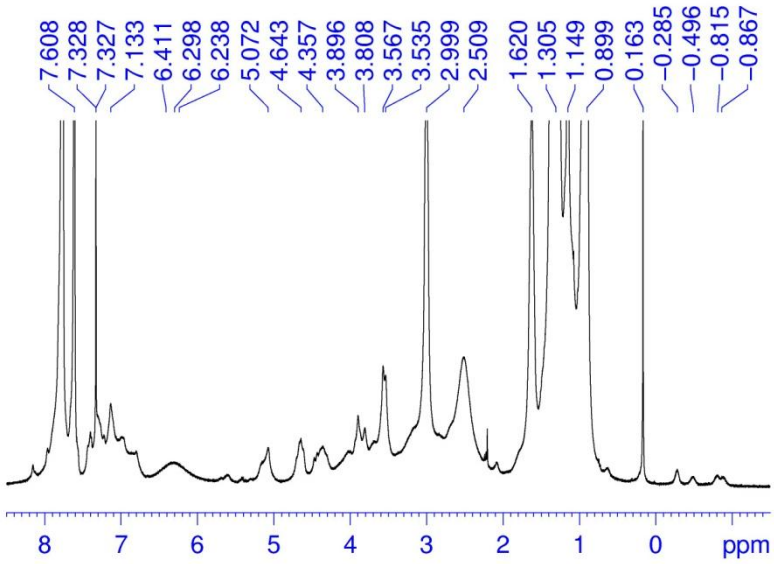

Figure 191. ^{1}H NMR spectrum (400 MHz, 298 K, $CDCl_3$) of the 1:3 mixture of **57** and **2**$^{+}$·TFPB^{-}.

Derivative 63^{3+}

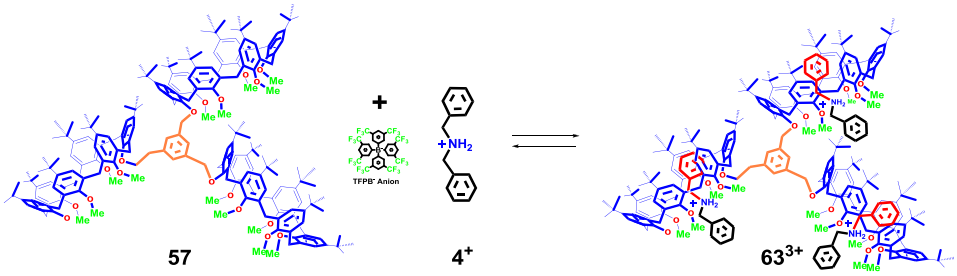

Triple-calixarene derivative **57** ($2.0\cdot10^{-3}$ g, $0.91\cdot10^{-3}$ mmol) and the dibenzylammonium derivative **4**$^{+}$ ($1.97\ 10^{-3}$ mmol) were dissolved in 0.5 mL of $CDCl_3$ and the mixture was stirred for 5 min at 25 °C. Then, the solution was transferred in a NMR tube for 1D and 2D NMR spectra acquisition. ESI(+) MS: *m*/*z* = 1245.6 [(**4**)$_3$⊂**57**]$^{3+}$. ^{1}H NMR ($CDCl_3$, 400 MHz, 298 K): δ 1.17 (s, Bu^{t}, 135H), 1.45 [(CH_2)$_{d}$, 6H], 2.94 [(CH_2)$_{f}$, 6H], 3.51 and 4.40 (AX, ArCH_2Ar, *J* =13.6 Hz, 18H each), 3.86 (s, OCH_3, 54H), 4.67 (d, ArH_o, *J*= 8.0 Hz, 6H), 5.34

(dd, $ArH_{\boldsymbol{m}}$, J_1=J_2=7.6 Hz, 6H), 5.40 [s $(OCH_2)_{bridge}$,6H], 6.01 (t, $ArH_{\boldsymbol{p}}$, J_1 = 7.6 Hz, 6H), 6.09 (*broad*, NH_2^+, 6H), 7.01 (s, ArH_{calix}, 36H), 7.48 (s, ArH_{TFPB}^-, 12H), 7.71 (ArH_{TFPB}^-, 24H).

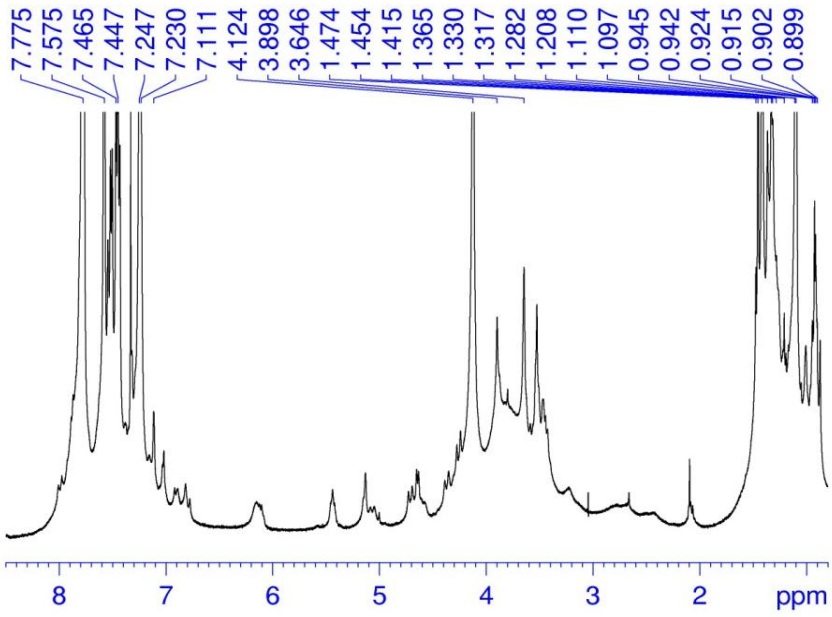

Figure 192. ^{1}H NMR spectrum (400 MHz, 298 K, $CDCl_3$) of the 1:3 mixture of **57** and $\mathbf{4}^+ \cdot TFPB^-$.

Derivative 66^{3+}

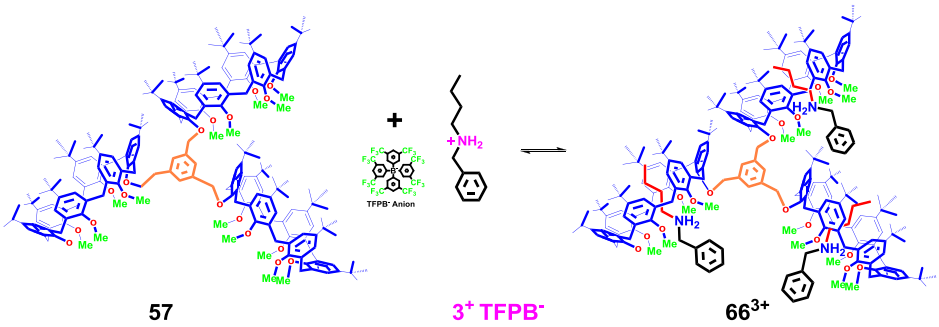

Triple-calixarene derivative **57** ($2.0\cdot10^{-3}$ g, $0.91\cdot10^{-3}$ mmol) and the alkylbenzylammonium derivative $\mathbf{3}^+$ ($2.73\cdot10^{-3}$ mmol) were dissolved in 0.5 mL of $CDCl_3$ and the mixture was stirred for 5 min at 25 °C. Then, the solution was transferred in a NMR tube for 1D and 2D NMR spectra acquisition.ESI(+) MS: *m*/*z* = 1239.6 $[(\mathbf{3})_3\subset\mathbf{57}]^{3+}$. ^{1}H NMR ($CDCl_3$, 400 MHz, 298 K): δ−1.01 [broad, $(CH_2)_\beta$, 6H], 0.03 [broad, $(CH_2)_\gamma$ + $(CH_3)_\delta$, 15H], 0.23 [broad, $(CH_2)_\alpha$, 6H], 2.27 [broad, ($^+H_2NCH^\alpha{}_2Ph$), 6H], 3.28, 3.59, 3.70 (s, OCH_3, 9H, 18H, 18H), 3.50 and 4.44 (broad, $ArCH_2Ar$, 12H), 3.52 and 4.32 (broad, $ArCH_2Ar$, 12H), 3.58 and 4.43 (broad, $ArCH_2Ar$, 12H), 4.97 (br s, OCH_2, 6H), 5.35 (br s, $^+NH_2$, 6H), 6.64–7.59 (overlapped, ArH, 75H).

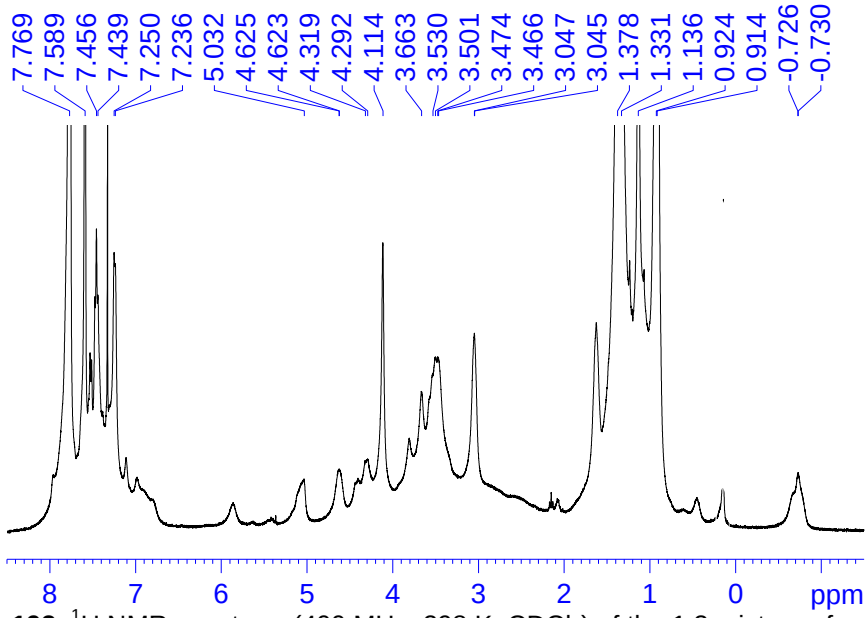

Figure 193. ^{1}H NMR spectrum (400 MHz, 298 K, $CDCl_3$) of the 1:3 mixture of **57** and **3**·TFPB^{-}.

6.5 Conclusion

In the last part of the Ph.D. thesis has been devoted to the threading abilities of triple-calix[6]arene hosts **57** with mono-ammonium axles in the presence of the TFPB superweak anion.

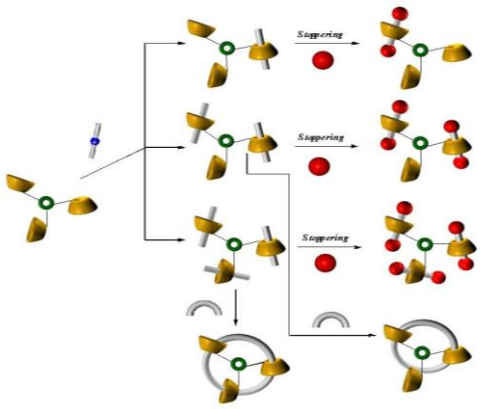

^{1}H NMR and ESI(+) MS spectra evidenced the stepwise formation of singly- doubly- and tply-threaded pseudorotaxane architectures by changing the host/guest stoichiometry from 1:1 to 1:3. The directional threading of nonsymmetrical *n*-butylbenzylammonium axle $\mathbf{3}^{+}$ with triple-calix[6]arene host **57** occurs with an *endo*-alkyl preference in accordance with the known "*endo*-alkyl rule".

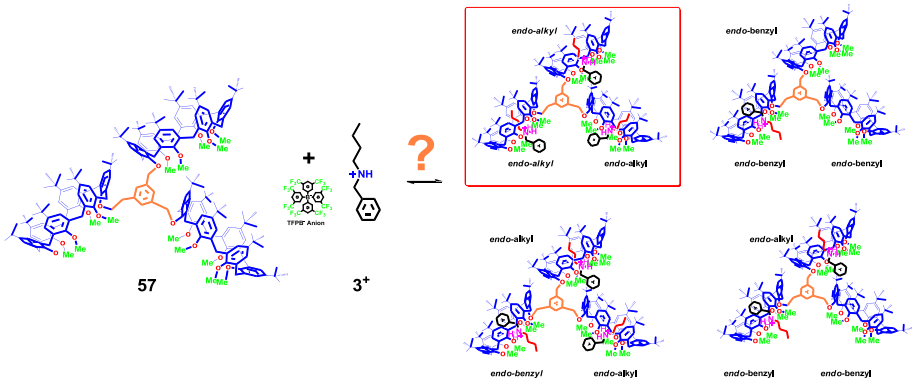

Figure 194. Possible triply-threaded pseudo[4]rotaxane stereoisomers by directional threading of **57** with the *n*-butylbenzylammonium axle $\mathbf{3}^{+}$.

CHAPTER VI

7. Conclusion

In this Ph. D. thesis, we have briefly introduced the main concepts of chemical topology in order to provide a rational perspective to frame what appear to be the most advanced molecular machines that chemistry has been able to assemble up to now.

From the considerable list of available approaches, it was decided to focus our study to the calixarene/dialkylammonium recognition motif, reporting some recently discovered peculiarities, which are related to the possible orientations of the directional calix-wheel.[77,78,79,]

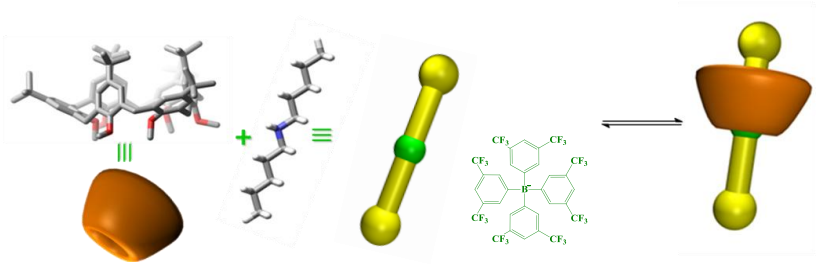

Figure 195. *endo*-Cavity Complexation and *Through-the-Annulus* Threading of Calixarenes Induced by Very Loose Alkylammonium Ion Pairs

Then, the Ph. D. thesis deals with the exploration of these stereochemical features in the threading of hosts containing multiple cavities. Therefore, the synthesis of double- and triple-calixarenes is reported, which is followed by the subsequent study of their threading abilities with dialkylammonium axles.

The results confirmed the well-known *endo-alkyl* preference of calix[6]arenes to give the inclusion of alkyl chains inside the calix-cavity. On this basis we were then able to build new chemical topologies such as oriented handcuff rotaxanes.

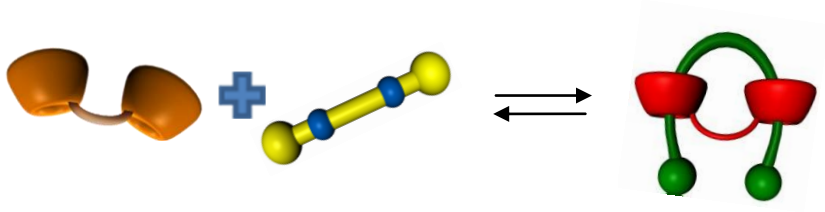

Figure 196. Threading of double calx[6]arene with bis-ammonium axle

The results were particularly satisfying and can be considered as a prelude to the possible use of multi-calixarenes in the synthesis of topologically more complex architectures.

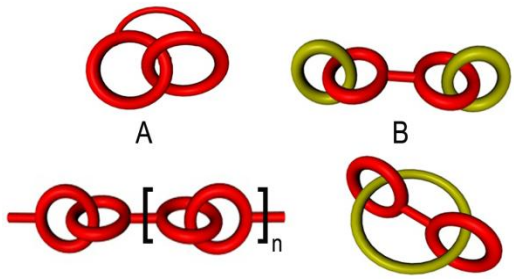

Figure 197. Topologically complex architectures.